Characterization of the trafficking pathway used by Pseudomonas aeruginosa Exotoxin A and application to oral drug delivery

Laurent, Floriane

Award date:
2016

Awarding institution:
University of Bath

Characterization of the trafficking pathway used by Pseudomonas aeruginosa Exotoxin A and application to oral drug delivery

Floriane Laurent

A thesis submitted for the degree of Doctor of Philosophy

University of Bath

Department of Pharmacy and Pharmacology

December 2015

ABSTRACT

Recent advances in biotechnology have enabled the development and large scale production of protein therapeutics, thereby providing new treatments for numerous diseases. However, oral delivery of biologics remains a challenge as macromolecules are poorly absorbed and rapidly degraded in the gastrointestinal tract. Several strategies have been studied to improve bioavailability, but to date, no safe, efficient and clinically relevant delivery system has been discovered. Here, the reprogramming of bacterial toxins for therapeutic purposes was investigated. Following cellular uptake, *Pseudomonas aeruginosa* exotoxin A (PE) and *Vibrio cholerae* cholix toxin (Cho) escape lysosomal degradation and are capable of both trafficking to the cytosol of non-polarised (NP) cells and undergoing transcytosis across polarised cells. This project aimed to investigate the trafficking routes exploited by these toxins to determine how they avoid degradation, and define their potential as vehicles for oral protein delivery.

The nature of the conformational change experienced by PE in acidic conditions was first investigated. It was shown that this transition consists of a subtle alteration in the protein's structure which does not affect its overall size, but results in the exposure of additional trypsin cleavage sites and hydrophobic residues. It was concluded that the transition is involved in the protein's escape from lysosomal degradation and was most likely caused by the protonation of two histidine residues when the pH was lowered, resulting in the formation of additional salt bridges and thus different structural constraints.

The interaction between PE and monosialoganglioside GM1 was also examined to determine whether it could act as a secondary receptor for PE. High-affinity binding was established in both acidic and physiological conditions, and interaction with GM1 was shown to be required for efficient protein internalisation by NP cells. These findings were concluded to be in agreement with GM1 acting as a secondary receptor for PE, leading the toxin away from lysosomal degradation following conformational change.

The potential of PE as a vehicle for delivery of biologics was studied using several versions of the toxin connected to a cargo protein. Results showed that a truncated version of PE is capable of carrying a cargo protein (green fluorescent protein, human growth hormone) inside NP cells *in vitro* and across polarised epithelium *in vivo*. These data strongly support the idea that PE has the potential to be used as a vehicle for oral delivery of biologics.

Similarly, these studies were also carried out on cholix to assess its ability to act as a drug carrier. Cholix was shown to undergo a conformational change similar to that experienced by PE. It was also demonstrated that an interaction with GM1 occurred, although in this case, increased binding appeared to result in decreased internalisation by NP cells. Finally, full-length and truncated cholix could transport a payload inside NP cells *in vitro* and across polarised epithelial cells *in vivo*. These results confirm that cholix could also represent a powerful tool for oral administration of macromolecular drugs.

DECLARATION OF AUTHORSHIP

This is all my own work, except where I have indicated via references or other forms of acknowledgment.

Date:

Signature:

ACKNOWLEDGEMENTS

First and foremost, I would like to express my sincere gratitude to my supervisor, Professor Randall Mrsny, for his advice and support over the years. I was fortunate to undertake my first steps in research under his supervision and believe his expertise, thought-provoking questions and inspired guidance led me to become a better researcher.

My thanks also go to the University of Bath for the studentship that funded this research.

I would also like to thank Dr David FitzGerald and Dr Thomas Hunter for their help and valuable advice.

My grateful thanks go to Dr Julia MacKay, Dr Hanne Kinnunen, Dr Emma Harvey and Dr Edward Carter for their friendship, practical advice and stimulating discussions. Many thanks also go to Alistair Taverner for his help with *in vivo* work.

I would also like to express my deepest gratitude to my family for their never-ending support. Finally, thank you to Iain, who never failed to provide the much needed encouragement to enable me to complete this PhD and who patiently proofread this entire thesis. This hasn't been an easy ride but it was all worth it.

CONTENTS

LIST OF TABLES

LIST OF FIGURES

List of Abbreviations and Acronyms

AA	Acetic acid
ADP	Adenosine diphosphate
AE	Anion exchange
AJ	*Adherens* junction
AJC	Apical junctional complex
ANS	8-Anilino-1-naphthalenesulfonic acid
APS	Ammonium persulfate
ATCC	American Type Culture Collection
ATP	Adenosine triphosphate
BSA	Bovine serum albumin
CD91	Cluster of differentiation 91
CHO	Chinese ovarian cancer
Cho	*Vibrio cholerae* cholix exotoxin
CO_2	Carbon dioxide
CP	Citrate-phosphate
CPP	Cell-penetrating peptide
CT	*Vibrio cholerae* cholera toxin
CTB	Cholera toxin B subunit
DAPI	4′,6-Diamidino-2-phenylindole dihydrochloride
dH_2O	Distilled water
DLS	Dynamic light scattering
DMEM	Dulbecco's modified eagle's medium
DMSO	Dimethylsulfoxide
DNA	Deoxyribonucleic acid
DRM	Detergent-resistant membrane
DT	*Corynebacterium diphtheriae* diphtheria toxin

DTT	Dithiothreitol
ECL	Enhanced chemiluminescence
E. coli	*Escherichia coli*
EDTA	Ethylenediaminetetraacetic acid
EE	Early endosome
eEF2	Eukaryotic elongation factor 2
EPO	Erythropoietin
ER	Endoplasmic reticulum
ERAD	ER-associated protein degradation
FBS	Fœtal bovine serum
FDA	Food and drug administration
FITC	Fluorescein isothiocyanate
FPLC	Fast protein liquid chromatography
Fv	Variable fragment
GF	Gel filtration
GFP	Green fluorescent protein
GIT	Gastro-intestinal tract
GM1	Monosialoganglioside
GS	Poly glycine-serine flexible linker
GSSG	Oxidised glutathione
HBSS	Hank's balanced salt solution
HCl	Hydrochloric acid
hGH	Human growth hormone
HPLC	High pressure liquid chromatography
HRP	Horseradish peroxidase
IF	Immunofluorescence
IgG	Immunoglobulin G
IMAC	Immobilised-metal affinity chromatography

IPTG	Isopropyl β-D-1-thiogalactopyranoside
IX	Ion exchange
KDEL-R	KDEL receptor
kPB	Potassium-phosphate buffer
L	Lysosome
LB	Lysogeny broth
LE	Late endosome
LRP	Low density lipoprotein receptor
LRP1	Low density lipoprotein receptor-related protein 1
LysoGM1	Lyso-monosialoganglioside
MeOH	Methanol
MQ H_2O	Milli-Q water
MW	Molecular weight
MWCO	Molecular weight cut-off
NaCl	Sodium chloride
NP	Non-polarised
ntCho	Non-toxic cholix
ntPE	Non-toxic *Pseudomonas* exotoxin A
P/S	Penicillin/streptomycin
PB	Phosphate buffer
PBS	Phosphate buffer saline
PDI	Protein-disulphide isomerase
PE	*Pseudomonas aeruginosa* exotoxin A
PFA	Paraformaldehyde
pI	Isoelectric point
PVDF	Polyvinylidene difluoride
RE	Recycling endosome
RIT	Recombinant immunotoxin

RME	Receptor-mediated endocytosis
RPMI	Roswell Park Memorial Institute
RT	Room temperature
SD	Standard deviation
SDS	Sodium dodecyl sulphate
SDS-PAGE	Sodium dodecyl sulphate polyacrylamide gel electrophoresis
SEC	Size exclusion chromatography
SI	Small intestine
siRNA	Small interfering ribonucleic acid
TBS	Tris buffer saline
TBS-T	Tris buffer saline supplemented with 0.1 % Tween 20
TE	Tris/EDTA
TEER	Transepithelial electrical resistance
TEMED	Tetramethylethylenediamine
TEV	Tobacco Etch Virus protease
TGN	*Trans* Golgi network
TJ	Tight junction
Tris	Tris(hydroxymethyl)aminomethane
UD	Undigested
UV	Ultra-violet
VIS	Visible
WB	Western blot

LIST OF APPENDICES

1 INTRODUCTION

Overview

Since the approval of the first recombinant protein drug by the US Food and Drug Administration (FDA) in 1982 (human insulin), the rapid development of new technologies within the pharmaceutical industry has enabled the large scale production of a wide range of recombinant proteins, offering new perspectives for the treatment of numerous diseases. Overall, the market is dominated by oncology, insulins, auto-immune and auto-suppressive agents (Figure 1-1) [1, 2]. Protein therapeutics represent an ever expanding market whose global sales increased from $33 billion in 2003 up to $137 billion in 2013 [1, 3], when seven out of the ten top global selling drugs were proteins and included five antibodies (Table 1-1) [4]. The sales of these seven compounds only accounted for more than $56 billion in 2013.

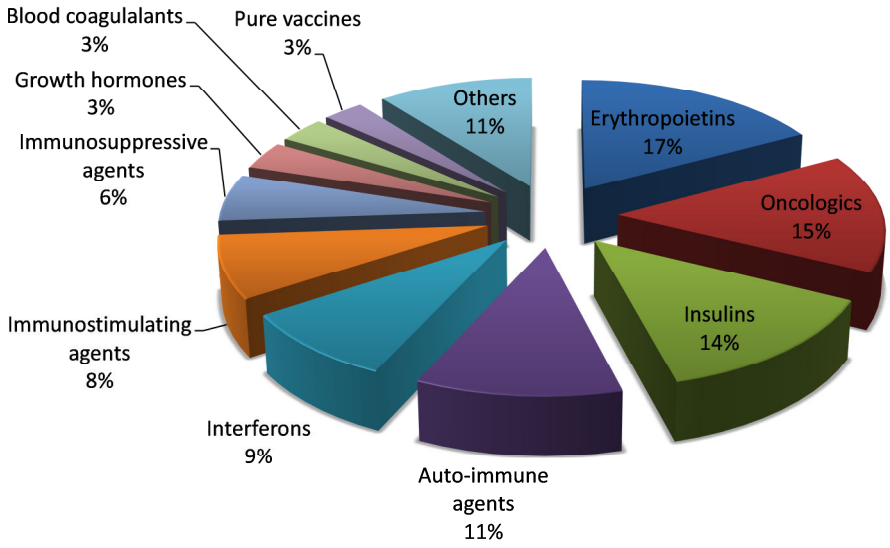

Figure 1-1 – Market share of the leading therapy classes in 2013 [2].

Table 1-1 – The world's top 10 best-selling prescription drugs in 2013 [4] and their current mode of administration. Stars indicate protein therapeutics.

Rank	Product	Company	Prescribed for treatment of	2013 sales ($USm)	Current mode of administration
1*	Humira	AbbVie	Rheumatoid arthritis/ autoimmune diseases	10.7	Subcutaneous injection [5]
2*	Enbrel	Pfizer/Amgen	Rheumatoid arthritis/ autoimmune diseases	8.8	Subcutaneous injection [6]
3*	Remicade	Johnson & Johnson/Merck & Co.	Rheumatoid arthritis/ autoimmune diseases	8.4	Intravenous infusion [7]
4	Seretide/ Advair	GlaxoSmithKline	Asthma	8.3	Inhalation [8, 9]
5*	Lantus	Sanofi	Diabetes	7.6	Subcutaneous injection [10]
6*	Rituxan	Roche	Rheumatoid arthritis	7.5	Intravenous infusion [11]
7*	Avastin	Roche	Bowel cancer	6.8	Intravenous infusion [12]
8*	Herceptin	Roche	Breast cancer	6.6	Intravenous infusion [13]
9	Crestor	AstraZeneca	Cholesterol	5.6	Oral [14]
10	Abilify	Otsuka Holdings	Depression/ schizophrenia	5.5	Oral/ intramuscular injection [12]

Protein therapeutics present several advantages over small-molecule drugs. First, they are highly specific molecules and their administration usually results in fewer side effects, less interference with regular biological processes and a more predictable behaviour [15]. Secondly, as most of these molecules are naturally produced by the body, they are often poorly immunogenic and well-tolerated [16]. Finally, proteins often fulfil various intricate functions which cannot be mimicked by traditional drugs [16]. This specific aspect gives

biologics the potential for far-reaching patent protection, thereby making them particularly attractive for pharmaceutical companies [17].

The use of protein therapeutics remains limited due to their poor oral bioavailability owing to the presence of physical, chemical and enzymatic barriers [18]. On average, less than 1% of most administered protein drugs reach the systemic circulation [18]. As a consequence, most biologics are currently delivered via parenteral injections (Table 1-1). However, the appearance of local reactions at the site of administration, systemic side-effects and immunogenicity concerns restrict the extent of their use as drugs [19]. For these reasons, the need for a new system, which allows for safe and efficient oral drug delivery, is greater than ever. Such a system would bring major improvements to the treatment of numerous chronic diseases. First, the convenience and ease of use would greatly improve patient compliance. Drug administration would also be safer, as the use of needles and syringes would no longer be required. As a result, the social stigma associated with the use of these items would be dramatically reduced, thereby improving the quality of life for patients [20]. Finally, from the economic standpoint, development of such systems is highly attractive, given that costs associated with prolonged patient hospitalisation and use of expensive devices could be significantly reduced [21].

In order to develop a system that is adequate for the oral delivery of macromolecules, numerous strategies have been investigated. These include the use of enzyme inhibitors and absorption enhancers, mucoadhesive polymeric and particulate carrier delivery systems [22, 23]. However, all of these strategies present major drawbacks and only a few approaches have reached the latter phases of clinical trials [24]. Another concept involves the use of virulence factors secreted by several bacterial pathogens, including *Corynebacterium diphtheriae*, *Vibrio cholerae* and *Pseudomonas aeruginosa*. The relevance of these toxins in the treatment of various types of cancers has been widely investigated [25]. Recently, it was suggested that they could be reprogrammed for drug delivery purposes [26, 27].

This chapter aims to provide an understanding of the various challenges faced during oral protein delivery and to discuss bacterial toxins as potential therapeutic tools. First, it offers an insight into how drug absorption takes place from the small intestine. In order to appreciate the requirements of successful oral protein delivery, a brief description of the anatomy of the gastrointestinal tract, the characteristics of the epithelium lining the small intestine, the different transport routes across this barrier, and the obstacles faced during oral protein administration are presented. The second part covers the use of bacterial toxins as therapeutic agents. It includes a summary of one strategy involving recombinant

immunotoxins, as well as a detailed account of the intoxication pathway and structure/function relationship of one particular toxin, *Pseudomonas* exotoxin A. The use of bacterial toxins as carriers for oral protein delivery is also introduced. This information predominantly aims to give a foundation to the studies described in this thesis and to underpin the main themes addressed in the following chapters.

1.1 Oral protein delivery

1.1.1 Anatomy of the gastro-intestinal tract

The role of the human gastro-intestinal tract (GIT) is to break down food particles and reduce them to small nutrients, which can be absorbed into the body to provide energy. The GIT is divided into several segments. Food uptake occurs in the oral cavity, where foodstuffs are mixed with saliva and mechanically processed. Food is then transported through the pharynx and oesophagus to the stomach, and further to the small intestine (SI), which is divided between the duodenum, jejunum and ileum. Digestion is initiated in the stomach: proteins, fats and carbohydrates are chemically broken into smaller peptides. Digestion is then completed in the small intestine, where most of the absorption of nutrients, via the epithelium, into the blood circulation, takes place. Undigested material travels from the ileum to the colon, before reaching the rectum and being evacuated.

Due to its large surface area (between 200 and 500 cm^2 [28]), absorption properties and a milder environment compared to the stomach, the SI represents a primary target for the absorption/uptake of drugs.

1.1.2 Epithelium in the SI

The SI epithelium performs several functions essential to the integrity of the body. It constitutes a physical barrier that separates the internal milieu from the exterior environment, while maintaining the homeostatic conditions of the body. To perform this function, the intestinal epithelium must establish and maintain a selective barrier regulating the movement of water and solutes between the intestinal lumen and the underlying matrix. In this way, the controlled absorption (nutrients) and secretion (waste products) of specific molecules can be performed, while the body remains protected from casual entry of potentially damaging materials and pathogens.

1.1.2.1 General organisation

The epithelium represents the innermost layer of the various segments of the GIT, including the SI. It is supported by a basement membrane, which is a specialised acellular structure that is organised through a process known as "self-assembly" [29]. It consists of laminins, collagens (mostly type IV), proteoglycans, calcium binding proteins such as fibulin, and various other structural or adhesive proteins [30]. Interactions between epithelial cells and the basement membrane influence their behaviour by controlling their shape, gene expression, adhesion, migration, proliferation and apoptosis [31]. Epithelial cells are anchored to components of the basement membrane by hemi-desmosomes [32]. The basement membrane is itself supported by an underlying layer of connective tissue called the lamina propria, which contains blood vessels, nerves, glands, lymphoid tissue and immune cells [33]. Beneath the lamina propria is the muscularis mucosa, which comprises layers of smooth muscles which can contract to change the shape of the lumen to mix and propel luminal contents [34] (Figure 1-2).

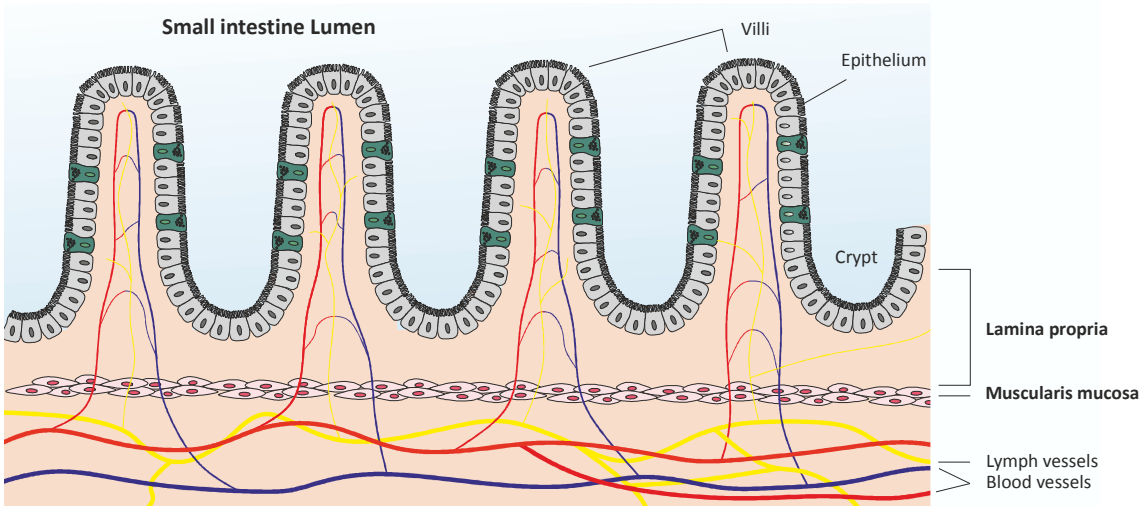

Figure 1-2 – Structure of the SI wall. The epithelium in the SI is supported by a basement membrane, which rests upon an underlying layer of connective tissue, the lamina propria. The lamina propria is itself supported by layers of smooth muscles known as the muscularis mucosa.

1.1.2.2 Polarity and barrier properties

Epithelial cells are polarised cells: their plasma membrane is divided between an apical surface which faces the intestinal lumen, and a basolateral domain which faces the neighbouring cells and establishes contact and communication between them [35]. Lateral cell-cell interactions are stabilised by desmosomes [36, 37], which form strong adhesive intercellular junctions and are also linked to cytoskeletal filaments, and gap junctions, which form channels connecting the cytoplasm of two adjacent cells, thus enabling rapid exchange of ions and small molecules (< 1 kDa) between adjacent cells [38].

The apical and basolateral domains of the plasma membrane are delimited by the apical junctional complex (AJC), which is composed of the tight junctions (TJs) and adherens junctions (AJs) [39]. Tight junctions are closely associated areas of the cells where membranes come together in such close approximation as to restrict the passage of water and electrolytes in the intercellular space. This is referred to as the "barrier" function of the TJs. The apical and basolateral domains of the plasma membrane are composed by different sets of proteins and lipids. For instance, the apical membrane is enriched in sphingolipids and cholesterol, while the basolateral membrane is mainly constituted of phospholipids [40]. TJs also regulate the lateral movement of these components between domains that could otherwise freely diffuse in the plasma membrane [41]. This is referred to as the "fence" function of the TJs.

Tight junctions are composed of several transmembrane proteins that include occludin, claudins and JAM-1 [42]. These proteins form the seal that limits the paracellular space and interact with proteins from the ZO family, connecting TJ structures to the cellular cytoskeleton [43]. Extracellular interactions established between claudins create paracellular pores that show size as well as charge selectivity and contribute to regulating the movement of molecules in the intercellular space [44, 45]. AJs are adhesive junctions that lie just below TJs on the basolateral cell membrane. A major constituent of AJs is a protein called E-cadherin, which forms calcium-dependent extracellular interactions and brings the adjacent cells into close proximity [39]. While TJs are impermeable barriers that seal the intercellular space completely, AJs and desmosomes establish 15-20 nm gaps between cell membranes and mechanically link adjacent cells.

1.1.2.3 Epithelium in the SI

The small intestine is lined by a monolayer of columnar absorptive epithelial cells called enterocytes, with scattered goblet cells and some enteroendocrine and microfold cells (M cells) [46]. The epithelium in the SI forms folds called villi. This particular geometry multiplies the surface area available for nutrient absorption by around 30-fold [47]. The crypts of Lieberkühn are located at the base of the villi, and the epithelium there also includes Paneth cells and stem cells [46] (Figure 1-3).

The apical surface of enterocytes is covered with small hair-like projections called microvilli, which can be as numerous as 3,000 per cell and are organised in a structure known as the brush border. The primary site for endocytosis is located between microvilli, which further increase the area of the epithelium available for nutrient digestion and uptake by 600-fold [47]. The membrane of enterocytes contains micro-domains enriched in cholesterol and sphingolipids and resistant to solubilisation by non-ionic detergents in physiological temperatures that are known as lipid rafts, or detergent-resistant membrane (DRM) micro-domains [48]. Lipids within DRMs are more ordered and tightly packed than in the surrounding membrane bilayer, and while these domains are mainly located on the apical membrane of enterocytes, they are also present within intracellular compartments (e.g. endosomes, Golgi network) [49, 50]. Many proteins involved in intracellular signal transduction are gathered in DRMs (e.g. G proteins, growth factor receptors and protein kinase C), which appear to act as signalling platforms by facilitating the interaction between various signalling pathway components [51].

While enterocytes are responsible for absorption through the epithelium, goblet and entero-endocrine cells have secretory functions. Goblet cells arise from differentiation of stem cells at the bottom of the crypts. They are responsible for the secretion of mucus and contain granules that fill with mucins as they migrate from the bottom to the opening of the crypt and release their content at the surface [52, 53]. Enteroendocrine cells secrete hormones regulating a variety of GIT functions. M cells are located individually or in lymphoid follicle-associated epithelium (Peyer's patches). They play an important role in immune response as they internalise antigens from the intestinal lumen via endocytosis and deliver them to the underlying lymphoid tissue [54, 55]. Stem cells also divide into Paneth cells that are located at the base of the crypts and secrete antimicrobial peptides, including lysosomal enzymes and α-defensins, into the crypt lumen. These peptides diffuse from the crypts and disperse further into the mucus layer, where they contribute to the protection of the epithelial surface [56].

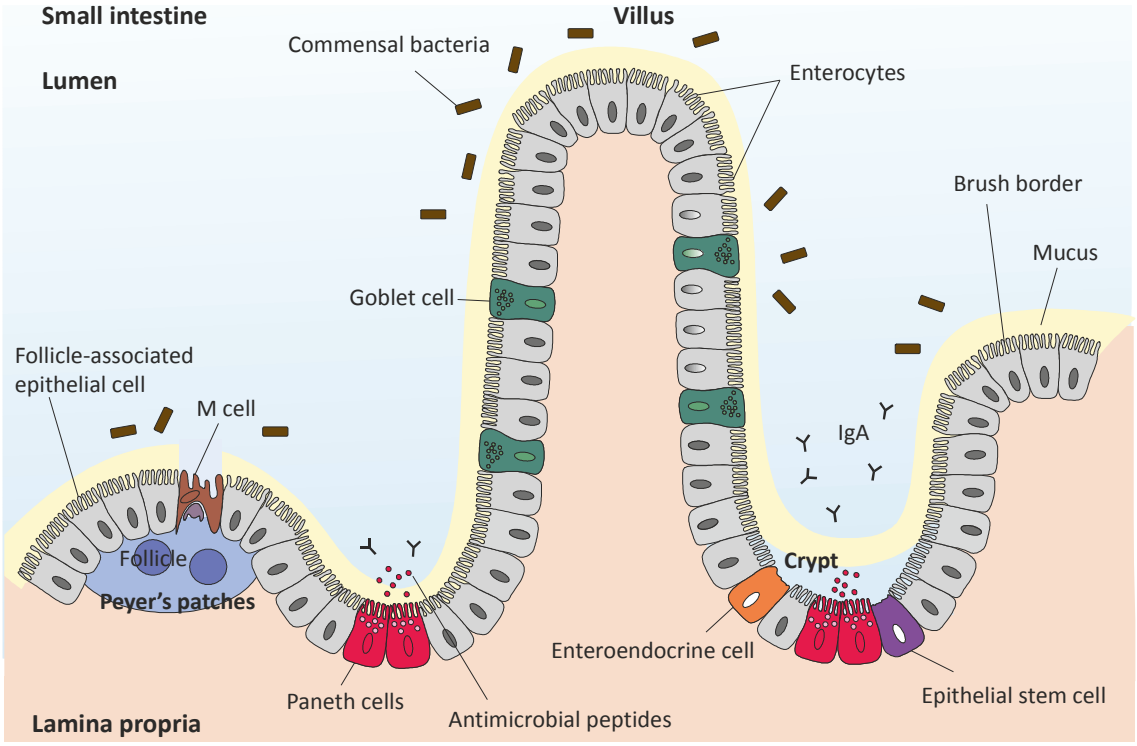

Figure 1-3 – The SI epithelium forms a barrier which maintains the homeostasis between the internal and external milieus. The epithelium is folded into villi and is mainly composed of a single layer of enterocytes interspersed with goblet cells. Paneth cells, entero-endocrine and epithelial stem cells are found in the crypts and M cells are associated with Peyer's patches. Secreted IgA are transported across epithelial cells by transcytosis and promote the clearance of antigens and pathogenic microorganisms from the intestinal lumen.

1.1.3 Transport across the intestinal epithelium

The transport of various materials across epithelial cells generally occurs using the paracellular pathway (between adjacent cells), transcellular pathway (through individual cells using pathways that access the cell cytosol), or via transcytosis (through individual cells using vesicles that do not involve access to the cell cytosol) (Figure 1-4).

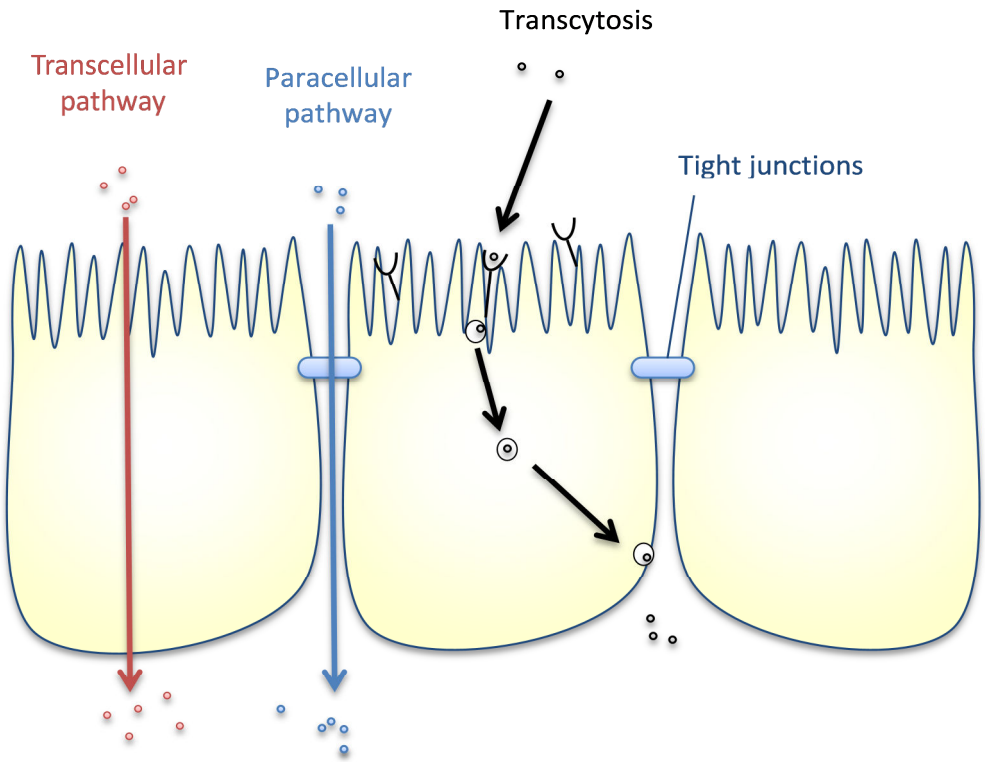

Figure 1-4 – Schematic representation of the intestinal epithelium and the pathways available for drug absorption. Depending on their properties, molecules can cross the epithelium via the transcellular or paracellular pathways, or by transcytosis.

1.1.3.1 Paracellular pathway

Transport of molecules across the intestinal epithelium via the paracellular pathway is a passive diffusion process that is limited by the presence of TJs. These molecular organisations form small pores that only allow compounds < 3.5 kDa to pass [57-59]. TJs also form claudin-dependent charge-selective channels that regulate the passage of ions and electrolytes [60]. Claudin proteins constitute a family of 24 transmembrane proteins localised exclusively at TJ structures. Each epithelium expresses a different pattern of claudin proteins that establish its permeability properties. Most epithelia express more than two claudin types in different combinations to form TJ strands. For instance, it has been shown that claudin-2, -4, -7 and -15 are the predominant types expressed in the mouse small intestine, with claudin-2 present in the deep crypt while claudin-7 is most favourably expressed in the upper villi [44, 61]. As a result of these combinations of claudins, the aqueous TJ pores they form vary in size.

1.1.3.2 Transcellular pathway

To cross the intestinal epithelial barrier using the transcellular pathway, molecules need to be reasonably small (< 700 Da), and able to passively and successively partition and diffuse through both lipidic (cell membrane) and aqueous (cytosol) compartments following a chemical potential gradient [62]. The flux of molecules crossing the epithelium using the transcellular pathway has been described according to Fick's first law of diffusion:

$$J = -D\frac{\partial Ø}{\partial x}$$

Where J diffusion flux (mol/m^2·s)

D diffusion coefficient specific to each molecule and obtained from the Stokes-Einstein equation (m^2/s)

$\partial Ø$ variation in concentration between the apical and basolateral side of the epithelium (mol/m^3)

∂x path length of the flux route (m).

In the hypothesis of a spherical particle, the Stokes-Einstein equation is as follow:

$$D = \frac{RT}{N_A}\frac{1}{6\pi\eta a}$$

Where D diffusion coefficient of the spherical particle (m^2/s)

a radius of the spherical particle (m)

R ideal gas constant (= 8.314 J/mol·K)

T is the temperature (K)

N_A is Avogadro's number (6.022 x10^{23} mol^{-1})

η is the viscosity of the fluid (Pa·s)

Molecule transport by the transcellular route can be either passive, when no energy is provided by the cell, or active, when cellular energy is required for transport. Passive transcellular transport can take place via simple diffusion, in which case movement is non-selective, and the flux of molecules can occur either in the apical to basolateral direction (absorption) or in the basolateral to apical direction (secretion) depending on the chemical gradient. In the context of ions and small molecules transport (e.g. some sugars and vitamins), diffusion can also be facilitated by integral membrane proteins (e.g. channel

or carrier proteins) which assist in the transit of specific substrates across the membrane bilayer [63]. During active transcellular transport, energy derived from ATP hydrolysis is used to modify the conformation of a carrier protein which then carries the substance across the plasma membrane against its concentration gradient [47, 62].

1.1.3.3 Transcytosis pathway

Transcytosis, with regard to the intestinal epithelium, describes the process of materials moving across enterocytes using an intracellular route involving vesicles. This process can occur in either direction, i.e. apical to basolateral or basolateral to apical. Materials transported by this process remain inside the vesicular structures and do not come in direct contact with the cytosol of the cell. The vesicular transport events involved in transcytosis are energy-dependent processes, which can be initiated by several endocytic mechanisms [64]. For instance, the process involving the bulk uptake of solid matter, including cell debris and microorganisms, is termed phagocytosis. In the SI, it can be carried out by specialised cells such as M cells, which specifically deliver their content to the underlying lymphoid tissue of the follicle-associated epithelium [65, 66]. Different types of fluid-phase uptake by pinocytosis can be classified according to the size and coating of the endocytic vesicle formed (Figure 1-5). Macropinocytosis is a non-specific uptake mechanism that accompanies cell-surface ruffling. It involves internalisation of large volumes of extracellular fluids and soluble macromolecules. The vesicles formed are usually > 500 μm in diameter [65] (Figure 1-5). Macropinocytosis is often induced as part of the response to stimulation by growth factors, but this process does not usually result in transcytosis [67]. Macropinocytosis is distinct from micropinocytosis, which includes clathrin-mediated endocytosis, caveolin-mediated endocytosis as well as clathrin- and caveolin-independent mechanisms [65, 68]. These processes proceed by invagination of selective plasma-membrane domains that are pinched off to form early stage endosomes as a first step in the process of transcytosis [65, 68]. These endocytic processes can be made more efficient through binding of extracellular molecules to the cell membrane by specific cell-surface receptors (i.e. receptor-mediated endocytosis) [65, 68]. Receptor-mediated endocytosis (RME) is involved in the transcytosis of molecules such as immunoglobulin G proteins [69] or Vitamin B_{12} [70] from the apical to the basolateral surface of epithelial cells.

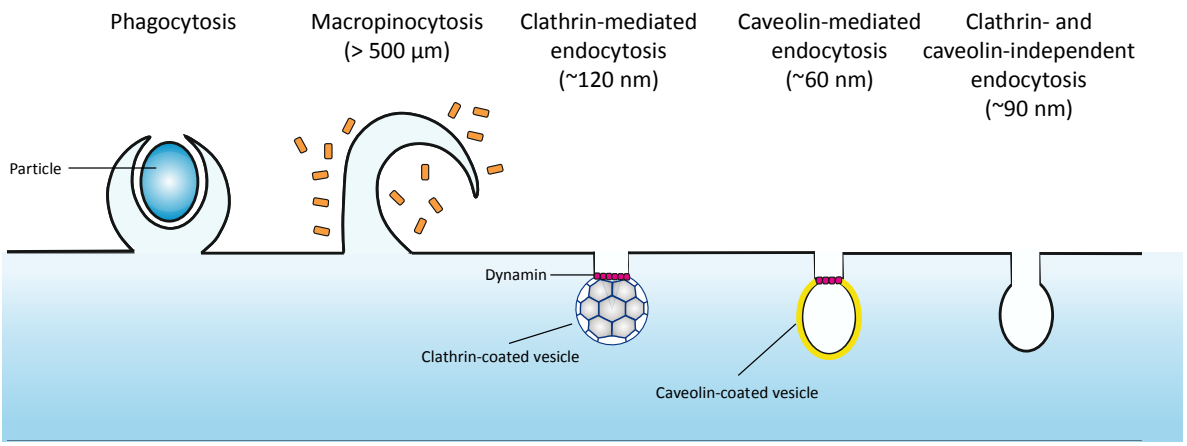

Figure 1-5 – Multiple pathways of entry into cells. Large particles can be taken up by phagocytosis, whereas fluid uptake occurs by macropinocytosis. The size of vesicles formed by these two processes is much larger than endocytic vesicles formed by micropinocytosis. Clathrin- and caveolin-mediated endocytosis usually depend on dynamin, a large GTPase which was suggested to play a role in the scission of newly formed vesicles from the plasma membrane [71]. Some clathrin- and caveolin-independent endocytic pathways can also be dynamin-independent. Adapted from [65, 68].

1.1.4 Challenges to oral protein delivery

The low oral bioavailability of biologics and consequently the limited use of such molecules as therapeutic agents are partly due to intrinsic properties of the protein drugs themselves. It is also linked, however, to the hostile conditions and other defence and upkeep mechanisms of the GI tract; these represent obstacles to non-selective protein absorption from the intestine into the systemic circulation.

1.1.4.1 Charge and size of protein drugs

Donovan *et al* (1990) demonstrated, using polyethylene glycol molecules, that transport across epithelia was independent of molecular weight for molecules smaller than 500-700 Da, but that permeation decreased steeply when molecular weight exceeded 700 Da [72]. For molecules to partition into cell membranes and be passively absorbed via the transcellular pathway, a minimum degree of lipophilicity is required [73]. However, most protein drugs are too hydrophilic to use this route of absorption, which represents a major obstacle for their oral intake. Besides, peptide and protein drugs are usually macromolecules larger than 3 kDa [15] and thus cannot be passively absorbed through the

paracellular pathway either, as the movement of molecules through this route is limited by the presence of TJs. The role of net protein charge in the degree of penetration of molecules is more controversial and, although some studies suggest that an overall positive charge could enhance transcellular protein transport across epithelial monolayers [74, 75], variations in global charge would affect mostly paracellular transport of low molecular weight compounds [76, 77]. Therefore, these conclusions do not apply to protein drugs.

1.1.4.2 Causes of protein degradation in the GIT

1.1.4.2.1 Acidity in the stomach

Before reaching the intestine, protein drugs have to travel through the stomach, where the harsh environmental conditions often lead to profound modifications or degradation of the molecule. In fact, due to secretion of hydrochloric acid by gastric glands, the stomach typically presents a very acidic environment (pH ~ 1-2) [78]. These conditions are essential for the efficient degradation of food materials. However, exposure of a protein to such a low pH can modify its ionisation state, which can in turn affect the drug's solubility, stability and conformation by modifying the electrostatic interactions and hydrogen bonding within the molecule. A change in conformation is often irreversible and may lead to protein denaturation [18]. Acidity can also result in proteolysis, breaking proteins into peptides [18]. Moreover, due to variations in gastric and pancreatic secretions between preprandial and postprandial states, the pH in the stomach (and more generally the GIT) can fluctuate significantly between fasting and fed states. This further complicates oral drug delivery as these differences can considerably influence protein drug release, stability and solubility [79]. Finally, secretion of pepsinogen (converted to its active form, pepsin, by acid cleavage) by mucosal cells further contributes to protein degradation in the stomach [18].

1.1.4.2.2 Enzymes in the small intestine

Biologics are exposed to a wide variety of enzymes along the GIT, and enzymatic degradation is one of the main factors reducing the bioavailability of orally administered drugs. This process has been coined as "pre-systemic metabolism" [80]. Degradation can occur either by hydrolysis of peptide bonds or by chemical modifications of the protein functional groups, such as oxidation, phosphorylation or deamidation [81].

Peptidases are numerous in the SI as they originate both from pancreatic secretions and from the enterocytes. Endopeptidases present in the intestinal lumen include trypsin, chymotrypsin and elastases, while the main exopeptidases are amino- and carboxypeptidases. Trypsin, chymotrypsin and other pancreatic enzymes are also present in the brush border of the epithelium, where they proceed to further facilitate protein degradation [82].

1.1.4.3 Mucus in the small intestine

Mucus covers the surface of the intestinal epithelium [83, 84], with the exception of M cells [85]. In the small intestine, mucus is secreted by goblet cells located at the top of the crypts of Lieberkühn and spreads between the villi [53]. The main components of intestinal mucus are gel-forming mucin proteins. Mucins are high molecular weight glycosylated proteins with oligosaccharide side chains attached to approximately 75% of the protein core [86]. This composition gives mucus its gel-like structure and water-retaining properties. The main mucin constituent of intestinal mucus is the gel-forming MUC2 glycoprotein [86]. Mucins are produced inside granules in goblet cells located at the base of the crypts. They become progressively glycosylated and densely packed in the granules as goblet cells migrate toward the villus tip [53]. Mucins are released into the extracellular milieu via exocytosis, at the top of the crypts, where they expand dramatically upon contact with water to form a gel-like structure [87, 88].

Mucus forms a semi-permeable barrier allowing for the exchange of nutrients and water while maintaining a hydrated surface which physically protects the epithelium against digestion enzymes, abrasive materials and pathogens present in the lumen. In fact, mucus is enriched in antimicrobial molecules from Paneth cells (α-defensins, lysozymes, etc.) [89] and secretory IgA from the enterocytes [69], which are entrapped within this viscous layer and thus maintained at high concentrations close to the cell surface. At the apical cell surface, mucus interacts with the glycocalyx structure [86], which forms a ~500 nm-thick coating layer between the cells and the mucus. It is composed of a negatively charged network of proteoglycans, glycolipids and glycoproteins, including densely packed transmembrane mucins (possibly MUC-3, -12 and -17 [83]), and a set of membrane-bound enzymes secreted by the enterocytes and present on the microvilli (brush border enzymes) [90, 91]. Due to the close association of these elements, the glycocalyx forms a size-selective diffusion barrier that prevents large particles such as pathogens from reaching the epithelium. Frey *et al* (1996) have shown that the functional pore size of the glycocalyx covering intestinal enterocytes is between 7.4 and 28.8 nm. This is much

smaller than the average size of a bacterium (~1 μm) or even a virus (~50 nm), and therefore greatly impedes the penetration of these agents across the glycocalyx [92].

Together, mucus and glycocalyx prevent auto-digestion and diffusion of pathogens from the intestinal lumen. They also constitute an important obstacle for oral drug delivery. Due to its viscosity, mucus can entrap lipophilic drugs and large delivery devices, blocking them from reaching the mucosal surface and consequently penetrating the epithelium [93], [94]. Brush border enzymes can also potentially reduce the bioavailability of orally administered biologics. Finally, mucus is continuously produced at a rate of ~10 L/day in the GIT [88]. As high volumes of fluids are secreted and washed away, drug residence times in the intestine are decreased, thereby reducing the amount of drug capable of crossing the epithelium.

1.1.4.4 Immunogenicity

Protein drugs used to treat patients can be either derived from non-human sources (e.g. salmon calcitonin) or produced from human genetic sequences using recombinant DNA technologies (e.g. human growth hormone, insulin). As a result, they sometimes present subtle differences with the endogenous compound(s), such as sequence variations, denaturation or alterations in their glycosylation pattern [95]. These factors, as well as the formulation, length of treatment, or genetic patient characteristics for example, account for the potential immunogenicity of biologics. The immune response induced by protein therapeutics can result in the formation of neutralising antibodies leading to decreased drug efficacy (e.g. interferon α-2b [96]), or to more serious adverse reactions if the secreted antibodies neutralise some physiologically important function [97]. Casadevall *et al* (2002) identified 22 patients presenting pure red-cell aplasia following treatment for anaemia from chronic renal failure, using recombinant erythropoietin alpha or beta (EPO), and suggested that the inhibition of erythropoiesis was caused by the development of neutralising anti-erythropoietin antibodies after an initial response to EPO [98].

Although the route of administration of a protein cannot make the protein less immunogenic *per se*, it can influence the extent of an immune response. Intramuscular and subcutaneous injections are viewed as more likely to induce severe immunogenic reactions compared to intravenous drug delivery [19] and topical application is considered the safest option. In the SI, the presence of numerous food-related antigens and a large population of commensal bacteria have allowed the intestinal mucosa to develop a mechanism of oral tolerance [99]. Therefore, despite the mechanism of mucosal immunity, which protects mucous membranes against potentially harmful microbes in the

GIT and controls the immune response in case these antigens penetrate further inside the body [100], the SI remains a target of choice for the delivery of potentially immunogenic protein therapeutics.

1.2 Bacterial toxins as therapeutic tools

1.2.1 Bacterial toxins

Bacterial pathogens secrete toxins as virulence factors in order to break through the body's defences. Some bacterial proteins are highly toxic to mammalian cells due to their ability to hijack cellular mechanisms to enter cells, reach the cytosol and attack essential constituents; events that can lead to cell death or modifications of cellular physiology [101]. Their toxicity is enhanced by the fact that these molecules have very few inhibitors.

Most of these proteins belong to the family of A-B toxins, a class of cytotoxic proteins that require cellular uptake through receptor-mediated endocytosis for activity [102, 103]. These toxins are structurally divided between a receptor-binding fragment (B subunit) that ferries an enzymatic fragment (A subunit) to its intracellular site of action. A-B toxins are secreted as pro-enzymes and their activation requires complete separation of the A and B subunits [102]. Toxins belonging to this family include diphtheria toxin (DT) secreted by *Corynebacterium diphtheriae*, *Pseudomonas aeruginosa* exotoxin A (PE), and one of the virulence factors secreted by *Vibrio cholerae*, cholix toxin (Cho) [101, 104, 105]. The A subunit of DT, PE and Cho is covalently linked to one B subunit that interacts with a single membrane receptor. The cellular receptors for DT and PE have long been identified as the heparin-binding epidermal growth factor-like precursor [106, 107] and the low density lipoprotein receptor-related protein 1 (LRP1), respectively [108]. The receptor for cholix remains unknown [105]. On the contrary, cholera toxin (CT) and Shiga toxin (Stx) present the characteristic structure of AB_5 toxins, in which the A subunit is non-covalently associated to a pentamer of B subunits, each interacting with a single receptor. The B subunits of CT and Stx bind with high affinity to the gangliosides GM1 and Gb3, respectively [109-111].

1.2.2 Reprogramming bacterial toxins for therapeutic purposes – Immunotoxins

The medical benefit of bacterial toxins has been demonstrated by the construction of recombinant immunotoxins (RITs), which are recombinant fusion proteins that have been engineered to replace the receptor-binding domain of the toxin by a ligand or variable fragment (Fv) of a monoclonal antibody (Figure 1-6) [25]. The toxin is delivered to the target cell by the new targeting moiety whereby it enters the cell and kills it.

DT, PE and the more recently identified cholix toxin, have been widely used to create new immunotoxins [25, 112, 113]. These proteins are all ADP-ribosylating toxins and share similar structures. In fact, they are composed of three distinct structural and functional domains. Domain I is responsible for cell-recognition and receptor-binding, while domain II mediates protein transport inside cells. Domain III is the catalytic domain carrying the cytotoxic activity [114]. Domains I and II compose the A subunit and domain III constitutes the B subunit. While PE and cholix domains I and III are located at the N- and C-termini of the protein, respectively, the orientation of DT is reversed, with its receptor-binding and catalytic domains positioned at the C- and N-terminal extremities of the sequence, respectively [114].

RITs are highly toxic and have been widely studied as a strategy for the treatment of different types of cancer such as B cell malignancies (RIT moxetumomab pasudotox), or lung cancer and mesothelioma (RIT SS1P). These RITs employ a strategy whereby the receptor-binding domain is replaced by a disulphide-stabilised Fv that targets the CD22 receptor and mesothelin, respectively. Both of these RITs are derived from PE and have reached clinical trials [115-120]. Similarly, a RIT constructed from DT and targeting the interleukin-2 receptor (denileukin diftitox) was approved by the FDA for treatment of T-cell lymphoma [120-122]. Compared to other cancer treatments, RITs selectively target cancer cells by recognition of specific cell-surface antigens, resulting in reduced toxicity issues for healthy tissues. Immunogenicity, leading to the development of neutralizing antibodies against the toxic domain present in the RIT, is the major obstacle hindering the development of RITs. In order to overcome this challenge, several strategies have been envisaged, including elimination of immunogenic B or T cell epitopes by mutation [123-125] and concurrent treatment of patients with immunosuppressive drugs [126, 127].

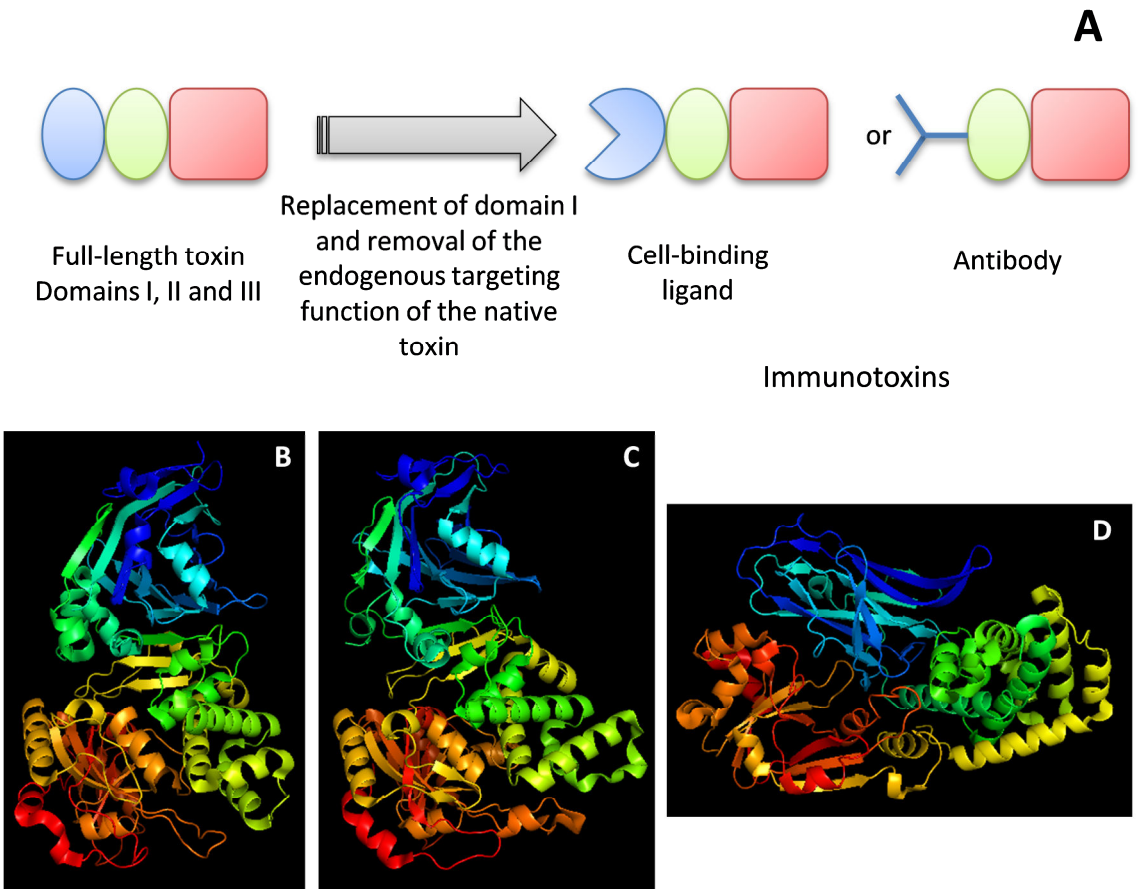

Figure 1-6 – ADP-ribosylating toxins are reprogrammed into immunotoxins for therapeutic purposes. (A) Immunotoxins are recombinant proteins in which the cell-recognition domain of the toxin has been replaced by another cell-binding ligand or antibody. (B), (C) and (D) Ribbon representations of ADP-ribosylating toxins PE, Cho and DT, respectively (PDB_ID: 1IKQ, 2Q5T and 1F0L, respectively). All three proteins are composed of a cell-binding domain, a translocation domain, and a catalytic domain. Cell-binding, translocation and catalytic domains are represented in blue, green and red, respectively. Figures were generated using PyMOL [128].

1.2.3 PE intoxication pathway in non-polarised cells

The cytotoxic pathway used by PE is now well characterised (Figure 1-7). In the extracellular milieu, carboxypeptidases can cleave the C-terminal lysine residue of the REDLK sequence carried by the protein in order to reveal the endoplasmic reticulum (ER) localisation sequence REDL [129]. PE then binds to the LRP1/B transmembrane receptor (also called CD91) [108, 130] and is internalised via receptor-mediated endocytosis (RME) in clathrin-coated vesicles [131]. LRP1is synthesized as a 600 kDa single-chain precursor,

which undergoes proteolytic cleavage within the TGN by furin (recognition sequence: RHRR) [132]. Mature LRP1 consists in a non-covalently associated heterodimer, constituted of an extracellular (515 kDa) α-chain and a transmembrane (85 kDa) β-chain. This proteolytic processing was shown to be dispensable for intracellular trafficking but suggested to be required for normal receptor activity [132]. The cytoplasmic domain of LRP1 is phosphorylated and carries multiple potential endocytosis motifs including two NPXY, one YXXL and two dileucine motifs [133]. Li *et al* (2000) have shown that the majority of LRP1 endocytosis is mediated by the YXXL and the distal dileucine motifs, whereas the two NPXY motifs and the proximal dileucine motif do not contribute to initial endocytosis [133]. Moreover, phosphorylation of this domain is mediated by protein kinase A at residue Ser76 and also contributes to RME [134]. The extracellular part of LRP1 can be cleaved, resulting in the formation of a soluble receptor which remains non-covalently bound to the transmembrane domain, retains ligand-binding capacity and acts as a decoy receptor [135]. A role for soluble LRP1 has also been suggested in inflammation [136]. The impact of soluble LRP1 on PE intoxication pathway remains unknown.

Following RME, PE-loaded vesicles traffic to the early endosome (EE), where a decrease in pH triggers a conformational change of the protein [137], allowing a furin cleavage site to be cut between residues Arg279 and Gly280 [138, 139]. This cleavage results in the separation of the polypeptide backbone between subunits A and B, and has been shown to be required, but not sufficient for, toxin activation, as the two fragments remain covalently linked by a disulphide bond between C265-C287 [140]. From the EE, PE was shown to exploit several pathways in order to reach the cytosol. In one scenario, the toxin can follow a Rab9/Arf1-dependent pathway which drives it to the late endosomes (LE) and further to the *trans* Golgi network (TGN) where interaction between the C-terminal REDL sequence and KDEL receptors (KDEL-R) facilitates its retrieval to the ER [141]. In another scenario, PE can traffic directly from the EE to the TGN using a Rab6/Syn16-dependent route, and subsequently transport to the ER using a lipid-dependent sorting pathway [142]. While Chaudhary *et al* (1990) demonstrated that the cytotoxic activity of PE in Swiss mouse 3T3 cells is fully dependent on the Rab9-mediated pathway and the presence of the REDL sequence [143], Smith *et al* (2006) showed that in HeLa cells, PE can use either pathway to reach the ER [142]. Therefore, the intracellular trafficking mechanism used by the toxin may be cell-dependent. McKee and FitzGerald (1999) showed that in the ER, the disulphide bond linking subunits A and B is reduced by protein-disulphide isomerases (PDIs) or PDI-like enzymes, resulting in the formation of two fragments of 37 kDa and 28 kDa, which correspond to the A and B subunits, respectively [137]. Only the C-terminal A

fragment is then transported to the cytosol. Although no direct evidence has been reported yet, PE might associate with the Sec61p translocon pore and exploit the ER-associated protein degradation (ERAD) pathway to exit the ER and reach the cytosol [144, 145]. There, the A subunit functions enzymatically to ADP-ribosylate eukaryotic elongation factor 2 (eEF2) and block its ability to transfer an ADP-ribosyl group from NAD^+ to the diphtamide moiety; this stops protein synthesis and leads to apoptosis [146, 147].

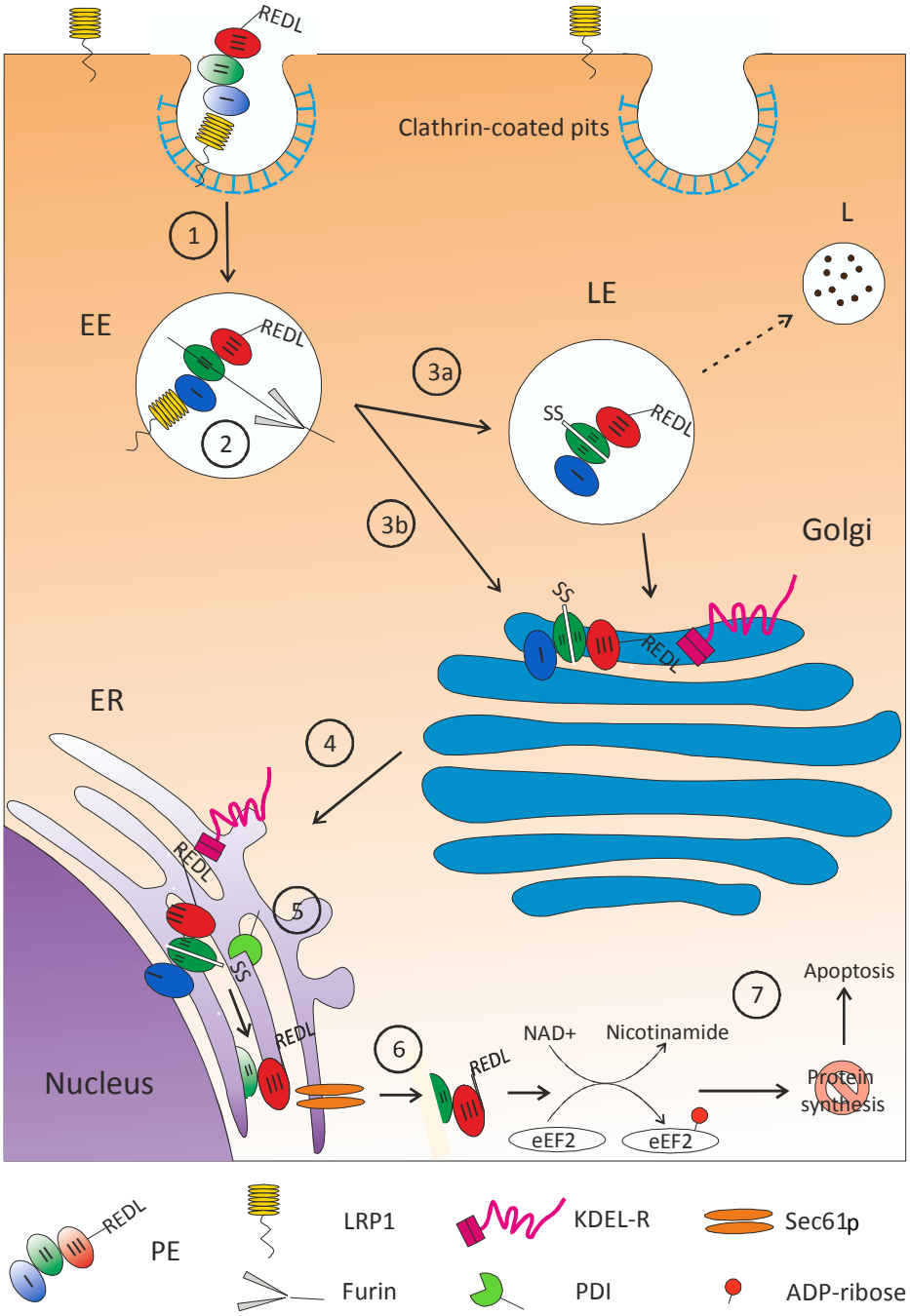

Figure 1-7 – PE intoxication pathway in NP cells. 1) PE binds to LRP1 on the cell surface and is internalised via RME. 2) In the endosome, PE is cleaved by furin at a site in domain II though the two fragments remain linked by a disulphide bond. 3) PE is transported to the Golgi network using a Rab6- or Rab9-dependent pathway ((a) and (b), respectively). There, it interacts with KDEL-R via its C-terminal REDL sequence. 4) Interaction with KDEL-R results in the transport of PE to the ER in a retrograde manner. 5) In the ER, the disulphide bond is reduced by PDIs. 6) Only the A fragment retro-translocates to the cytosol using Sec61p. 7) In the cytosol, PE catalyses the ADP-ribosylation of eEF2 leading to arrest of protein synthesis and cell death. L, lysosome.

1.2.4 Protein escape from the lysosomal degradation pathway and sorting mechanisms

Most extracellular components internalised following RME are transported to the EE, where they are either directed to the recycling endosome (RE) and further carried to the plasma membrane (receptors), or transferred to lysosomes through the LE for degradation (cargos) [148, 149]. Interestingly, bacterial toxins hijack the early endocytic pathway to penetrate target cells and traffic to their destination within cells, but avoid lysosomal degradation [104]. How this is achieved remains unclear. It has been suggested that following exposure to low pH in the EE, some bacterial toxins would undergo a conformational change that would allow them to escape lysosomal degradation [101, 150-152]. Although PE was demonstrated to experience such a transition in acidic conditions, the conversion remains poorly characterised and the mechanism used by the toxin to evade endosomes has yet to be established [150, 153, 154].

Two trafficking routes from the plasma membrane to the Golgi can be exploited by PE, but the mechanisms involved in sorting the toxin to the Rab6- or Rab9- dependent pathway remain incompletely understood. Recent studies by Carter (2014) suggested that the monosialoganglioside GM1 could be involved in directing PE to follow one route or the other [27]. GM1 is the host receptor for CT [109, 155, 156] and, as a ganglioside, is composed of a hydrophilic head group linked to a hydrophobic ceramide moiety which anchors the lipid into the cell membrane. Chinnapen *et al* (2012) showed that alterations in the ceramide chains led to variations in the intracellular transport of GM1 and associated CT molecules [157]. Furthermore, preliminary studies by Mrsny *et al* (personal communication) suggested that PE could also bind to GM1, which might therefore act as a secondary receptor for the toxin and be involved in sorting mechanisms within cells.

1.2.5 Structure/function relationship of PE

Pseudomonas exotoxin A is the virulence factor secreted by the bacterium *Pseudomonas aeruginosa*. PE is a 66 kDa protein made of 613 amino acids, and analysis of its three-dimensional crystal structure have shown that the toxin is a single polypeptide chain divided into three distinct domains (Figure 1-8) [158]. Domains I and II compose the A subunit and domain III constitutes the B subunit. The N-terminal domain is composed of domain Ia (1-252), responsible for cell recognition and receptor binding, and domain Ib (365-404), whose function remains undetermined [159]. Siegall *et al* (1989) have

suggested that this Ib domain may be required for secretion by the bacterium [160]. Although Ia and Ib are not sequential, they are structurally adjacent. Domain II (253-364) is responsible for protein translocation across the cells and intracellular trafficking, and the C-terminal domain III (405-613) is the catalytic domain which carries the cytotoxic activity of the protein [159]. Domain III contains a terminal KDEL-like sequence (REDLK) that is required for cytotoxicity in certain cell lines [143]. The native toxin contains eight cysteine residues that are arranged into four disulphide bonds: C11-C15 and C197-C214 (domain Ia), C265-C287 (domain II) and C372-C379 (domain Ib) [158]. Douglas *et al* (1987) have shown that the amino acid Glu553 within domain III is crucial for cytotoxic activity, as a punctual mutation replacing it by Asp dramatically reduced the cytotoxicity of the mutant protein, termed ntPE [161]. A furin-cleavage site (RQPR) is located within the protein's second domain between Arg279 and Gly280 [138, 162].

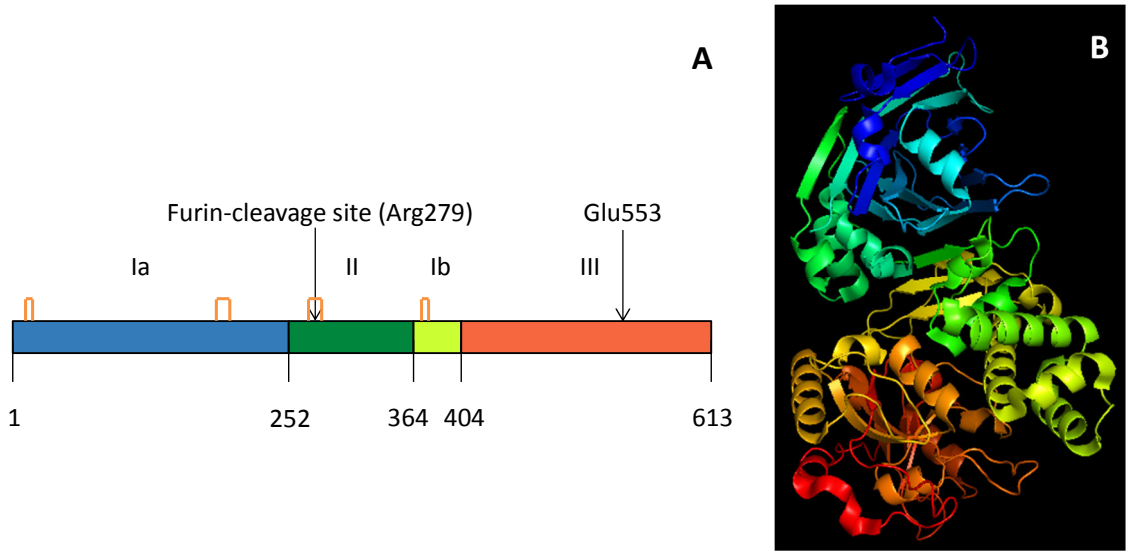

Figure 1-8 – (A) Schematic and (B) Ribbon representations of the structure of *Pseudomonas* exotoxin A. The protein is divided into domain Ia (1-252) responsible for cell recognition and receptor binding (blue), domain II (253-364) that controls protein translocation and contains the furin-cleavage site (green), domain Ib (364-404) (yellow) and domain III (405-613), which is the enzymatic domain of the toxin (red). Disulphide bonds are indicated orange in (A). Note the deletion of E553 in domain III that renders PE non-toxic (ntPE). Figure (B) was generated using PyMOL [128].

1.2.6 PE and cholix as vehicles for oral protein delivery

As previously described (Section 1.1.4), one of the hurdles in oral delivery of protein therapeutics is the presence of an impermeable layer of polarised epithelial cells in the intestine. Macromolecules are too large to transport through this barrier using the paracellular pathway, and most of them are too hydrophilic to passively cross the lipid bilayer of cell membranes. Remarkably, PE specifically targets non-polarised cells in the body, especially antigen-presenting cells present in the submucosal space, and also appears to translocate across polarised epithelial cells. The transcytosis pathway used by the toxin to traffic through polarised cells is currently poorly understood. However, this characteristic was exploited, and PE has been used as a tool for mucosal immunisation [163, 164].

Alternatively, PE has been used for intracellular delivery of biologics by replacement of its catalytic domain by a therapeutic protein. Mohammed *et al* (2012) exploited PE's ability to reach the cytosol following internalisation and showed that fusion of a cell-penetrating peptide (CPP) sequence to the N-terminus of PE domain II facilitated the cytosolic delivery of a cargo protein [165].

Recently, Carter (2014) showed that PE could not only deliver siRNA into macrophages to elicit a knockdown effect, but also transport the siRNA cargo across polarised cells and deliver it into macrophages [27]. Furthermore, Mrsny *et al* (personal communication) showed that a molecule of green fluorescent protein (GFP) attached to the C-terminal of ntPE could be carried across intact epithelium both *in vitro* and *in vivo*. Besides, replacement of PE domain III by GFP, rat or human growth hormones led to the same observation. These studies have concluded that ntPE is organised in a carrier-cargo format: the first two domains being essential for transport across polarised cells, while presence of domain III is not required for transcytosis (Figure 1-9). A remarkable fact is that cargo proteins seemed fully functional after transport across the epithelial layer. These findings suggest that ntPE could be used as a carrier for delivery of orally administered protein drugs.

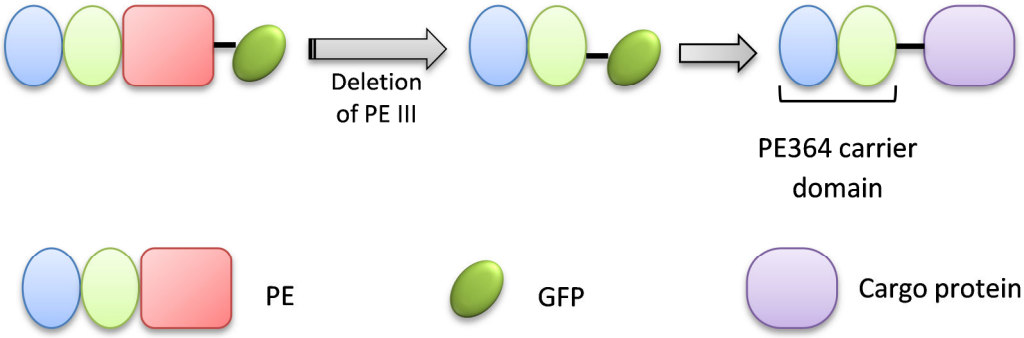

Figure 1-9 – PE is constructed on a carrier-cargo format and could be used as a drug delivery system. PE can transport a C-terminal molecule of GFP (dark green) across polarised monolayers, and replacement of domain III (red) by GFP results in the same outcome. Therefore domain I (blue) and domain II (light green) could be used as a carrier system for delivery of protein therapeutics (purple) across the intestinal barrier. The carrier domain constituted of PE domains I and II (residues 1-364) will be referred to as PE364.

Jørgensen *et al* (2008) characterised a new ADP-ribosylating toxin, cholix toxin (Chapter 4), which presents striking structural similarities with PE [105]. Both proteins are divided in three distinct domains, critical disulphide bonds align in each toxin, and sequence alignment revealed that they share 33% identity [105]. While PE originates from the airway bacterium *Pseudomonas aeruginosa*, cholix is the virulence factor secreted by the intestinal pathogen *Vibrio cholerae* and, if operating in a similar way to PE, might therefore be more efficient than PE with regards to oral drug delivery. It therefore appears essential to determine if the similarities observed between the structures of the two toxins extend to their respective functions, and if cholix could also be able to carry proteins across polarised epithelial cells.

For these reasons, it is crucial to study the transcytosis mechanisms of both PE and cholix in polarised cells to further understand the potential and limitations of these toxins as protein carriers for oral drug delivery.

1.2.7 Potential cargo proteins

The use of PE (and potentially cholix) as a vehicle for the transport of biopharmaceuticals (such as therapeutic proteins and peptides) across the intestinal epithelial cell barrier would undoubtedly improve delivery prospects for this class of therapeutic agents. However, not all protein therapeutics would represent appropriate cargo drugs for this system. For instance, an antibody for the treatment of cancer which needs to circulate in

the body at high concentrations would not constitute a plausible candidate, as such elevated quantities would probably not be achieved following oral administration. Therefore, cargo proteins would have to be judiciously considered with regards to their target site and mechanism of action as well as the dose they need to be delivered at in order to show therapeutic effects. Here, the human growth hormone and interleukin-10 are proposed as potential cargo candidates.

Human growth hormone

Human growth hormone (hGH) is a peptide hormone that stimulates cell growth, reproduction and regeneration in tissues [166]. It has been broadly used as a medicine to treat human diseases such as growth hormone deficiency syndrome or AIDS-associated wasting [167, 168] and is, at present, mainly administered via subcutaneous or intramuscular injections [169, 170]. Due to its most common use in paediatric patients, development of a non-injectable dosage form would greatly improve patient compliance. As the highest concentration of growth hormone receptors is found in the liver [171], oral delivery of this protein using PE as a vehicle would result in direct absorption following administration (first-pass effect), thereby increasing protein targeting and making hGH a possible cargo candidate.

Interleukin-10

Interleukin-10 (IL10) is an anti-inflammatory cytokine that plays a central role in immunoregulation and inflammation by limiting and ultimately terminating inflammatory responses [172, 173]. IL10 is being investigated as a potential treatment for several diseases, including inflammatory bowel disease, malignant neoplasms, skin disorders (e.g. psoriasis and reduction of scarring), rheumatoid arthritis and hepatitis C [172, 174, 175]. In these studies, IL10 was administered by subcutaneous or intravenous routes and was found to induce side-effects (flu-like symptoms) at doses of up to 100 µg/kg [176]. Because the IL10 receptor is particularly expressed at the surface of immune cells [176], oral administration of IL10 would enable its targeted delivery to the cells of the mucosal immune system in the intestine, and would therefore allow for a decrease of the doses administered thereby reducing side-effects.

1.3 Aims and objectives

Despite all the research that has taken place over the years, the mechanism that allows PE to escape lysosomal degradation and traffic through cells remains unclear. A possible role for GM1 in this process has been suggested, but no evidence yet exists to substantiate this hypothesis. Furthermore, although the catalytic activity of bacterial toxins has been widely used to produce immunotoxins and kill targeted harmful cells, their ability to traffic through intact polarised epithelial cells and carrier-cargo organisation has not been fully investigated.

Therefore, the aim of this project was two-fold. Firstly, some aspects of the intracellular trafficking of PE, which appear crucial to explain its ability to transport across cells, were investigated. Secondly, the ability of bacterial toxins to cross epithelial barriers and their potential as vehicles for oral delivery of macromolecular drugs were explored. Defining the interactions that govern the trafficking route exploited by PE within a cell might help enhance its potential as drug carrier.

In *Chapter 3*, the conformational change experienced by PE in acidic conditions was investigated in terms of protein size, structure rearrangement and domains/residues involved. This chapter aimed to define the characteristics of this transition and understand its role in the protein's escape from the intracellular degradation pathway that terminates in delivery to lysosomes.

Chapter 4 describes the study of the interaction between PE and GM1 and its impact on the protein's intracellular trafficking route. The aim here was to provide a better understanding of the role of GM1 as a possible secondary receptor for PE.

Chapter 5 investigates the respective and combined effects of toxin truncation and addition of a cargo protein on the trafficking of PE. This chapter aimed to characterise some of the structural requirements for PE to function as an efficient drug carrier in non-polarised cells and across the intestinal epithelium.

In *Chapter 6*, the effects of pH on the conformation of cholix were examined, along with the protein's interaction with GM1 and the effects of truncation and attachment of a cargo molecule. The aim of this chapter was to provide a better understanding of the intracellular pathway used by cholix, and to supply sufficient information to allow for a comparison with PE, in terms of drug delivery.

2 GENERAL MATERIALS AND METHODS

2.1 Cell culture

Caco-2 cells were obtained from American Type Culture Collection (ATCC). This cell line was originally derived from a human colorectal adenocarcinoma [177].

M40-1 hybridomas were a gift from Dr David FitzGerald (NCI/NIH, Bethesda, MD). These cells secrete a mouse monoclonal antibody targeting the amino acids 264-308 of PE [153].

2.1.1 Preparation of trypsin/Ethylenediaminetetraacetic acid (EDTA) solution

2% EDTA solution: 0.5 g EDTA dissolved in 25 ml PBS and sterile-filtered using a 0.2 µm filter

0.25% trypsin/0.02% EDTA solution:	100 ml 10X trypsin
	10 ml 2% EDTA solution
	890 ml sterile PBS

2.1.2 Media preparation

Different media were employed in order to culture various cell lines.

- Caco-2 cells growth medium: DMEM containing 10% heat-inactivated foetal bovine serum (FBS) and 50 IU of each penicillin/streptomycin (P/S)
- M40-1 hybridomas growth medium: RPMI containing 10% heat-inactivated FBS and 50 IU P/S
- M40-1 hybridomas secretion medium: RPMI containing 50 IU P/S

2.1.3 Subculture of adherent cells

Caco-2 cells are adherent cells and were trypsinized one to three times a week in order to maintain them in the exponential phase and at a desired confluency of 70-80%. After trypsinization, they were seeded into T75 flasks in fresh growth medium.

Medium was removed from flasks and discarded. Cells were washed with PBS and incubated with 0.25% trypsin/0.02% EDTA at 37 °C under 5% CO_2 until they detached. The trypsin medium was then inactivated by adding growth medium in a 1:1 ratio. The resulting suspension was centrifuged at 125 x *g* for 10 min. Pelleted cells were suspended in fresh growth medium, counted under a light microscope using a haemocytometer and diluted before being seeded at an appropriate density into a new T75 flask.

2.1.4 Subculture of suspension cells

M40-1 hybridomas are suspension cells that were grown in T175 flasks. When the cell density reached ~1 x10^6 cells/ml, 90% of the cell suspension was aspirated and replaced by fresh complete growth medium.

2.1.5 Thawing and freezing cell lines

Vials containing frozen cells were removed from liquid nitrogen storage and quickly thawed by gently swirling the tube in a 37 °C water bath. The cells were added drop wise to 10 ml of pre-warmed complete growth medium, gently mixed, and spun at 125 x *g* for 10 min. The pellet was subsequently suspended in complete growth medium. Cells were seeded in a T25 flask and subcultured as described in 2.1.3 after reaching confluency.

Cells were frozen while still in the log phase of growth. They were trypsinized and centrifuged at 125 x *g* for 10 min before being suspended in freezing medium (DMEM or RPMI + 20% FBS + 10% DMSO) at a density of ~1 x10^6 cells/ml. Aliquots were placed in cryotubes and frozen slowly by storing initially at -20 °C for 1 h, followed by -80 °C overnight before being transferred to liquid nitrogen the following day.

2.2 Sodium dodecyl sulphate polyacrylamide gel electrophoresis (SDS-PAGE) and Western blot (WB)

2.2.1 SDS-PAGE

2.2.1.1 Recipes

Reducing sample buffer 2X (1ml):

Reagent	**Volume (µl)**
4X NuPAGE® LDS buffer	500
NuPAGE® reducing agent	200
dH_2O	300

Running buffer (Tris-Glycine) 10X (1 l):

Reagent	**Weight (g)**
Tris	30.3
Glycine	144
Sodium dodecyl sulphate (SDS)	10.0

Staining solution (1 l):

Reagent	**Amount**
Coomassie brilliant blue R-250 (mg)	500
Ethanol (EtOH) (ml)	400
Glacial acetic acid (AA) (ml)	100
dH_2O (ml)	500

Destain solution (1 l):

Reagent	**Volume (ml)**
Methanol (MeOH)	100
Glacial AA	70
dH_2O	830

Polyacrylamide gels recipe for 10 gels, 12% Bis-tris acrylamide, 1 mm thick gels:

Resolving gel:

Reagent	**Volume (ml)**
MQ H_2O	24.0
40% Bis-Tris acrylamide	16.8
1.5 M Tris-HCl pH 8.8	14.0
10% SDS	0.560
10% ammonium persulfate (APS)	0.560
Tetramethylethylenediamine (TEMED)	0.056

Stacking gel:

Reagent	**Volume (ml)**
MQ H_2O	11.6
40% Bis-Tris acrylamide	3.00
0.5 M Tris-HCl pH 6.8	5.00
10% SDS	0.20
10% APS	0.20
TEMED	0.02

All the resolving gel reagents were mixed together and poured into gel cassettes to about 75% total volume. A layer of butanol was applied in the remaining volume to ensure that the gel set flat and that they were no bubbles. Gels were left to polymerise for 45 min.

Once set, the butanol was discarded and the stacking gel solution applied. Gel combs containing either 10, 12 or 15 wells were inserted into the stacking gel at the top of the cassette prior to polymerisation and gels were left to set.

2.2.1.2 Method

A fully polymerised gel was placed in an XCell™ Sure Lock® Mini-cell tank with running buffer. Samples were mixed with reducing sample buffer in a 1:1 ratio and loaded in the wells. The first well was generally filled with 5 µl of a standard protein ladder (10-170 kDa). Gels were run for 35-40 min at 250 V.

2.2.1.3 Coomassie staining

Following sample separation, gels were incubated overnight in Coomassie stain solution on a rocking platform. They were then destained as many times as required in order to observe the bands.

2.2.1.4 Silver staining

Gels were silver-stained using the SilverXpress® Silver staining kit. Following sample separation, gels were fixed in MeOH:AA:MQ H_2O in a 10:2:9 ratio for 10 min on a rocking platform. They were then sensitized, stained and developed according to the manufacturer's recommendations for Bis-Tris gels.

2.2.2 Western Blot

2.2.2.1 Recipes

Transfer buffer (1 l):

Reagent	**Amount**
Tris (g)	3.0
Glycine (g)	14.4
MeOH (ml)	200
dH_2O (ml)	800

Tris Buffer Saline (TBS) (1 l):

Reagent	**Volume (ml)**
Tris, HCl 1M pH 8.0 (ml)	10.00
NaCl 4M (ml)	37.50
dH_2O (ml)	952.5

TBS-T: 1 l of TBS + 1 ml Tween-20

Blocking solution: depending on the antibody, dissolve 2.5 g of either non-fat dry milk or 2.5 g bovine serum albumin (BSA) in 50 ml TBS-T.

2.2.2.2 Method

Following SDS-PAGE, proteins were transferred to a 0.2 µm polyvinylidene difluoride (PVDF) membrane at 30 V (170 mA) for 1.5 h using XCell II™ Blot Module. The membrane was briefly washed with distilled water, blocked for 1 h at room temperature (RT) and incubated overnight at 4 °C with a primary antibody diluted in TBS-T (Table 9-2). The membrane was then washed three times with TBS-T before being incubated for 1 h at RT with an enhanced chemiluminescence (ECL)-linked secondary antibody diluted in TBS-T (Table 9-3). The membrane was washed again three times with TBS-T, incubated with the ECL solution and developed using an X-ray film developer.

2.3 Cloning of PE364-hGH and Cho386-hGH

Human growth hormone (hGH) was earlier suggested as a cargo protein that could be orally delivered in association with PE or possibly cholix. It is a 22.1 kDa protein whose nucleotide sequence contains 573 bp coding for the mature protein. A 24-nucleotide long N-terminal pre-sequence was engineered by Goeddel *et al* (1979) and inserted into pHGH107 to allow synthesis and secretion of hGH in microbial cells [178]. In order to test the ability of PE or cholix to transport hGH across polarised epithelium, two fusion proteins were engineered, composed of either PE364 or Cho386 (residues 1-364 and 1-386, respectively) linked to a C-terminal hGH molecule via a flexible poly glycine-serine linker. The resulting proteins were called PE364-hGH and Cho386-hGH.

The cloning strategy followed and primers employed for polymerase chain reaction (PCR) and sequencing are detailed in Figure 2-1 and Table 2-1, respectively.

Table 2-1 – Sequences of primers used during cloning of PE364-hGH and Cho386-hGH. PCR and S indicate primers used for PCR and sequencing, respectively.

Name	PCR/S	Sequence
hGH_F	PCR	5'-ACTCTTAAGTTCCCAACTATACCACTATCTCGTCTATTCGAT-3'
hGH_R	PCR	5'-AGTCGAATTCGAAGCCACAGCTGCCCTCCAC-3'
GS linker	PCR	5'-GGTAGTGGTAGTGGTTCTGGTAGT-3'
Cholix_F	PCR	5'-CCAATTCATATGGTCGAAGAAGCTTTAAAC-3'
Cho386_R	PCR	5'-CCATATACTAFTATAATCGTTATAGATCTGACG-3'
T7_F	S	Provided by Source Bioscience
PE_Nterm_F	S	5'-CAAATGGGCGGTAGGCGTGTAC-3'
PE_mid_F	S	5'-CAACCAGCTCAGCCACATGTC-3'
PE_mid_R	S	5'-GACATGTGGCTGAGCTGGTTG-3'
PE364_F	S	5'-CGACCAGGTGATCCGCAAC-3'
Cho_mid_F	S	5'-CGGTAACGCGTCCTGAAC-3'
Cho_mid_R	S	5'-GCCACCAAACCAATTATCCCCT-3'
Cho386end_R	S	5'-CTTGTGCACCCGCACTGGT-3'

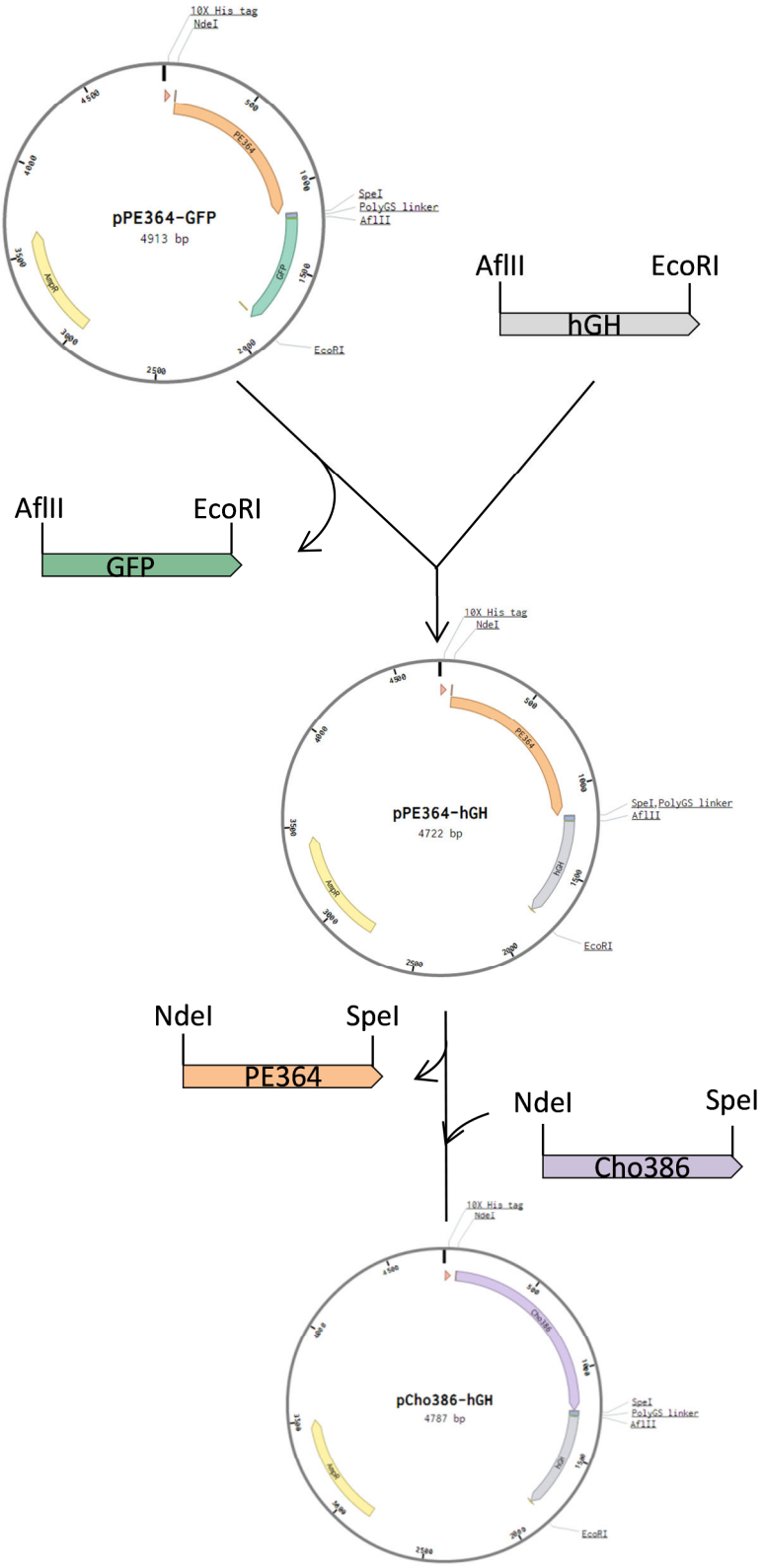

Figure 2-1 – Cloning of PE364-hGH and Cho386-hGH. PE364 and Cho386 are orange and purple, respectively, GFP is green, hGH is light grey, and the ampicillin resistance gene is depicted yellow.

2.3.1 Cloning of PE364-hGH

hGH was amplified from pHGH107 (ATCC) by PCR using Phusion High-Fidelity DNA Polymerase and either GC buffer, GC buffer + DMSO or HF buffer according to manufacturer's instructions. The forward (hGH_F) and reverse (hGH_R) primers carried an AflII and EcoRI restriction sites, respectively. The thermocycling conditions used to amplify the DNA fragment are detailed in Table 2-2.

Table 2-2 – Thermocycling conditions used for amplification of hGH from pHGH107.

	Step	Temperature (°C)	Duration
1	Initialisation	95	5 min
2	Denaturation	98	30 sec
3	Annealing	60	30 sec
4	Elongation	72	60 sec
5	Amplification	Go to step 2	20 x
6	Final elongation	72	5 min
7	End	10	-

pPE364-GFP is a plasmid containing PE364 linked to a C-terminal GFP inserted between the AflII and EcoRI restriction sites (Figure 2-1). The two protein sequences are separated by a poly glycine-serine linker of SGSGSGSGS (5'-AGTGGTAGTGGTAGTGGTTCTGGTAGT-3'). It also includes an N-terminal 10X His tag and a resistance gene for ampicillin.

Both pPE364-GFP and the amplified hGH fragment were digested by the restriction endonucleases AflII and EcoRI-HF® in the conditions specified by the manufacturer and purified by agarose gel electrophoresis (1% agarose in 40 mM Tris containing 20 mM AA and 1 mM EDTA at pH 8.0, 20 min) using GeneJET™ Gel Extraction Kit. The digested plasmid and hGH fragment were then ligated together using Quick Ligation Kit and 10 µl competent DH5α cells were transformed with the resulting plasmid, termed pPE364-hGH (DH5α) (Figure 2-1). This plasmid was further transformed into 10 µl competent One Shot™ BL21 Star™ cells for expression of the fusion protein PE364-hGH, and labelled pPE364-hGH (BL21).

2.3.2 Cloning of Cho386-hGH

The sequence of Cho386 was obtained from pETCHO, a plasmid that encodes for the full-length, non-toxic, cholix sequence (Appendix 1, Figure 9-1). It was amplified by PCR using the Phusion High-Fidelity DNA Polymerase and the same thermocycling conditions used for amplification of hGH (Table 2-2). The forward (Cholix_F) and reverse (Cho386_R) primers contain the NdeI and SpeI restriction sites, respectively.

Both pPE364-hGH (DH5α) and the amplified Cho386 fragment were digested using NdeI and SpeI-HF® endonucleases before being ligated together using Quick Ligation Kit. The plasmid obtained after transformation of 10 µl competent DH5α cells was named pCho386-hGH (DH5α) (Figure 2-1). This plasmid was used for further transformation of 10 µl competent Shuffle cells for expression of Cho386-hGH and the resulting plasmid was labelled pCho386-hGH (Shuffle).

2.4 Protein expression in *E. coli*

For each protein, information about the expression plasmid, calculated molecular weight and isoelectric point can be found in Appendix 1 (Table 9-1).

2.4.1 Expression of ntPE

A non-toxic mutant of *Pseudomonas* exotoxin A, termed ntPE, was engineered to delete the glutamic acid at position 553 [161]. The plasmid containing ntPE (pVC45D) was kindly provided by Dr David FitzGerald (NCI/NIH, Bethesda, MD, USA) [179].

Protein expression in the periplasm

50 ml of Lysogeny broth (LB) medium containing 50 µg/ml ampicillin was inoculated with pVC45D and grown overnight at 37 °C with shaking at 250 RPM. LB medium (1 l) containing 50 µg/ml ampicillin was inoculated with 25 ml overnight culture and grown at 37 °C with shaking at 250 RPM until the OD_{600} reached 0.6-0.8. Monitoring of the OD_{600} was achieved using a NanoDrop™ 2000c. The incubation temperature was then dropped to 18 °C and the cultures were induced with 0.5 mM isopropyl β-D-1-thiogalactopyranoside (IPTG) and grown overnight.

Periplasm fractionation

In order to collect the secreted protein, the outer membrane was broken by osmotic shock, releasing the protein present in the periplasm while keeping the cell membrane intact.

Cells were centrifuged (JA-10 fixed angle rotor on Beckman J2-MC centrifuge) at 6,400 x *g* at 4 °C for 20 min and the pellets were resuspended in 30 mM Tris-HCl, 20% sucrose, pH 8.0 at 80 ml per gram wet weight and kept on ice. EDTA was added drop wise until a final concentration of 1 mM was reached and the cells were incubated on ice for 10 min with gentle shaking. They were then centrifuged at 8,000 x *g* (JA-14 fixed angle rotor) for 20 min at 4 °C and the supernatants were collected. Pellets were suspended in the same volume (80 ml per gram wet weight) of ice-cold water and cells were incubated on ice for 10 min with gentle shaking. They were then centrifuged at 8,000 x *g* (JA-14 fixed angle rotor) for 20 min at 4 °C and the supernatant was collected and concentrated to 50 ml using a Vivaflow 200 with a 30 kDa MWCO membrane. The supernatant was then dialysed overnight at 4 °C against 50 mM Tris pH 7.4, 50 mM NaCl, 1 mM EDTA.

Protein purification

Following overnight dialysis, ntPE was purified by anion-exchange (AE) chromatography and size exclusion chromatography as described in Sections 2.6.1 and 2.6.4.

2.4.2 Expression of ntPE GS TEV and ntCho GS TEV

ntPE GS TEV and ntCho GS TEV are modified versions of PE and cholix that are non-toxic and were engineered to contain the poly glycine-serine linker of SGSGSGSGS (5'-AGTGGTAGTGGTAGTGGTTCTGGTAGT-3') between the protein and a C-terminal TEV cleavage sequence (ENLFQS). This sequence is located between two cysteine residues that form a disulphide bond. The flexible linker was added to increase cleavage efficiency by making the digestion site more accessible to the TEV enzyme. The resulting protein can be coupled to various elements (including fluorescent tags or other proteins) via a thiol linkage. Both ntPE GS TEV and ntCho GS TEV were soluble when expressed in *E. coli*.

Protein expression

50 ml LB medium containing 50 μg/ml kanamycin was inoculated with plasmids containing ntPE GS TEV or ntCho GS TEV and grown overnight at 37 °C with shaking at

250 RPM. LB medium (1 l) containing 50 µg/ml of kanamycin was inoculated with 25 ml overnight culture and grown at 37 °C with shaking at 250 RPM until the OD_{600} reached 0.6-0.8. Monitoring of the OD_{600} was achieved using a NanoDrop™ 2000c. The temperature was then dropped to 18 °C and cultures were induced with 0.25 mM IPTG and grown overnight. Cells were harvested by centrifugation (J2-MC with JA-10 fixed angle rotor) at 6,400 x *g* at 4 °C for 20 min. Pellets were suspended in 50 mM Tris pH 8.0, 300 mM NaCl, 20 mM imidazole in the presence of cOmplete EDTA-free protease inhibitors. Cells were then sonicated on ice twice at 30% power 6 during 3 min. Samples were then centrifuged (J2-MC with JA-20 fixed angle rotor) at 48,300 x *g* at 4 °C for 30 min to remove any unbroken cells. The supernatant was collected and dialysed overnight at 4 °C against 50 mM Tris pH 7.4, 50 mM NaCl, 1 mM EDTA.

Protein purification

ntPE GS TEV and ntCho GS TEV were purified using anion exchange chromatography (Section 2.6.1). The protein-containing fractions were collected and further enriched by size exclusion chromatography as described in Section 2.6.4.

2.4.3 Expression of PE GS TEV and Cho GS TEV mutants

While ntPE GS TEV and ntCho GS TEV were soluble and expressed as described above, their respective mutants were insoluble and had to be expressed as inclusion bodies. Isolation of proteins expressed into inclusion bodies entails three major steps prior to purification: first, the aggregates have to be extracted from the bacterial cytoplasm (cell lysis), then isolated from the cellular debris, and finally solubilised and refolded, before being purified.

Expression of PE GS TEV and Cho GS TEV mutants as inclusion bodies

In order to express these proteins as inclusion bodies, 50 ml LB medium containing 50 µg/ml kanamycin was inoculated with the relevant plasmids and grown overnight at 37 °C with shaking at 220 RPM.

LB medium (1 l) containing 50 µg/ml of kanamycin was then inoculated with 25 ml overnight culture (1:40 dilution) and grown at 37 °C with shaking at 220 RPM until the OD_{600} reached 0.6-0.8. Monitoring of the OD_{600} was achieved using a NanoDrop™ 2000c.

The temperature was then dropped to 16 °C and the cultures induced with 1 mM IPTG and grown overnight.

The cells were centrifuged (JA-10 fixed angle rotor on J2-MC) at 6,400 x *g* for 20 min at 4 °C. Pellets were suspended in 50/20 TE buffer (50 mM Tris, 20 mM EDTA, pH 8) and lysozyme was added at a concentration of 0.01 mM in order to disrupt the cells. Samples were incubated at RT for 30 min on a rocking platform. They were then sonicated on ice twice for 1.5 min (power 6, 30%) and incubated for another 30 min at RT on a rocking platform to ensure maximal cell disruption. In order to completely disintegrate membrane fragments, 0.3 M NaCl and 2% Triton X-100 were added to the samples, which were incubated at RT for 30 min on a rocking platform and centrifuged (JA-14 fixed angle rotor on J2-MC) at 15,300 x *g* for 45 min at 4 °C. Pellets were suspended in 50/20 TE buffer containing 2% Triton X-100. Samples were homogenised (Tissue Master 240) and centrifuged (JA-14 fixed angle rotor on J2-MC) at 15,300 x *g* for 30 min at 4 °C. Again, pellets were suspended in 50/20 TE buffer, homogenised and centrifuged (JA-20 fixed angle rotor on J2-MC) at 17,400 x *g* for 30 min at 4 °C. This step was repeated three times in order to wash the pellets from any detergent residues.

Solubilisation of PE GS TEV and Cho GS TEV mutants

Solubilisation of the aggregates was achieved by complete unfolding of the protein: the pellets were suspended in 6 M guanidine-HCl, 100 mM Tris pH 8, 2 mM EDTA. Guanidine is a strong chaotropic agent that denatures proteins by disrupting intramolecular interactions mediated by non-covalent forces, such as hydrogen bonds and van der Waals forces [180]. Samples were homogenised, incubated at RT for 1.5 h on a rocking platform and centrifuged (JA-20 fixed angle rotor on J2-MC) at 27,200 x *g* for 15 min at 4 °C. The concentration of soluble protein in the supernatant was then determined by Bradford assay. In order to reduce disulphide bonds and further increase protein solubility, dithiothreitol (DTT) was added to the supernatant to a final concentration of 10 mg/ml and samples were incubated at RT for 1.5 h on a rocking platform.

Refolding of PE GS TEV and Cho GS TEV mutants by dilution and dialysis

After solubilisation, removal of the denaturant and reducing agent was necessary in order to provide the protein with a suitable environment for spontaneous and correct refolding.

Full-length PE and cholix contain four disulphide bonds [105, 140], and at least three of them should be conserved among the mutants. The solubilised protein was added drop

wise to 100 mM Tris buffer pH 8.0 containing 500 mM L-Arginine, 2 mM EDTA, and 0.9 mM oxidised glutathione (GSSG) and left stirring overnight at 4 °C. These low molecular weight compounds promote correct refolding and disulphide bond formation. Protein concentration was maintained at a final concentration < 100 µg/ml to prevent aggregation.

The refolded protein was then dialysed 1:10 against 20 mM Tris pH 8, 100 mM urea. This step was performed four times at 4 °C, the dialysis buffer being changed every 3 h. Samples were subsequently concentrated using Vivaflow 200 (30 kDa MWCO membrane) to an adequate volume for purification, typically about 50 ml. Finally, proteins were dialysed overnight at 4 °C stirring against 50 mM Tris pH 7.4, 50 mM NaCl, 1 mM EDTA.

Purification of PE GS TEV and Cho GS TEV mutants

All proteins were filtered using a 0.45 µm filter and purified using anion-exchange chromatography (Section 2.6.1). They were then further enriched using size exclusion chromatography (Section 2.6.4).

2.4.4 Expression of Cho-GFP mutants

ntCho-GFP is a fusion protein constituted of full-length, non-toxic (deletion of E581), cholix connected by the previously described poly glycine-serine (GS) flexible linker to a C-terminal GFP molecule. The resulting protein carries an N-terminal 6X His tag, which allows ntCho-GFP to be purified by immobilised-metal affinity chromatography (IMAC).

While ntCho-GFP was soluble and expressed as ntCho GS TEV, its mutants were insoluble and had to be expressed as inclusion bodies. All proteins belonging to the Cho-GFP series were purified by immobilised metal affinity chromatography (Section 2.6.2) followed by size exclusion chromatography (Section 2.6.4).

2.4.5 Expression of PE364-hGH and Cho386-hGH

Both PE364-hGH and Cho386-hGH were insoluble and therefore had to be expressed as inclusion bodies using pPE364-hGH (BL21) and pCho386-hGH (Shuffle), respectively. Proteins were then purified using AE (Section 2.6.1) and size exclusion chromatography (Section 2.6.4).

The calculated molecular weight and pI values for PE364-hGH and Cho386-hGH are presented in Table 2-3.

Table 2-3 – Calculated molecular weight and pI values for PE364-hGH and Cho386-hGH [181].

Protein	Calculated molecular weight (kDa)	Calculated pI
PE364-hGH	66.4	5.84
Cho386-hGH	67.8	5.34

2.5 Antibody expression in mouse hybridomas

In order to express the M40-1 monoclonal antibody, the culture medium containing this hybridoma was collected when the cell density reached ~1 x10^6 cells/ml and spun at 500 x *g* for 10 min. Pelleted cells were suspended and seeded in serum-free medium in triple T175 flasks and left to secrete the antibody. After 10 days, the culture medium was collected and 0.45 μm-filtered. The filtered medium of at least four flasks was concentrated down to ~50 ml using a stirred Amicon-type ultrafiltration cell and dialysed overnight against 20 mM sodium-phosphate, pH 7.0 (binding buffer).

2.6 Protein purification using fast protein liquid chromatography

Fast protein liquid chromatography (FPLC) is a technique commonly used to purify mixtures of proteins. Here, all chromatography methods were performed using a ÄKTA FPLC system with the eluted protein, detected by monitoring absorbance at 280 nm, being captured using an automated fraction collector. The letters/numbers indicated above protein purification gels and chromatograms therefore correspond to the fractions collected from the fraction collector tray used for these studies (Figure 2-2).

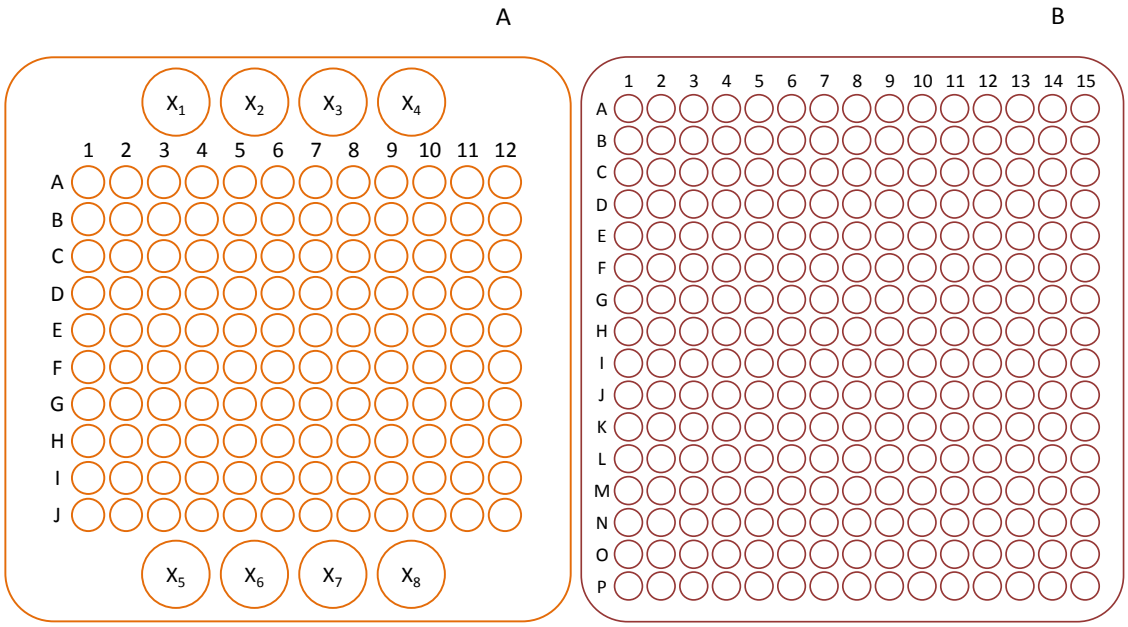

Figure 2-2 – Schematic representation of the trays used with the automated fraction collector during protein purification. (A) represents the tray used for ion exchange and immobilised metal ion affinity chromatography. X-labelled tubes were used to collect flow-through fractions, and tubes placed in rows A-J were used to collect elution fractions. (B) represents the tray used to collect fractions following ion exchange, protein G or gel filtration chromatography.

2.6.1 Ion exchange chromatography

Ion exchange (IX) chromatography is a technique that allows for separation of proteins according to their net charge. It relies on the reversible adsorption of charged molecules to opposite charge ions immobilised on a matrix support. The IX columns used in this project are anion-exchange (AE) Q columns, i.e. they are functionalised with positively charged quaternary amine groups. Proteins bearing a positive net charge do not bind to the positively charged beads and thus are eluted first. On the contrary, negatively charged proteins adsorb to the support. The stronger their negative charge, the stronger proteins will adsorb to the matrix. These molecules are released and eluted from the column using a gradient of increasing ionic strength (Figure 2-3).

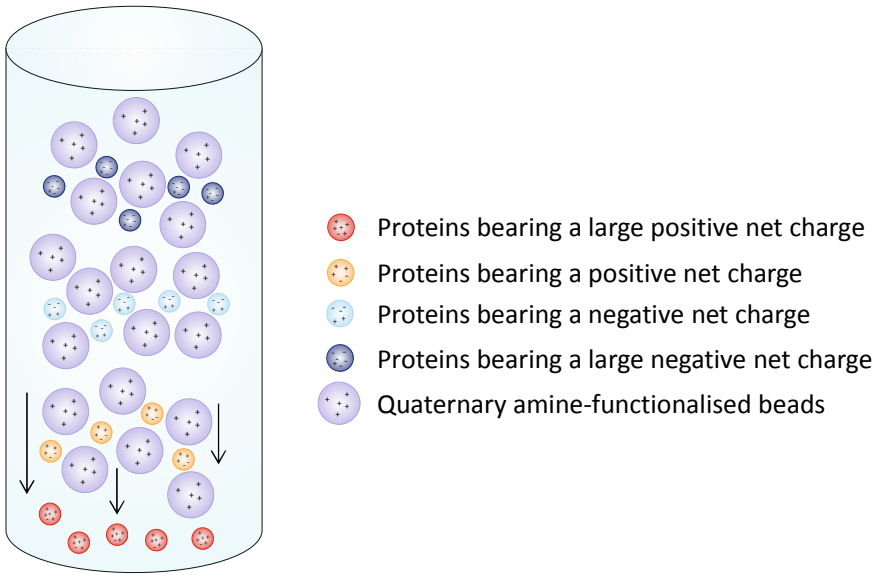

Figure 2-3 – Principle of IX chromatography. On an AE column functionalised with quaternary ammonium groups (purple), proteins bearing a net positive charge (red and orange) will be eluted first while molecules which overall charge is negative (light and dark blue) will bind to the column with more or less strength.

The sample was applied to an AE column (HiTrap Q HP column) which was eluted with a linear gradient of NaCl (0 to 1.0 M) in 50 mM Tris pH 7.4, 1 mM EDTA at a flow rate of 1 ml/min. Fractions containing the protein were collected and concentrated to 1 ml sample using a Millipore 10 kDa MWCO spin filter.

2.6.2 Immobilised metal ion affinity chromatography

Proteins carrying an N- or C-terminal His tag can be purified on a nickel column using immobilised metal ion affinity chromatography (IMAC). These protein samples were 0.45 µm-filtered and loaded on an agarose column functionalised with chelating ligands that are Ni^{2+}-charged (HisTrap FF column).

His-tagged proteins bind to nickel ions with high affinity and were eluted from the column using a linear gradient of imidazole (20 to 500 mM) in 50 mM Tris pH 8.0, 300 mM NaCl at a flow rate of 1 ml/min. Due to their structural resemblance (Figure 2-4), imidazole competes with the His tag for Ni^{2+} binding, progressively releasing the tagged protein from the column. Protein-containing fractions were collected and concentrated to 1 ml using 10 kDa MWCO spin filters.

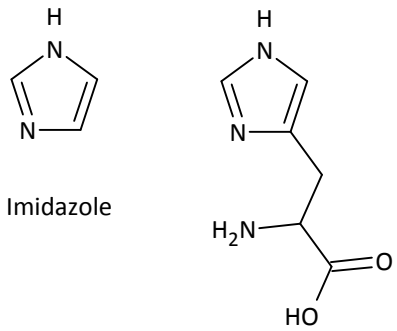

Figure 2-4 – Molecular structures of imidazole and histidine.

2.6.3 Immobilised protein G affinity chromatography

Protein G is a modified version of the bacterial cell wall protein isolated from Streptococcus group G. It binds to the constant domain of immunoglobulins from various species but lacks the albumin-binding region. Immobilised protein G affinity chromatography was used to purify the M40-1 mouse monoclonal antibody against PE.

M40-1 samples were loaded on a HiTrap protein G HP column, which is functionalised with immobilised protein G. The unbound material was washed off with binding buffer (20 mM sodium-phosphate, pH 7.0), after what the antibody was eluted with 0.1 M Glycine-HCl, pH 2.7 at a flowrate of 1 ml/min. The collection tubes were prefilled with 1 M Tris-HCl, pH 9.0 as a precaution to prevent degradation of the antibody in acidic conditions. IgG-containing fractions were collected and buffer-exchanged into PBS before being concentrated down to 1 ml using 10 kDa MWCO spin filters.

Several characteristics of the final product were examined by SDS-PAGE and WB. Following the gel filtration step, fractions corresponding to the peak that could contain antibody were separated by SDS-PAGE and Coomassie stained to confirm the size of the final compound.

To confirm that the final product specifically targeted ntPE as antigen, 10 µg of both the toxin and BSA were loaded on a gel and transferred to a PVDF membrane, which was first blocked with 5% milk in TBS-T for 1 h at RT before being incubated overnight at 4 °C with the collected product. The antibody concentrations used ranged from 1/1,000 to 1/20,000 from a 1 mg/ml stock solution. The membrane was finally incubated with an anti-mouse HRP-linked secondary antibody (Table 9-3) for 1 h at RT and developed.

2.6.4 Size exclusion chromatography

Size exclusion chromatography (SEC), also known as gel filtration (GF) chromatography, is a technique used to separate molecules according to their size. Proteins migrate through a porous matrix at different speeds: large proteins are excluded from the pores of the beads and are thus eluted first, while smaller molecules diffuse through these pores and are eluted last from the column (Figure 2-5). The molecular weight (MW) and three dimensional structure of proteins both affect migration of a compound through the resin. Size exclusion chromatography is usually used as the last "polishing" step, in order to remove any aggregates that would have co-migrated with the protein of interest during the previous purification steps, and to place the protein into a desired buffer appropriate for storage and/or subsequent applications.

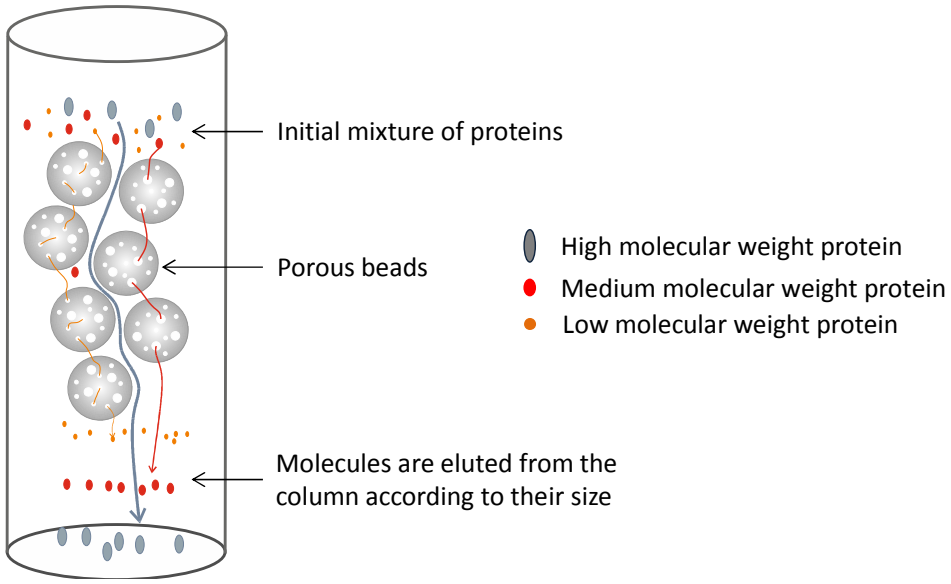

Figure 2-5 – Size exclusion chromatography. While large proteins are excluded from the pores of the resin and are eluted first, smaller molecules travel through these pores and thus are eluted last from the column.

The column matrix used for GF chromatography was Superdex™ 200 HR10/30. It is useful to purify samples containing proteins whose MW ranges from 10 to 600 kDa. Samples previously enriched by IX, IMAC or protein G chromatography were concentrated down to 1 ml before being loaded on the GF column and eluted with PBS at a flow rate of 0.5 ml/min. Components corresponding to the UV peaks were separated by SDS-PAGE to identify which fractions contained the protein of interest.

2.7 Determination of protein concentration

2.7.1 By UV spectrophotometry

Concentration of various samples was determined by measuring the absorbance of proteins at 280 nm using a NanoDrop™ 2000c spectrophotometer. This instrument was used in pedestal and UV-VIS modes. A blank measurement was first performed on 1.5 µl of the buffer in which the protein was diluted. Then, the absorbance of the sample was assessed and, using Beer-Lambert's law (Equation 2-1), converted to a concentration.

Equation 2-1 – Beer-Lambert law $$c = \frac{A}{l.\varepsilon}$$

With c concentration of the protein solution (M)

A sample absorbance at 280 nm

l path length (cm)

ε molar absorptivity ($mol^{-1}.l.cm^{-1}$)

Extinction coefficients ε were calculated for each protein at 280 nm in water using ProtParam [181].

2.7.2 By Bradford assay

Bradford assay is a colorimetric method that involves the use of Coomassie blue to quantify proteins in solution. When Coomassie blue binds to a protein in solution its absorption maximum shifts from 465 nm (unbound dye, brown) to 595 nm (dye-protein complex, blue). Here, Bradford assay was performed using a Coomassie protein assay kit according to the manufacturer's instructions.

First, a standard curve was established using bovine serum albumin (BSA) samples over the 100-1,500 µg/ml working range (Table 2-4). Standards were prepared in the same buffer as the protein.

Table 2-4 – Preparation of BSA standards for Bradford assay. Adapted from [182].

Vial	Volume of diluent (µl)	Volume of BSA (µl)	Final BSA concentration (µg/ml)
A	0	300 at 2mg/ml	2,000
B	125	375 at 2mg/ml	1,500
C	325	325 at 2mg/ml	1,000
D	175	175 of B	750
E	325	325 of C	500
F	325	325 of D	250
G	325	325 of E	125
H	400	100 of G	25
I	400	0	0

Each standard, blank (buffer) and protein sample were run on a microplate in triplicate: 10 µl was added to three microplate wells and 300 µl of Coomassie blue reagent was added to each well. The plate was placed on a microplate shaker for 30 sec and incubated at RT for 10 min before absorbance was measured at 595 nm (A_{595nm}).

After subtracting the average blank value to all other measurements, the standard curve representing A_{595nm} vs. BSA concentration was plotted and used to determine the unknown protein concentration of each sample.

2.8 Protein labelling

2.8.1 TEV cleavage

Proteins which carry a C-terminal TEV cleavage sequence (ENLYFQS) [183] can be used for chemical coupling via thiol linkage (Figure 2-6). The enzyme used for cleavage is the AcTEV, which is an enhanced version of the native TEV protease. 2 mg of TEV substrate containing protein was diluted into 50 mM Tris-HCl pH 8.0, 0.5 mM EDTA in presence of 0.5 mM DTT. After addition of the AcTEV enzyme, the mixture was left to incubate for 2 h at RT or overnight at 4 °C. The sample was then separated using a Ni^{2+} affinity chromatography column that was eluted with PBS. The protein was finally buffer-exchanged into PBS and sample concentration was assessed using a NanoDrop™ 2000c.

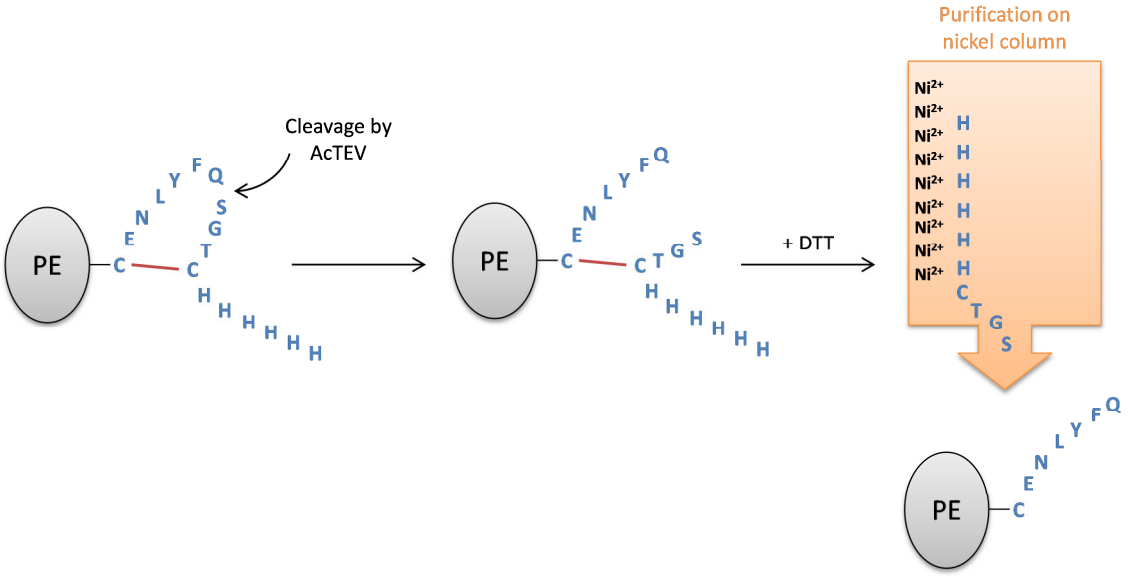

Figure 2-6 – PE coupling strategy using TEV cleavage. Following cleavage, reduction of the disulphide bond and purification, the protein carries a free cysteine that is used for further coupling via thiol linkage.

2.8.2 Protein coupling to a fluorescent tag

Thiol reactive Alexa Fluor® dyes carrying a maleimide group (Table 2-5) were added drop wise to the TEV-cleaved protein in a 20-fold molar excess. The mixture was incubated at RT for 2 h. The sample was then concentrated down to 1 ml using 10 kDa MWCO spin filters and purified using GF chromatography. The tagged protein was eluted with PBS at a flow rate of 0.5 ml/min.

Table 2-5 – Molecular weight, excitation and emission maximum wavelengths of Alexa Fluor® C_5 maleimide dyes used in this study. All parameters were obtained from the Life Technologies website.

Alexa Fluor® dye	Excitation max (nm)	Emission max (nm)	Molecular weight (g/mol)
488	496	519	720.66
546	556	573	1034.37
568	578	603	880.92

2.8.3 Protein coupling to biotin

Protein biotinylation was achieved using the sulfhydryl-reactive EZ-Link® Maleimide-PEG_2-Biotin reagent (MW = 525.62 g/mol). The biotinylation reagent was dissolved in PBS to obtain a 20 mM stock solution and added drop wise to the TEV-cleaved protein in a 50-fold molar excess. The mixture was incubated at RT for 3 h. At this point, labelling was considered complete and the excess biotinylation reagent was removed using a Zeba® Desalting Spin Column with a 7 kDa MWCO.

2.9 Size exclusion high pressure liquid chromatography (HPLC)

All experiments were performed on a Flexar HPLC system using a BioSep-SEC-s3000 (300 x 7.8 mm) size exclusion column. The HPLC system contained a LC column oven, pump, solvent manager and UV-VIS detector. Before any run, the column was rinsed with mobile phase for 30 min at 1 ml/min. 10 µl of sample was manually loaded on the column and injected. For all experiments, samples were run at 1 ml/min in 0.1 M potassium-phosphate buffer (kPB), containing 0.1 M NaCl at pH 5.8 or 7.4 at 37 °C for 15 min and the compounds eluted were detected by UV measurement at 254 nm.

2.10 Trypsin digestion

To obtain the first trypsin cut of the protein, 10 µg of protein was diluted up to 10 µl in citrate-phosphate buffer containing 0.1 M NaCl at different pH values. The protein was then incubated in presence of 0.4 µg trypsin on ice for 30 min. Control samples (undigested protein) were prepared by diluting 10 µg protein in PBS before incubation on ice. The reaction was stopped by addition of reducing sample buffer in a 1:1 ratio and heating at 95 °C for 10 min. Digestion fragments were separated by SDS-PAGE, and gels were either stained with Coomassie blue, silver-stained or transferred to PVDF membrane for immunodetection.

For N-terminal sequencing, the bands of interest were cut out of the gel and sent to Alta Bioscience Ltd., Birmingham, UK.

2.11 Dynamic light scattering

Principle

Dynamic light scattering (DLS) is a technique used to assess the size of particles in a monodisperse solution [184]. It measures Brownian motion of the sample, i.e. the random movement of molecules caused by collision between particles themselves and solvent molecules around them. The larger the particles, the slower they will move. The velocity of the Brownian motion is defined by the translational diffusion coefficient *D*, which enables the determination of a particle's hydrodynamic diameter using the Stokes-Einstein equation:

$$\boldsymbol{d(H) = \frac{kT}{3\pi\eta D}}$$

Where *d(H)* hydrodynamic diameter of the particle (m)

k the Boltzman constant (k = 1.38 $m^2.kg.s^{-2}.K^{-1}$)

T absolute temperature (K)

η viscosity of the solvent ($kg.m^{-1}.s^{-1}$)

D translational diffusion coefficient ($m^2.s^{-1}$)

The hydrodynamic diameter refers to how a particle diffuses within the solvent and, for a protein, represents the diameter of a perfect sphere which has the same translational diffusion coefficient as the molecule in solution. Therefore, due to its low limit of detection (0.3 nm for a 30% w/v sucrose solution in water [185]), DLS can discriminate between two protein conformations if the difference in size or shape between them is sufficient to affect their diffusion speed in solution.

Experimental conditions

Samples were diluted in citrate-phosphate buffer containing 0.1 M NaCl at different pH values. Buffers were filtered through Minisart® 0.20 µm filters before use to eliminate dust particles present in solution. For each run, 100 µl of sample at 1 mg/ml were dialysed against buffer at the desired pH for 2 h at RT using Slide-A-Lyser dialysis devices (10 kDa MWCO). The buffer was then changed and dialysis carried on overnight at 4 °C. Samples were then filtered through a 0.20 µm filter and introduced in a quartz cuvette, which had been rinsed twice with 0.20 µm-filtered water and twice with 0.20 µm-filtered buffer. Size

measurements were performed on a Zetasizer Nano S at 37 °C using a viscosity of 0.67 mPa.s. (= 0.000692 $kg.m^{-1}.s^{-1}$). The instrument was equipped with Zetasizer Software V. 7.03, and results were collected in terms of size distribution by intensity.

2.12 Spectrofluorometry

Principle

8-anilinonaphthalene-1-sulfonic acid (ANS) is a dye (Figure 2-7) whose fluorescence is minimal in polar solvents such as aqueous solutions, but increases drastically in non-polar environments. This increase in fluorescence intensity is accompanied by a blue shift in the wavelength of the maximum emission from about 520 nm in water to 464 nm in very non-polar solvents [186]. ANS readily binds to exposed hydrophobic residues on proteins via hydrophobic interactions mediated by the aromatic rings [187]. This binding is reflected by alterations in the fluorescence spectrum of the dye, which makes it an ideal probe to study protein behaviour in solution, and more specifically to characterise protein conformational changes as well as kinetics of folding and unfolding [188, 189], exposure of accessible hydrophobic surfaces [190] and ligand binding (displacement assays) [191, 192].

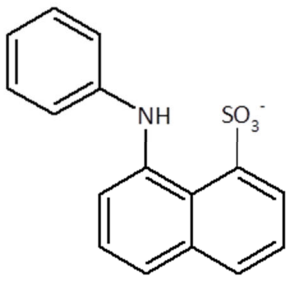

Figure 2-7 – Molecular structure of 8-anilinonaphthalene-1-sulfonic acid (ANS).

ANS is anionic over most of the commonly used pH range and therefore can also bind to external cationic sites on a protein's surface via electrostatic interactions. However, as ANS molecules bound to cationic sites exposed to the aqueous solvent are quenched due to monopolisation of the charge, it is assumed that the characteristic strong fluorescence observed when the dye binds to proteins is due to hydrophobic interactions.

Here, ANS was used to further characterise ntPE conformational change by investigating the effect of pH on the protein surface hydrophobicity.

Experimental conditions

Fluorescence measurements were performed on a Hitachi F-4500 fluorescence spectrophotometer connected to a water bath for temperature control. Buffers used for these experiments were citrate-phosphate containing 0.1 M NaCl at pH 5.8 or 7.4. Stock solutions of ANS 200 µM and protein 3.04 µM were prepared in buffer at both pHs. First, fluorescence measurements were carried out on 100 µM ANS alone in buffer in order to establish a blank. The dye was then mixed with protein in the corresponding buffer in a 1:1 volume ratio and fluorescence was measured [193, 194]. Final protein and ANS concentrations were always 1.52 µM and 100 µM, respectively. In all studies, emission slit width was 2.25 nm and excitation wavelength was set to 380 nm. Fluorescence spectra were acquired by scanning from 400 to 700 nm at a speed of 240 nm/min. Shifts in $\lambda_{em,max}$ were obtained by averaging the values collected for several independent runs. The difference in fluorescence intensity under various conditions, defined as the ratio ΔF, was examined by comparing the respective areas under the curve (AUC) minus the background fluorescence due to ANS alone at the studied pH.

$$\boldsymbol{\Delta F = \frac{AUC\ (P + ANS, 5.8) - AUC\ (ANS, 5.8)}{AUC\ (P + ANS, 7.4) - AUC\ (ANS, 7.4)}}$$

With AUC = area under curve, P = protein

When the influence of an additional compound (C) was examined, samples were blanked with the fluorescence of ANS + C.

2.13 Bio-layer interferometry

Principle

Bio-layer interferometry (BLI) is an optical analytical technique which uses a fibre-optic biosensor to measure the shifts in interference patterns between waves of reflected light. The biosensor tip is made of two interfaces: an optical layer (reference layer) and a biocompatible layer on the surface of the tip (Figure 2-8). Ligand molecules are immobilised on the latter and the tip is dipped into an analyte sample. White light is then directed down the biosensor and reflects from each of the reference and ligand-coated surfaces. The reflected beams can interfere either constructively or destructively, creating changing interference patterns at different wavelengths in the spectrum. As analyte molecules bind to the immobilised ligands on the sensor surface, a layer of molecules is formed and its thickness increases as more analyte molecules bind to the surface. As a

result, the distance between the two reflective layers of the tip also increases, resulting in changes in the interference pattern detected. These fluctuations are proportional to the extent of binding and are hence reported on a sensorgram as a change in wavelength (nm shift). Monitoring the spectral shifts in real time provides kinetic data on molecular interactions.

BLI presents several advantages with regards to binding kinetics and affinity measurements. In fact, due to the use of standard microplates (96- or 384-well plates), the volume of sample required for analysis can be as low as 40 µl. Moreover, BLI is not a destructive technique, and depending on the immobilisation method employed, samples can be recovered intact after the assay. The biosensors used are disposable and cost-effective, and because measurements can be performed in parallel in microplates, assay time is significantly reduced (compared to surface plasmon resonance for instance). Finally, high sensitivity allows for measurement of binding affinity up to the millimolar range, which represents a considerable improvement compared to techniques such as ELISA or immunoprecipitation, where the requirement for washing steps might result in dissociation between the species studied.

Here, streptavidin-functionalised biosensors were used to immobilise biotinylated ntPE on the sensing surface during BLI measurements (Figure 2-9). This method of ligand immobilisation presents several advantages: the interaction between streptavidin and biotin is non-covalent but rapid, stable and essentially non-reversible. Moreover, biotinylation is performed at neutral pH and therefore gentle on proteins. Finally, the coupling can be easily monitored and controlled biotinylation of ntPE in one specific location ensured that one molecule of protein was bound per functional group and therefore that all the protein molecules were oriented in a similar manner.

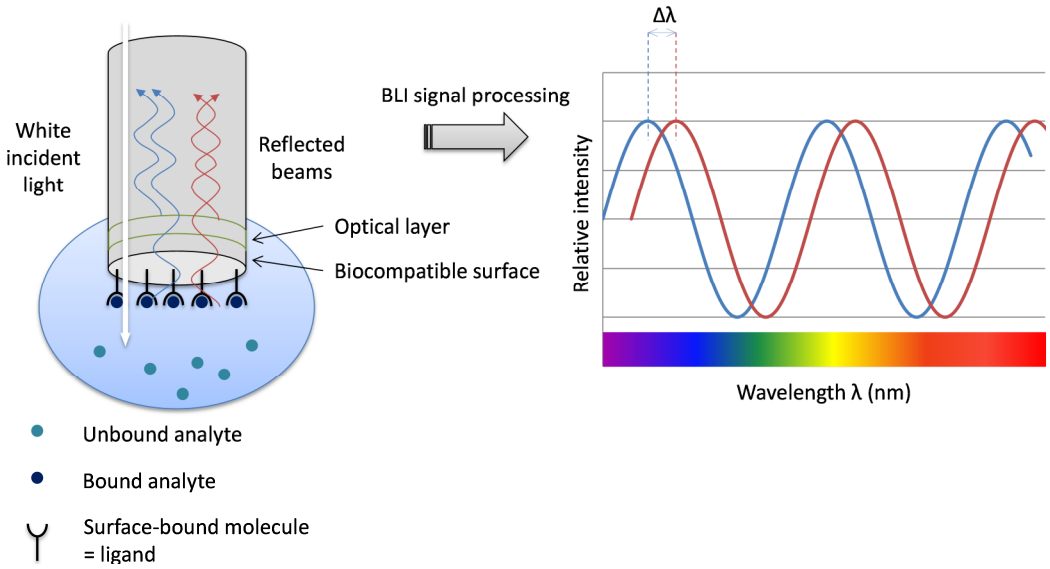

Figure 2-8 – Diagrammatic representation of the principles involved in BLI. A ray of white light illuminates the sample, and interference patterns from the reflected beams are analysed. Variations in the number of molecules bound on the sensor tip surface result in shifts in the interference pattern which are proportional to the total number of bound analyte molecules. Adapted from [195].

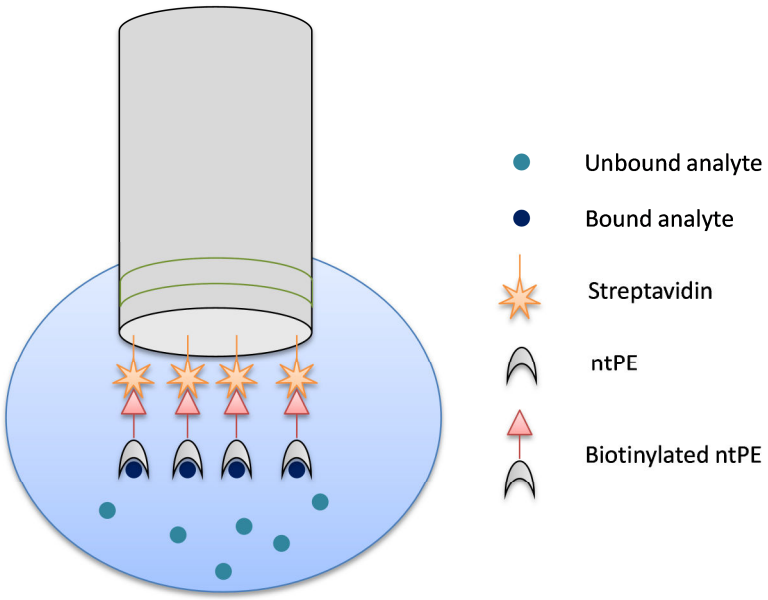

Figure 2-9 – Streptavidin-functionalised sensor tip. Biotinylated ntPE was immobilised on the surface of the biosensor via streptavidin-biotin interactions, and the tip was subsequently dipped into a solution of analyte.

Experimental conditions

Studies were performed on an Octet® RED96 instrument (Pall ForteBio Corp., CA, USA). All measurements were carried out in 0.1 M potassium-phosphate buffer at 37 °C at a flow rate of 1,000 RPM (plate shaking). For each sample, three independent measurements were performed in parallel. The biosensor was first exposed to 0.1 M potassium-phosphate buffer at 37 °C for 60 sec in order to establish a stable baseline. It was then immersed in biotinylated protein for 120 sec to allow for immobilisation of the protein on streptavidin-coated tips. Protein concentration at the surface was 1 nM. The biosensor was exposed to buffer for another 35 sec before being dipped in a 103.6 nM (= 159.5 µg/l) solution of GM1. Complex formation was monitored in real time over 120 sec. Finally, the biosensor was moved to buffer one last time and dissociation of the protein-GM1 complex was monitored over 95 sec. A reference well devoid of attached ligand but exposed to the same ganglioside concentration was used to measure the effect of analyte passing through the cell, i.e. when the concentration of unbound analyte remained constant. Data were collected as sensorgrams representing the evolution of the shift in the interference pattern over time. The reference well was subtracted from the raw data and the data obtained was then Y- and X-aligned (i.e. the curves were zeroed on baseline and the starts of injection were aligned with respect to each other).

2.14 Generation of antigen-binding fragments (Fab)

The monoclonal antibody (mAb) M40-1 was expressed in mouse hybridomas as explained. It was fragmented using Pierce Fab preparation kit following the manufacturer's instructions: 3.8 mg of IgG diluted to a total volume of 500 µl in PBS were incubated in presence of papain for 5 h at 37 °C in an end-over-end mixer. The sample was then loaded on an immobilised protein A column, and unbound Fab fragments were eluted with PBS. Crystallisable fragments (Fc) and intact IgG were later detached from the column using the elution buffer provided with the kit (Figure 2-10). Samples collected following the different elution washes were separated by SDS-PAGE following mixture 1:1 with reducing sample buffer and then maintained at room temperature or heated at 95 °C for 10 min.

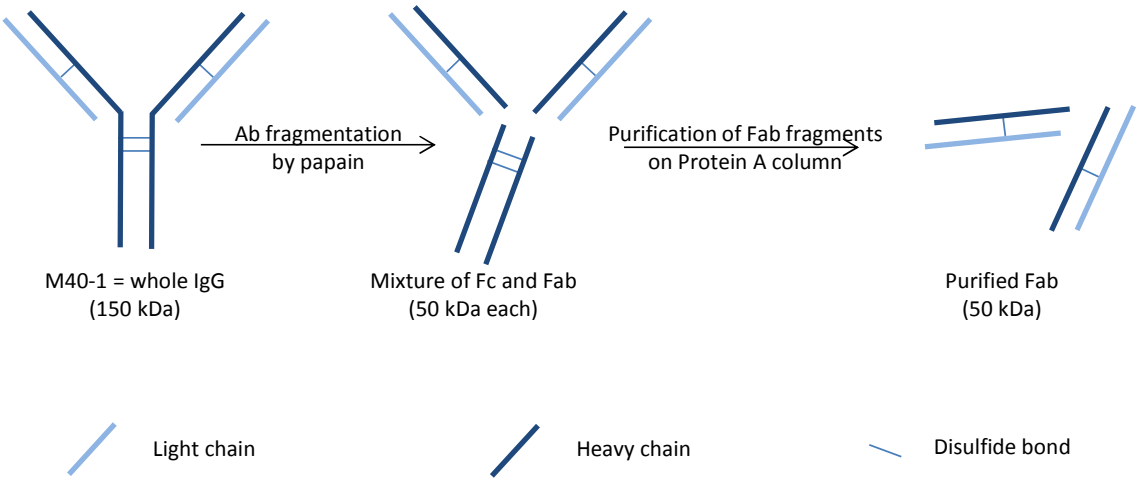

Figure 2-10 – Generation of Fab fragments by enzymatic cleavage. The IgG is digested by papain and the resulting mixture of Fc and Fab fragments is run on a protein A column, which retains only the Fc fragments and potential undigested IgG.

After purification, the Fab concentration was assessed by measuring the absorbance of the sample at 280 nm using an extinction coefficient of ε = 1.4.

PE and Fab (M40-1) were then mixed in a 1:1 ratio and the resulting sample was subsequently loaded on FPLC gel filtration column for purification of the complex.

2.15 Protein uptake by non-polarised epithelial cells

Caco-2 cells were cultured in complete growth medium on 12 mm glass coverslips in 12-well plates at a density of ~10 x10^4 cells/ml. After 48-72 h, cells were washed with fresh medium twice and 20 µg of protein diluted in 100 µl fresh medium was applied on the cells. For each assay, final molar concentrations are detailed individually in the corresponding Results section. Following 2 h incubation at 37 °C, cells were washed three times with PBS in order to remove excess protein and fixed using 4% (w/v) paraformaldehyde (PFA) in PBS for 20 min. When the Golgi network was visualised, cells were subsequently permeabilised and blocked in 5% BSA in PBS containing 0.5% Triton X-100 for 1 h at RT and incubated with an anti-GM130 antibody diluted in 3% BSA in PBS containing 0.5% Triton X-100 overnight at 4 °C (Appendix 2, Table 9-2). After being washed three times with PBS, cells were incubated with an Alexa Fluor® 568 (A568)-conjugated anti-rabbit secondary antibody diluted in 3% BSA in PBS + 0.5% Triton X-100 for 1 h at RT (Appendix 2, Table 9-3), washed again and treated with 4',6-diamidino-2-

phenylindole (DAPI) for 20 min before being mounted on microscope slides. Finally, samples were observed under confocal microscope (Section 2.18).

For competition assays, 20 µg of each cholera toxin B subunit (CTB) (final concentration = 3.5 µM) and protein diluted in 100 µl complete medium were simultaneously applied to the cells for 2 h. When applicable, cells were pre-incubated with 1 U/ml neuraminidase for 15 min or 2 h at 37 °C. A solution containing the protein(s) and 1 U/ml neuraminidase was then applied to the cells for 2 h.

2.16 *In vitro* transport assay in polarised epithelial cells

2.16.1 Transcytosis

Caco-2 cells were plated on Transwell® filters (polycarbonate membrane, 12 mm, 0.4 µm pore size) at a density of 70,000 cells/well and grown in 500 µl complete growth medium for 14-21 days. The volume of medium applied to the basolateral compartment was 1 ml. Transepithelial electrical resistance (TEER) was measured using EVOM2 epithelial voltohmmeter and cells were considered polarised when TEER > 350 $\Omega \cdot cm^2$. Both apical and basolateral compartments were then washed twice with HBSS, and cells were left to equilibrate in HBSS for 30 min at 37 °C. The protein was then diluted in 300 µl HBSS and applied to the apical compartment of the filters and to a blank well (filter with no cells) in order to assess the effect on the polycarbonate semi-permeable membrane on protein transport. HBSS from the basolateral well was collected at t = 15, 30, 60, 120 and 240 min of incubation and replaced each time with fresh medium. Total basolateral HBSS volume was kept constant at 600 µl. Each sample collected was plated in triplicate (90 µl) in a black 96-well plate (to minimise fluorescence background), using HBSS as a blank, and fluorescence intensity was measured using a fluorescence microplate reader. Excitation and emission filters are indicated in Table 2-6.

Table 2-6 – Excitation and emission filters used for quantification of Alexa Fluor®-labelled proteins used in this study with a microplate reader.

Alexa Fluor® dye	Excitation max (nm)	Emission max (nm)	Excitation filter (nm)	Emission filter (nm)
A488	496	519	480	520
A568	578	603	540	610

2.16.2 Dextran permeability

Dextran is a polymer of glucose which is unable to transport efficiently across polarised epithelial barriers. Therefore, it can be used to assess monolayer integrity by monitoring permeability across Caco-2 cells cultured on Transwell® filters. Dextran labelled with a fluorescent dye (e.g. fluorescein isothiocyanate (FITC)-labelled dextran) was applied to the apical cell surface, and measurement of the amount that transported to the basal compartment provided information about the integrity of the cell monolayer.

After the last time point of a transport study was collected, the filters were washed and 200 µl of 0.5 mg/ml 4 kDa FITC-dextran were added to the apical compartment. Cells were then incubated for 30 min at 37 °C, with the medium from the basal compartment collected and its fluorescence intensity measured (excitation and emission filters: 480 nm and 520 nm, respectively).

2.16.3 Cell preparation for confocal microscopy

Following transcytosis and evaluation of dextran permeability, Transwell® filters were rinsed three times with PBS and cells were fixed in 4% PFA for 20 min at RT. After another three washes in PBS, cell nuclei were stained with DAPI for 20 min at RT. Membranes were then cut off the wells and mounted on microscope slides.

2.16.4 Analysis

Dextran fluorescence intensities of each sample well (F_{Dex}), a blank well (no cells) ($F_{Dex,blank}$) and background HBSS ($F_{background}$) were measured using a microplate reader and used to calculate a relative permeability factor (P) defined by:

$$\boldsymbol{P} = \frac{\boldsymbol{F_{Dex}} - \boldsymbol{F_{background}}}{\boldsymbol{F_{Dex,blank}} - \boldsymbol{F_{background}}}$$

P allows for the normalisation of fluorescence values obtained for each well with regards to the well's dextran permeability. Therefore, the basolateral fluorescence ($F_{protein}$) due to protein transport across the monolayer is calculated from the measured fluorescence (F) and defined by:

$$\boldsymbol{F_{protein}} = (\boldsymbol{F} - \boldsymbol{F_{background}}) - ((\boldsymbol{F} - \boldsymbol{F_{background}}) * \boldsymbol{P})$$

2.17 *In vivo* transport assay in rat small intestine

2.17.1 Transepithelial transport assay

Adult (7-8 weeks old) male Wistar rats (250-300 g) were anesthetised using 5% isoflurane and maintained in an anesthetised state using 4% isoflurane (administered by mask) during surgery. A midline abdominal incision was made in order to expose the gastrointestinal system. A dose of 1.86 $x10^{-9}$ mol protein was injected into the lumen of the small intestine as a 50 µl bolus in PBS. After 5-10 min, animals were euthanized using CO_2 and a 2 cm tissue section originating at the injection site was collected, cut longitudinally and washed free of luminal contents with PBS. Each segment was then fixed overnight in 4% PFA in PBS at 4 °C.

2.17.2 Immunohistochemistry

Fixed tissue samples were dehydrated by successive 2 h-immersions in diluted ethanol solutions (70, 80, 90 and 100% ethanol). They were then immersed in paraffin for 2 h twice before being embedded and placed overnight at 4 °C. Sections of small intestine (5 µm) were subsequently cut using a microtome and mounted onto polylysine slides that were left to dry overnight at RT.

Paraffin-embedded tissues were rehydrated by successive 5-min immersions into Histoclear (solution 1), Histoclear (solution 2), and 100%, 90%, 80%, 70% ethanol solutions. They were then washed three times with PBS for 5 min. Antigen retrieval was achieved by immersing the slides into boiling 10 mM sodium-citrate buffer at pH 6.0 for 10 min. Tissue sections were washed three times with PBS for 5 min, permeabilised for 30 min at RT using 0.2% Triton X-100 in PBS and blocked with 2% BSA in PBS for 1 h at RT. Finally, they were incubated overnight at 4 °C in a humidified container with primary antibodies diluted into PBS containing 0.1% Triton X-100 and 1% BSA (Appendix 2, Table 9-2).

Slides were washed again in PBS and tissue sections were incubated for 2 h at RT with fluorescent secondary antibodies diluted in PBS containing 0.1% Triton X-100 (Appendix 2, Table 9-3). Following another three washes in PBS, slides were incubated with DAPI for 30 min at RT and rinsed again. Water was used for the last wash in order to remove any remaining salts. Slides were finally dehydrated by successive immersion into 70% and

100% ethanol for a few minutes each, Histoclear 1 for 5 min, 100% ethanol, and mounted using Vector Shield mounting medium.

2.18 Confocal microscopy

Confocal fluorescent images were obtained using a Zeiss LSM 510 META confocal laser scanning fluorescence microscope with a 63x objective. Sequential excitation at 405 nm, 488 nm and 543 nm was achieved using a laser diode and argon and helium-neon (HeNe) gas lasers, respectively (Table 2-7). Emission filters BP420-480, BP505-530 and LP550 were used for collecting blue, green and red fluorescence, respectively. Maximum excitation and emission wavelengths (λ_{ex} and λ_{em}, respectively) for the fluorophores used are detailed in Table 2-8. Images were analysed using Zeiss LSM Image Browser software. The term co-localisation refers to the coincidence of green and red fluorescence, as measured by the confocal microscope.

Table 2-7 – Lasers used for observation of fluorescently-labelled samples in confocal microscopy.

Laser	Excitation line (nm)	Corresponding fluorophore
Diode	405	DAPI
Argon/2	458, 477, 488, 514	GFP, fluorescein (FITC), A488
HeNe	543	A546, A568

Table 2-8 – Maximum excitation and emission wavelengths of the various fluorophores used in confocal microscopy.

Fluorophore	λ_{ex} (nm)	λ_{em} (nm)
DAPI	358	461
GFP	488	509
FITC	490	525
A488	490	525
A546	556	573
A568	578	603

2.19 FlexPred, Protparam and ProtScale

FlexPred is an online software which predicts, from a protein sequence or crystal structure, amino acid residues within a protein that are likely to be involved in conformational changes due to high flexibility [196, 197]. Here, the crystal structure of PE and cholix (PDB_ID: 1IKQ and 2Q5T, respectively) were submitted for estimation of amino acids that could be involved in the conformational changes experienced by these proteins.

ProtParam and ProtScale are also both online software applications. ProtParam was used to calculate the molecular weight and isoelectric point (pI) values of the various truncated and GFP-tagged versions of PE and cholix [181]. ProtScale was used to calculate and represent the profiles produced by three amino acid scale on PE and cholix from each protein's sequence. The scales "% buried residues", "% accessible residues" [198] and "Average flexibility" [199] were here of interest to gain information about the conformational change undergone by these two toxins.

2.20 Statistical analysis

The statistical significance of the data obtained was tested using either an unpaired t-test (for comparison of two groups of data) or a 1-way ANOVA followed by Tukey post-hoc test. P values < 0.05 were considered to be statistically significant.

2.21 Reagents and Materials

Table 2-9 – Table of reagents.

Reagent	Catalogue Number	Supplier
4´,6-diamidino-2-phenylindole, dilactate (DAPI, dilactate)	D3571	Invitrogen, Paisley, UK
8-Anilinonaphthalene-1-sulfonic acid (ANS)	A1028	Sigma-Aldrich, Dorset, UK
Acrylamide/bis-acrylamide, 40% solution	A7802	Sigma-Aldrich, Dorset, UK
AcTEV Protease	12575	Invitrogen, Paisley, UK
AflII restriction endonuclease	R0520	New England BioLabds, Herts, UK
Agarose	BP-1356	Fisher Scientific, Loughborough, UK
Alexa Fluor® C_5 maleimide 488	A-10254	Invitrogen, Paisley, UK
Alexa Fluor® C_5 maleimide 546	A-10258	Invitrogen, Paisley, UK
Alexa Fluor® C_5 maleimide 568	A-20341	Invitrogen, Paisley, UK
Alexa Fluor® 546-conjugated anti-rabbit IgG (donkey)	A-10004	Invitrogen, Paisley, UK
Alexa Fluor® 568-conjugated anti-rabbit IgG	A10042	Invitrogen, Paisley, UK
Ampicilin for LB media	BP-1760	Fisher Scientific, Loughborough, UK
Ammonium persulfate	A/P470/46	Fisher Scientific, Loughborough, UK
Anti-Cho386 GS TEV antibody		INNOVAGEN AB, Lund, Sweden
Anti-GM130 antibody	Ab52649	Abcam, Cambridge, UK
Anti-hGH antibody	AF1067	R&D Systems, Abington, UK
Anti-*Pseudomonas* exotoxin A whole antiserum	P2318	Sigma-Aldrich, Dorset, UK

Arginine	W381918	Sigma-Aldrich, Dorset, UK
β-Mercaptoethanol	63689	Sigma-Aldrich, Dorset, UK
Bovine Serum Albumin (BSA)	A7906	Sigma-Aldrich, Dorset, UK
Butanol	B/4800/08	Sigma-Aldrich, Dorset, UK
Caco-2 cells, C2BBe1 clone	CRL-2102	ATCC, Teddington, UK
Cholera toxin B subunit	C9903	Sigma-Aldrich, Dorset, UK
Cholera toxin B subunit, Alexa Fluor™ 488 conjugate	C22841	Invitrogen, Paisley, UK
cOmplete EDTA-free protease inhibitors	11873580001	Roche Diagnosted Ltd., Burgess Hill, UK
Coomassie brilliant blue R-250	BP101	Fisher Scientific, Loughborough, UK
Coomassie Plus (Bradford) Assay Reagent	23238	Fisher Scientific, Loughborough, UK
DH5α competent cells	C2987	New England BioLabds, Herts, UK
Dialysis tubing SnakeSkin, 10 kDa	10781755	Fisher Scientific, Loughborough, UK
Dithiothreitol (DTT)	R0862	Fisher Scientific, Loughborough, UK
DMEM cell culture medium	41965039	Invitrogen, Paisley, UK
DMSO	D1435	Sigma-Aldrich, Dorset, UK
DNA gel loading dye	B7021S	New England BioLabds, Herts, UK
ECL Western Blotting Detection Reagent	RPN2209	GE Healthcare, Amersham, UK
EcoRI-HF® restriction endonuclease	R3101	New England BioLabds, Herts, UK
Ethanol	32221	Sigma-Aldrich, Dorset, UK
Ethidium bromide	E1510	Sigma-Aldrich, Dorset, UK
Ethylenediaminetetraacetic acid (EDTA)	BP118	Fisher Scientific, Loughborough, UK

EZ-Link® Maleimide-PEG_2-Biotin reagent	21901BID	Fisher Scientific, Loughborough, UK
Fermentas PageRuler™ Prestained Protein Ladder (10-170 kDa)	26616	Fisher Scientific, Loughborough, UK
Fluorescein-conjugated anti-goat IgG (rabbit)	FI-5000	Vector Laboratories Ltd., Peterborough, UK
Fluorescein Isocyanate (FITC) Dextran, 4 kDa	FD4	Sigma-Aldrich, Dorset, UK
Foetal bovine serum, heat-inactivated (FBS)	16000036	Invitrogen, Paisley, UK
Glacial acetic acid	27225	Sigma-Aldrich, Dorset, UK
Glutathione, oxidised	G4376	Sigma-Aldrich, Dorset, UK
Glycine	BP381-1	Fisher Scientific, Loughborough, UK
Guanidine hydrochloride	BP178-500	Fisher Scientific, Loughborough, UK
Hanks' Balanced Salt Solution (HBSS), 1X	14025050	Invitrogen, Paisley, UK
Heat inactivated foetal bovine serum	10500-064	Invitrogen, Paisley, UK
Histo-Clear	HS-200	National Diagnostics,
HRP-liked anti-mouse IgG	NXA931	GE Healthcare, Amersham, UK
HRP-linked anti-rabbit IgG	NA934	GE Healthcare, Amersham, UK
Hydrochloric acid	07102	Sigma-Aldrich, Dorset, UK
Imidazole	301870010	Fisher Scientific, Loughborough, UK
IsoFlo® (isoflurape, USP)	05260-05	Abbott Laboratories, Maidenhead, UK
Isopropyl β-D-1-thiogalactopyranoside (IPTG)	BPE1755	Fisher Scientific, Loughborough, UK
L-Arginine	W381918	Sigma-Aldrich, Dorset, UK

L-cysteine	168149	Sigma-Aldrich, Dorset, UK
L-Glutathione, oxidized	G4376	Sigma-Aldrich, Dorset, UK
Lyso-monosialoganglioside, lysoGM1	G5660	Sigma-Aldrich, Dorset, UK
Lysozyme chloride	L2879	Sigma-Aldrich, Dorset, UK
M40-1 antibody		David FitzGerald, NIH/NCI, MD, USA
Methanol	34860	Sigma-Aldrich, Dorset, UK
Monosialoganglioside, GM1	G7641	Sigma-Aldrich, Dorset, UK
Mounting medium, Vectashield®	H-1000	Vector Laboratories Ltd., Peterborough, UK
Neuraminidase	N2876	Sigma-Aldrich, Dorset, UK
NdeI restriction endonuclease	R0111	New England BioLabds, Herts, UK
Non-fat dry milk		Morrisons
NuPAGE™ LDS Sample Buffer (4X)	NP0007	Invitrogen, Paisley, UK
NuPAGE™ Sample Reducing Agent	NP0009	Invitrogen, Paisley, UK
One Shot™ BL21 Star™ (DE3) chemically competent cells	C6010	New England BioLabs, Herts, UK
Tissue-Tek V.I.P.™ Paraffin	62580-08	Science Services, Munich, Germany
Paraformaldehyde	P6148	Sigma-Aldrich, Dorset, UK
Penicillin/Streptomycin	P0781	Sigma-Aldrich, Dorset, UK
pHGH107 plasmid	31538	ATCC, Teddington, UK
Phosphate Buffer Saline (PBS)	BR0014G	Fisher Scientific, Loughborough, UK
Phusion High-Fidelity DNA Polymerase	M0530	New England BioLabs, Herts, UK
Primer synthesis		Sigma-Aldrich, Dorset, UK

Protease Inhibitor Cocktail III Animal Free for Mammalian Cells	P2302-1	Fisher Scientific, Loughborough, UK
Rat tail collagen I	A10486-01	Invitrogen, Paisley, UK
RPMI 1640 cell culture medium	A1049101	Invitrogen, Paisley, UK
Shuffle competent cells	C3026	New England BioLabds, Herts, UK
SilverXpress® Silver staining kit	LC6100	Invitrogen, Paisley, UK
Sodium chloride	S9625	Sigma-Aldrich, Dorset, UK
Sodium citrate, dehydrate	W302600	Sigma-Aldrich, Dorset, UK
Sodium dodecyl sulphate (SDS)	S/5200/53	Fisher Scientific, Loughborough, UK
Sodium phosphate, dibasic	71636	Sigma-Aldrich, Dorset, UK
Sodium phosphate, monobasic	71507	Sigma-Aldrich, Dorset, UK
SpeI-HF® restriction endonuclease	R3133	New England BioLabds, Herts, UK
Sucrose	16104	Sigma-Aldrich, Dorset, UK
TEMED	T/P190/04	Fisher Scientific, Loughborough, UK
Tris	T6066	Sigma-Aldrich, Dorset, UK
Tri-sodium citrate, dihydrate	S1804	Sigma-Aldrich, Dorset, UK
Triton X-100	X100	Sigma-Aldrich, Dorset, UK
Trypsin (protein digestion)	T1426	Sigma-Aldrich, Dorset, UK
Trypsin, 10X (cell culture)	SV30037.01	Fisher Scientific, Loughborough, UK
Tryptone	T1332	Fisher Scientific, Loughborough, UK
Tween-20	P1379	Sigma-Aldrich, Dorset, UK
Urea	U5378	Sigma-Aldrich, Dorset, UK
Vectashield® mounting medium	H-1000	Vector Laboratories Ltd, Peterborough, UK
Yeast Extract	BP1422	Fisher Scientific, Loughborough, UK

Table 2-10 – Table of materials.

Material	Catalogue number	Supplier
AccuSpin™ 400 Benchtop centrifuge	FB56652	Fisher Scientific, Loughborough, UK
ÄKTA Explorer FPLC system		GE Healthcare, Amersham, UK
BioSep-SEC-s3000 GF HPLC column		Phenomenex Inc., Macclesfield, UK
Centrifure J2-MC		Beckman Coulter Ltd., High Wicombe, UK
Chromera Chromatography Data System V 3.3.0		Perkin Elmer Inc., West Midlands, UK
Confocal laser scanning microscope	LSM 510 META	Carl Zeiss Ltd., Cambridge, UK
Costar® 10 ml Stripette® Serological Pipets, Sterile	4488	Corning B.V. Life Sciences, Amsterdam, The Netherlands
Coverslips, glass, 12 mm diameter	A67761333	Fisher Scientific, Loughborough, UK
Dialysis flask, 10K MWCO, 250mL	87762	Fisher Scientific, Loughborough, UK
Dialysis tubing 10 kDa	68100	Fisher Scientific, Loughborough, UK
Disposable gel cassette, 1 mm	NC2010	Invitrogen, Paisley, UK
Disposable PD10 Desalting columns	17-0851-01	GE Healthcare, Amersham, UK
Evom^2 epithelial voltohmmeter	EVOM2	World Precision Instruments, Hitchin, UK
Extra thick blot paper	1703966	Bio-rad, Hertfordshire, UK
F-4500 fluorescence spectrophotometer		Hitachi Ltd., Tokyo, Japan

Fab preparation kit	10269923	Fisher Scientific, Loughborough, UK
Fixed angle rotor JA10		Beckman Coulter Ltd., High Wicombe, UK
Fixed angle rotor JA14		Beckman Coulter Ltd., High Wicombe, UK
Fixed angle rotor JA20		Beckman Coulter Ltd., High Wicombe, UK
Flexar HPLC system		Perkin Elmer Inc., West Midlands, UK
Fuji X-Ray film	2731261	Fisher Scientific, Loughborough, UK
Gel Cassette Combs, 1.0 mm, 12 well	NC3012	Invitrogen, Paisley, UK
Gel Cassette Combs, 1.0 mm, 15 well	NC3015	Invitrogen, Paisley, UK
Gel Cassette Combs, 1.0 mm, 10 well	NC3010	Invitrogen, Paisley, UK
Glass coverslips	BB018018A0D3	Thermo Scientific Gerhard Menzel
Glass pasteur pipette	FB502553	Fisher Scientific, Loughborough, UK
GeneJET™ Gel Extraction Kit	K0691	Fisher Scientific, Loughborough, UK
GeneJET™ Plasmid Miniprep	K0502	Fisher Scientific, Loughborough, UK
Haemocytometer	AC1000	Hawksley, Lancing, UK
Hellma® fluorescence cuvettes	Z802433	Sigma-Aldrich, Dorset, UK
HisTrap FF column for ÄKTA FPLC system, 1 ml	17-5319-01	GE Healthcare, Amersham, UK
HisTrap HP Crude column for ÄKTA FPLC system, 5 ml	17-5248-01	GE Healthcare, Amersham, UK
HiTrap Protein G HP column for ÄKTA FPLC system, 1 ml	17040403	GE Healthcare, Amersham, UK
HiTrap Q HP column for ÄKTA FPLC system, 1 ml	17-1153-01	GE Healthcare, Amersham, UK

ImmEdge hydrophobic barrier pen	H-4000	Vector Laboratories Ltd, Peterborough, UK
Membrane filter ultrafiltration, 1 kDa NMWL	PLAC06210	Fisher Scientific, Loughborough, UK
Microplate reader, FluoStar Omega		BMG LABTECH Ltd., Bucks, UK
Microtome	Biocut 2035	Leica Microsystems (UK) Ltd., Milton Keynes, UK
Microscope slide Polysine adhesion	J2800AMNZ	Fisher Scientific, Loughborough, UK
Millipore 0.45 µm filters	FDR-050-071N	Fisher Scientific, Loughborough, UK
Millipore 10 kDa MWCO spin filter, 15 ml	UFC901008	Fisher Scientific, Loughborough, UK
Millipore 10 kDa MWCO spin filter, 4 ml	UFC801024	Fisher Scientific, Loughborough, UK
Millipore 100 kDa MWCO spin filter	UFC810024	Fisher Scientific, Loughborough, UK
Minisart® high flow Syringe filters, 0.2 µm	16532	Sartorius UK Ltd., Surrey, UK
NanoDrop™ 2000c	ND2000c	Fisher Scientific, Loughborough, UK
Nunc® cell culture-treated 12-well plate	150628	Fisher Scientific, Loughborough, UK
Nunc® cell culture-treated 24-well plate	142475	Fisher Scientific, Loughborough, UK
Nunc® cell culture-treated 6-well plate	140675	Fisher Scientific, Loughborough, UK
Nunc® CryoTubes®, 1 ml	Z763659	Fisher Scientific, Loughborough, UK
Nunc® MicroWell™ 96-well microplates	167008	Fisher Scientific, Loughborough, UK
N-terminal protein sequencing		Abington Health Laboratory Services,

		Birmingham, UK
Octet® RED96 instrument		Pall ForteBio Corp., CA, USA
Polypropylene tube for ultracentrifuge, 3.2 ml	362333	Beckman, High Wycombe, UK
Prism 4 software		GraphPad Software Inc., CA, USA
PVDF membrane, 0.2 µm	88520	Fisher Scientific, Loughborough, UK
Quick Ligation Kit	M2200	New England BioLabs, Herts, UK
Slide-A-Lyser MINI Dialysis Device, 10 KDa MWCO, 0,5 ml	88401	Fisher Scientific, Loughborough, UK
Sonicator 102c and Sonifier 250		Branson Ultrasonics, Danbury, UK
Sponge pad for blotting	EI9052	Invitrogen, Paisley, UK
Sterilin polystyrene tubes, sterile	128B/FS	Fisher Scientific, Loughborough, UK
Stirred ultrafiltration cell	5123	Fisher Scientific, Loughborough, UK
Superdex™ 200 HR10/30	17-1088-01	GE Healthcare, Amersham, UK
Syringe filter, 0.45 µm	SLHA033SS	Fisher Scientific, Loughborough, UK
Syringe needles, gauge 27, L 1 ¼ in., BD Precisionglide®	Z192376	Sigma-Aldrich, Dorset, UK
T100™ Thermal cycler for PCR	186-1096	Bio-rad, Hertfordshire, UK
Tissue culture flask TripleFlasks, 500 cm^2	132913	Fisher Scientific, Loughborough, UK
Tissue culture flask, 175 cm^2	159910	Fisher Scientific, Loughborough, UK
Tissue culture flask, 25 cm^2	156367	Fisher Scientific, Loughborough, UK
Tissue culture flask, 75 cm^2	156499	Fisher Scientific, Loughborough, UK
Tissue Master 240		Omni International, Kennesaw, GA, USA
Tissue Master 240 homogeniser		Omni International, kennesaw, GA, USA

Tissue processor	TP 1020	Leica Microsystems (UK) Ltd., Milton Keynes, UK
Transwell polycarbonate membrane, 12 mm, 0.4 μm	CLS3401	Sigma-Aldrich, Dorset, UK
Vivaflow 200	VFS204	Vivascience, Goettingen, Germany
Vivaflow 200, PES membrane, 30 kDa MWCO	VF20P2	Vivascience, Goettingen, Germany
Wax embedder	EG 1150 c	Leica Microsystems (UK) Ltd., Milton Keynes, UK
Whatman® Anatop® 10 syringe filter, 0,1 μm, 10 mm	WHA68091012	Sigma-Aldrich, Dorset, UK
XCell II™ Blot Module	EI9051	Invitrogen, Paisley, UK
XCell™ *Sure Lock*® Mini-cell electrophoresis system	EI0001	Invitrogen, Paisley, UK
X-ray film developer		Photon Imaging Systems, Swindon, UK
Zeba® Desalting Spin Column, 7 Kda MWCO, 2ml	89890	Fisher Scientific, Loughborough, UK
Zeba® Desalting Spin Column, 7 Kda MWCO, 5ml	89892	Fisher Scientific, Loughborough, UK
Zetasizer Nano S		Malvern Instruments Ltd., Malvern, UK

3 RESULTS 1 – PE CONFORMATIONAL CHANGE

3.1 Introduction

Although major steps of the *Pseudomonas aeruginosa* exotoxin A (PE) intoxication pathway have now been elucidated, the potential for a pH-induced conformational change experienced by the protein in the endosomes and its implications in terms of protein translocation across polarised epithelial cells remain obscure.

It is now widely acknowledged that domain II is responsible for translocation of the toxin across membranes [159, 160, 200]. Domain II of PE comprises amino acids 253-364 and is made of six α-helices (Figure 3-1)[158]. Helices B (Glu282-Ala301) and E (Pro333-Gly354) are long enough to span a membrane [201], although domain II does not contain any hydrophobic stretches that could explain how PE inserts into lipidic membranes [202], as in the case of DT where the B fragment becomes hydrophobic at low pH, driving the A fragment of the protein into the cytosol [203, 204]. Helices A (Leu267-Arg274), C (Ser304-Ser318), D (Gly322-Glu331) and F (358-364) are much shorter, and while deletion of any of the helices A-E was shown to significantly impair the translocation process, removing helix F actually enhanced it [205].

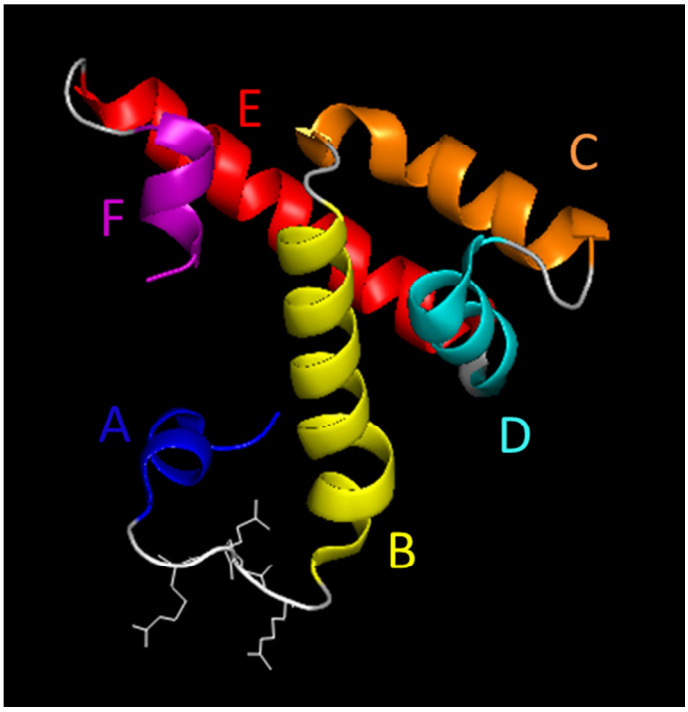

Figure 3-1 – Ribbon representation of PE translocation domain. α-helices are lettered and the white loop carries the four residues constituting the furin cleavage site (RQPR). The figure was generated using PyMOL [128].

Although researchers were, at the time, looking for an explanation to PE's entry into non-polarised cells, a pH-induced conformational change within domain II was first suggested in the late 1990s [150, 206, 207]. Since, several techniques such as measurement of tryptophan intrinsic fluorescence [150], trypsin digest [202, 206], detergent affinity and insertion into vesicles [150, 154, 206, 207], and ^{125}I-labelling [202] have been employed to investigate how this structural rearrangement happened.

Several hypotheses have been advanced. Méré *et al* (2005) put forward a mechanism involving an N-cap residue and a "membrane anchor" which would explain how PE could translocate directly from endosomes to ER. At neutral pH, Trp305 is buried into a hydrophobic pocket closed by helix F. Following access to the endosomal compartment and a drop in pH, Asp358 (the N-cap residue of helix F proposed here to act as a pH sensor) would become protonated. As a result, helix F would be destabilised and the side chain of Trp305 (membrane anchor) would become exposed to a more hydrophilic environment, leading to its insertion into the endosomal membrane [208] and, somehow, to the transport of the entire protein through the membrane to the ER. As several trafficking routes have previously been suggested for PE (Section 1.2.3), this mechanism would be applicable only in a scenario in which PE would use the Rab9-independent pathway to bypass the LE and reach the Golgi directly from the early endosome [142].

Using a refined crystallographic structure of PE, Wedekind *et al* (2001) suggested that various ionic interactions within domain I and II might control the toxin's pH-induced conformational change [209]. Although it is now acknowledged that PE undergoes this structural reorganisation when the pH drops below pH 6.0, the aforementioned authors rightly pointed out that whether the conversion occurs as a localised perturbation of the furin cleavage site or in a more "global" dissociation of domain I from domain II remains unknown. Simulations involving individual protonation of the carboxyl groups of His, Asp or Glu side chains did not show any significant perturbation within the protein structure. Therefore, Wedekind *et al* concluded from these studies that such a conformational change couldn't result from the protonation of a single residue within the protein. Thus, these authors proposed that a combination of destabilisations (due to protonation of several amino acids) might be more likely to trigger the observed transformation.

However, experimental data corroborating any of these theories has yet to be published. The aim of the work presented in this chapter was to investigate the modifications in the protein structure which lead to this conformational change. A thorough characterisation of the behaviour of PE would be invaluable to understand how large and hydrophilic molecules may translocate to the cytosol and to elucidate PE's transcytosis pathway. In fact, a similar conversion is thought to take place in the endosomes of polarised cells and could be a major step in getting the protein across the epithelial barrier. Further characterisation of this conversion was attempted by comparing and combining data obtained at neutral and acidic pH by various techniques, including trypsin digestion, DLS, HPLC and eventually by preparing samples in an attempt to crystallise PE in acidic conditions.

3.2 Methods

Determination of possible trypsin cleavage sites from digestion fragments

Following digestion of PE GS TEV mutants by trypsin, the size of the resulting fragments was used to estimate potential cleavage sites. The protein sequence (PDB_ID: 1IKQ) was run into PeptideCutter and only digestion sites with a 100% cleavage probability were displayed [183]. The molecular weight of the resulting fragments was then calculated with ProtParam [181].

3.3 Results and discussion

3.3.1 Protein expression and purification

3.3.1.1 Expression and purification of ntPE

pVC45D encodes a non-toxic version of PE lacking the Glu553 codon [161]. It contains an OmpA signal sequence that triggers protein secretion into the bacterial periplasm. This method of protein expression is of particular interest for molecules which, like ntPE, contain disulphide bonds [210], as it provides a milieu that contributes to their proper folding. In fact, the environment in the periplasm is more oxidizing than in the cytoplasm, and it contains two foldases (disulphide oxidoreductase and disulphide isomerase) that catalyse the formation and isomerisation of disulphide bonds [211, 212].

After protein expression (into the periplasm) and fractionation of the periplasm, ntPE was purified in a two-phase procedure that included a first purification step using AE chromatography, followed by a polishing step involving size exclusion chromatography.

Protein loading on an AE column and elution with a gradient of NaCl resulted in the detection of two peaks of UV-absorbing materials (Figure 3-2 (A)). The first peak (~220 mAU) corresponded to the flow-through i.e. elements that did not interact with the column and were eluted before the NaCl gradient was applied to the system. The second peak (~230 mAU) corresponded to material eluted at 0.12 to 0.65 M NaCl (12 to 65% gradient). Fractions containing the compounds eluted in these two peaks were separated by SDS-PAGE (Figure 3-2 (B)).

In the flow-through fractions, a strong band was observed at ~72 kDa (fractions E_2 and E_3). This band could also be observed in the fractions corresponding to the eluted protein of interest. This suggests that some ntPE did not interact with the column and was eluted with the non-specific materials. This could be due to overloading of the column as suggested by the relatively high peak intensity for the flow-through. In this case, the flow-through fractions were re-run on the column in order to collect the excess protein and maximise the amount of protein purified. Fractions E_7-E_{10} were concentrated together down to 1 ml and loaded on a gel filtration column.

The resulting chromatogram showed a relatively broad peak that likely contained several sub-peaks (Figure 3-3 (A)). Collected fractions contained ntPE plus minor amounts of several discrete contaminants with molecular weight lower than ntPE (e.g. 45 kDa, 30 kDa) (Figure 3-3 (B)). Due to the relatively negligible proportion of these contaminants

compared to that of enriched full-length ntPE, fractions F_{10}-G_1 were combined and the purified protein was used for the following studies.

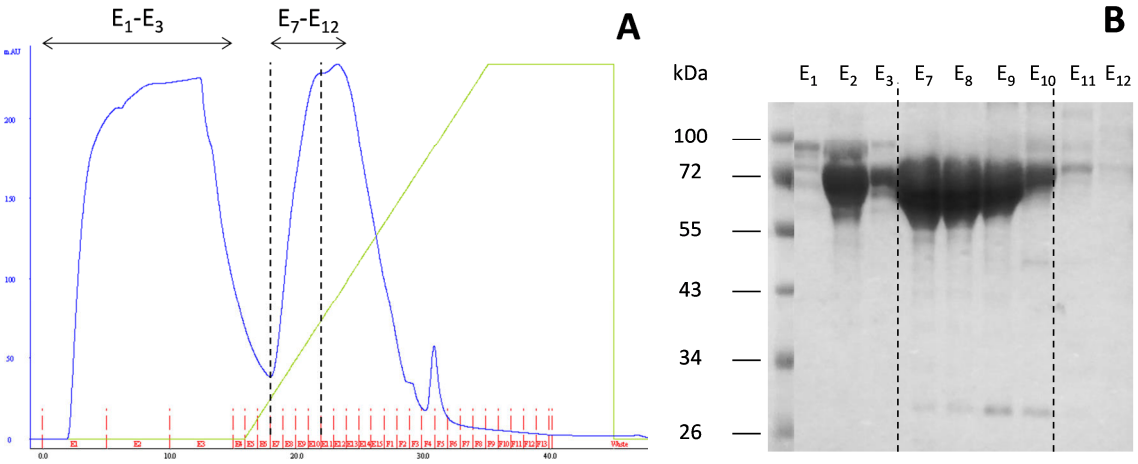

Figure 3-2 – Initial enrichment of ntPE by AE chromatography. (A) Chromatogram obtained for AE separation. (B) Coomassie-stained SDS-PAGE of fractions corresponding to the UV peaks. E-labelled lanes in (B) correspond to arbitrary tray row and column reference on the fraction collector and are illustrated by the red dashes on (A). Fractions covered by the arrow in (A) indicate the complete range of fractions displayed in (B). The black dotted lines marked on both (A) and (B) indicate the fractions containing ntPE that were collected.

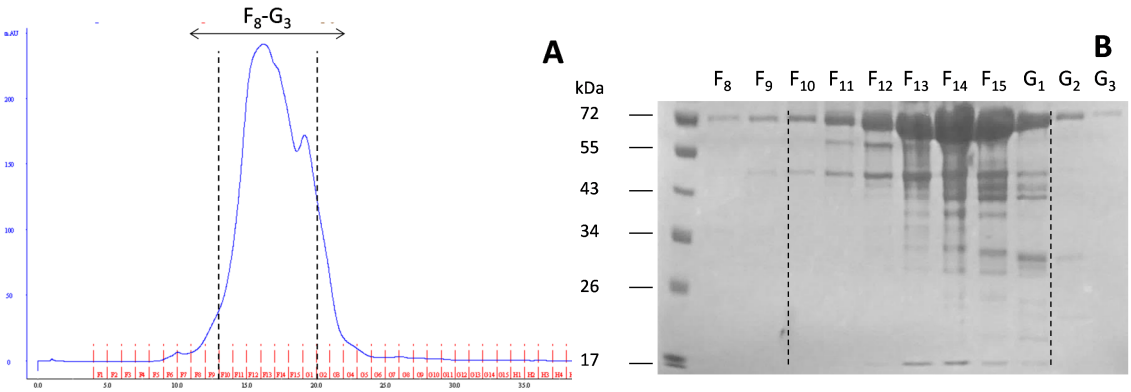

Figure 3-3 – Further enrichment of ntPE by GF chromatography. (A) Chromatogram obtained for GF column separation. (B) Coomassie-stained SDS-PAGE of fractions corresponding to the UV peak. F- and G-labelled lanes in (B) correspond to arbitrary tray row and column reference on the fraction collector and are illustrated by the red dashes on (A). Fractions covered by the arrow in (A) indicate the complete range of fractions displayed in (B). The black dotted lines marked on both (A) and (B) indicate the fractions containing ntPE that were collected.

3.3.1.2 Expression and purification of ntPE GS TEV and its mutants

The proteins described in this section were cloned by Dr Julia Mackay (engineering of the expression plasmids). Dr Emma Harvey contributed to their expression (isolation of inclusion bodies under supervision).

ntPE GS TEV is a modified version of ntPE that was engineered to contain the poly glycine-serine linker of SGSGSGSGS (5'-AGTGGTAGTGGTAGTGGTTCTGGTAGT-3') between the protein and a C-terminal TEV cleavage sequence (ENLFQS). This flexible linker was added to increase cleavage efficiency by making the digestion site more accessible to the TEV enzyme.

Five truncated versions of ntPE GS TEV were also produced: PE408 GS TEV, PE364 GS TEV, PE351 GS TEV, PE320 GS TEV and PE303 GS TEV. Numbers indicate the last amino acid of the truncated PE protein.

Truncations were engineered so that for each mutant, one or several helices of domain II were removed (Figure 3-4). The shortest mutant (PE303 GS TEV) contains helices A and B, PE320 GS TEV terminates after helix C, PE351 GS TEV contains helices A-E and PE364 GS TEV comprises all six helices A-F. The last mutant, PE408 GS TEV, was composed of all three domains Ia, II and Ib. The molecular weight and isoelectric point of each version of ntPE GS TEV were calculated using ExPASy ProtParam (Table 3-1) [181].

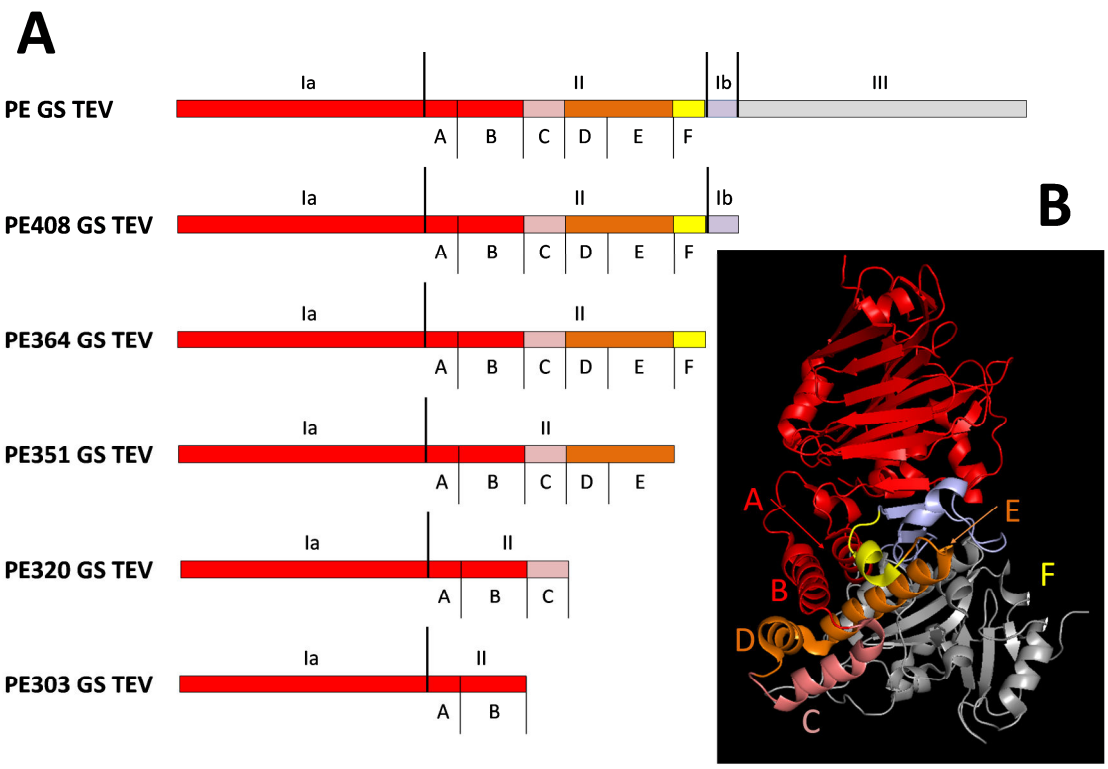

Figure 3-4 – (A) Schematic representation of the different versions of ntPE GS TEV used in this study. Note the deletion of E553 in domain III that renders PE non-toxic (ntPE). (B) Ribbon representation of PE highlighting the various helices in domain II. The figure was generated using PyMOL [128]. Letters A-F refer to the six α-helices of domain II.

Table 3-1 – Physicochemical properties of PE GS TEV truncated mutants. Both pI and molecular weight were calculated using ExPASy ProtParam [181].

Protein designation	Calculated pI	Calculated molecular weight (kDa)
ntPE GS TEV	5.28	66.7
PE408 GS TEV	5.28	44.4
PE364 GS TEV	5.86	40.1
PE351 GS TEV	5.97	38.9
PE320 GS TEV	6.33	35.6
PE303 GS TEV	6.33	33.8

While ntPE GS TEV was soluble, the truncated mutants were insoluble and had to be expressed as inclusion bodies, which are aggregates of misfolded protein, and subsequently refolded using a disulphide exchange shuffle buffer system (see below). A summary of the expression and purification outcomes is presented in Table 3-2.

Table 3-2 – Summary of expression and purification outcomes for PE GS TEV mutants.

Protein designation	Solubility	Expression protocol used	Purification	Yield
ntPE GS TEV	Soluble	Soluble	IX, GF	Good
PE408 GS TEV	Insoluble	Inclusion bodies	IX, GF	Medium
PE364 GS TEV	Insoluble	Inclusion bodies	IX, GF	Low
PE351 GS TEV	Insoluble	Inclusion bodies	IX, GF	Low
PE320 GS TEV	Insoluble	Inclusion bodies	IX, GF	Low
PE303 GS TEV	Insoluble	Inclusion bodies	IX, GF	Medium

Inclusion body formation results from the accumulation of partially folded proteins in the cytoplasm of *E. coli*, but it can also arise from the reducing environment of the cytoplasm that does not allow for the formation of disulphide bonds, which can be crucial for a protein to adopt its native, soluble and biologically active conformation [213].

After their collection and washing by repeated centrifugation to reduce lipopolysaccharide content, inclusion bodies were solubilised in guanidine-HCl, which promotes complete protein unfolding by disrupting intermolecular interactions [214], and DTT, which reduces disulphide bonds by thiol disulphide exchange [215]. The amount of solubilised protein was assessed by Bradford assay. A defined amount of total protein was then subjected to a di-sulphide shuffle buffer refolding method that utilized arginine and glutathione. Although its mechanism of action has not yet been elucidated, the presence of arginine seems to help protein refolding by reducing aggregation. It has been suggested that this amino acid could interact favourably with most amino acids' side chains, thereby reducing intermolecular interactions (e.g. hydrogen bonds, ionic, and hydrophobic interactions) between proteins [216]. For instance, Tsumoto *et al* (2004) reported that interaction between the guanidinium group of arginine and the side chain of tryptophan (which is normally buried in folded proteins but exposed to solvent in unfolded states)

contributes to increasing protein solubility by preventing misfolding and protein aggregation mediated by hydrophobic interactions [217]. It has also been proposed that arginine in refolding solutions could act as a "neutral crowder" that can slow protein association and dissociation by being preferentially excluded from protein-protein encounter complexes, but not from dissociated protein molecules [217, 218]. Oxidised glutathione (GSSG) reportedly promotes the formation of correct disulphide bonds by encouraging rapid "reshuffling" of improper disulphide bonds [213]. In the protocol used, the protein was added drop-wise and maintained at low concentration (< 100 µg/ml) during refolding to further reduce the chance of aggregation.

Following refolding, samples were dialysed in order to remove these low molecular weight compounds and purified using AE and GF chromatography. Presented below as examples are the chromatograms and an SDS-PAGE of column fractions obtained following purification of PE303 GS TEV. The protein was eluted from an AE column with a NaCl gradient. A single peak could be observed at 10-60% NaCl (= 0.1-0.6 M NaCl) (Figure 3-5 (A)).

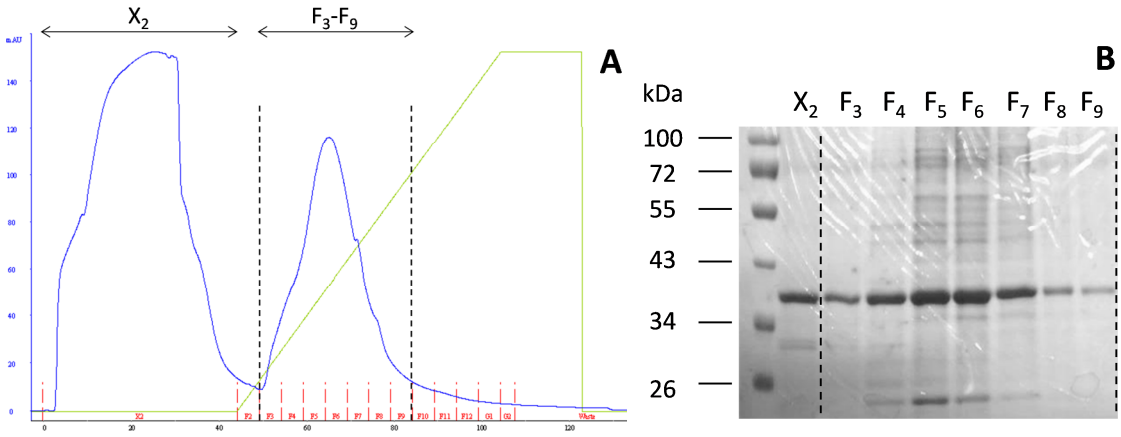

Figure 3-5 – Initial enrichment of PE303 GS TEV by AE chromatography. (A) Chromatogram obtained for AE separation. (B) Coomassie-stained SDS-PAGE of fractions corresponding to the UV peaks. X- and F-labelled lanes in (B) correspond to arbitrary tray row and column reference on the fraction collector and are illustrated by the red dashes on (A). Fractions covered by the arrow in (A) indicate the complete range of fractions displayed in (B). The black dotted lines marked on both (A) and (B) indicate the fractions containing PE303 GS TEV that were collected.

Fractions corresponding to this peak as well as the flow-through (molecules which were not retained by the column) were separated by SDS-PAGE (Figure 3-5 (B)). A band was observed for the flow-through at the same size as the protein. This band was relatively strong, and the presence of protein in the flow-through might have been due to column

overloading. In this case, the flow-through was re-run on the AE column. In the elution fractions, a single band was visible around 40 kDa for all fractions. These were concentrated together down to 1 ml for further purification by size exclusion chromatography (Figure 3-6 (A)).

Following the second purification step, fractions corresponding to the UV-absorbing material were separated by SDS-PAGE. As the UV peak obtained was less well defined, an SDS-PAGE of individual column fractions was used to assess the amount and purity of the protein of interest, providing the rationale for fractions that were pooled; for example, PE303 GS TEV was collected from fractions M_5-M_{11} (Figure 3-6 (B)). Analysis of the Coomassie-positive bands showed a dominant one visible at ~20 kDa in fractions M_{12}-M_{14}. Due to the presence of this contaminant, these fractions were not added to the final batch of enriched PE303 GS TEV.

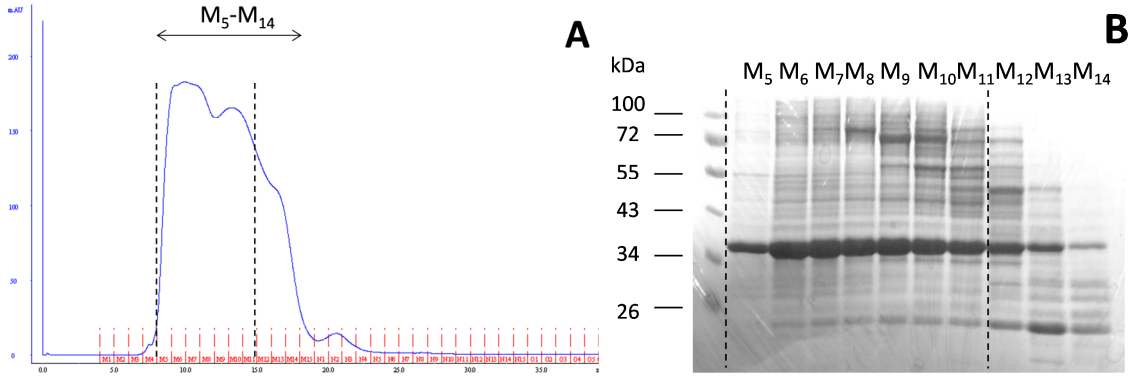

Figure 3-6 – Further enrichment of PE303 GS TEV by GF chromatography. (A) Chromatogram obtained for GF column separation. (B) Coomassie-stained SDS-PAGE of fractions corresponding to the UV peak. M-labelled lanes in (B) correspond to arbitrary tray row and column reference on the fraction collector and are illustrated by the red dashes on (A). Fractions covered by the arrow in (A) indicate the complete range of fractions displayed in (B). The black dotted lines marked on both (A) and (B) indicate the fractions containing PE303 GS TEV that were collected.

3.3.1.3 M40-1 expression and purification

M40-1 is a monoclonal antibody which targets a region located between residues 264-308 of the native protein and was expressed using mice hybridomas generated by Ogata *et al* (1991) [153]. After collection and concentration, the cell culture medium was first filtered to remove the dead cells and loaded on a Protein G column to isolate the IgG. Elution with a linear gradient of glycine-HCl produced one peak of UV-absorbing material (~100 mAU),

eluting at 42-63% glycine-HCl (= 0.042-0.063 M glycine-HCl) (Figure 3-7 (A)). As Protein G chromatography is a rather specific purification method, only IgG were likely to elute within this peak. Therefore, pooled fractions corresponding to the peak were concentrated to 1 ml and further purified using GF chromatography. One compound emerged in a single symmetrical peak at 14-16 ml (28-32 min) (Figure 3-7 (B)) and was examined by SDS-PAGE with two main bands at ~50 kDa and 25 kDa being observed (Figure 3-8). These bands correspond to the heavy and light chains of the antibody, respectively, confirming the nature of the product collected. Furthermore, no contaminants could be seen on the gel, which suggested a relatively high purity of the antibody. This is largely due to the very specific interaction between the IgG and the Protein G column, which eliminates the main impurities present in the cell culture medium, including BSA from FBS.

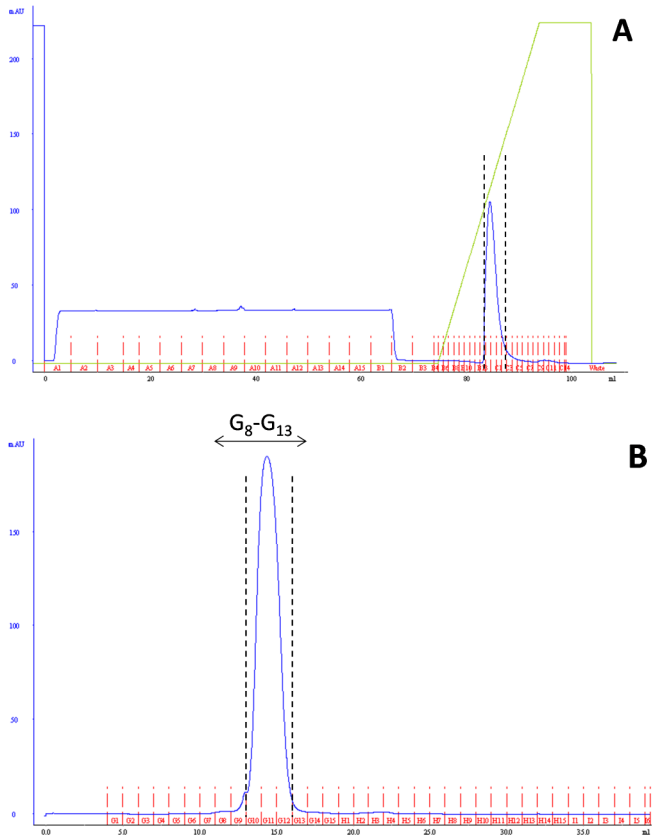

Figure 3-7 – Chromatograms obtained after purification of M40-1 by (A) Protein G and (B) size exclusion chromatography. Fractions covered by the arrow in (B) indicate the complete range of fractions displayed in Figure 3-8. The black dotted lines marked on both (A) and (B) indicate the fractions containing M40-1 that were collected.

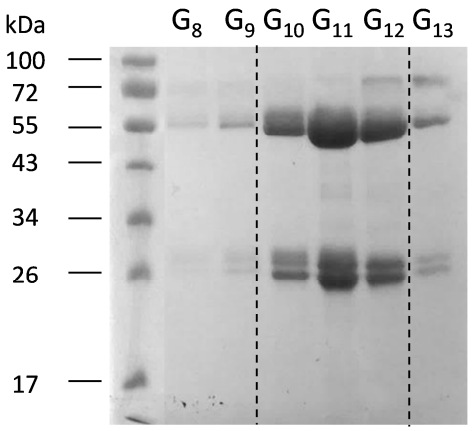

Figure 3-8 – Coomassie-stained SDS-PAGE of fractions collected after running M40-1 on a GF column. Bands migrating at ~50 and 25 kDa correspond to the reduced heavy and light chains of the IgG, respectively. G-labelled lanes correspond to arbitrary tray row and column reference on the fraction collector and are illustrated by the red dashes on Figure 3-7 (B). The black dotted lines indicate the fractions containing M40-1 that were collected.

The functionality and specificity of the M40-1 antibody were assessed by WB using ntPE as the antigen (Figure 3-9). One strong band could be detected after development at ~70 kDa and corresponded to the native toxin, showing that the purified antibody did target ntPE. Furthermore, no band could be observed when blotting BSA with M40-1, confirming the specificity of the product. This therefore established that the product expressed from the hybridoma cells was able to selectively interact with ntPE.

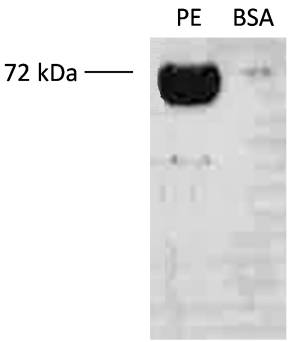

Figure 3-9 – WB analysis of the purified antibody (M40-1). 10 µg PE or BSA was studied by SDS-PAGE and transferred to PVDF membrane that was probed with the purified antibody diluted at 1 in 10,000 in TBS-T from a 1 mg/ml stock solution.

The purified M40-1 antibody preparation was divided in two batches: one lot was stored at 1 mg/ml in 1:1 PBS: glycerol for Western blot, and the rest was stored in PBS at 12 mg/ml for HPLC and crystallisation studies. The presence of glycerol helps preserve the

integrity of the antibody when subjected to several freeze/thaw cycles at low concentration.

3.3.2 ntPE undergoes a pH-induced and reversible conformational change

In order to confirm that the protein expressed and used here presented the same pH-dependent behaviour as described in the literature, the structural behaviour of ntPE in solution was probed by trypsin digestion. Like in many experiments described here, BSA was used as a control protein. In fact, the mature BSA is composed of 583 amino acids and was particularly appropriate as a control since its molecular weight (66.5 kDa vs. 66.8 kDa) and calculated pI (5.6 vs. 5.3) are very close to the 613 amino acids of mature ntPE [181]. Different from PE, BSA has been reported to undergo structural transitions below pH 5.0 and above pH 7.5, but it appears to have a conserved conformation within the working pH range of 5.0-7.0 [219, 220]. Moreover, the isoelectric point of BSA in aqueous solution containing 0.15 M NaCl is ~4.7 which means that BSA should remain stable in solution over the studied pH range [221, 222].

BSA and ntPE were diluted in citrate-phosphate buffer at different pHs (5.8, 6.2 and 7.4) and digested by trypsin before being analysed by SDS-PAGE (Figure 3-10). In the case of BSA, no difference in the digestion pattern could be observed between the three pHs: one main band appeared at ~70 kDa, corresponding to the undigested protein, and one fainter secondary band could be seen at ~60 kDa. It showed that digestion of BSA by trypsin was minimal and pH-independent within the range studied. On the contrary, ntPE presented a different digestion pattern depending on the pH. At pH 7.4, one strong band appeared at ~70 kDa and corresponded to the undigested protein, while a faint secondary band was visible at ~60 kDa. This indicated that enzymatic digestion of ntPE at pH 7.4 was minimal. When the pH was lowered to 6.2 and 5.8, a shift in the digestion pattern could be observed. The band at ~70 kDa disappeared and a band at ~50 kDa appeared instead, which progressively became the main digestion fragment. Trypsin activity is highest around pH 7.0, and therefore the increase in protein digestion at lower pH could not be explained by a change is enzyme efficacy [223]. Instead, it seemed that the site for trypsin cleavage became more accessible for enzyme digestion at pH 5.8. These results confirmed that when transferred to acidic pH, the ntPE expressed here undergoes a conversion from a native state in which trypsin cleavage is limited, to a second conformation in which the enzyme recognition sequence seems to be more exposed and thus available for digestion.

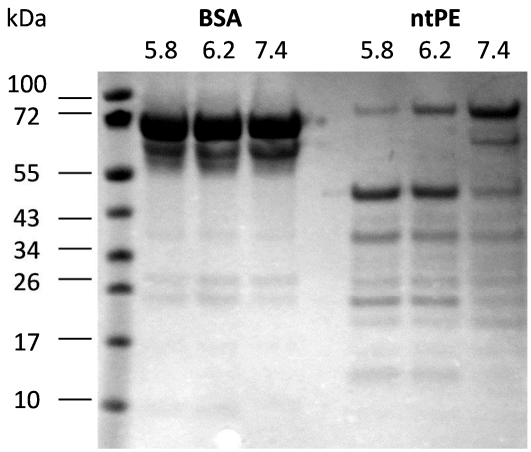

Figure 3-10 – Trypsin digestion of ntPE but not BSA is pH-dependent. Coomassie-stained SDS-PAGE of ntPE and BSA diluted in citrate-phosphate buffer at pH 5.8, 6.2 and 7.4 and digested using 0.4 µg trypsin at 4 °C for 30 min.

In order to refine the pH range where the conformational change occurred, the size of ntPE over the 5.8-7.4 pH interval was determined by dynamic light scattering (DLS).

In Figure 3-11 (A), the determined mean hydrodynamic diameter is plotted against the pH of the solution. Statistical analysis of the results is presented in Figure 3-11 (B). On each graph, two distinct areas emerge: when pH > 6.2, ntPE presented an average tumbling volume of 9.5 nm and variations in size were small (± 0.4 nm, ~4.2%). When pH ≤ 6.2, the average protein size increased by ~12.0% to 10.8 ± 0.7 nm that suggested a slightly greater size variability of ~6.5%. Two sets of data collected over a three year-interval described the same trend, with the first set of data being collected by Dr Julia Mackay in May 2011 and the second in October 2014. Minimal variations in pH shift between the two curves could be explained by sample preparation method. While samples prepared in October 2014 were dialysed against buffer at the indicated pH (as described in Section 2.11), in May 2011 the protein was diluted directly in buffer, thereby slightly increasing the pH by addition of PBS into the mixture.

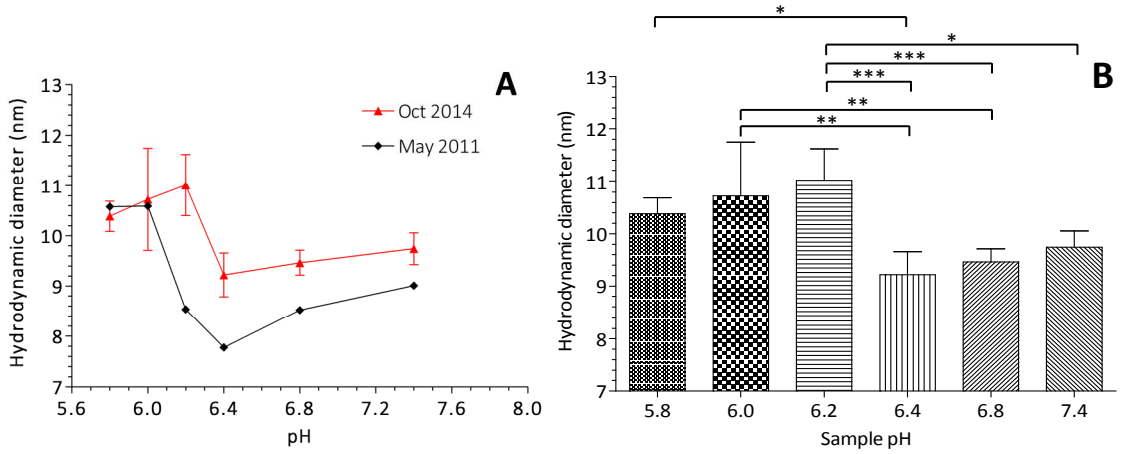

Figure 3-11 – (A) Measurement of the size of ntPE at different pH values in citrate-phosphate buffer using DLS. (B) Statistical analysis of the results obtained in (A). Bars show mean ± SD for n = 6 independent experiments where *** P < 0.001, ** P < 0.01 and * P < 0.05.

To confirm these results, the ntPE preparations used for DLS measurements were separated by SDS-PAGE and Coomassie-stained (Figure 3-12). The conformational change could be observed as a progressive transition and pH 6.2 appeared as the conversion point between the two conformations. In fact, while the intensity of undigested protein (band 1, ~70 kDa) slowly decreased with the pH, band 2 (~55 kDa) nearly entirely disappeared and band 3 (~47 kDa) began to emerge below pH 6.2. Furthermore, the amount of undigested material was much less at lower pH.

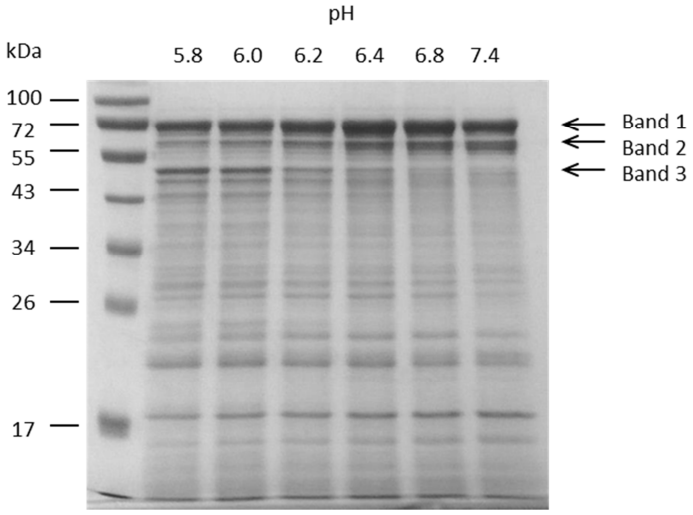

Figure 3-12 – Determination of the transition point between two conformations by trypsin digestion. Coomassie-stained SDS-PAGE of DLS samples following digestion of 10 µg sample with 0.4 µg of trypsin at 4 °C for 30 min.

To rule out the possibility that the transition observed only reflected protein denaturation or hydrolysis due to exposure to acidic environment, reversibility of the conversion was assessed. ntPE was incubated in citrate-phosphate buffer, 0.1 M NaCl at pH 5.8 and the pH was reversed back to 7.4. The digestion pattern of the reversed sample (REV) was identical to the one of ntPE in buffer at pH 7.4 when analysed by SDS-PAGE (Figure 3-13), which suggests that the conformational transformation undergone by the protein was reversible when the pH was switched back to more physiological values.

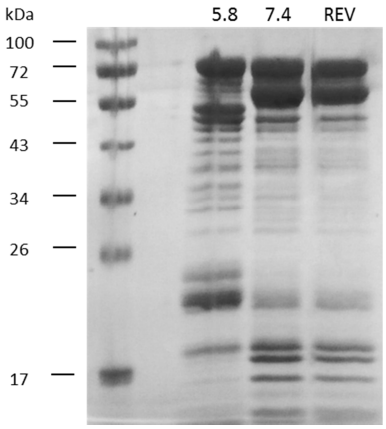

Figure 3-13 – pH-dependency of ntPE digestion by trypsin is reversible. Coomassie-stained SDS-PAGE of ntPE in citrate-phosphate buffer at pH 5.8 or 7.4 and of a sample incubated at pH 5.8 for 5 min and returned to pH 7.4 by dialysis (REV). All samples were digested using 0.4 µg trypsin at 4 °C for 30 min.

The apparent total reversibility observed in the trypsin digest studies suggests that ntPE does not go through a global reorganisation of structure when exposed to low pH values, as an extensive modification would be less likely to reverse so completely. Instead, it would seem more likely that the difference in trypsin sensitivity observed with pH would result from a subtler, local switch in conformation. DLS measurements and examination of protein cleavage by trypsin indicate that this switch takes place around pH 6.2 in the present experimental conditions. This hypothesis was verified using HPLC GF.

3.3.3 The conformational change experienced by ntPE is not a global change in tertiary structure

Characterisation of ntPE by size exclusion HPLC using 0.1 M potassium-phosphate buffer (kPB) containing 0.1 M NaCl at pH 7.4 or 5.8, showed that the protein eluted at 9.282 and 9.383 min, respectively (Figure 3-14 (A)). By comparison, BSA, whose conformation has been shown to remain constant within studied pH range [219, 220], eluted at 9.061 and

9.082 min at pHs 7.4 and 5.8, respectively (Figure 3-14 (B)). These results show that switching to a more acidic environment did not modify significantly the elution time of ntPE. This would support the idea that ntPE does not go through any global structural rearrangements (e.g. major unfolding or change of orientation of a whole domain) as the pH is lowered.

If in fact ntPE did undergo a local rather than an overall conformational change, a complete reorientation of one domain relatively to the others would seem unlikely as this would involve extensive structure modifications. Instead subtle alterations of the protein's structure, within or possibly at the interface between, one or several domains would appear to be more probable. Domain II has been demonstrated to be responsible for toxin translocation through the cells [200] and it is assumed that the conformational change described here is responsible for the re-routing of PE away from the lysosomal degradation pathway, towards the Golgi and eventually the cytosol. It could therefore be anticipated that the conformational change could occur within domain II [200, 224]. Supporting this hypothesis are the observations that replacing either or both domains I and III by an alternative protein does not alter the ability of PE to reach the cytosol of the target cell [145, 165].

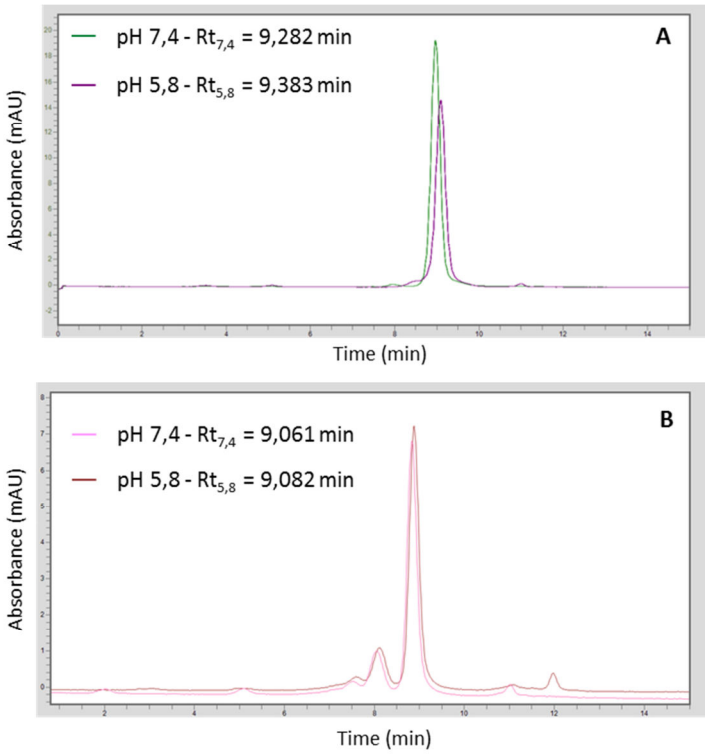

Figure 3-14 – HPLC chromatograms of (A) ntPE and (B) BSA after elution on a HPLC GF column in kPB + 0.1M NaCl at pH 7.4 and 5.8 at 37 °C. UV measurements were performed at 254 nm. The chromatograms presented here were taken as representative of 6- and 3-run sets for ntPE and BSA, respectively.

3.3.4 Truncation of ntPE results in the increased exposure of trypsin cleavage sites

In order to better define the region in which this conformational change happens, a series of truncated proteins were cloned and expressed from PE. These truncated mutants were shortened up to the end of α-helix B and their ability to undergo the same conformational change as ntPE was examined by trypsin digestion.

Truncated mutants of ntPE GS TEV were subjected to trypsin cleavage at either pH 5.8 or 7.4 at 4 °C for 30 min and separated by SDS-PAGE. Gels were stained with Coomassie blue (Figure 3-15).

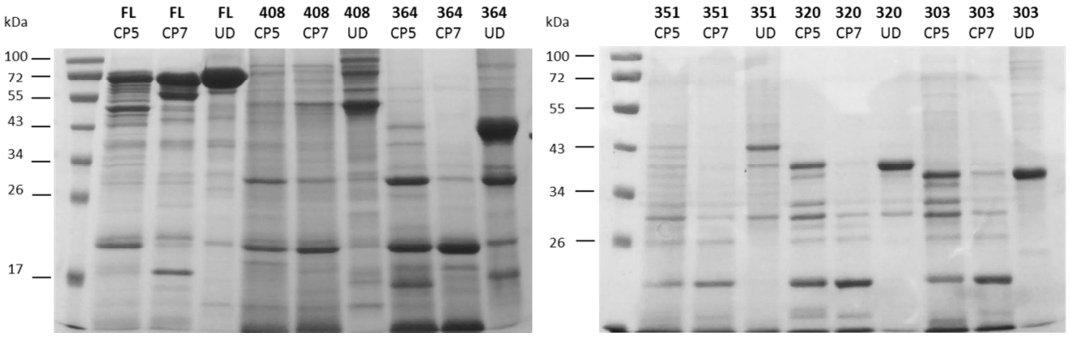

Figure 3-15 – Trypsin digestion of PE GS TEV mutants. 10 μg protein was incubated with 0.4 μg trypsin for 30 min at 4 °C and analysed by SDS-PAGE. Undigested samples were incubated in PBS without trypsin. Top line indicates the mutant used; full-length (FL), PE408 GS TEV (408), PE364 GS TEV (364), PE351 GS TEV (351), PE320 GS TEV (320) or PE303 GS TEV (303). Bottom line indicates the conditions of the digestion in citrate-phosphate at pH 5.8 or 7.4 (CP5 and CP7, respectively), or undigested protein (UD).

In the case of the full-length ntPE GS TEV (FL), the pattern observed was significantly different depending on the pH. At neutral pH, cleavage was scarce with only a band at ~55 kDa detectable and most protein left undigested (~72 kDa band). This pattern is consistent with previous reports detailing cleavage of PE by trypsin after Arg490 [225]. In mildly acidic conditions (pH 5.8), protein cleavage was more extensive. A band corresponding to the unprocessed sample was still present though far less intense than at pH 7.4. Four main bands could be observed on the gel at approximately 45, 40, 30, and 20 kDa. N-terminal sequencing revealed that both 20 and 30 kDa bands matched the N-terminal end of the protein (AEEAF). This suggests that ntPE GS TEV was cut at two distinct positions, and that two pairs of bands were actually detected by SDS-PAGE (one

cleavage, cleavage 1, C1, resulted in bands at 20 and 45 kDa while another, cleavage 2, C2, produced bands at 30 and 40 kDa). Further N-terminal sequencing (Alta Bioscience Ltd., Birmingham, UK) showed that the 40 kDa fragment starting sequence was GWEQL, therefore demonstrating that one of the trypsin digestion sites, most likely C2, corresponds to the furin cleavage site. This would be in agreement with previous reports showing that this region of the protein is exposed to enzymatic cleavage only under acidic conditions [162]. N-terminal sequencing of the 45 kDa band did not provide satisfactory results, and consequently the location of C1 could not be determined accurately. However, based on the approximate molecular weight of the fragments (~20 and 45 kDa) and the location of each residue (Figure 3-16), it could be assumed that the protease would most likely cleave after either Arg186 or Arg213 (Table 3-3).

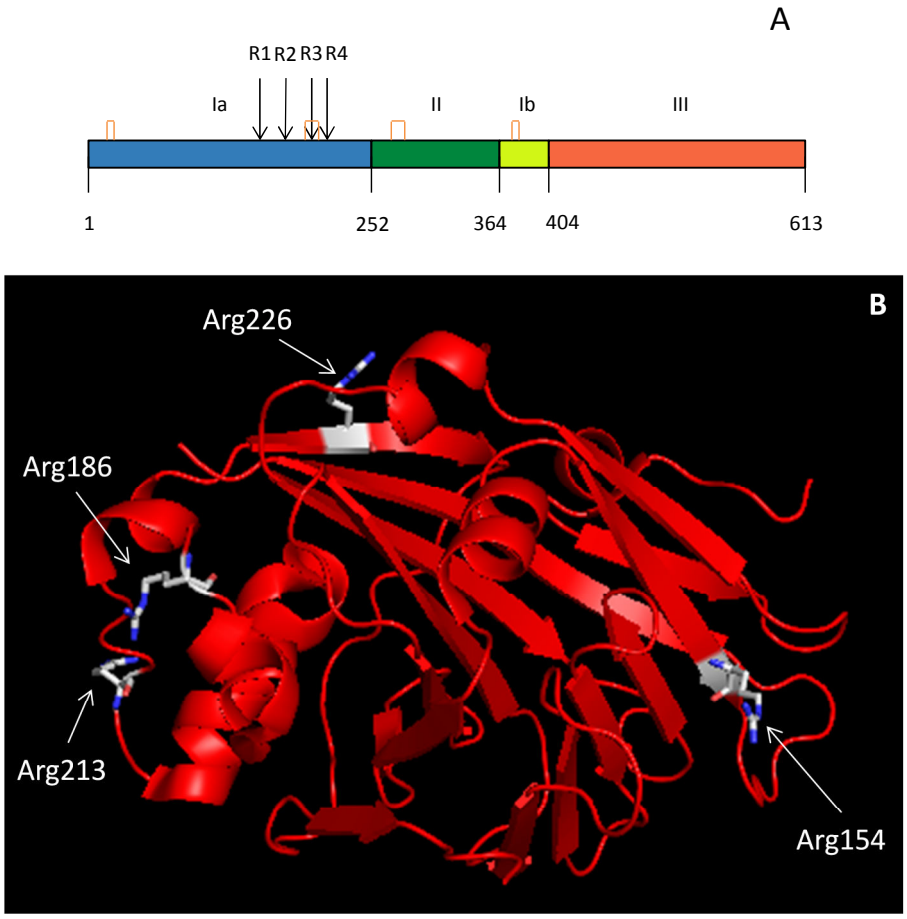

Figure 3-16 – Positions of the potential trypsin cleavage sites corresponding to the 20 and 45 kDa fragments that were detected in Figure 3-15. (A) Schematic representation of the full-length PE and (B) Ribbon representation of PE domain I. Arg186 (R2) and Arg213 (R3) are both located on loops, while Arg154 (R1) and Arg226 (R4) are in the middle of β-strands. Disulphide bonds are indicated orange in (A). Figure (B) was generated using PyMOL [128].

Table 3-3 – Potential trypsin cleavage sites corresponding to the 20 and 45 kDa fragments detected. ExPASy Peptide Cutter and ExPASy ProtParam were used to generate the fragments and calculate their molecular weight, respectively. Only 100% probability cleavage sites are displayed.

Position of cleavage site	MW (fragment 1) (kDa)	MW (fragment 2) (kDa)
Arg154	16.9	49.9
Arg186	20.5	46.4
Arg213	23.6	43.3
Arg226	25.2	41.7

The bands detected after trypsin digestion of the truncated mutants denoted strikingly different behaviour compared to the FL protein; sensitivity to the protease was inversed compared to FL for all five. At pH 5.8, a ~20 kDa N-terminal band was detected and represented the main fragment. These results suggested C1 became the main cutting site in these truncated proteins. In some cases, bands possibly corresponding to the 30 kDa N-terminus and the undigested sample (e.g. PE364 GS TEV and PE303 GS TEV) were also identifiable. Proteins seemed to be digested more at pH 7.4, with fewer fragments retrieved and a complete absence of uncleaved material. A ~20 kDa band could also be detected with reasonably strong intensity. These results suggested that the mutants examined in these studies were more extensively digested by trypsin, making them more difficult to detect by SDS-PAGE.

These studies show that lowering the pH promotes a conformational change of the FL protein resulting in exposure of additional trypsin cutting sites, and that these same sites appear to be more exposed at neutral pH in all truncated mutants. This would imply that in native PE, domain III could conceal a cleavage site at pH 7.4, or might impose conformational constraints on the protein to prevent exposure of these sites. Removal of domain III seemed to lift these restrictions and reveal the additional cleavage sequences. The fact that all mutants still displayed a difference in their digestion patterns with the pH suggests not only that a conformational change still occurs, despite removal of III, but also that the origin/trigger of this conformational change is located, at least in part, somewhere between amino acids 1 and 303 (shortest mutant), i.e. either in domain I or, more probably, in the N-terminal half of domain II.

The reversibility test previously performed on the FL protein was then applied to all mutants (Figure 3-17). The pattern observed for samples that had been diluted in buffer at

pH 5.8 before being returned to neutral pH and digested with trypsin matched that obtained previously for samples cut at pH 7.4. Thus, the conformational change(s) undergone by the mutants, just like the FL protein, seemed to be completely reversible. This observation reinforced the idea that removing amino acids 304-613 did not prevent the conformational change from occurring in these truncated proteins, and that this process must originate from transformations in residues located before position 303.

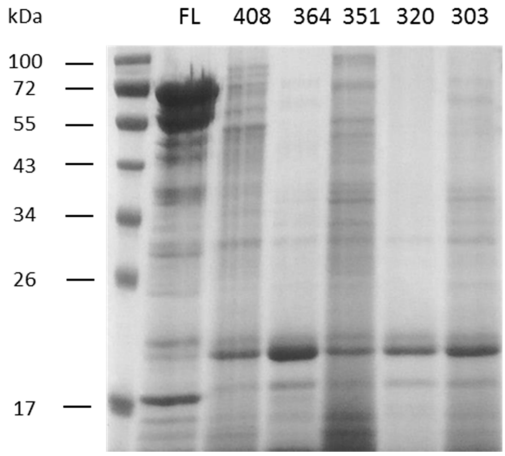

Figure 3-17 – Assessment of the reversibility of the pH-induced conformational change in PE GS TEV mutants. Coomassie-stained SDS-PAGE of PE GS TEV mutants incubated in citrate-phosphate buffer at pH 5.8 for 5 min and returned to pH 7.4 by dialysis. All samples were digested by 0.4 µg trypsin for 30 min at 4 °C.

These results support the hypothesis that the pH-dependent conformational change undergone by ntPE is local and could occur within domain II, and that this change may be focused between amino acids 252 and 303. This segment contains a region rich in hydrophobic residues (amino acids 256-280: **LAAL**T**A**HQ**A**CH**LPL**ET**F**TRHRQ**P**R**G**, hydrophobic residues are highlighted in bold) [154, 201] which, if subject to a conformational change, could be more or less exposed to solvent depending on the pH. To investigate the relative exposure of this region in acidic and neutral conditions, the overall hydrophobicity of the protein at pH 5.8 and 7.4 by spectrofluorometry was investigated.

3.3.5 The conformational change experienced by ntPE results in the exposure of hydrophobic residues

ANS was used to further characterise ntPE conformational change by investigating the effect of pH on the protein surface hydrophobicity. The pKa of ANS is 0.37 [226], thus it was assumed that the dye was always present under its anionic form in the pH range

studied (5.8-7.4). The hypothesis was that lowering the pH would trigger a change in the conformation of the protein and result in the exposure of buried (hydrophobic) residues.

Fluorescence measurements were performed in citrate-phosphate buffer containing 0.1 M NaCl at pH 5.8 and 7.4. The fluorescence emission spectrum was scanned from 400 to 700 nm (Figure 3-18), after what areas under the fluorescence curves (AUC) were calculated and values of $\lambda_{em,max}$ were determined (Table 3-4). BSA was used as a control at the same concentration as ntPE.

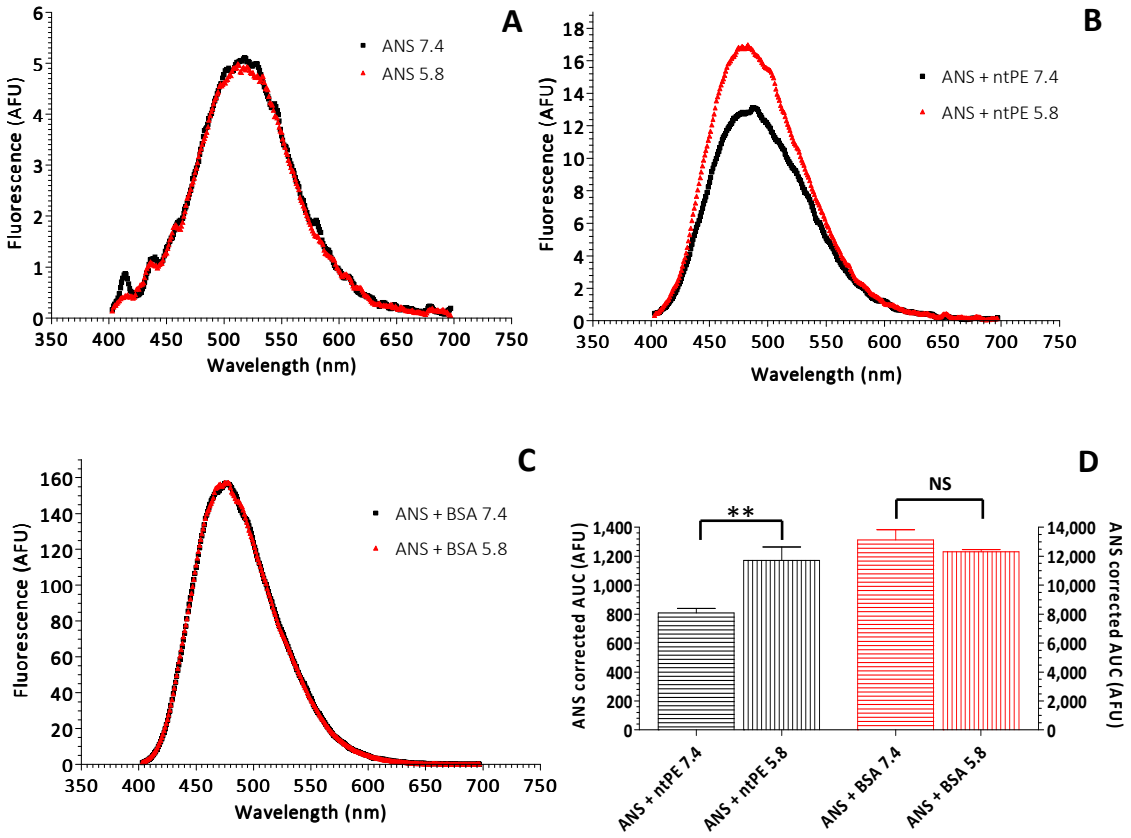

Figure 3-18 – Hydrophobic residues are exposed on the surface of ntPE when the protein is exposed to acidic pH. Fluorescence spectra of (A) ANS, (B) ANS + ntPE and (C) ANS + BSA at pH 5.8 (red) and 7.4 (black) for [ANS] = 100 µM and [ntPE] = [BSA] = 1.52 µM. (D) Areas under the fluorescence curves of ntPE and BSA at both pHs. Black bars refer to left-hand y axis; red bars refer to right-hand y axis. Bars show mean ± SD for n = 3 independent samples where ** P < 0.01 and NS is non-significant.

Table 3-4 – Values of *ΔF* and $\lambda_{em,max}$ collected by spectrofluorometry for samples composed of ANS, ANS + ntPE or ANS + BSA.

Sample	*ΔF*	$\lambda_{em,max}$ (nm)
ANS 7.4	0.976	518
ANS 5.8		517
ANS + ntPE 7.4	1.449	483
ANS + ntPE 5.8		475
ANS + BSA 7.4	0.938	476
ANS + BSA 5.8		475

As expected, ANS in solution at 100 µM displayed minimal fluorescence, and no differences between the spectra collected at either pH could be observed (*ΔF* = 0.98, identical $\lambda_{em,max}$). Addition of ntPE at a concentration of 1.52 µM (0.1 mg/ml) to ANS in solution at pH 7.4 led to a 2.5-fold increase in total fluorescence intensity and a shift of $\lambda_{em,max}$ from 518 to 483 nm. When the pH was lowered to 5.8, the fluorescence intensity of ANS in presence of ntPE increased by 1.5-fold compared to ANS + ntPE at pH 7.4 and a blue shift in $\lambda_{em,max}$ from 483 to 475 nm could be observed. When BSA was mixed to ANS in solution, a significant increase in fluorescence could be observed compared to ANS alone, but $\lambda_{em,max}$ were similar at both pHs and *ΔF* was equal to 0.938.

These results suggest that in their native conformational state, both ntPE and BSA present surface hydrophobic residues that are accessible to solvent and thus available for interaction with ANS (Figure 3-19). The dramatic increase in ANS fluorescence for BSA suggested that this protein presented a significant number of surface hydrophobic sites. This would be in agreement with one of the major functions of serum albumins which bind to fatty acids in the blood, thereby increasing their solubility, and transport them through the plasma [227, 228]. In fact, hydrophobic interactions between fatty acids hydrocarbon tails and the uncharged side chains of amino acids lining the binding sites were previously reported to be important in the binding process [229-231]. When the pH of the protein samples was lowered to 5.8, the two proteins behaved in very dissimilar ways. The fluorescence spectrum of BSA remained identical to the one obtained at pH 7.4, with both fluorescence quantum yield (*ΔF* = 0.938) and $\lambda_{em,max}$ unchanged, which was in agreement with the fact that the protein does not undergo any conformation change within this pH range. In contrast, results collected for ntPE suggested that the number of hydrophobic

sites available for ANS binding was greater at acidic pH. These data suggest that at a more acidic pH, extra hydrophobic residues accessible to solvent appear on the surface of ntPE and that ANS could interact with them. This would support the earlier stated hypothesis that when the pH is lowered, ntPE would undergo a local conformational change, resulting in the unfolding of a specific region of the protein, and exposure of additional hydrophobic residues.

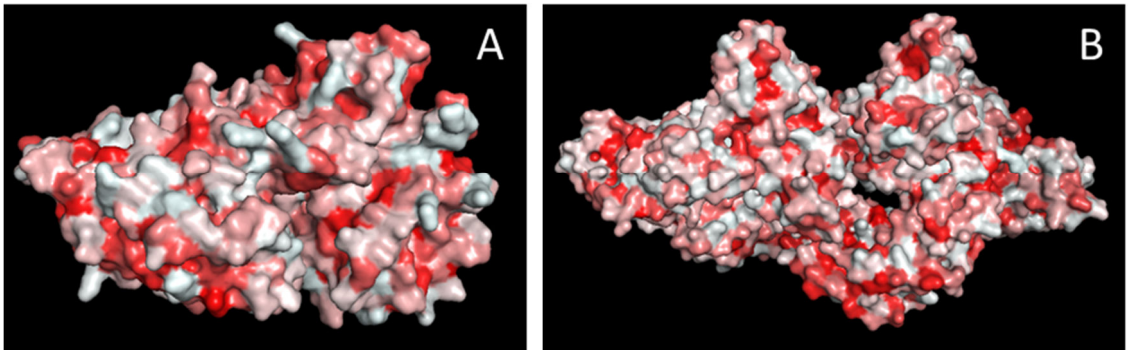

Figure 3-19 – Surface hydrophobicity of (A) PE and (B) BSA at pH 7.4 (based upon crystal structure information). Red and white refer to hydrophobic and hydrophilic residues, respectively. Even in their native conformations, PE and BSA present solvent-exposed hydrophobic sites that could bind ANS. The figures were generated using PyMOL [128].

3.3.6 Sample preparation for crystallisation studies of PE in acidic conditions

In order to test the hypothesis that unfolding of a specific region of the protein could account for the pH-dependent differences observed in ntPE, crystallisation of PE in acidic conditions would be ideal. However, several attempts to obtain ordered crystals for X-ray analysis have failed, likely due to the instability of the protein at slightly acidic pH. It was suggested that the region surrounding the furin cleavage site (amino acids 276-280) would be particularly suitable for the conformational change to take place due to its pH-dependent exposure and hydrophobicity.

The monoclonal antibody M40-1 was generated by Ogata *et al* (1991) as part of a series of monoclonal antibodies (mAbs) designed to probe and gain a better understanding of the transformations that arise in PE's structure under different sets of conditions. Although the exact residues required for binding remain unknown, M40-1 was reported to specifically target a site located within a 45 amino acid-long segment at the N-terminal end

of domain II (amino acids 264-308). Therefore, its binding site could potentially envelope the proposed region of conformational flexibility.

Several studies have reported the advantages of co-crystallisation between a protein and one of its ligands [232-235]. Here, it was proposed that the interaction between M40-1 and PE at pH 5.8 could be used to stabilise the protein enough to obtain ordered crystals.

3.3.6.1 M40-1 binding properties are not pH-dependent

Before any attempt at crystallising the protein/antibody complex, the interaction between the two components had to be tested at both neutral and acidic pH to ensure that the antibody expressed here presented similar characteristics to the one described by Ogata *et al* [153].

The monoclonal antibody M40-1 run on a HPLC GF column in potassium-phosphate buffer at 1 mg/ml came out as two main peaks which eluted at similar retention times at both pHs (Figure 3-20 and Table 3-5). The small difference observed between retention times was, as in the case of ntPE, non-significant.

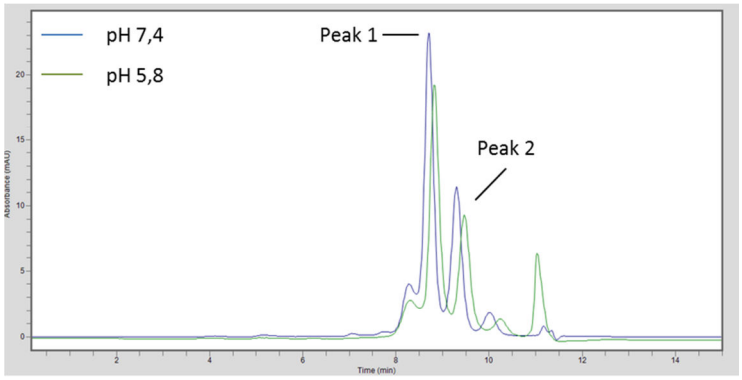

Figure 3-20 – The elution profile of M40-1 is not dramatically affected by changes in pH. Chromatograms were collected for M40-1 at either pH 7.4 or 5.8 using HPLC GF. Eluted compounds were detected by UV measurements at 254 nm.

Table 3-5 – Elution times and areas of main peaks obtained for M40-1 by HPLC GF at pH 5.8 and 7.4 and corresponding to Figure 3-20.

	Rt (Peak 1) (min)	Rt (Peak 2) (min)	Area (Peak 1) (AU)	Area (Peak 2) (AU)
pH 5.8	8.90	9.50	121,120	67,732
pH 7.4	8.69	9.17	128,873	77,496

ntPE was then diluted in 0.1 M potassium-phosphate buffer at pH 5.8 or 7.4 to a concentration of 1 mg/ml and M40-1 was added in a 2:1 or 4:1 molar ratio. 10 µl samples were separated by HPLC GF at 1 ml/min. The chromatograms obtained seemed to suggest that the protein-antibody interaction was not affected by pH as in both 2:1 and 4:1 ratio samples the complex formed was eluted at the same retention time (6.80 min) whether at neutral or acidic pH (see Figure 3-21).

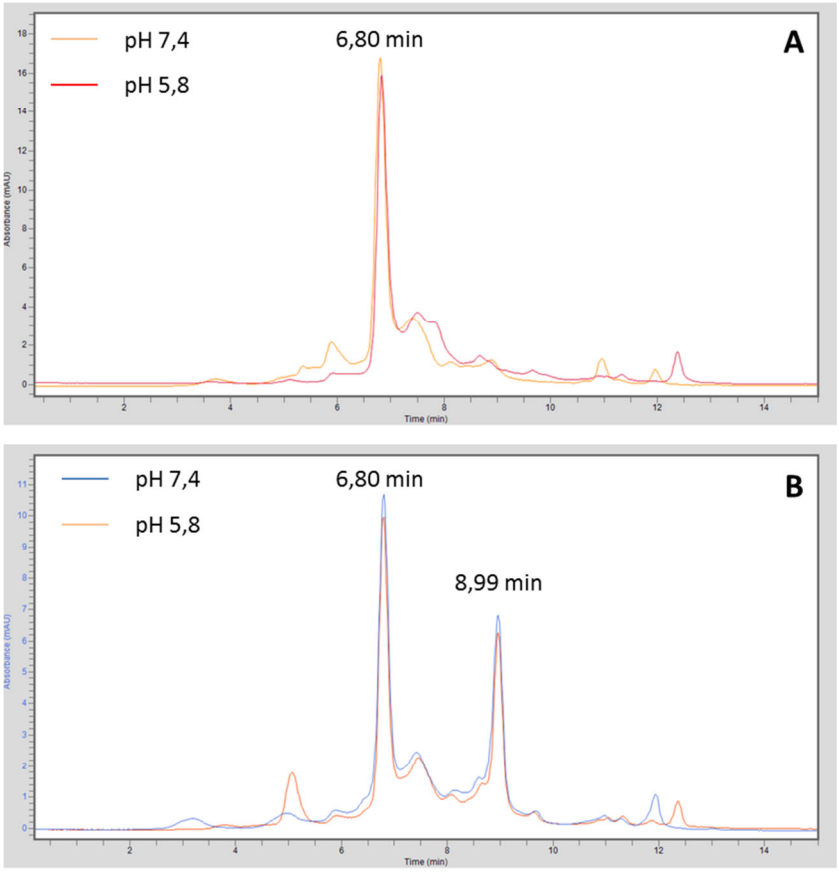

Figure 3-21 – Elution profiles for solutions of ntPE and M40-1 in (A) 2:1 or (B) 4:1 molar ratio. ntPE concentration was maintained constant at 1 mg/ml.

Ogata *et al* (1991) reported that no changes in M40-1 binding to PE were observed between pH 5.0 and 7.4, indicating that pH variations within this range do not influence the binding affinity of the antibody for PE [153]. Assuming that the region surrounding the furin cleavage site is, in effect, key to the conformational change, these results could be explained by the fact that the antibody would interact with residues located in the second half of the proposed binding site (residues 264-308) (Figure 3-22). Therefore, its affinity for PE would not be affected by a localised modification in the first half of the sequence. However, it was also demonstrated that treatment of PE with both urea and DTT (which commonly lead to protein unfolding, exposure of the loop carrying the furin recognition site and reduction of the disulphide bond between Cys267-Cys285 [236]) resulted in a decrease in M40-1 reactivity for the protein. This suggests a transformation within the IgG binding site which would be more likely to occur in the region encompassed by the two cysteine residues rather than in α-helix B itself, and therefore include at least part of the loop connecting α-helices A and B. In this case, the absence of variation in binding affinity between M40-1 and PE when the pH is lowered could be due to a local variation in the protein's 3D organisation that would be structurally small but functionally significant.

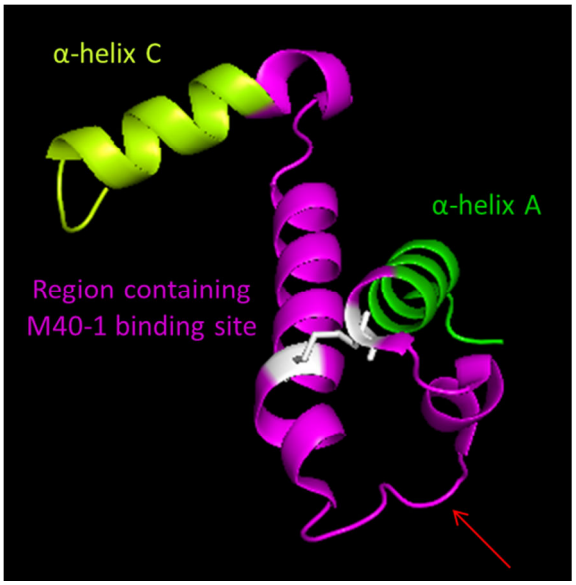

Figure 3-22 – Ribbon representation of the region suggested as M40-1 binding site. The red arrow indicates the loop connecting helices A and B and carrying the furin cleavage site. Highlighted in white are the two cysteine residues (C265 and C287) which form a disulphide bond. The structure was generated using PyMOL [128].

Furthermore, these results seem to indicate that one molecule of antibody is able to bind two molecules of ntPE. In fact, no leftover protein or antibody could be detected in the 2:1 ratio sample, whereas a peak could be observed at 8.99 min in the 4:1 ratio sample. This

peak probably corresponds to the unbound antibody, for whose retention time was determined to be 8.69 and 8.90 min at pH 7.4 and 5.8, respectively.

As a conclusion, the epitopes for M40-1 interaction with ntPE seem to be sufficiently accessible for binding at either pH. However, the whole IgG is a relatively large molecule (150 kDa), and thus too bulky for co-crystallisation. Therefore it was cleaved in order to generate fragments that could be used for crystallisation studies.

3.3.6.2 Antibody fragmentation and complex isolation

Antibody fragments such as Fab (antigen-binding fragments), Fv (variable fragments) or scFv (single-chain variable fragments), can be used as crystallisation chaperones (Figure 3-23) [237]. They are specific and high-affinity protein-binding partners, and facilitate the formation of well-ordered crystals by reducing the conformational freedom of the target protein, enhancing solubility or, alternatively, helping crystallisation of proteins which are too soluble to form crystals [234, 235, 237-239]. Besides, antibody fragments are often able to match the size of the chaperone (15-50 kDa) to the specific target.

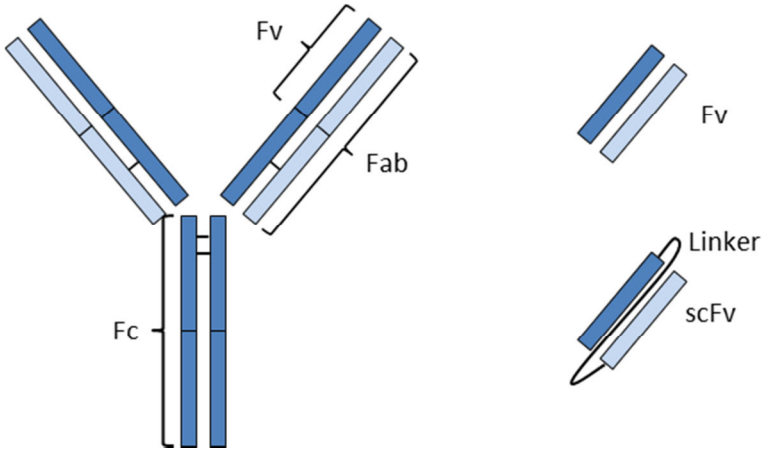

Figure 3-23 – Schematic representation Fc, Fab, Fv and scFv fragments from whole IgG.

The interaction between a fragment of M40-1 and PE at pH 5.8 could be enough to stabilise the protein in its conformation at low pH and allow crystallisation of the complex for further determination of the protein structure in acidic conditions. Therefore the antigen-binding portion of the antibody (Fab fragment) was generated and used for crystallisation studies.

Fab fragments were generated by digestion of the whole IgG by the enzyme papain, whose cleavage site is located above the hinge region containing the disulphide bonds that link the heavy chains, but below the site of the disulphide bond joining the heavy and light

chains. They were further isolated by elution on an immobilised protein A column, to which both undigested IgG and Fc fragments will bind via the Fc domain.

After purification, 2.1 mg (4.2×10^{-8} mol) of Fab were collected. As 3.8 mg whole IgG (2.53×10^{-8} mol) was initially used for fragmentation and one mole of IgG generates 2 moles of Fab, the final yield was calculated to be 83.0%. This result was confirmed by running samples eluted in PBS (Fab_1 and $Fab_{2,3}$) and elution buffer (IgG_1, IgG_2 and IgG_3) on SDS-PAGE under denaturing and non-denaturing conditions (Figure 3-24). As expected, only reduced Fab fragments (25 kDa) and light chains (23 kDa) were present in the denatured flow-through fractions of Fab_1 and $Fab_{2,3}$. The presence of a second pair of bands in the non-denatured lanes for these samples results from the partial denaturation of the Fab fragments due to incubation with reducing buffer at RT. Materials detached from the column by the elution buffer appeared as a single ~27 kDa band on the gel following reduction. When samples were only mixed with reducing buffer without being boiled, this band was located at ~45 kDa. These results are consistent with data previously described for analysis of M40-1 by SDS-PAGE (Figure 3-8). In both cases, only a very faint band could be observed > 130 kDa. The absence of bands at either ~50 kDa (denatured samples) or ~150 kDa (non-denatured samples) suggests that no undigested IgG remained after fragmentation and that all material recovered in these samples after elution were Fc fragments.

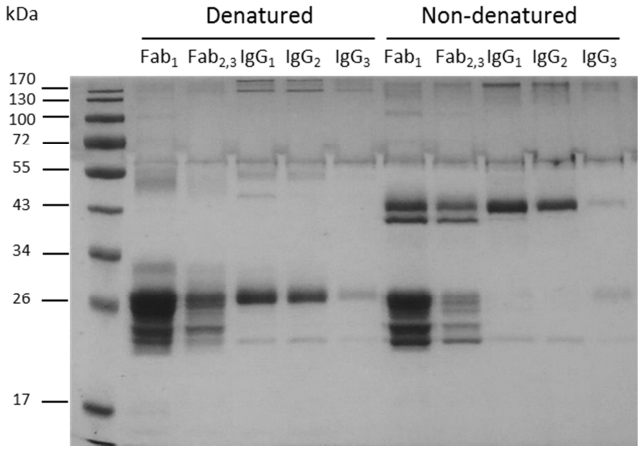

Figure 3-24 – Fragmentation of M40-1. Coomassie-stained SDS-PAGE of the fractions obtained after purification of the digested sample on immobilised protein A column. Fab and IgG samples were eluted with PBS and elution buffer, respectively. Subscripts indicate wash number.

All Fab fragments were mixed with ntPE in a 1:1 molar ratio and the sample was run on a gel filtration column in order to isolate the protein-Fab complex from any unbound material present in solution.

One main peak could be observed on the UV chromatogram (Figure 3-25 (A)), which corresponded to fractions J_{10} and J_{11} and contained the ntPE-Fab (M40-1) complex (Figure 3-25 (B)). These fractions were therefore collected. Due to time constraints, crystallisation studies could not be initiated and the purified complex was handed out to Dr Julia MacKay who, in collaboration with Dr Jean van den Elsen, set up crystallisation studies of PE in acidic conditions. Unfortunately, at the time of writing, no results had been obtained yet.

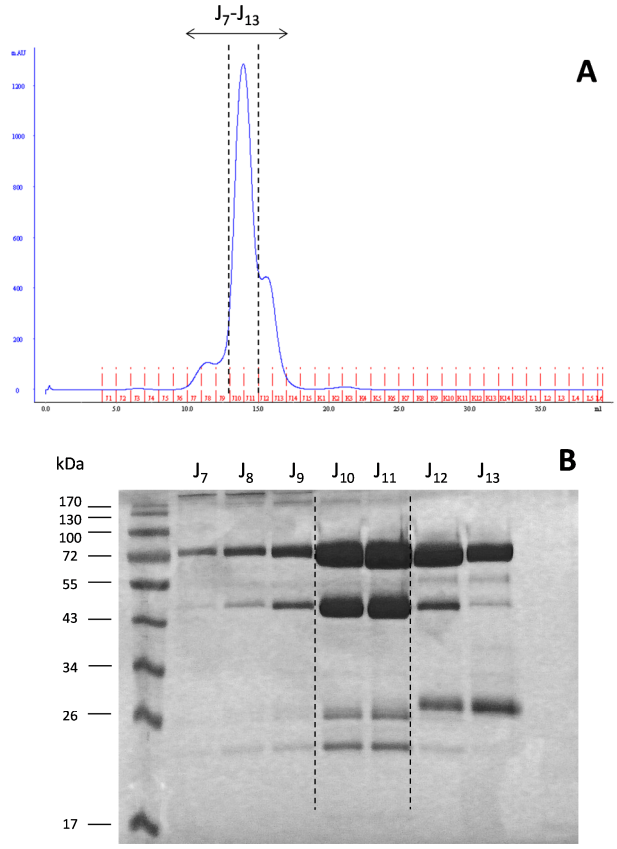

Figure 3-25 – Purification of the ntPE-Fab (M40-1) complex by GF. (A) Chromatogram and (B) Coomassie-stained SDS-PAGE of the fractions corresponding to the UV peaks. J-labelled lanes in (B) correspond to arbitrary tray row and column reference on the fraction collector and are illustrated by the red dashes on (A). Fractions covered by the arrow in (A) indicate the complete range of fractions displayed in (B). The black dotted lines marked on both (A) and (B) indicate the fractions containing the ntPE-Fab (M40-1) complex that were collected.

3.4 General discussion

In this chapter, the transformations undergone by PE upon lowering the pH of its environment have been examined. It is shown that ntPE undergoes a conformational

change when the pH is dropped from 7.4 to 5.8. This confirmed earlier reports describing this transition [150, 154, 206, 240, 241]. However, in most of these studies, influence of pH on the protein's behaviour was examined at pH 4.0 or lower, which is not in the physiological pH range. In fact, no cellular compartment of the endocytic pathway, which has been suggested for PE entry, reaches these acidic pH values. The most acidic compartments described being the late endosome and lysosome with respective pHs of 5.5 and 4.7 [242]. Moreover, the isoelectric point of PE (the pH value where the protein bears no charge) has been reported to be ~5.0 [154, 241]. Above this value, PE carries an overall negative charge, whereas below it, the protein bears an overall positive charge. Therefore if an inversion of its polarity occurred, the protein would behave differently in solution. Such observations would not necessarily reflect physiologically relevant changes. Fryling *et al* (1992) showed that protease cleavage of PE at pH < 5.5 was more extensive than at pH ≥ 5.5. However, in this case the recovery of defined fragments was diminished, suggesting that at pH < 5.5 the protein's digestion pattern is different. This outcome could result from further change(s) associated with exposure to a pH that is near its pI [210].

The results presented here suggested that the transition in conformation in response to an increasing acidity in its environment occurs around pH 6.2. Previous studies reported pH values for this conversion between 4.2 and 6.0 [139, 150, 154, 207, 241]. These discrepancies could derive from the various methods of detection (e.g. fluorescence, trypsin digestion, binding/insertion into membranes) and experimental conditions used by different groups (e.g. temperature, salt and denaturant concentrations). A shift occurring at pH 6.2 would imply that ntPE could undergo a conformational change in the early endosome (pH ~6.3) [242], which is the first compartment the toxin would enter in the endocytic pathway following receptor-mediated endocytosis. It has been demonstrated that the furin cleavage site is not accessible to the protease at neutral pH, and that PE needs to go through structural changes for it to take place [162]. As this activation step was suggested to happen within the endosomal compartment [210], this pH seems to be a reasonable value for the transition point.

The change observed was apparently fully reversible when studied by trypsin digest as the same fragments where generated when compared to the native toxin at neutral pH. While findings by Farahbakhsh *et al* (1987) are in agreement with these data [150], work by Idziorek *et al* (1990) only reported 80% reversibility in the protein structure [154]. However, their work was carried out at pH < 4.0 which could explain why the protein did not return to its original conformation (as a certain degree of protein denaturation cannot be excluded in such conditions). Therefore, additional studies such as assessment of ADP-

ribosylating activity and translocation would be needed to confirm these results. The apparent complete reversibility of the transition suggests that the conformational change experienced by ntPE might be more likely to involve a localised modification in the toxin's structure rather than a major disruption of its molecular organisation. Indeed, intramolecular interactions such as hydrogen and disulphide bonds as well as electrostatic interactions would be harder to re-establish properly by solely re-increasing the pH after disruption. This notion was further supported by HPLC studies that monitored the elution time of the protein run either by itself or in complex with a monoclonal antibody. Importantly, the antibody used in these studies targeted a region of the toxin that encompassed the furin loop but wasn't affected by changes in pH.

Although studies by Méré *et al* (2005) would support the idea that the conformational change described here does not involve a global rearrangement of structure (since creation of a disulphide bond between residues 253 and 364 doesn't affect translocation or cytotoxicity), the data presented in this chapter does not seem to promote the role of Asp358 as a pH sensor whose protonation would be the trigger to the conformational change [202]. In fact, the pKa value of aspartic acid (pKa = 3.65) makes this residue unlikely to become protonated within the pH range considered here. Furthermore, trypsin digestion on truncated mutants seemed to indicate that shortening the protein up to amino acid 303 did not prevent the conformational change from occurring, which would be unlikely if the interaction between Asp358 and Trp305 was critical for this process.

Wedekind *et al* (2001) determined a refined crystallographic structure of PE at a 1.62 Å resolution and suggested that residues located at the interface of the different structural domains might be responsible for inducing the observed pH-dependent conformational change [243]. Their work highlighted specific donor/acceptor interactions that might control (or at least play a role in) conformational change(s) due to their involvement in the formation of salt bridges (= combination of two non-covalent interactions, hydrogen bonding and electrostatic interaction) at lower pH. This is shown in Figure 3-26.

After examining the pKa values of amino acids' side chains (Table 3-6) and relating them to the determined transition pH (pH = 6.2), it appeared that histidine would constitute the most likely residue involved in the shift. Its pKa is the only one between 5.0 and 7.4 and makes it the most probable amino acid susceptible to see its protonation state modified within this pH range.

Three possible histidine residues were indicated as potential salt bridge partners; His249, His262 and His275. All three amino acids are fairly close to the loop carrying the furin-cleavage site (Arg276-Gly280) within PE's primary sequence. As previously mentioned,

this loop has been described as inaccessible to the enzyme at neutral pH [162]. On the contrary, in more acidic environments and supposedly following the protein's conformational change, it becomes exposed to solvent and accessible for cleavage. Therefore it would seem reasonable to believe that the switch triggering the conformational change could be localised in the vicinity of this loop.

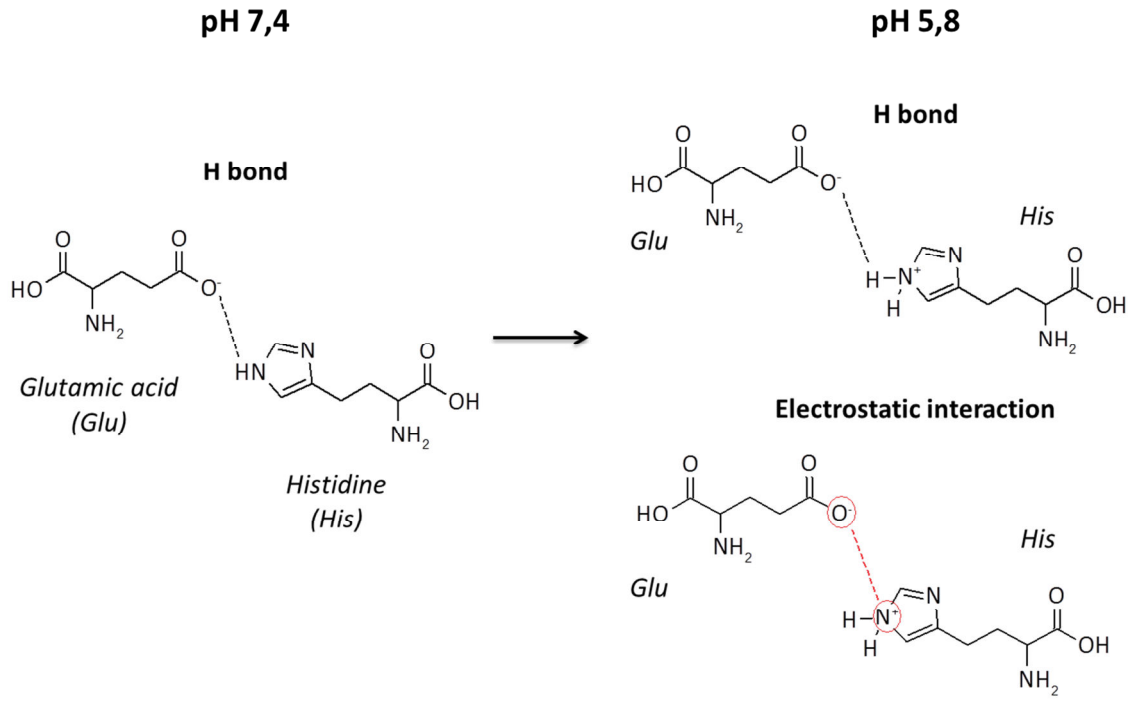

Figure 3-26 – Interactions between Histidine (His) and Glutamic acid (Glu) residues. At neutral pH, only an H-bond is formed between the two amino acids' side chains. When the pH is lowered below pKa (His), one of the nitrogen atoms becomes protonated, leading to an additional (electrostatic) interaction between His and Glu and resulting in the formation of a salt bridge.

Table 3-6 – Three-letter abbreviations and list of the pKa for amino acids' side chains. Data obtained from [244].

Amino acid	Abbreviation	pKa (side chain)
Arginine	Arg	12.48
Aspartic acid	Asp	3.65
Cysteine	Cys	8.18
Glutamic acid	Glu	4.25
Histidine	His	6.00
Lysine	Lys	10.53
Tyrosine	Tyr	10.07

ExPASy ProtScale [181] was used to calculate, for each amino acid in the structure, the degree of solvent concealment (in terms of % buried), the degree of accessibility (% accessible) and the flexibility (Figure 3-27). The region extending from cysteine 265 to proline 290, which includes the loop between α-helices A and B and thus the mentioned His residues, was revealed as particularly interesting. In fact, this section is one of the least buried segments of the protein (% buried as low as 0.25), but is also scored as one of the least accessible areas in the structure (% accessible is 0.38-0.5). Moreover, this zone seems to be especially flexible compared to the average protein flexibility. These observations suggest that this region, which is neither excessively buried nor accessible at neutral pH, but is fairly flexible, has the potential to become solvent-exposed following a minor change in the protein structure. They also confirm that His249, His262 and His275 could be potential candidates involved in the conformational change.

The protein sequence of PE was then run into FlexPred in order to examine the individual flexibility of each of the amino acids involved in these three salt bridges [196]. FlexPred attributes a value between 0 and 1 to each residue depending on their likelihood to be involved in protein conformational switches, and only amino acids with scores > 0.75 are considered as reasonably flexible [197]. It occurred that amongst the six residues involved in the salt bridges of interest, all His249, His262, Asp366 and Glu391 displayed low scores (Table 3-7). On the contrary, Glu80 could be categorised as flexible and His275 is clearly more flexible than the average amino acid as its score nears the 0.75 threshold. These two residues would thus be more likely to trigger the conformational change upon lowering the pH.

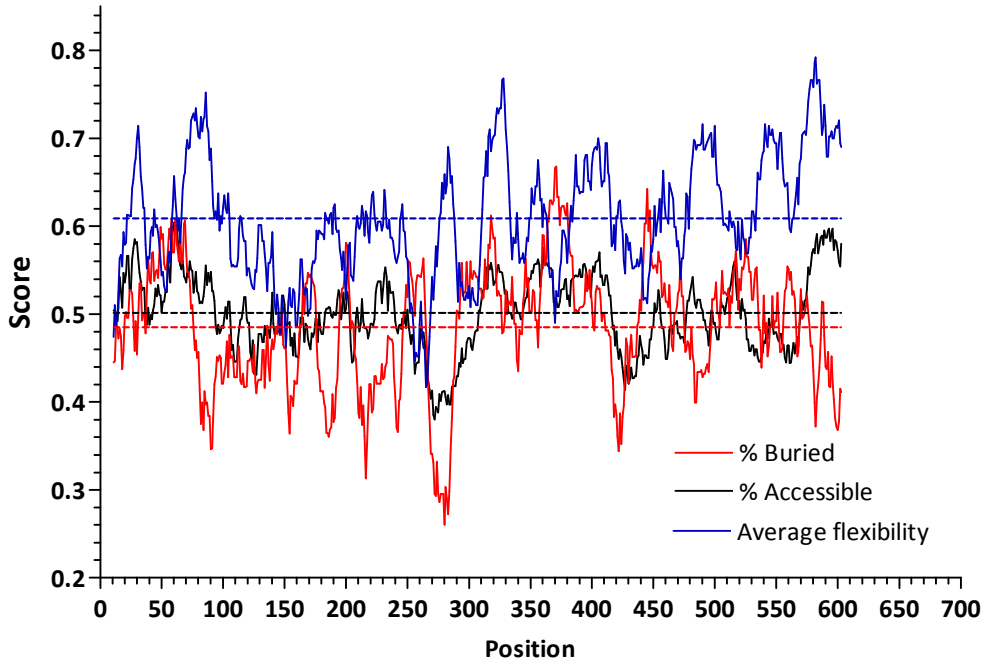

Figure 3-27 – Graphic representation of the relative degree of amino acid flexibility, accessibility and concealment from the surface. Dotted lines represent the respective average values for each curve. (Data were generated using ExPASy ProtScale [181]).

Table 3-7 – Relative individual flexibility of the residues involved in the formation of salt bridges with His. (Scores were calculated using FlexPred [196]).

Acceptor residue	Flexibility score	Donor residue	Flexibility score
Glu80	0.8680	His275	0.7302
Asp366	0.4120	His249	0.4210
Glu391	0.5374	His262	0.2952

These results can be explained by looking at the relative arrangement of the residues on the protein tertiary structure. His262, which presented the lowest flexibility score, is fairly close to the furin site but located in the middle of the α-helix A, while Glu391 is in the centre of a β-strand and its side chain completely solvent inaccessible. Wedekind *et al* suggested that the protonation of His262 might trigger an *untethering* of the loop carrying the furin-cleavage site and, potentially, result in a more global disruption of the protein' structure [243].

His249 is located just at the interface of domains I and II, on a loop preceding the α-helix, and Asp366 is positioned at the beginning of domain Ib. They are also part of a larger set of interactions involving His246, Arg247, Asp384 and Asp387 [243]. Brinkmann *et al*

(1992) mentioned that when the trio His246, Arg247 and His249 was mutated to glutamic acid, the resulting protein did not need activation by DTT and urea to express ADP-ribosylation activity [225]. Chaudhary *et al* (1990) had previously demonstrated that the same mutations resulted in a loss of toxicity on 3T3 cells. However, when all three amino acids were mutated to lysine, which retained their positive charge and hydrogen atoms, toxicity remained unchanged [245]. This could possibly indicate that, due to a lack of hydrogen or electrostatic interactions between Glu and Asp, the protein was unfolded to a greater degree than its native counterpart, and that His249 could play a role in maintaining a "close" conformation in which the loop would be kept from solvent exposure at neutral pH. To confirm the specific role of His249, individual mutations of each of these three amino acids would be required.

His275 is the first residue on the loop connecting α-helices A and B. It is relatively flexible, adjacent to the furin cleavage site, and its position on the loop would thus make it fairly inaccessible to solvent at neutral pH (but possibly exposed under more acidic conditions). Furthermore, Glu80 is also located on a rather long loop which explains its flexibility. Kasturi *et al* (1992) reported that mutation of His275 into Ala (H275A) resulted in a decrease in toxicity in L929 and A431 cells [246]. However, the mutant protein retained its ADP-ribosylating activity, even in the absence of DTT and urea, which are normally required for activation of the native toxin *in vitro*. Moreover, the H275A mutant of PE was much more sensitive to chymotrypsin action but less sensitive to trypsin at neutral pH than native PE. A possible explanation could be that the mutated protein was folded differently compared to PE due to the absence of interaction between the Ala and Glu residues at neutral pH. The increased sensitivity to chymotrypsin could suggest that the mutant protein was more unfolded than its native counterpart, in such a way that the loop would be more accessible, and thus protease-induced cleavage increased. Finally, α-helix A is short and protonation of one residue might be enough to destabilise the entire helix. These observations support the role of His275 as an N-cap residue, which protonation would contribute to the exposure of the furin-cleavage site and thus activation of the toxin.

Studies describing trypsin digestion of the PE mutants truncated at various positions in domain II revealed that removal of domain III changes the protein's sensitivity to the protease. Therefore, as previously discussed, domain III could be imposing structural constraints on the molecule that would contribute to preventing its early activation by furin cleavage. On the other hand, even after removing amino acids 304-613, the protein still seems to undergo a pH-induced and reversible conformational switch. Therefore, one or several residues located prior to this position are likely to be involved in this transition.

Finally, fluorescence techniques were used in this chapter to demonstrate that upon lowering the pH, additional non-polar residues are exposed to solvent and made available for binding to a hydrophobic probe. The region 256-280 is rich in hydrophobic residues [154]. In particular, the last amino acid present on the loop carrying the furin-cleavage site is tryptophan 281 (Trp281). Therefore, the exposure of the loop between helices A and B and of this tryptophan residue following a drop in pH would be in agreement with the increase in hydrophobicity described here by the fluorescence assay. Moreover, it was shown that mutation of Trp281 into alanine increased the toxin's sensitivity to trypsin but completely inhibited its cytotoxic activity on three cell lines [246]. Similarly, replacement of this tryptophan residue by a methionine slightly enhanced intracellular furin cleavage but reduced toxicity by about 100-fold [138]. In this last case, the authors suggested that the observed loss of catalytic activity on cells could be due to a defect in translocation caused by a change in protein conformation. These reports reinforce the idea that exposure of this residue, and more generally of the loop on which it is positioned, are crucial for protein translocation.

Localised modifications which result in small but functionally significant protein conformational changes have been described elsewhere for viral and bacterial proteins [152, 247-251]: glycoprotein B from Herpes simplex virus type 1 (gB) constitutes a particularly interesting case. Crystallisation of gB at pH 8.5 and 5.5 showed that this protein undergoes a pH-induced conformational change which does not affect its overall conformation [252]. Instead, it was suggested that a histidine residue would become protonated upon lowering the pH and act as a "switch" by creating new electrostatic interactions that would force the side chain to move out. This seemingly minor change would actually result in a significant conformational transformation by pulling the second fusion loop F2 out. However, the difference between the two conformations (neutral and acidic pHs) could only be characterised following crystallisation, which reinforces the need to find suitable conditions for crystallisation of PE at pH 6.0. A similar mechanism has also been proposed to explain the membrane-insertion process of another ADP-ribosylating toxin, DT. Conformational change from a *membrane-incompetent* state to a *membrane-competent* state was suggested to originate from the protonation of six histidine residues, which would disrupt several salt bridges between different helices. In particular, Kurnikov *et al* (2013) hypothesised that following protonation, the repulsion between His223 and His257, whose side chains are facing each other, would lead to the destabilisation of one α-helix of DT followed by exposure of a hydrophobic helical hairpin, important for membrane insertion [253].

These results seem to strongly suggest the involvement of histidine residues in the conformation switch undergone by PE under acidic conditions. While the furin-cleavage site remains concealed from the protease at neutral pH to prevent early activation, a decrease in pH in the early endosome would lead to protonation of histidine residues and result in the creation of salt bridges. His249 and His275 appear to be strong contenders for the role, and it cannot be discounted that a combination of their respective protonation's effects might be required to complete the conformational switch. In fact, evidence suggests that mutation of His249 to a negatively-charged residue could lead to early protein activation and defect in translocation activity [245]. Similarly, point mutation of His275 to an uncharged amino acid seems to trigger a defect in toxin translocation [246].

The conformational change undergone by PE in acidic conditions is thus suggested to contribute to protein diversion from the lysosomal degradation pathway towards the Golgi and eventually either the cytosol of non-polarised cells or basal side of polarised cells. In fact, this conformational change could decrease the affinity of PE for the LRP1 receptor, leading to the dissociation of the complex. While the receptor would then recycle to the plasma membrane, the protein would then be free to bind another receptor in the endosome, whose role would be to lead the protein away from the lysosomal pathway.

4 Results 2 – Role of GM1 in the uptake and trafficking of PE

4.1 Introduction

Monosialoganglioside GM1 belongs to the family of gangliosides. It bears two hydrocarbon chains, which constitute the ceramide moiety and are connected to a hydrophilic sugar head composed of two galactose rings (*II* and *IV*) and one of each glucose (*I*), N-acetylgalactosamine (*III*) and sialic acid (*V*) moieties (Figure 4-1 (A)). GM1 has an important role in the physiology of the brain [254-256] and is also the host receptor used by cholera toxin (CT), one of the virulence factors secreted by the intestinal pathogen *Vibrio cholerae*. CT binds to GM1 on the apical surface of polarised epithelial cells and is internalised via receptor-mediated endocytosis [257]. Similarly, other toxins penetrate their target cells following interactions with cell surface lipids [102], which then mediate their transport to the ER in a retrograde manner [104, 111, 258, 259]. PE appears to be an exception, as its endocytosis in non-polarised cells is mediated by a surface protein receptor, the α-2-macroglobulin receptor/low density lipoprotein receptor-related protein (LRP1 aka CD91), rather than a lipid receptor [108], and because the intracellular pathway it exploits to reach the ER has been shown to vary from those of the lipid-binding proteins [142, 143]. One study has suggested that LRP1 may be involved in the uptake of PE by polarised cells that results in epithelial transcytosis [164].

However, preliminary studies performed by Dr Thomas Hunter (personal communication) using bio-layer interferometry (BLI) have shown that PE can interact moderately and reversibly with GM1, and that the binding affinity was greater at mildly acidic rather slightly alkaline pH. These results were complemented by HPLC studies that demonstrated incubation of PE with asialoGM1 instead of GM1 did not result in complex formation, suggesting the protein interacts with the sialic acid moiety of the ganglioside. Furthermore, Carter (2014) suggested that GM1 could be involved in the transcytosis of PE, as addition of CT considerably reduced the transport of fluorescent PE across a monolayer of polarised epithelial cells [27]. These results suggest that interaction between the protein and the ganglioside might be required for efficient transcytosis. However, neither the location, nor the role of this interaction in the trafficking of PE in polarised or non-polarised systems, has been elucidated.

In this chapter, the role of GM1 in the uptake and early trafficking of PE was investigated in non-polarised epithelial cells. First, BLI was employed to quantify the interaction between the protein and the ganglioside at different pH values. The location of the binding site on PE was then examined by spectrofluorometry. Finally, the role of GM1 in the internalisation and intracellular transport of PE was studied using a fluorescently-labelled protein.

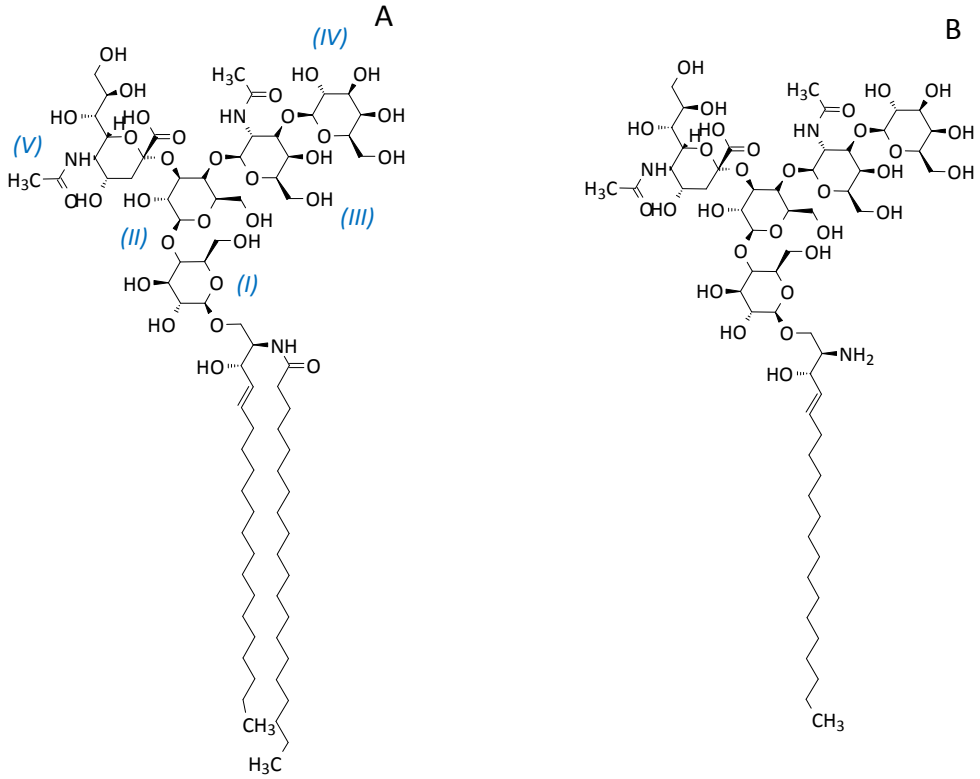

Figure 4-1 – Molecular structures of (A) monosialoganglioside GM1 and (B) lysoGM1.

4.2 Methods

Determination of the critical micellar concentration of lysoGM1 using the dye micellisation method

LysoGM1 is a version of GM1 lacking one of the two hydrophobic chains (Figure 4-1 (B)) [260] that was used in spectrofluorometry studies to investigate the location of the GM1 binding site on PE. Its critical micellar concentration (CMC) was determined using the dye micellisation method with eosin Y [261]. Eosin Y (Figure 4-2) is a dye which maximum absorption occurs at 518 nm in the absence of micelles. Due to encapsulation of the dye into surfactant micelles, increasing the surfactant concentration results in a progressive shift of the maximum absorption wavelength from 518 nm to 538 nm. It has been reported that the variation can be better followed at 542 nm (A_{542}) and that the inflection point on the A_{542} = f ([lysoGM1]) or λ_{max} = f ([lysoGM1]) curves corresponds to the CMC [261].

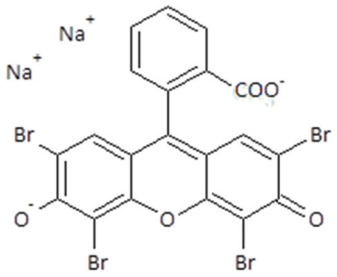

Figure 4-2 – Molecular structure of eosin Y.

5 µl lysoGM1 samples were prepared in phosphate buffer (PB) 5.8 containing 0.1 M NaCl at concentrations ranging from 1 x10^{-9} to 1 mM and eosin Y was added to each sample to a final concentration of 0.19 mM. Absorbance data were collected at 542 nm (A_{542}) using a NanoDrop™ 2000c on pedestal setting [261].

4.3 Results and discussion

4.3.1 Quantitative characterisation of the interaction between PE and GM1 using BLI

In order to quantify the interaction between PE and GM1 in both acidic and neutral conditions using BLI, ntPE was biotinylated to be immobilised on the biosensor tip via biotin-streptavidin interactions, and GM1 was used as the analyte in solution in buffer. Characterising the strength of the interaction between the protein and its receptor at

different pHs is essential to determine at which stage the interaction between PE and GM1 is most prone to take place.

4.3.1.1 Preparation of biotin-labelled PE

In order to obtain biotinylated protein, the C-terminal TEV sequence of ntPE GS TEV was digested with a commercial AcTEV protease; 1.28 mg (19 nmol) of cleaved ntPE GS TEV was collected in 3.5 ml PBS and incubated in presence of 50-molar excess sulfhydryl-reactive EZ-Link® Maleimide-PEG_2-Biotin reagent (950 nmol ≡ 0.5 mg) for 3 h at RT (Figure 4-3). Following desalting, buffer exchange and concentration, 200 µl of ntPE-biotin at 3.5 mg/ml were collected in PBS.

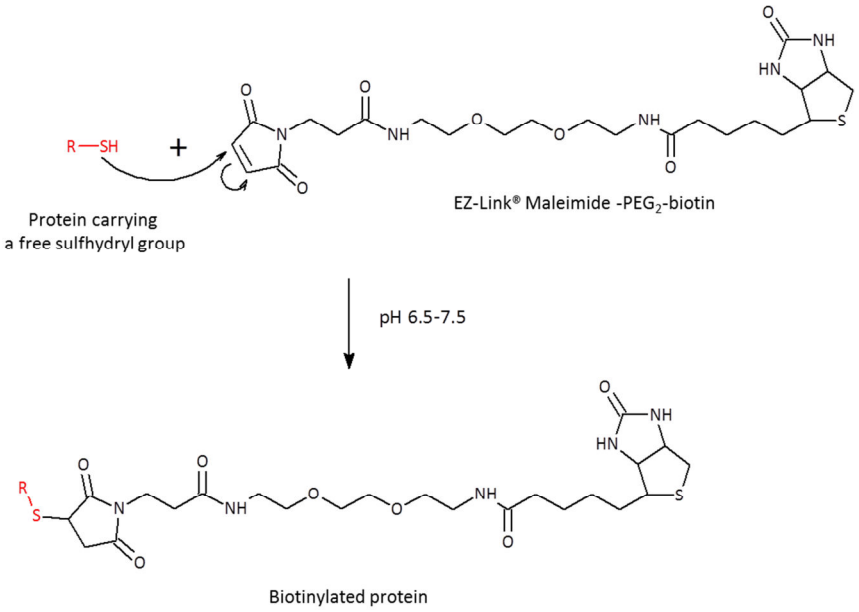

Figure 4-3 – Reaction scheme for biotinylation of a sulfhydrylated protein (R) with EZ-Link® Maleimide-PEG_2-biotin.

4.3.1.2 Characterisation of the PE-GM1 interaction by BLI

BLI was used here to characterise the interaction between PE and GM1 in neutral and mildly acidic conditions. Measurements were performed in collaboration with Dr Thomas Hunter who had access to a BLI instrument.

Experiments were conducted at 37 °C in 0.1 M potassium-phosphate buffer at pH 5.5 or 7.5. The plate layout used is presented in Figure 4-4. The biosensor tip was first dipped in buffer in order to establish a baseline (Equilibration, Column 1). Biotinylated ntPE was then loaded on the sensing surface (Loading, Column 2). A second baseline step was

performed to remove unbound ligand from the biosensor and assess for possible drifts caused by non-specific binding (Baseline, Column 3). The association between GM1 and ntPE was then monitored in real time (Association, Column 4). Finally, the biosensor was dipped into buffer one last time and dissociation was observed (Dissociation, Column 5). A summary of the kinetics assay step times is presented in Table 4-1 and the sensorgrams obtained for each condition are displayed in Figure 4-5. For each pH, a reference well, devoid of attached ligand but exposed to the same ganglioside concentration, was used to measure non-specific binding of GM1 to the sensor surface (Lanes G and H).

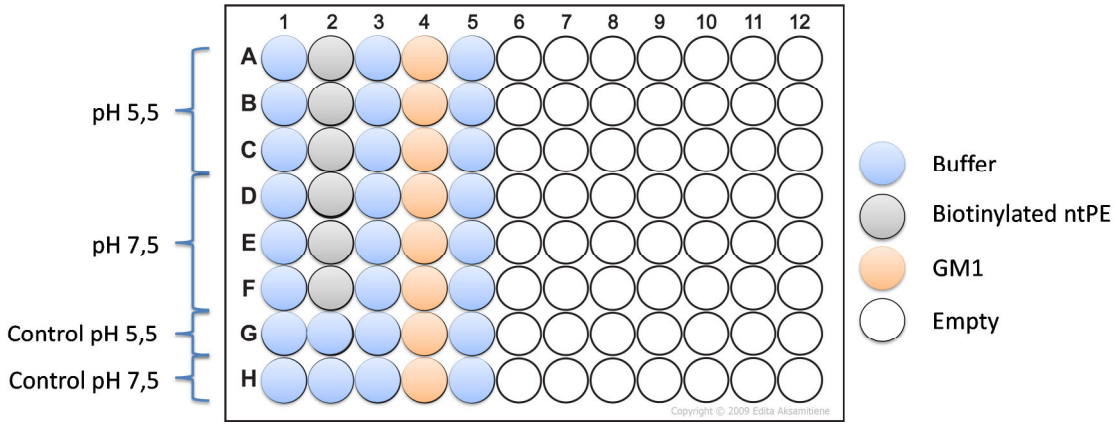

Figure 4-4 – Plate layout diagram for the kinetics assay.

Table 4-1 – Summary of kinetics assay procedure.

Step #	Step name	Time (sec)	Sample plate column
1	Equilibration	60	1
2	Loading	120	2
3	Baseline	35	3
4	Association	120	4
5	Dissociation	95	5

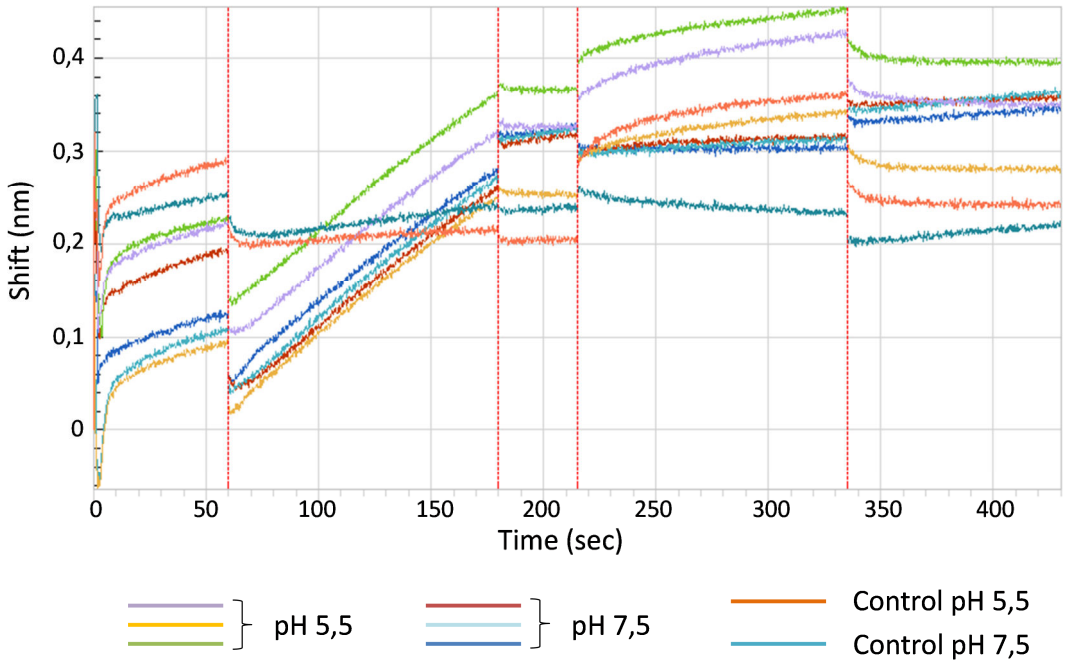

Figure 4-5 – Kinetic characterisation of the interaction between ntPE and GM1. Sensorgrams obtained following interaction of GM1 and immobilised, biotin-labelled ntPE at pH 5.5 and 7.5.

Observation of the sensorgrams revealed that the curves were biphasic, especially at lower pH. This indicates that more than one interaction was taking place. As a result, data were fitted to a 2:1 heterogeneous ligand binding model (Figure 4-5) as described in Equation 4-1, where A is the analyte in solution, and B_1 and B_2 represent two different ligands on the surface [262]. K_D is the dissociation constant (expressed in M) and k_a and k_d are the association and dissociation constant rates, respectively. This model is used when one molecule of analyte can bind to two different ligands immobilised on the surface. It also assumes that there are no cooperative interactions and that the analyte in solution is a single species. The observed binding is then the sum of the interaction with the two different ligands. This is an appropriate model for samples in which the ligand is not homogeneous or fully active, e.g. when the ligand prepared contains a small amount of misfolded protein which could still bind to the analyte or when the immobilisation of the ligand on the surface can alter its activity. The fact that the heterogeneous ligand binding model provided a best fit for the data collected here, especially at pH 5.5 (r^2 = 0.996), could be related to the instability and dynamic behaviour of PE in mildly acidic conditions, as previously described in Chapter 3. In fact, if the conformation adopted by ntPE in acidic conditions is unstable, then the protein could bind to GM1 as two different entities. A summary of the parameters obtained following data fitting is presented in Table 4-2.

Equation 4-1 – 2:1 heterogeneous ligand model.

$$A + B_1 \underset{k_{d1}}{\overset{k_{a1}}{\rightleftharpoons}} AB_1 \quad K_{D1} = \frac{k_{a1}}{k_{d1}}$$

$$A + B_2 \underset{k_{d1}}{\overset{k_{a2}}{\rightleftharpoons}} AB_2 \quad K_{D2} = \frac{k_{a2}}{k_{d2}}$$

Table 4-2 – Summary of the parameters obtained by fitting experimental data to a heterogeneous ligand binding model. Parameters are the average of three individual lanes.

Sample	K_{D1} (M)	K_{D2} (M)	k_{a1} (1/M.s)	k_{a2} (1/M.s)	k_{d1} (s^{-1})	k_{d2} (s^{-1})	r^2
7.5	7.06×10^{-6}	7.06×10^{-6}	4.43×10^{2}	4.43×10^{2}	2.60×10^{-3}	2.60×10^{-3}	0.711
5.5	$< 1 \times 10^{-12}$	3.01×10^{-9}	6.72×10^{5}	1.33×10^{7}	$< 1 \times 10^{-7}$	3.70×10^{-2}	0.996

The calculated K_D values indicate that ntPE binds to GM1 at pH 5.5 and 7.5 with relatively high affinities as in both cases $K_D < 10^{-5}$ M. However, the protein and receptor complex constitutes a higher affinity pair in acidic conditions ($K_{D5.5} < 10^{-9}$ M). The results obtained following data fitting confirmed that while the protein was immobilised under one state only at pH 7.5 ($K_{D1} = K_{D2}$), more than one species of ntPE was attached to the tip surface at pH 5.5 ($K_{D1} \neq K_{D2}$). Since both samples originated from the same batch of protein, this discrepancy likely reflects the dynamicity of ntPE in acidic conditions mentioned above, and its presence under different conformations on the tip surface. One of these conformations interacted much more tightly with GM1 ($K_{D1} < 1 \times 10^{-12}$ M and $k_{d1} < 1 \times 10^{-7}$ s^{-1}) than the other ($K_{D2} = 3.01 \times 10^{-9}$ M and $k_{d2} = 3.70 \times 10^{-2}$ s^{-1}). This could suggest that the pair showing the highest binding affinity involved a protein which had fully undergone its conformational change, while the other species could be a protein which was either still in transition, unable to reach its final state, or even kept alternating between the two states.

It was shown in Chapter 3 that following internalisation, ntPE undergoes a conformational change, which is likely to occur in the early endosomal compartment. Together with the results presented here, data seem to indicate that the pH-dependent difference in binding

affinity observed for ntPE interactions with GM1 could be due to a difference in binding site exposure reflecting an ntPE-associated conformational change. Moreover, it was previously concluded that the rearrangement in the toxin's structure is likely to occur within domain II, particularly between amino acids 252 and 303, and that it results in the exposure of formerly buried hydrophobic residues. Therefore, it is possible for GM1 to interact, at least partially, with the region of changing hydrophobicity revealed by ANS studies (Section 3.3.5). Consequently, if GM1 was added in solution to ntPE, and did interact with a hydrophobic region of the protein, it would then prevent contact between the dye and these exposed residues and inhibit any increase in fluorescence at pH 5.8. Spectrofluorometry was therefore employed in an attempt to further characterise the interaction(s) of GM1 with ntPE.

4.3.2 Investigation of the GM1 binding site by spectrofluorometry

ANS was employed here to determine whether the GM1 binding site is located in a region of variable hydrophobicity, possibly within domain II. Such studies are complicated by the fact that GM1, as a ganglioside, contains a highly hydrophobic tail that is prone to ANS binding and thereby would increase the dye's fluorescence in solution (Figure 4-6).

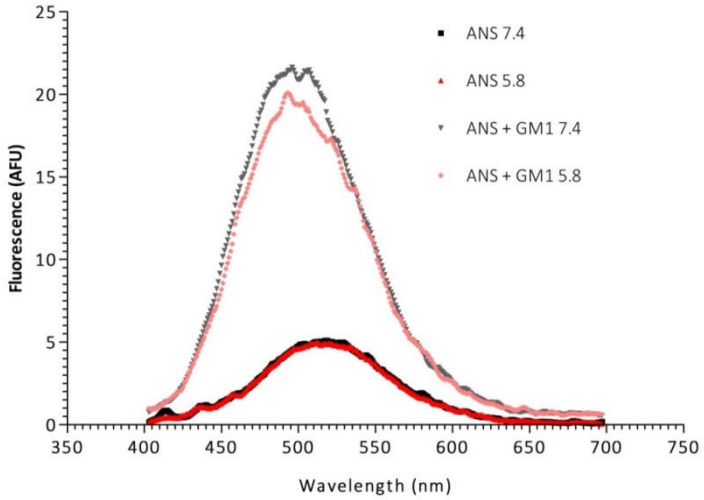

Figure 4-6 – ANS readily binds to GM1 in solution. Fluorescence spectra of ANS and ANS + GM1 at pH 7.4 or 5.8 with [ANS] = 100 µM and [GM1] = 2.5 µM.

In order to reduce this effect, GM1 was substituted in these experiments by lysoGM1, which is a version of GM1 lacking one of the two hydrophobic chains, which dramatically decreases its hydrophobicity (Figure 4-1). The hypothesis underlying this work was that the interaction between protein and ganglioside occurred via the sialic acid moiety of the head group, and therefore substituting GM1 by lysoGM1 should not affect the ability to

accurately test this hypothesis since it would not affect the nature of the ganglioside binding properties being studied.

For these studies, it was important to maintain lysoGM1 concentration below its CMC, as the steric hindrance due to the formation of ganglioside micelles could affect the protein-receptor interaction. Unfortunately, CMC information for lysoGM1 could not be found in the literature. Therefore, this data was determined empirically for the conditions to be used in subsequent studies.

4.3.2.1 Determination of lysoGM1 CMC

Eosin Y was employed to record the appearance of lysoGM1 micelles using the dye micellisation method. The shift from monomeric to micellar form was monitored by changes in maximum absorption wavelength (λ_{max}) as a function of lysoGM1 concentration. Figure 4-7 illustrates lysoGM1 CMC determined by the shift in λ_{max} as the concentration of ganglioside was increased from 1 $x10^{-9}$ to 1 mM. Three phases could be observed: i) when [lysoGM1] < 0.05 mM, λ_{max} remained stable at 518 ± 2 nm, characterising the concentration range where the ganglioside was present as a monomer and the dye was free in solution. ii) A second stable zone could be observed as λ_{max} reached 528 ± 1 nm when [lysoGM1] ≥ 0.2 mM. The majority of the ganglioside was then present under micellar form and most of the dye was encapsulated into these micelles. Between i) and ii) was a region of rapid transition in λ_{max}, characteristic of the progressive encapsulation of the dye into the lysoGM1 micelles as these started to form. This zone was characterised by the presence of lysoGM1 under both monomeric and micellar form. Figure 4-8 depicts the three phases of the micelle formation process.

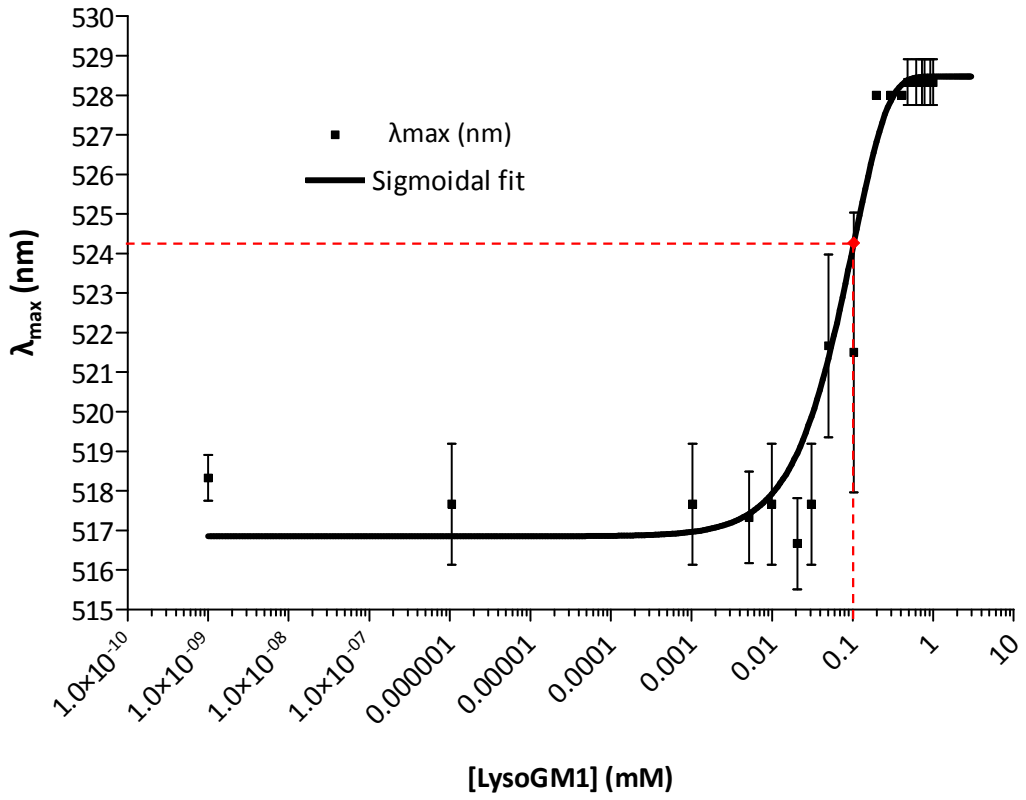

Figure 4-7 – Critical micellar concentration determination of lysoGM1 using the dye micellisation method. λ_{max} values were determined over a concentration range of the ganglioside. Eosin concentration was 0,19 mM. Bars represent mean ± SD for n = 3 independent samples. The plain black line represents a sigmoidal fit of the data. The red dashed line indicates the coordinates of the inflection point to the sigmoidal curve.

A sigmoidal curve could be fitted to the experimental data (r^2 = 0.9647) (Equation 4-2) and determination of the inflexion point allowed for an evaluation of the critical micelle concentration of lysoGM1. Using this method, the CMC was calculated to be 0.09 mM. This value is in agreement with the graphic data which suggested that micelle formation was initiated for [lysoGM1] ≥ 0.05 mM.

Equation 4-2 $$y = 528/(1 + exp((0.3817 - x)/(0.1006)))$$

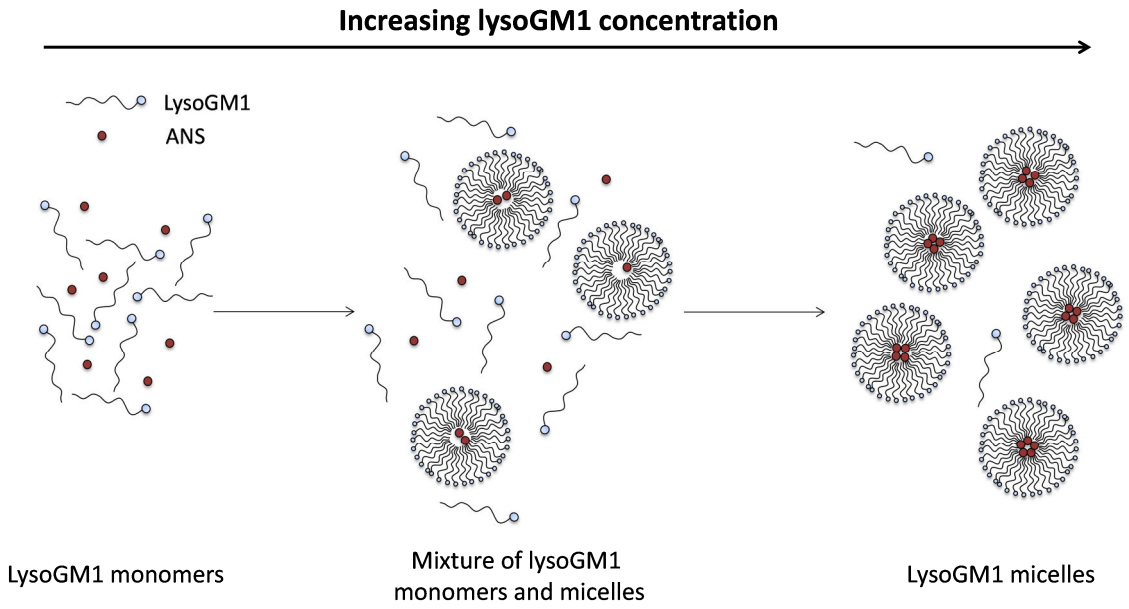

Figure 4-8 – Micelle formation process with increasing concentrations of lysoGM1.

The dye micellisation technique using eosin Y was shown to procure CMC values comparable to those obtained by surface tension measurements and could thus be considered a reliable method for determination of surfactant CMC [261]. Here, it was used to determine an approximate CMC for the ganglioside lysoGM1, in order to ensure that further fluorescence studies would be performed on the monomeric form of this compound. It was concluded that for any concentration below 0.09 mM, lysoGM1 would not form micelles in the particular conditions used here. CMC data for gangliosides, including GM1, remain controversial. While some reports suggest that the critical micellar concentration for GM1 is of the order of 10^{-8} M [263-265], others have determined that GM1 only forms micelles at micromolar [266] or even higher concentrations [267]. The discrepancy in these data might be due to variations in experimental conditions as solvents (aqueous or partly organic) and techniques used (conductivity, surface tension and spectrophotometry) typically differ in most of these studies; challenges that are further complicated by the fact that the degree of purity of the gangliosides has a significant impact on the end result and these are likely different between studies [261]. The greater CMC value for lysoGM1 compared to GM1 was expected as the propensity to form micelles would be dependent upon the reduced hydrophobic character resulting from the presence of one versus two acyl chains [268]. In that respect, the values determined here with the dye micellisation technique seem coherent.

4.3.2.2 Fluorescence studies

It was previously shown that as the pH decreases, PE undergoes a conformational change which both results in exposure of hydrophobic residues and increased GM1 binding. To investigate a potential connection between these two events and the possibility that the newly exposed hydrophobic sites might be part of the GM1 binding site, displacement studies were performed using ANS fluorescence. ANS fluorescence is increased at lower pH due to interaction with additional hydrophobic residues. However, if these residues are involved in GM1 binding to PE, ANS should not be able to interact with these sites and no increase in fluorescence should be observed [191, 269].

As mentioned earlier, GM1 was replaced by lysoGM1 in order to minimise binding of ANS to the ganglioside's ceramide moiety. To test for specificity and ensure that the remaining hydrophobic tail of the ganglioside did not interfere with ANS fluorescence measurements, N-acetylneuraminic acid (NANA) (sialic acid) was used as a control. Measurements were also performed after replacing lysoGM1 by sucrose to investigate whether potential interactions would be sugar-specific (Figure 4-9).

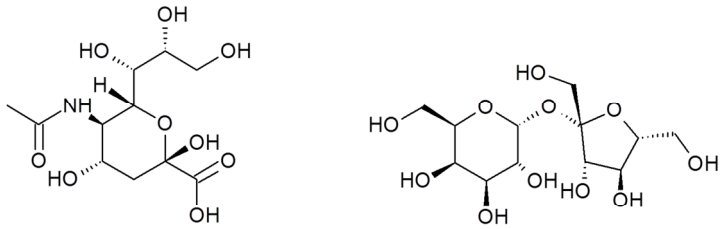

Figure 4-9 – Molecular structures of N-acetyl neuraminic acid (sialic acid) and sucrose.

Each sample was corrected with either the intrinsic fluorescence of ANS or that of ANS in the presence of lysoGM1 or one of its substitutes, and values of AUC, ΔF and $\lambda_{em,max}$ were determined (Table 4-3). The study of the influence of each lysoGM1, NANA and sucrose on the fluorescence of ANS revealed that none of these components had a significant effect on the dye fluorescence spectrum within the 400-700 nm range that was used for analysis in these studies. In fact, the AUC were similar and $\lambda_{em,max}$ remained unchanged (Table 4-3 and Figure 4-10 (A)). Moreover, no pH-induced difference could be observed between the fluorescence spectra of ANS in presence of each of these compounds (Figure 4-10, (A), (C), (E), (G)). Therefore, none of these compounds seemed to affect ANS fluorescence in the present experimental conditions.

When ntPE was added to ANS in solution, only the variation between $AUC_{5.8}$(ANS + ntPE) and $AUC_{5.8}$(ANS + ntPE + lysoGM1) was recorded as statically significant (Figure 4-11 (B)). However, the ratios ΔF between ANS + ntPE and ANS + ntPE + lysoGM1 were not significantly different (Figure 4-11 (C)), suggesting that the addition of lysoGM1 did not affect the fluorescence of ANS in the presence of ntPE at either pH. Similarly, the fluorescence of the protein and ANS solution was unaffected by the presence of NANA or sucrose.

Overall, these data revealed that the presence of lysoGM1 in solution did not affect the exposure of hydrophobic residues available for ANS binding on the surface of ntPE at either pH. These results did not support the hypothesis that lysoGM1 binding to ntPE could occur through a hydrophobic surface area exposed due to conformational change(s) induced at acidic pH. This finding would be coherent with the hypothesis that GM1 and lysoGM1 interact with PE via their sialic acid moiety as NANA is a fairly polar group (Log P = -3.56 [226]). However, to ensure that the absence of variation was due to the lack of ANS displacement, a positive control with a molecule known to dislocate ANS from one of its binding sites would be required.

Table 4-3 – Values of *ΔF* and $\lambda_{em,max}$ collected by spectrofluorometry for different mixtures of ANS, ntPE and lysoGM1 or one of its substitutes.

Sample	*ΔF*	$\lambda_{em,max}$ (nm)
ANS 7.4		518
	0.976	
ANS 5.8		518
ANS + lysoGM1 7.4		520
	0.952	
ANS + lysoGM1 5.8		518
ANS + NANA 7.4		515
	1.020	
ANS + NANA 5.8		516
ANS + sucrose 7.4		516
	0.964	
ANS + sucrose 5.8		518
ANS + ntPE 7.4		483
	1.449	
ANS + ntPE 5.8		475
ANS + ntPE + lysoGM1 7.4		488
	1.526	
ANS + ntPE + lysoGM1 5.8		479
ANS + ntPE + NANA 7.4		483
	1.432	
ANS + ntPE + NANA 5.8		480
ANS + ntPE + sucrose 7.4		489
	1.506	
ANS + ntPE + sucrose 5.8		478

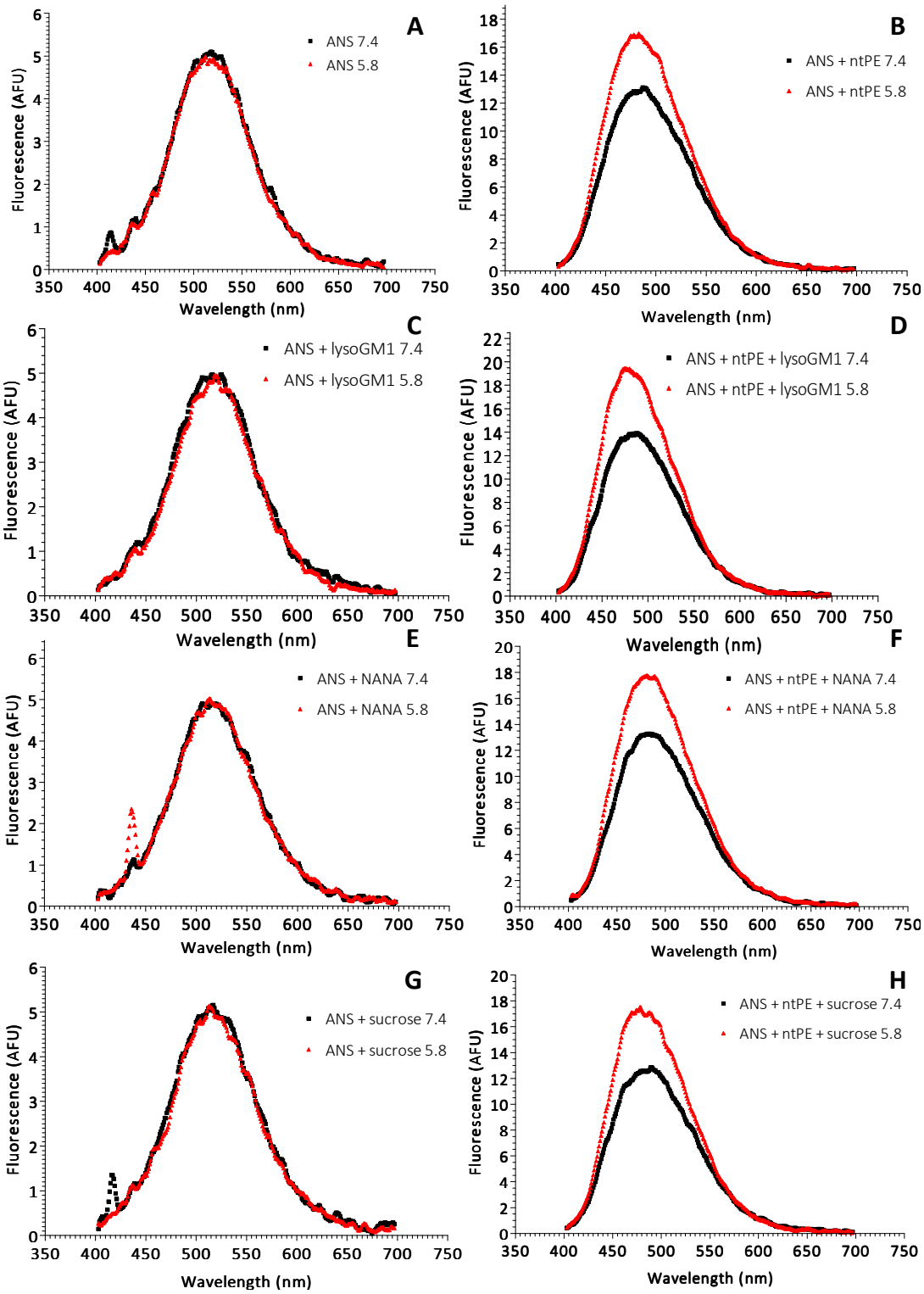

Figure 4-10 – Fluorescence spectra of (A) ANS, (B) ANS + ntPE, (C) ANS + lysoGM1, (D) ANS + ntPE + lysoGM1, (E) ANS + NANA, (F) ANS + ntPE + NANA, (G) ANS + sucrose and (H) ANS + ntPE + sucrose in CP 5.8 (red) and 7.4 (black). For all measurements, [ANS] = 100 µM, [ntPE] = 1.52 µM and [lysoGM1] = [NANA] = [sucrose] = 2 µM.

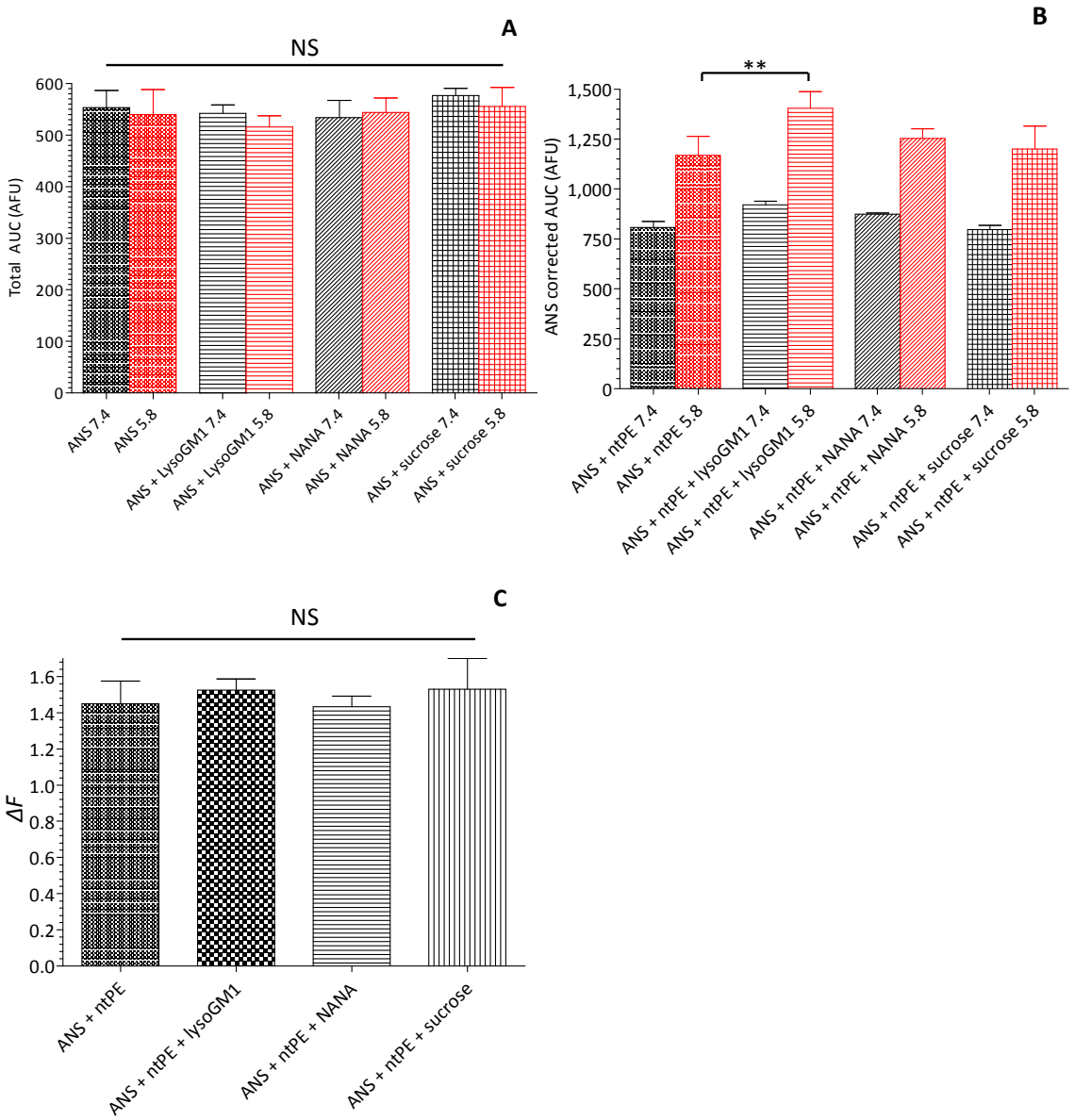

Figure 4-11 – Statistical analysis of the areas under the curves of (A) ANS and (B) ANS + ntPE in presence of lysoGM1, NANA and sucrose and (C) Variations in *ΔF* in different samples. In (A) and (B) data at pH 7.4 are represented in black and data at pH 5.8 are displayed in red. Bars show mean ± SD for n = 3 independent samples where ** P < 0.01 and NS is non-significant.

4.3.3 GM1 is involved in the uptake and early trafficking of PE in non-polarised cells

In non-polarised (NP) cells, internalisation of PE has been reported to occur by endocytosis following binding to LRP1 as a cell-surface receptor [108]. However, BLI studies showed that ntPE also binds to GM1 at both pH 5.5 and 7.5, and that the

interaction is stronger in mildly acidic conditions. This could suggest a role for GM1 as a PE receptor not only inside the cell (endosomal compartment), but also on the cell surface, where the pH is closer to physiological values. The involvement of GM1 in the uptake and early intracellular trafficking of PE by NP cells was therefore examined using a fluorescently-labelled protein. Further, the individual and combined effects of neuraminidase treatment on the cells and addition of cholera toxin B subunit (CTB) to the protein mixture were also analysed.

4.3.3.1 Coupling of PE to a fluorescent tag

All coupling experiments were performed and purified using the same protocol. As an example, coupling of full-length ntPE GS TEV to Alexa Fluor® 568 is described below.

After cleavage of the C-terminal TEV sequence with a commercial AcTEV protease, ntPE GS TEV was incubated with a maleimide-functionalised Alexa Fluor® 568 tag (ntPE-A568). In order to separate the tagged protein from unreacted materials (uncoupled tag), the sample was loaded on a size exclusion column and purified by FPLC. The different components were eluted with PBS, and the fractions corresponding to the UV-absorbing peaks were separated by SDS-PAGE (Figure 4-12).

Purification by GF chromatography resulted in the separation of two main UV-absorbing compounds. While the first peak (fractions M_{12}-N_1) corresponded to a band at ~70 kDa on Coomassie-stained gel, no bands corresponding to the second peak (fractions N_5-N_9) could be observed. This shows that the coupled ntPE-A568 and unbound dye were eluted in fractions M_{12}-N_1 and N_7-N_9, respectively. In fact, the dye is a very small molecule (MW = 880.9 Da [270]) and thus could not be seen on the gel, whose MW range was between ~17 and 100 kDa. The absence of secondary bands revealed that the coupled material was, as expected, very pure. Thus, fractions M_{14}-M_{15} were concentrated together for further use.

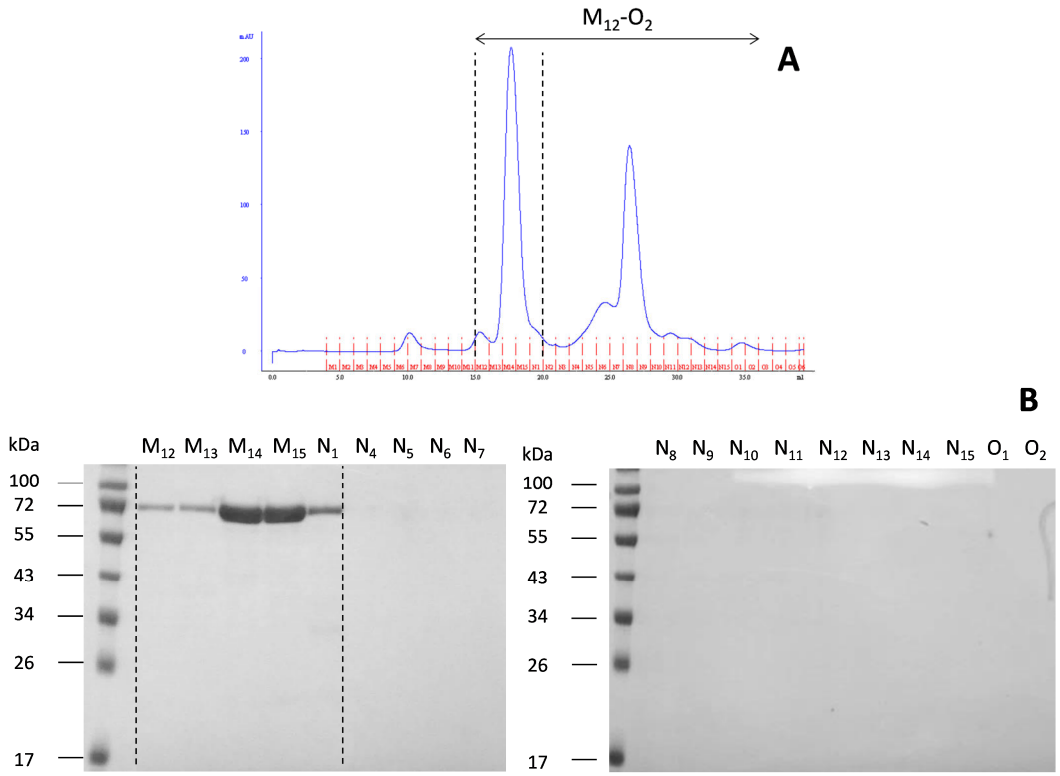

Figure 4-12 – Enrichment of ntPE-A568 by GF chromatography. (A) Chromatogram obtained for GF column separation. (B) Coomassie-stained SDS-PAGE of fractions containing the UV-absorbing material. M-, N- and O-labelled lanes in (B) correspond to arbitrary tray row and column reference on the fraction collector and are illustrated by the red dashes on (A). Fractions covered by the arrow in (A) indicate the complete range of fractions displayed in (B). The black dotted lines marked on both (A) and (B) indicate the fractions containing ntPE-A568 that were collected.

4.3.3.2 Uptake of PE by non-polarised epithelial cells

Non-confluent, non-polarised (NP) Caco-2 cells seeded on glass coverslips were incubated with 20 µg ntPE labelled with a fluorescent tag (ntPE-A568) diluted in 100 µl complete growth medium (= 3 µM final protein concentration). After 2 h, ntPE-A568 could be observed inside these NP cells, localising to individual spots at the periphery of the nuclei (Figure 4-13). Next, the effect of neuraminidase on protein entry was tested; NP cells were treated with the enzyme using several experimental formats. Initially, the effect of cell pre-treatment with neuraminidase on the fate of added ntPE-A568 was examined. The pattern of intracellular fluorescence was observed to be similar for untreated NP Caco-2 cells compared to those following a 15-min pre-treatment with 1 U/ml neuraminidase. On the other hand, when the length of pre-treatment was extended to 2 h, a net increase in the amount of internalised protein could be detected, suggesting that removal of sialic acid

residues by the action of neuraminidase resulted in increased ntPE-A568 internalisation. To explore this possibility further, NP Caco-2 cells were subjected to the same treatment and 3.5 μM cholera toxin B subunit (CTB), which selectively binds to sialic acid residues of the ganglioside GM1, was added to ntPE-A568 during incubation. In this case, hardly any intracellular fluorescence could be detected. Similarly addition of 3.5 μM CTB to ntPE-A568 in the absence of neuraminidase (Figure 4-13; bottom) decreased the amount of fluorescent material that could be observed inside the cells compared to ntPE-A568 alone (Figure 4-13; top). Although no co-localisation studies were performed to determine exactly which final intracellular compartment the internalised ntPE-A568 reached, observation of the fluorescence patterns were consistent with the possibility that the protein could have travelled to the Golgi and/or possibly the ER. Importantly, the pattern of ntPE-A568 was inconsistent with EE or lysosome compartments as these are not typically adjacent to the nuclei of NP Caco-2 cells.

Neuraminidase is an enzyme that cleaves sialic acid (SA) groups from glycoproteins and glycolipids [271]. In particular, gangliosides are progressively transformed from di-, tri- and tetrasialogangliosides to mono- and asialogangliosides by neuraminidase. Although the enzyme used here originated from *Clostridium perfringens*, neuraminidase is also secreted by bacteria, such as *Pseudomonas aeruginosa* and *Vibrio cholerae* [272, 273]. The role of bacterial neuraminidase isn't well defined, but it has been suggested that one of its functions might be to prepare the cell surface for microbial attack. In fact, mucosal surfaces are heavily glycosylated [274] and neuraminidase could participate in the intoxication process by clearing the way to the epithelium through cleavage of SA groups from surface glycolipids and glycoproteins [275]. In the case of *Pseudomonas aeruginosa*, Soong *et al* (2006) suggested that neuraminidase might facilitate infection by taking part in the formation of biofilms [276]. In fact, the enzyme would modify the surface of epithelial cells in order to facilitate bacterial attachment; an event that might be exaggerated in cystic fibrosis patients, whose airway epithelia are more prone to modification than that of healthy patients.

Another potential role for this enzyme could be to expose cell-surface receptors for bacterial toxins, thereby increasing their internalisation and facilitating the subsequent cell intoxication process. This mode of neuraminidase action has been mentioned in the case of cholera toxin (CT). It was suggested that following its release from the bacteria, the enzyme could digest SA groups from surface glycolipids and especially gangliosides, which would be transformed into additional monosialoganglioside molecules. GM1 is the host cell receptor for CT [109, 155, 156] and was proven to be resistant to *Vibrio cholerae*-

secreted neuraminidase [277]. Its cleavage into asialoGM1 by the enzyme is thus limited. With more GM1 molecules unmasked on the cell surface by the removal of sialic acid from non-ganglioside molecules, the uptake of CT would be promoted and cell intoxication increased [277-279]. However, findings by Galen *et at* (1992) revealed that neuraminidase was not essential for CT action, and that the enzyme might actually be an accessory virulence factor whose action and enhancement of pathogenicity would be noticeable only if conditions for the uptake of CT were not optimal [277].

Here, pre-treating the cells with neuraminidase aimed at clearing cell-surface SA groups on non-ganglioside molecules before applying ntPE [271]. The data collected showed that neuraminidase treatment was not compulsory for protein internalisation but indicated that pre-incubating the cells for 2 h in the presence of the enzyme enhanced protein entry. This effect could be due to removal of cell-surface SA groups unrelated to GM1 that could act to distract an interaction between ntPE and the SA group of GM1. Thus, removing the bulk of surface SA could promote ntPE internalisation. On the contrary, nearly no protein could be observed in the cells following addition of CTB (whether the cells were exposed to neuraminidase or not), implying that targeted GM1 blocking greatly reduced the cellular uptake of ntPE and supporting the likelihood that interaction with GM1 may play a role in ntPE internalisation.

As neuraminidase action seemed to be both optional and beneficial to protein uptake, but specific GM1 blocking appeared detrimental to this process, these results suggest that this ganglioside functions in the internalisation of PE and *P. aeruginosa*-secreted neuraminidase could play a role in such a process by helping the toxin efficiently access the receptor. Although neuraminidase treatment should remove SA moieties from most surface proteins and lipids simultaneously, the recycling rate of lipids is much faster than that of proteins (minutes compared to hours) [280-282]. In fact, one of the lipid metabolic pathways allows for membrane lipids to be directed from the early endosome to the Golgi apparatus, where additional glycosylation can take place before the lipid is recycled back to the plasma membrane [281]. On the contrary, most proteins have to be entirely resynthesized (although the proportion of direct reglycosylation and recycling through the TGN compared to *de novo* synthesis depends both on the cell line and the protein considered) [283-285]. As a consequence, monosialated gangliosides would be recycled to the cell surface long before the bulk of sialated proteins were restored. Moreover, although the overall number of functional surface GM1 molecules might be reduced compared to untreated cells, the remaining gangliosides would be more accessible for binding by the toxin, which would itself be less distracted by surrounding sialated surface

proteins. Finally, it would not be impossible for neuraminidases secreted by *Vibrio cholerae* and *Pseudomonas aeruginosa* to present comparable characteristics, and for the enzyme secreted by the latter to be unable to cleave the SA moiety from monosialiogangliosides. As a conclusion, neuraminidase could improve GM1 binding by a combination of effects that would reduce the non-specific interaction between PE and sialated surface proteins and increase the potential for enhanced interactions with exposed GM1 molecules concomitantly. The studies presented here indicate that removal of the bulk of sialated protein from the cell surface could improve the GM1-associated cellular uptake of PE and support the role of neuraminidase as an accessory virulence factor.

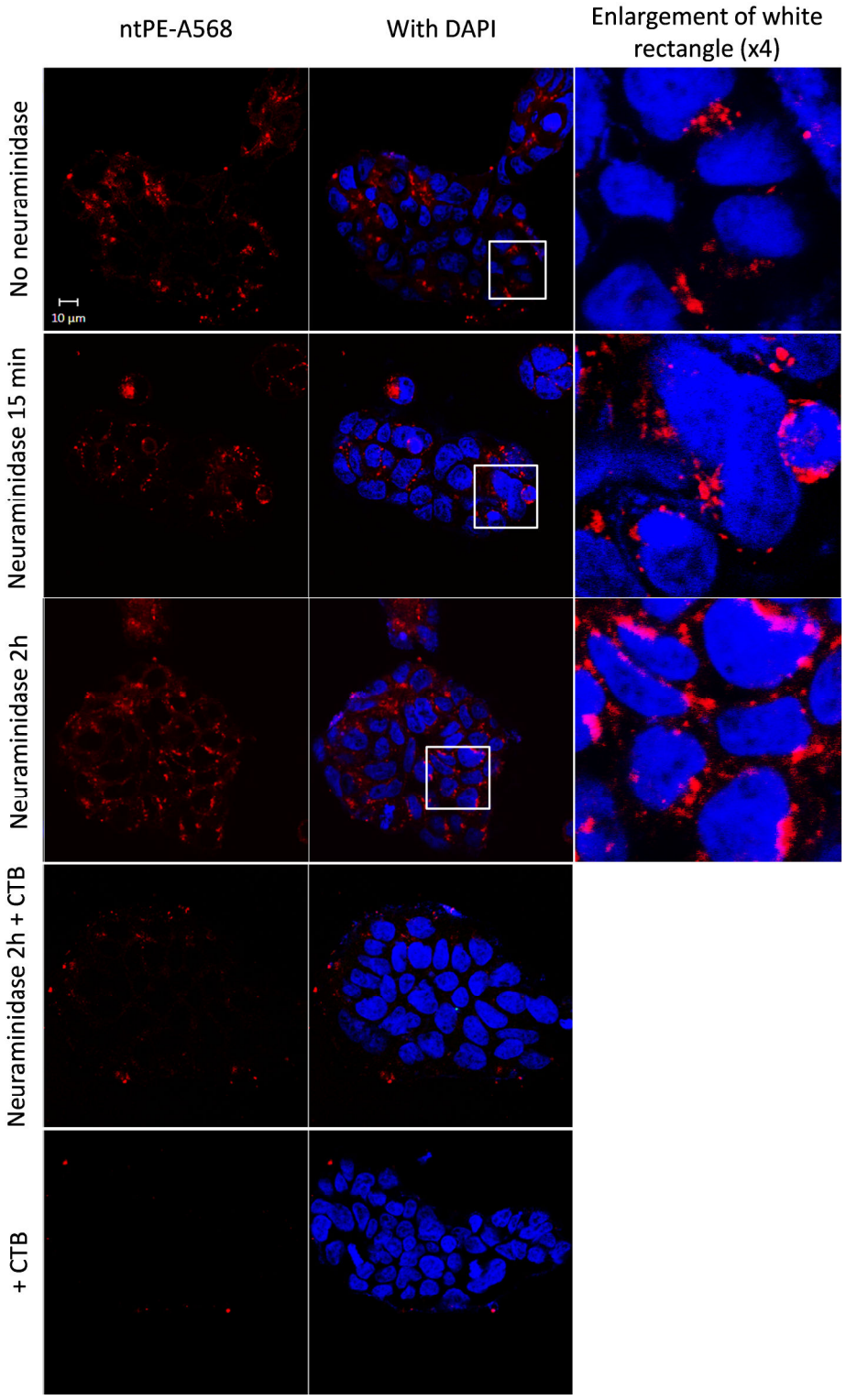

Figure 4-13 – Neuraminidase and CTB affect the entry of PE in NP epithelial cells. Fluorescent images of NP Caco-2 cells incubated for 2 h with 3 µM ntPE-A568 under various conditions, including cell treatment with 1 U/ml neuraminidase for the indicated duration and/or addition of 3.5 µM CTB in solution with ntPE-A568. Cell nuclei were stained with DAPI (blue). Images are representative of three independent experiments.

4.4 General discussion

In this chapter, the interaction between PE and GM1 was characterised at neutral and acidic pH and the role of GM1 in the uptake and early endocytic pathway of PE was investigated in non-polarised (NP) epithelial cells. BLI was used to show that the ganglioside binds to ntPE with relatively high affinity at the neutral pH of 7.5, and that the interaction is even stronger at the mildly acidic pH of 5.5. By relating these results with data described in Chapter 3, it was hypothesised that the increased binding observed in mildly acidic conditions could be due to an improved exposure of the GM1 binding site on PE following a conformational change of the protein. It was therefore suggested that the ganglioside binding site(s) on PE could be located within or near the region of the protein undergoing this localised structure rearrangement (domain II), although spectrofluorometry studies did not allow confirmation or rejection of this hypothesis. Such a configuration could allow the protein to bind simultaneously to LRP1 and GM1 (Figure 4-14).

The fact that ntPE could interact with GM1 at neutral pH seems to indicate that binding could take place at the cell surface. This was confirmed by uptake assays in NP intestinal epithelial cells. GM1 is the host cell-membrane receptor for CT [109, 155, 156] and addition of CTB following neuraminidase treatment greatly decreased the amount of fluorescent protein detected in the cells. Moreover, it was revealed that the action of neuraminidase increased the uptake of ntPE most likely by removing the bulk of sialic acid moieties on the cell surface, thereby enhancing the specific binding of ntPE to GM1 and increasing its internalisation into cells. It was concluded that this enzyme could be acting as an accessory virulence factor, which would be released by the bacteria, and which action would be required only when conditions are not optimal for toxin uptake at the cell membrane [277].

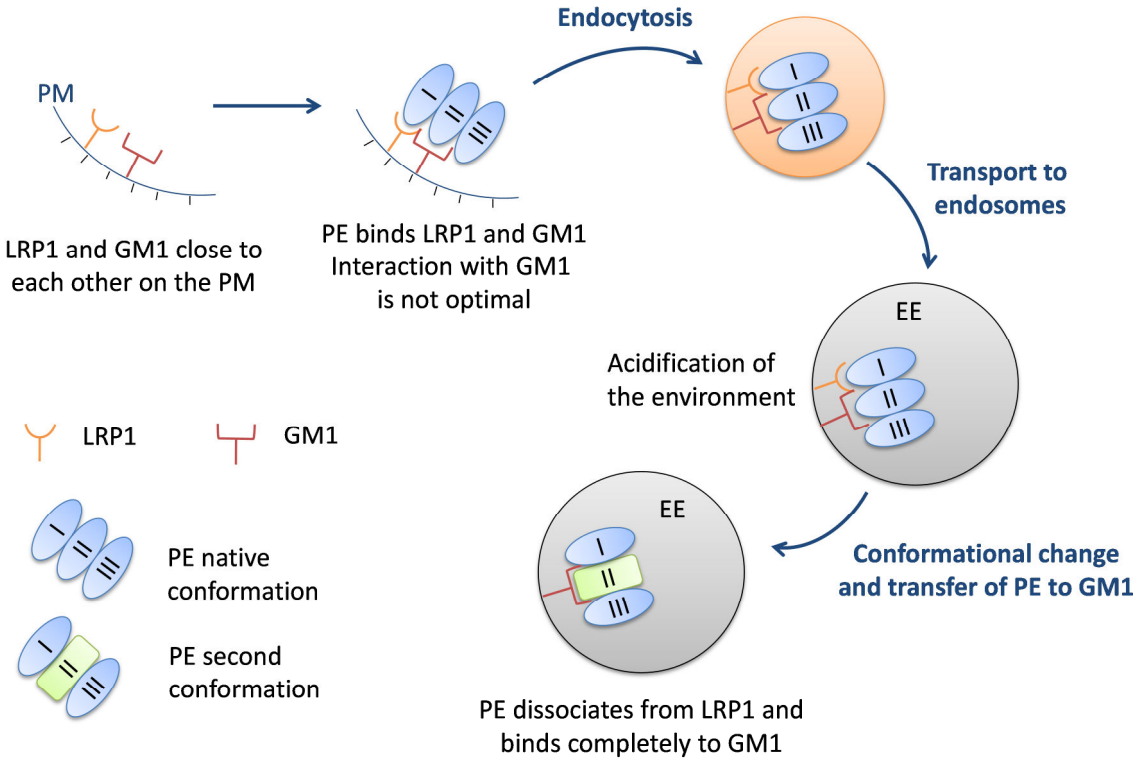

Figure 4-14 – Proposed mechanism for the interaction of PE with GM1 both at the plasma membrane and in the endosome. PM, plasma membrane; EE, early endosome.

Several pathways may be involved in the entry and early trafficking of PE in non-polarised Caco-2 cells. This possibility was mentioned previously by Smith *et al* (2006), whose work indicated that PE could exploit two independent trafficking pathways to reach the ER in HeLa cells (Figure 4-15) [142]. The first route proposed is the KDEL receptor-mediated pathway, which is characterised by protein endocytosis mediated by LRP1 and subsequent trafficking from the EE to the LE, and further to the TGN, in a Rab9-dependent manner. In the TGN, KDEL receptors would interact with the C-terminal KDEL-like sequence of PE, leading the toxin to the ER in a retrograde manner. The alternative pathway considered by these authors is Rab6-dependent and involves the recruitment of LRP1 in detergent-resistant membrane (DRM) micro-domains, which are highly ordered plasma membrane domains rich in glycosphingolipids and cholesterol [286]. Following internalisation, PE would traffic directly from the EE to the Golgi and then the ER following a lipid-dependent sorting pathway. A similar pathway has been described for shiga toxin intoxication [287, 288]. The relative contribution of each pathway to the intracellular transport of PE was shown to vary in a cell-type specific manner [142].

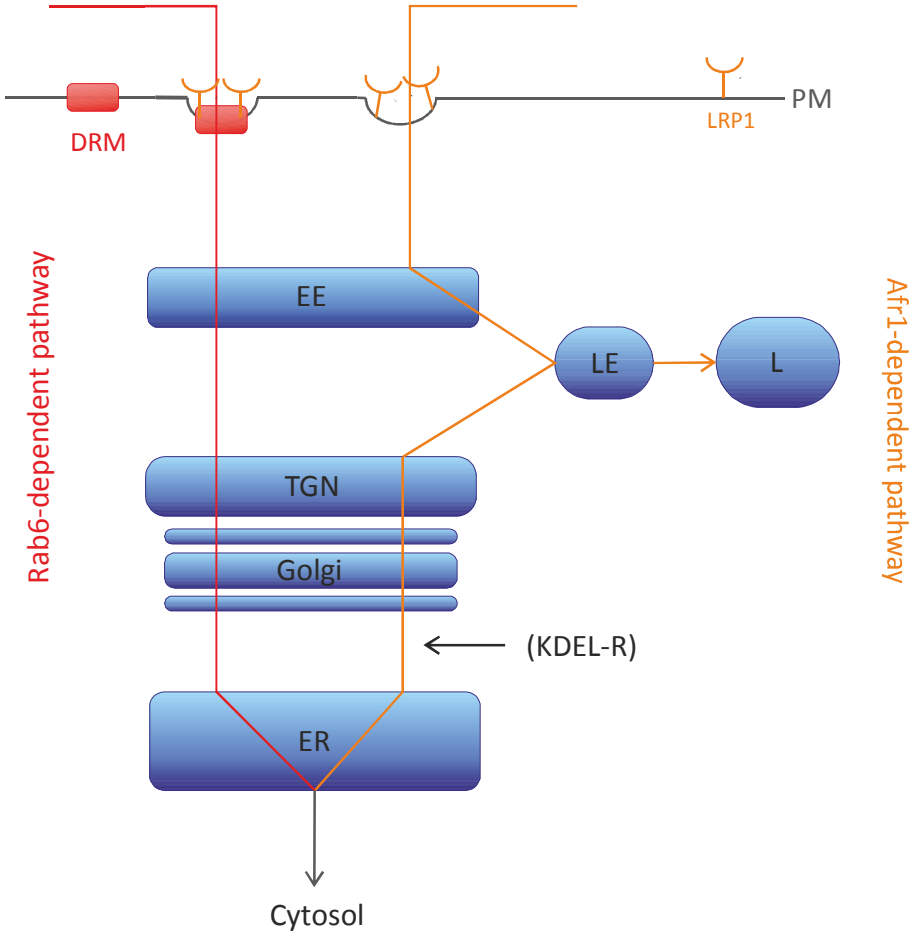

Figure 4-15 – PE can exploit multiple pathways to traffic from the plasma membrane to the ER in HeLa cells. PM, plasma membrane; DRM, detergent-resistant membrane micro-domain; EE, early endosome; LE, late endosome; L, lysosome; TGN, *Trans* Golgi network; ER, endoplasmic reticulum; KDEL-R, KDEL receptor. Adapted from [142].

Data obtained in (NP) Caco-2 cells seemed to support and perhaps complete this hypothesis. It is proposed here that in untreated cells, specific interaction between PE and GM1 is prevented at the plasma membrane by the mass of sialated surface components and the toxin would therefore enter the cells by LRP1-mediated endocytosis. A fairly small amount of protein would then be internalised. However, due to the high potency of the toxin, only a few molecules need to reach the cytosol to intoxicate the cells [289, 290]. Activation of this sole pathway might therefore be enough for the virulence factor to carry out its catalytic activity and lead to the arrest of protein synthesis following infection by *Pseudomonas aeruginosa*.

Application of neuraminidase to the NP cells likely resulted in the cleavage of sialic acid groups from glycoproteins and glycolipids at the plasma membrane [271]. The faster recycling rate of lipids [280-282] probably resulted in the overall number of "functional"

GM1 molecules available for specific binding to PE being greater than in untreated cells. Protein binding to the ganglioside would then result in the opening of a second pathway and in the subsequent increased uptake of PE by the cells. GM1 has been shown to be fairly evenly distributed on the cell membrane [291], but can also be also concentrated in structures including, but not limited to, caveolae [292, 293], clathrin-coated pits [292, 293] and DRM domains [294]. However, it has been suggested that only DRM-associated GM1 molecules could efficiently mediate the transport of CT to the ER via the Golgi and thereby cause toxicity [295]. This could explain why molecules of GM1 located near LRP1 but not associated with DRM did not trigger protein endocytosis following this pathway. As a conclusion and as suggested by Smith *et al* [142], the second pathway exploited by PE could be initiated by protein associated with DRM domains.

Upon addition of CTB and ntPE, the two proteins would compete for GM1 binding on the cell surface. Because the affinity of CTB for GM1 (K_D = 4.61 x 10^{-12} M at pH 7.5 [296]) is greater than that of PE (K_D = 7.06 x10^{-6} M at pH 7.5), the binding of CTB would dominate and as a result, the amount of PE internalised by the DRM-associated pathway would be reduced. Moreover, the small amount of PE that managed to enter the cell via this pathway would also have to compete for GM1 binding upon any conformational change that occurred in the EE. This could further reduce the amount of PE trafficking to the Golgi and possibly redirect it to the lysosome for degradation.

CT has been shown to also exploit different pathways to enter the cells depending on the cell line [257, 297]. In particular, CT can be internalised via clathrin-dependent and clathrin-independent mechanisms following GM1 binding; the respective fractions of each pathway varying with the cell line considered [257]. Furthermore, although the A subunit of CT bears a C-terminal KDEL sequence, this has been demonstrated to not be required for transport to the ER as its absence slows down, but does not inhibit, the action of CT on cells [295, 298]. Instead, evidence strongly suggests that following internalisation, CT remains bound to GM1 molecules associated with lipid rafts, and that the ganglioside leads the toxin from the plasma membrane to the ER via the Golgi apparatus [295]. Moreover, the A subunit is not required for transport from the plasma membrane to the ER via the Golgi apparatus [295]. Therefore, as in the case of PE, the KDEL sequence might not be a requirement for transport to the ER but it might help to retain CT in the ER in order to increase the fraction of A1 subunit transporting to the cytosol [295]. It is an interesting possibility that the previously described Rab6-dependent pathway used by PE to reach the Golgi [142] might be associated with GM1 binding at the cell surface and in the endosome,

and that this trafficking route might resemble the lipid transport pathway suggested for CT intracellular transport [299].

The two pathways of PE cellular trafficking described in this chapter seem to vary mainly in the way the protein enters the cells. However, it would be possible for them to be connected in the cell, perhaps in the early endosome. Independent of its entry mechanism, PE could dissociate from LRP1 and fully interact with GM1 following a pH-dependent structural rearrangement. This could allow all internalised PE to traffic to the Golgi using a lipid transport pathway, and would explain why even in untreated cells the addition of CTB seemed to reduce the amount of fluorescent PE detected inside the cells.

Based on the results presented here and by making comparisons with CT, a mechanism for the entry and early intracellular pathway of PE can be proposed (Figure 4-16). This mechanism correlates with previous reports from Smith *et al* (2006) and seems to complement their hypothesis [142]. Two different processes could be involved in the entry of PE into non-polarised epithelial cells. The first one involves protein endocytosis following binding to the LRP1 receptor and its subsequent transport to the EE. The second mechanism proposed here would involve protein binding to the DRM-associated GM1 ganglioside present on the plasma membrane and transport to the EE. Whether this binding would occur in conjunction to LRP1 binding is unknown. However, previous reports showed that PE is able to recruit a fraction of the LRP1 receptors in DRM [142], and data presented in this chapter suggests that the toxin might interact with GM1 via its second domain. It is therefore possible that protein endocytosis from DRM would involve simultaneous binding to LRP1 (via domain I) and GM1 (via domain II). The two pathways could then either carry on separately to the ER or connect in the EE, where independently of how it was internalised, PE would dissociate from LRP1 and bind completely to GM1. The ganglioside would then lead the protein to the ER through the Golgi. Alternatively, a fraction of the protein could transport from the EE to the Golgi via the LE before carrying on to the ER following binding to KDEL receptors, as previously suggested [142].

Physiologically, the lipid transport pathway used by PE to reach the ER might not be the main trafficking pathway, as the studies presented here have suggested that that the exposure of GM1 might need to be increased for specific protein binding and activation of this trafficking route. Thus, the toxin might utilise this route only when conditions for transport via the KDEL-dependent pathway are not optimal. In this case, neuraminidase secreted by the bacteria upon infection would clear the cell surface from SA groups thereby enhancing toxin binding to GM1, a sialic acid-expressing ganglioside. This would result in the initiation of this secondary pathway and in the increase in the amount of PE

penetrating the cells. It is important to point out that these findings were obtained *in vitro* using NP Caco-2 cells; more discrimination *in vivo* between these various internalisation and trafficking pathways may occur in specific populations of NP cell types of an infected host.

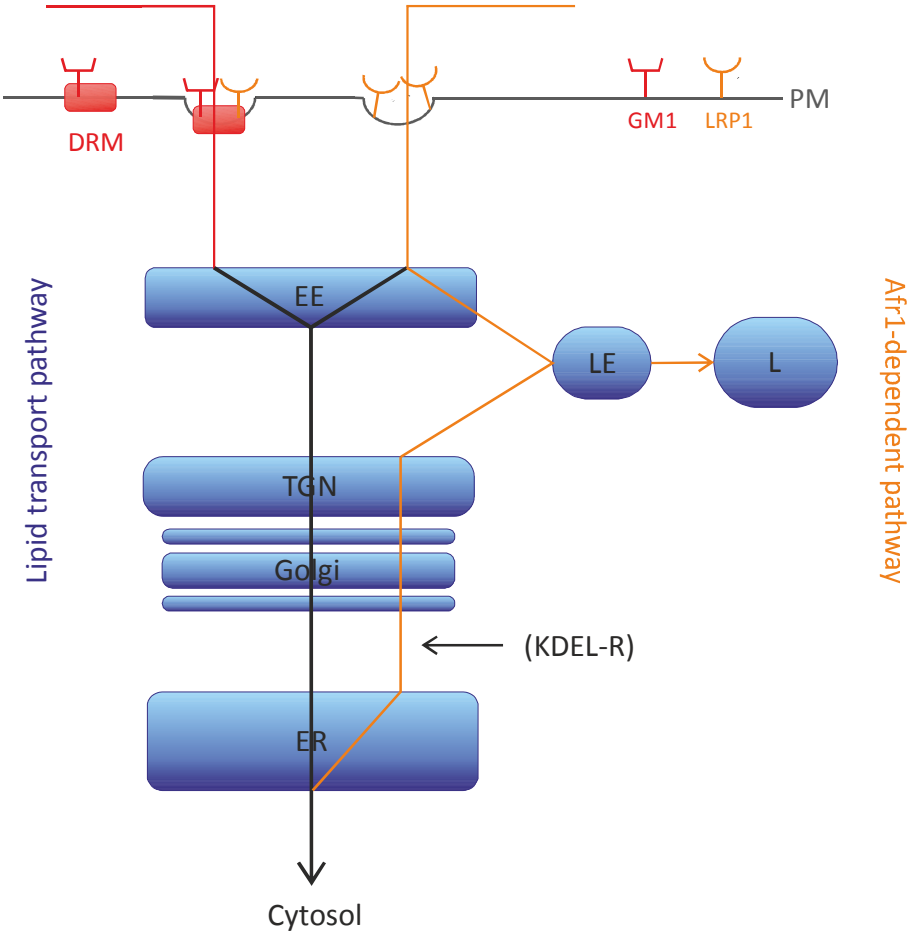

Figure 4-16 – PE can exploit a lipid transport pathway as well as a KDEL-dependent pathway to traffic to the ER. PM, plasma membrane; DRM, detergent-resistant membrane micro-domain; EE, early endosome; LE, late endosome; L, lysosome; TGN, *Trans* Golgi network; ER, endoplasmic reticulum; KDEL-R, KDEL receptor.

As a conclusion, it is proposed that efficient binding and transport of at least a fraction of PE to the ER are mediated by interaction with DRM-associated GM1 molecules. The different routes exploited by the protein to reach its intracellular target have been studied here, and by others, using the native toxin [108, 139, 142, 300]. Understanding the characteristics and requirements of the protein for efficient uptake and translocation is essential if PE is to be used as a drug carrier. Similarly, it is crucial to appreciate how the addition of a cargo macromolecule may impact the intracellular trafficking of PE in order to define the acceptable features a protein drug would need to present to be transported.

5 RESULTS 3 – PE AS A DRUG DELIVERY VEHICLE: STRUCTURAL REQUIREMENTS FOR CELLULAR UPTAKE AND DRUG TRANSPORT

5.1 Introduction

In the last 20 years, the use of bacterial toxins such as PE and DT as therapeutic tools has been widely explored by replacing their receptor-binding domain with a cell-specific antibody, thereby transforming these natural cell killers into highly potent immunotoxins for the treatment of cancer [120]. Recently, Mohammed *et al* (2012) exploited PE's ability to reach the cell cytosol following internalisation, and showed that fusion of a cell-penetrating peptide (CPP) sequence to the N-terminus of domain II of PE facilitated the cytosolic delivery of a cargo protein [165]. Moreover, these toxins are characterised by their remarkable ability to translocate across the polarised cells of mucosal surfaces without causing any obvious damage to the epithelium, but to subsequently target and kill antigen-presenting cells located in the submucosal space [164]. Carter (2014) showed that PE could not only deliver siRNA into macrophages to elicit a knockdown effect, but also

transport the siRNA cargo across polarised cells and deliver it into macrophages of the underlying mucosa [27].

Altogether, these observations suggest that PE could represent a highly efficient delivery system for transport of drugs across epithelial barriers such as those present in the lung or intestine. This would allow oral administration of macromolecular drugs, which currently have to be delivered by injection. Importantly, the crystal structure of PE and information regarding functional properties of various regions of the molecule suggest that this protein is organised in a carrier-cargo format: domain I and II appear to be required for protein transport and responsible for carrying domain III across polarised cells and delivering it to non-polarised cells where it can incite cell death. Thus, removal of domain III should not prevent transcytosis, and this cytotoxic domain could potentially be replaced by a therapeutic payload (protein, siRNA, etc.) that could be carried across epithelial barriers.

The use of PE as a drug carrier following the replacement of domain III with a therapeutic protein would exhibit various advantages over currently existing delivery systems for macromolecules. First, it would allow the drug to be transported across the epithelium without causing any damage to the mucosa, which would represent a major advance compared to the current systems used to improve epithelial absorption of macromolecular drugs. Moreover, several studies have reported that there is no competition between PE and other LRP1 ligands for the binding of the LRP1 receptor [301-303]. Therefore, cellular uptake of the PE-cargo drug complex would not be limited by the presence of endogenous LRP1 ligands, as is currently the case for other delivery systems that involve competition with endogenous ligands [304, 305]. Finally, removal of PE domain III, which carries the cytotoxic activity, should decrease the immunogenic potential of this delivery system.

This chapter describes an attempt at characterising a non-toxic form of PE (ntPE) as a delivery system for protein therapeutics. First, truncated mutants of the toxin were used to investigate the minimal protein length required for uptake into non-polarised cells; a fluorescent cargo protein was then attached to these versions of PE and the resulting fusion proteins were employed to determine the impact of such an addition on internalisation and transcytosis events *in vitro*. This fluorescent element was then replaced by a therapeutic cargo, and transepithelial transport of this compound was studied *in vivo*. Finally, the role of the ganglioside GM1 in the uptake of truncated PE mutants by non-polarised cells was examined.

5.2 Methods

Co-localisation analysis using Image J

Each image was visually inspected and co-localisation of GFP (green) and GM130 (red) was qualitatively tested using the Image Correlation J [306] and Colocalization [307] plugins on Image J [308] in order to establish, for each image, a scatter plot and a mask image, respectively. The latter was generated from the overlay of two masks encompassing the fluorescent signal for the labelled protein and GM130 immunofluorescence, respectively. The sites of co-localisation appear in white on the final image.

5.3 Results and discussion

5.3.1 Cloning, expression and purification of PE364-hGH

Cloning of PE364-hGH

Human growth hormone (hGH) was amplified from pHGH107 by PCR using a set of different buffers (GC buffer, GC buffer + DMSO or HF buffer) and primers containing the AflII and EcoRI restriction sites. While use of HF buffer results in a lower error rate of Phusion polymerase, GC buffer is more adapted to primers with GC-rich content and presence of DMSO can help in the denaturation of such templates [309]. Amplification in each of these conditions produced bands at ~0.6 kbp of comparable intensities (Figure 5-1 (A)). As HF is the recommended buffer for high-fidelity amplification, the PCR was scaled up using this buffer, and the insert was digested by AflII and EcoRI-HF® restriction enzymes.

In parallel, pPE364-GFP was digested at the AflII and EcoRI restriction sites in order to release the GFP fragment (Figure 5-1 (B)). Digestion products were separated by agarose gel electrophoresis, and three bands were observed: one strong band ~4 kbp (undigested plasmid) and two very faint bands at ~3 kbp (digested plasmid) and 0.7 kbp (GFP). The strong intensity of the 4 kbp band compared to the other bands shows that digestion was not very effective, and only a small amount of the original DNA was cleaved. However, by scaling up the reaction, enough of the digested plasmid was collected to proceed to the next steps.

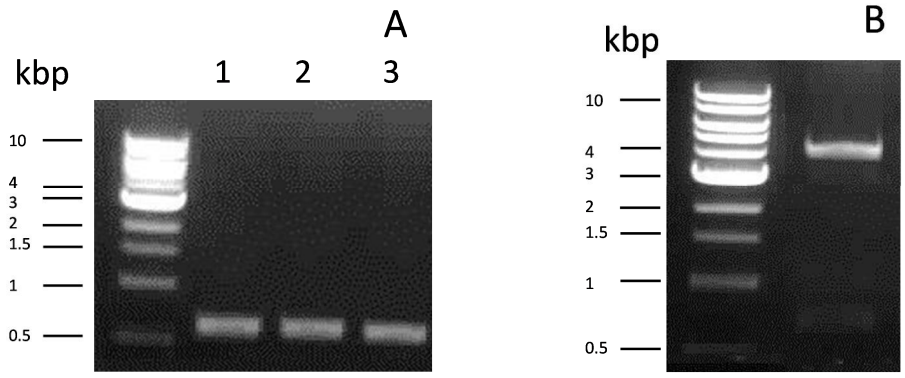

Figure 5-1 – (A) Amplification of hGH by PCR. Lane 1 contains the fragment amplified in GC + DMSO, and lanes 2 and 3 correspond to GC and HF buffers, respectively. (B) Fragments obtained following digestion of pPE364-GFP by AflII and EcoRI-HF®.

The plasmid obtained after ligation of the insert (hGH) and the digested plasmid and transformation on competent DH5α cells was named pPE364-hGH (DH5α). Confirmation of the nature of the plasmid was obtained by sequencing (Sanger sequencing, Source BioScience, Oxford, UK). This plasmid was further transformed in competent BL21 cells to obtain pPE364-hGH (BL21) for protein expression.

Expression and purification of PE364-hGH

PE364-hGH was insoluble when expressed in *E. coli*, as shown in Figure 5-2: after centrifugation of bacterial cells, virtually no protein was present in the supernatant, while the pellets were loaded with protein.

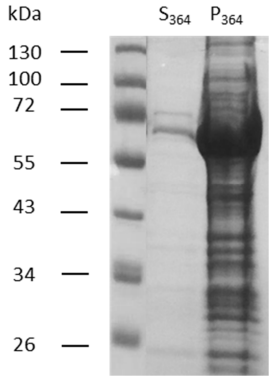

Figure 5-2 – PE364-hGH is insoluble when expressed in *E. coli*. S_{364}, sample containing the soluble protein fractions (supernatant) and P_{364}, sample containing the insoluble protein fractions (pellet).

As a consequence, PE364-hGH was expressed as inclusion bodies from pPE364-hGH (BL21). Despite the presence of an N-terminal His tag, the expressed protein was not retained on His column (Figure 5-3). This could be due to column degradation, or alternatively the tag could have been masked during protein refolding and therefore could be unable to interact with nickel groups on the column. As a result, PE364-hGH was purified using AE and GF chromatography. First, PE364-hGH was eluted from an AE column with a NaCl gradient. A single peak could be observed at 15-55% NaCl (= 0.15-0.55 M NaCl) (Figure 5-4 (A)).

Fractions corresponding to this peak as well as the flow-through were separated by SDS-PAGE (Figure 5-4 (B)). A single band at ~70 kDa was detected in fractions D_3-D_7 which corresponds to PE364-hGH (Section 2.4.5 and Appendix 1). As the band observed in the flow-through fraction (X_6) was relatively faint compared to bands detected in fractions D_3-D_7, these fractions were concentrated together down to 1 ml for further purification by size exclusion chromatography (Figure 5-5) and X_6 was discarded.

Following this second purification step, fractions corresponding to the UV-absorbing material were separated by SDS-PAGE. As the UV peak obtained was less well defined, an SDS-PAGE of individual column fractions was used to assess the amount and purity of the protein of interest, providing the rationale for fractions that were pooled; PE364-hGH was collected from fractions J_6-J_{12} (Figure 5-5 (B)). Analysis of the Coomassie-positive bands showed a dominant one visible at ~37 KDa in fractions J_{13}-J_{15}. This band could correspond to incompletely expressed PE364-hGH.

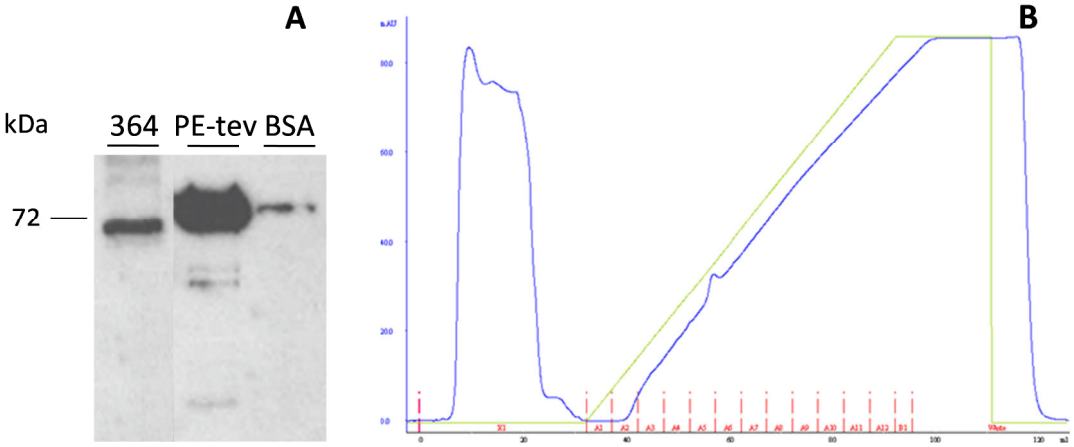

Figure 5-3 – Despite carrying an N-terminal His tag, PE364-hGH was not retained on a His column. (A) WB of the purified PE364-hGH. 10 µg of protein was separated by SDS-PAGE and transferred to PVDF membrane that was probed with an anti-His antibody diluted at 1 in 3,500 in TBS-T. PE-tev is a version of PE carrying a C-terminal His tag and was used as a positive control. BSA was used as a negative control. (B) Chromatogram obtained following elution of PE364-hGH on a Ni^{2+}-functionalised column.

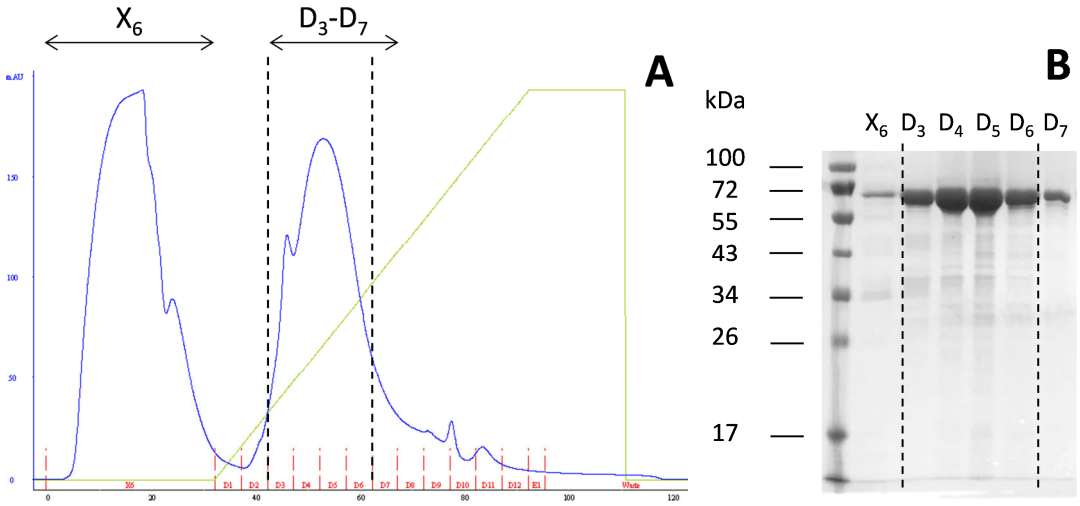

Figure 5-4 – Initial enrichment of PE364-hGH by AE chromatography. (A) Chromatogram obtained for AE separation. (B) Coomassie-stained SDS-PAGE of fractions corresponding to the UV peaks. X- and D-labelled lanes in (B) correspond to arbitrary tray row and column reference on the fraction collector and are illustrated by the red dashes on (A). Fractions covered by the arrow in (A) indicate the complete range of fractions displayed in (B). The black dotted lines marked on both (A) and (B) indicate the fractions containing PE364-hGH that were collected.

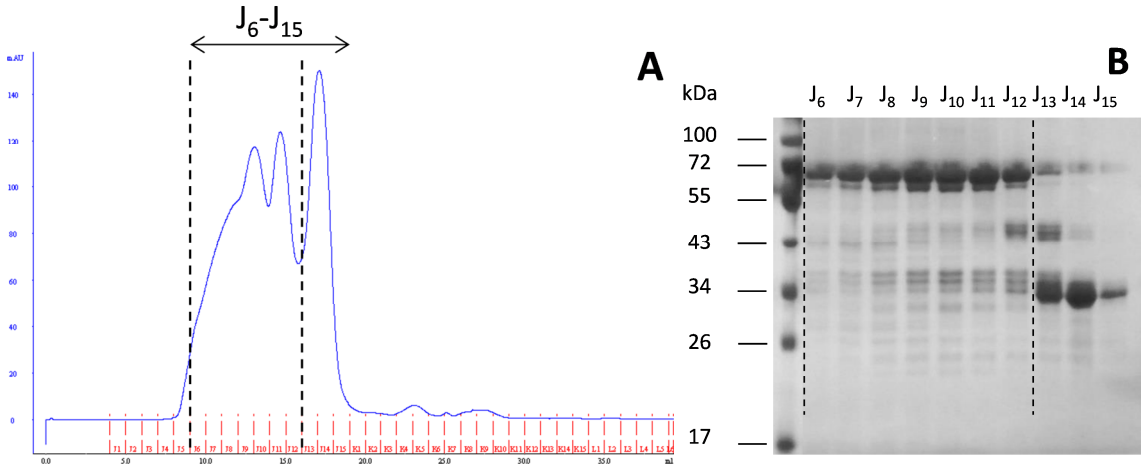

Figure 5-5 – Further enrichment of PE364-hGH using GF chromatography. (A) Chromatogram obtained for GF column separation. (B) Coomassie-stained SDS-PAGE of fractions corresponding to the UV peaks. J-labelled lanes in (B) correspond to arbitrary tray row and column reference on the fraction collector and are illustrated by the red dashes on (A). Fractions covered by the arrow in (A) indicate the complete range of fractions displayed in (B). The black dotted lines marked on both (A) and (B) indicate the fractions containing PE364-hGH that were collected.

5.3.2 Properties of PE-GFP mutants

A series of six PE-GFP versions was cloned and expressed in collaboration with Dr Julia MacKay. ntPE-GFP is a fusion protein that is constituted of full-length ntPE GS TEV connected to a C-terminal GFP molecule and was isolated by IMAC. Five truncated versions of ntPE-GFP were also produced, corresponding to the PE GS TEV protein series: PE408-GFP, PE364-GFP, PE351-GFP, PE320-GFP and PE303-GFP. Numbers indicate the last amino acid of the truncated protein. Physiochemical properties of these proteins are presented in Table 5-1.

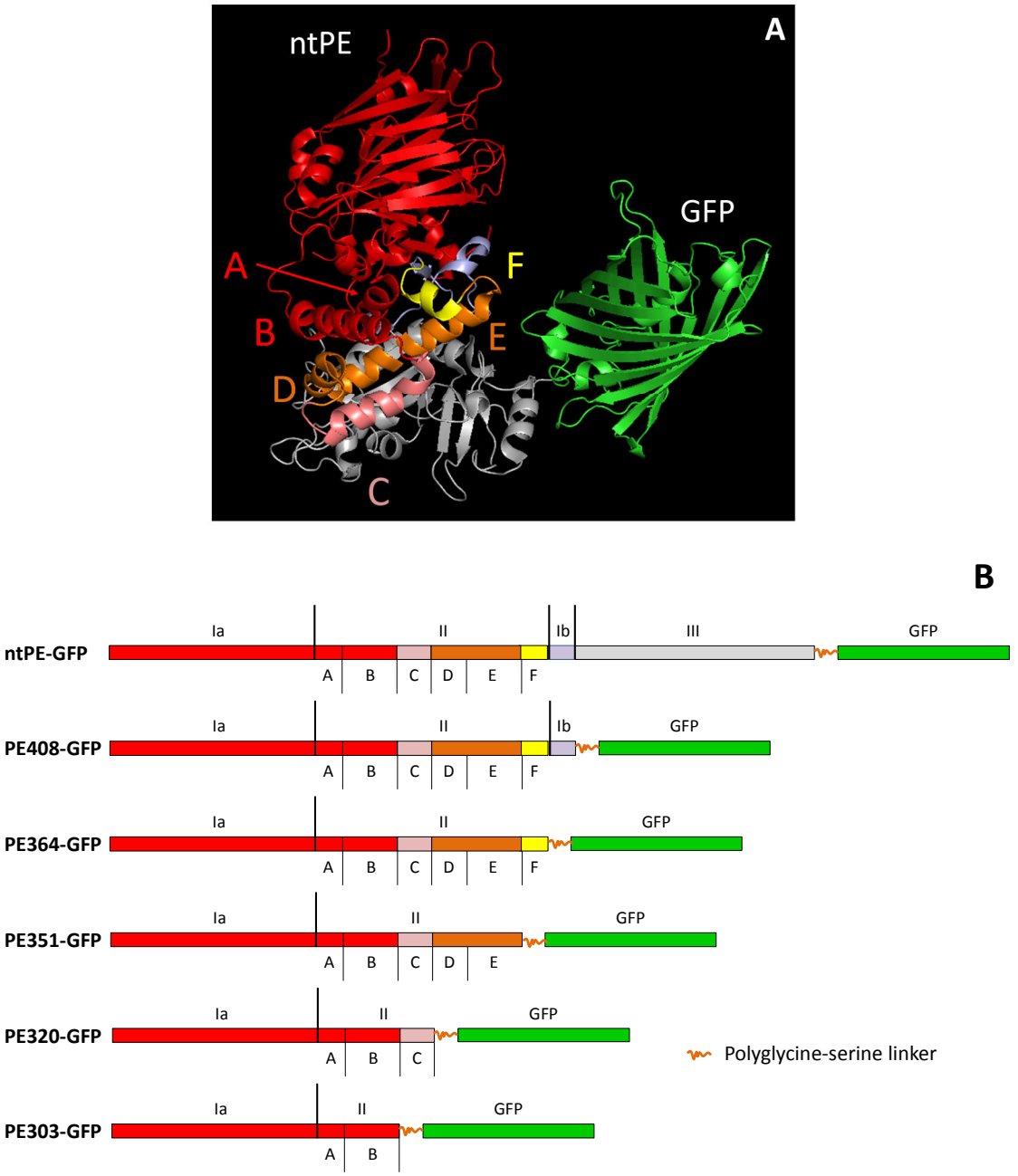

Figure 5-6 – (A) Ribbon representation of ntPE-GFP structure. ntPE GS TEV was fused to a C-terminal GFP molecule. The figure was generated using PyMOL [128]. (B) Schematic representation of the different versions of PE-GFP used in this study. Note the deletion of E553 in domain III that renders PE non-toxic (ntPE). Letters A-F refer to the six α-helices of domain II.

Table 5-1 – Physicochemical properties of PE-GFP truncated mutants. Both pI and molecular weight were calculated using ExPASy ProtParam [181].

Protein designation	Calculated pI	Calculated molecular weight (kDa)
ntPE-GFP	5.34	93.2
PE408-GFP	5.36	71.4
PE364-GFP	5.33	69.2
PE351-GFP	5.41	67.6
PE320-GFP	5.53	64.4
PE303-GFP	5.53	62.5

5.3.3 In vitro uptake of two truncated versions of PE

It is proposed that utilising the internalisation mechanism and intracellular trafficking used by PE would be an effective method for the delivery of biopharmaceuticals. This concept involves the use of domains I and II that appear to be specifically involved in these internalisation and trafficking processes; domain III could be eliminated. In an attempt to better understand the requirements of domain II in these processes, PE was genetically truncated at residues 303 or 364 and modified at the new C-terminus with a sequence of amino acids that could be specifically cleaved by tobacco etch virus (TEV) protease and that allowed for a site-selective chemical coupling with the fluorescent Alexa Fluor® tag 568 (A568). The two PE-derived materials, denoted as PE303 GS TEV (short-length mutant) and PE364 GS TEV (medium-length mutant), respectively, were evaluated for their internalisation and trafficking properties in NP epithelial cells *in vitro*.

NP Caco-2 cells seeded on coverslips were incubated with 20 μg of each fluorescently-tagged protein diluted into 100 μl complete growth medium (concentration of ntPE-A568 = 3.0 μM, PE364-A568 = 5.0 μM, and PE303-A568 = 5.9 μM, respectively) for 2 h at 37 °C before being fixed and stained with DAPI (Figure 5-7).

Importantly, fluorescent images obtained by confocal microscopy showed that both truncated PE proteins retained their ability to be taken up by NP cells *in vitro*. However,

the intracellular distribution of PE364-A568 and PE303-A568 may have been somewhat distinct. No co-localisation studies were performed here and therefore the proposed intracellular location of each protein remains purely speculative at this time. In the absence of these co-localisation studies, it appears that full-length ntPE-A568 could be detected primarily in a compartment that might correspond to the ER/Golgi apparatus (Figure 5-7; top, green arrow). In the case of PE364-A568, the protein was found as well-defined fluorescent dots surrounding the nuclei in some cells (white arrow), while in others it was present as a single fluorescent spot close to the nucleus (green arrow). The pattern observed for PE303-A568 is less clear and only small and poorly-defined fluorescent protein dots around cell nuclei could be identified. These observations could suggest that while some of PE364-A568 might have reached the Golgi/ER (similar pattern to ntPE-A568), a substantial fraction of the protein might have remained inside endocytic vesicles or alternatively, trafficked to the lysosome. It appeared that PE303-A568 may have reached these peri-nuclear locations less efficiently than PE364-A568 or with a slightly different pattern of intracellular distribution. Rigorous co-localisation studies involving intracellular markers for the Golgi (GM130, TGN46), EE (Rab4, EEA1), LE (Rab7, Rab9a) or lysosome (LAMP1) would be required to accurately determine the intracellular localisation of ntPE-A568, PE364-A568, and PE303-A568 [310-312].

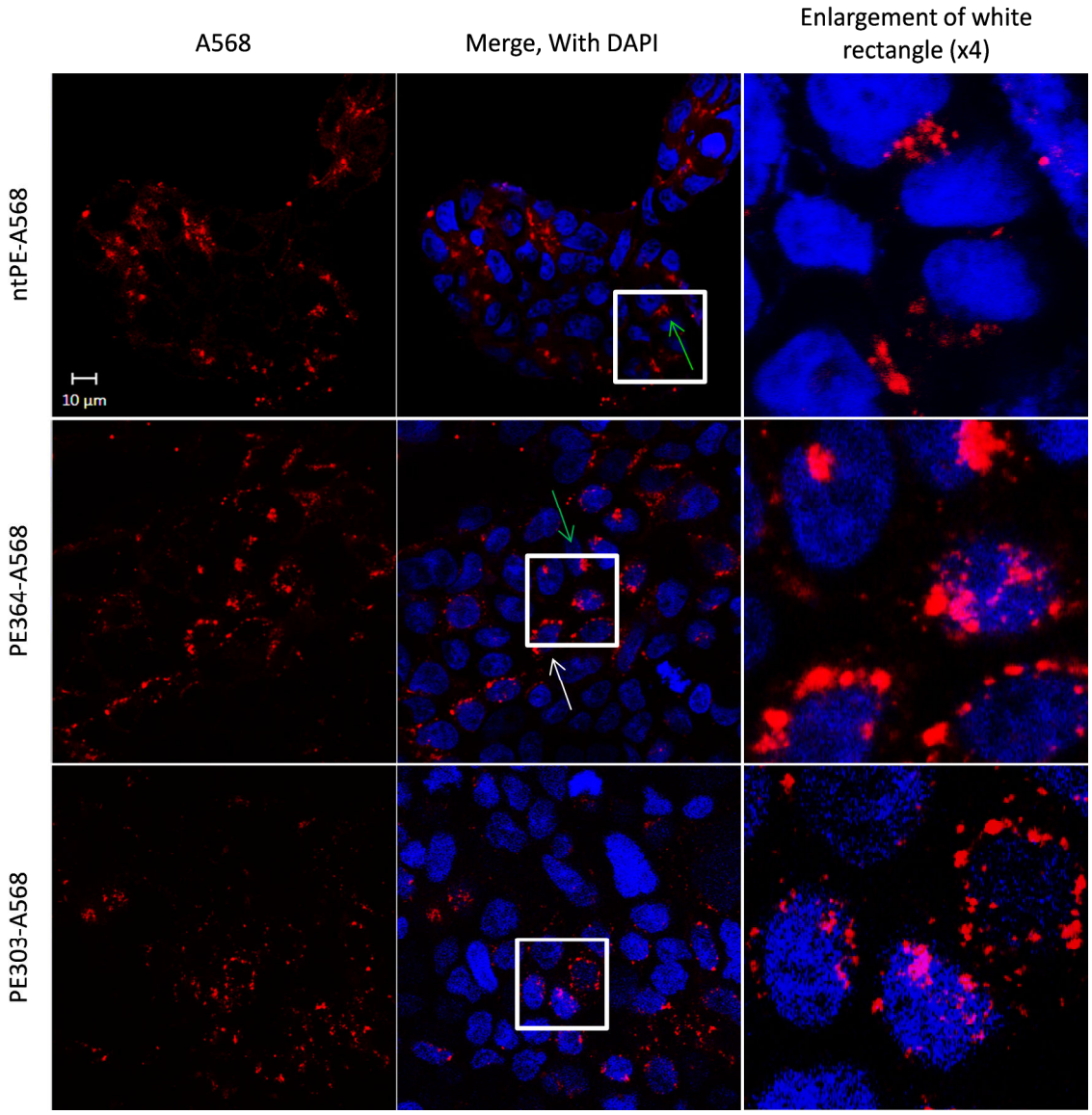

Figure 5-7 – Truncated forms of PE are internalised by NP epithelial cells. Fluorescent images of NP Caco-2 cells incubated for 2 h with 20 µg of protein tagged with Alexa Fluor® 568 and diluted in 100 µl complete growth medium (red). Final protein concentrations were 3.0 µM ntPE-A568, 5.0 µM PE364-A568 and 5.9 µM PE303-A568. Cell nuclei were stained with DAPI (blue). Arrows indicate protein suggested, but not demonstrated, to be localised in endocytic vesicles (white) and Golgi network (green). Images are representative of three independent experiments.

It was reported that following receptor-mediated endocytosis, the intoxication pathway of PE in NP cells involves vesicular transport through the endocytic pathway to the Golgi [145]. In Chapter 4 two trafficking routes were proposed as exploitation strategies used by the toxin to reach the ER, and it was suggested that the dominant pathway in untreated

cells could involve interaction with KDEL receptors in the Golgi via the protein's C-terminal REDL sequence and further transport to the ER in a retrograde manner (Section 4.4). In the studies presented above, the REDL sequence of full-length ntPE-A568 is not accessible to KDEL receptors due to attachment of the C-terminal fluorescent tag. Therefore, the protein's capacity to reach the ER in a retrograde manner should be greatly decreased, and the toxin should not be able to transport further than the Golgi apparatus. The fluorescence pattern observed for full-length ntPE-A568 could be in agreement with this assumption as it appeared to be restricted to a peri-nuclear vesicular structure (green arrow) rather than diffusely distributed in the cytosol, where the protein would retro-translocate to after reaching the ER [145]. Again, this hypothesis would need to be confirmed by co-localisation studies.

If PE364-A568 was shown to be present in the Golgi and inside endocytic vesicles simultaneously, this could indicate that a fraction of the protein was redirected to the lysosome for degradation after trafficking to the Golgi. In fact, quality control in the secretory pathway allows properly folded proteins to traffic from the ER to the Golgi and subsequent compartments, while incompletely folded or misfolded proteins which escape to the Golgi are recycled back to the ER using their ER-retrieval sequence (KDEL-like sequences) [313]. Here however, none of the proteins used carried any accessible ER-retrieval sequence. Therefore, it would be possible for truncated proteins to be perceived as misfolded in the Golgi apparatus and subsequently redirected to the lysosome for degradation. In this case, it would be plausible that quality control mechanisms in the Golgi were quicker to perceive PE303 compared to PE364 as misfolded, resulting in its faster redirection to the lysosome. Thus, it would be interesting to determine if there are differences in the extent of PE364-A568 or PE303-A568 that traffic to lysosomes versus the Golgi apparatus.

As a conclusion, all three versions of PE tested here (full-, medium- and short-length) seemed able to enter into NP cells. Observation suggested that these proteins could have different intracellular fates and could therefore imply that truncation might affect the proteins' capacity to traffic through the endocytic pathway. Further studies are required to determine the nature and extent of these differences in intracellular fate.

5.3.4 In vitro uptake of PE-GFP mutants –effects of neuraminidase

In order to determine the ability of truncated forms of PE to transport a cargo protein inside the cells, fusion proteins carrying a C-terminal green fluorescent protein (GFP) molecule were cloned. This system presents the advantage of having each mutant conveying a cargo protein that has approximately the same molecular weight as PE domain III and is fluorescent, hence easy to detect. 20 µg of a truncated PE-GFP protein diluted in 100 µl complete growth medium was applied to NP Caco-2 cells and incubated at 37 °C for 2 h. Final molar concentrations for all proteins applied are given in Table 5-2. Cells were then fixed with PFA, labelled with an anti-GM130 antibody and prepared for confocal microscopy. GM130 belongs to the Golgin family of proteins, which are present specifically in the Golgi matrix [314]. Confocal images showed that although a limited amount of ntPE-GFP seemed to have entered the cells, the internalised protein was frequently co-localised with GM130 labelling (Figure 5-9; top). Therefore a full-length ntPE carrying a cargo molecule of GFP conserved its ability to be taken up by NP cells and to be trafficked, at least partially, to the Golgi apparatus. The low fraction of internalised material is consistent with data obtained in Chapter 4, which demonstrated that only a minor fraction of ntPE applied to untreated NP Caco-2 cells could be taken up (Section 4.3.3.2). Conversely, none of the five truncated versions of PE-GFP seemed able to enter NP Caco-2 cells.

Studies presented in Chapter 4 suggested that increasing the number of accessible GM1 molecules on the surface of NP cells greatly enhanced the efficiency of toxin uptake. Therefore, cells were pre-treated with 1 U/ml neuraminidase for 2 h. Following this, 20 µg of protein diluted in 100 µl complete growth medium containing 1 U/ml neuraminidase was applied for another 2 h (Figure 5-10).

Table 5-2 – Molar equivalent of 20 µg protein for the PE-GFP mutant series and concentrations used in uptake assays in NP Caco-2 cells.

Protein designation	Molar equivalent of 20 µg protein (nmol)	Protein concentration in 100 µl medium (µM)
ntPE-GFP	0.21	2.1
PE408-GFP	0.28	2.8
PE364-GFP	0.29	2.9
PE351-GFP	0.29	2.9
PE320-GFP	0.31	3.1
PE303-GFP	0.32	3.2

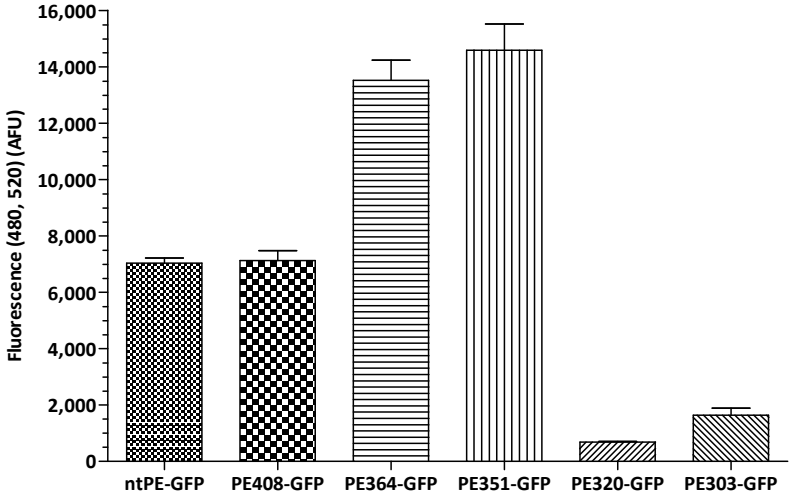

Figure 5-8 – Fluorescence of PE-GFP mutant proteins. Fluorescence intensity of 20 µg of fusion protein in HBSS (λ_{ex} = 480 nm, λ_{em} = 520 nm). Corresponding molar concentrations are presented in Table 5-2. Data are presented as mean ± SD for each sample, for n = 3 microplate wells.

All proteins appeared to be internalised when administered in conjunction with neuraminidase treatment. However, they seemed to show little co-localisation with GM130, indicating that most of the internalised material observed was not in the Golgi, as shown in Table 9-4 and Appendix 4. This was striking as even the ntPE-GPF, which showed some Golgi apparatus co-localisation when initially tested, lost that co-localisation behaviour when administered with neuraminidase. On the other hand, the fluorescence pattern observed in neuraminidase-treated cells did not strongly suggest lysosomal degradation either. This could thus imply that, following cell penetration, the proteins might have remained held within endosomal compartments, were unable to escape, and

possibly underwent constant cycling between the early and recycling endosomes. This hypothesis would need to be tested by carrying out co-localisation studies using organelle markers such as EEA1 or Rab11, which target the early and recycling endosomes, respectively [315].

In order to determine if the internalisation and trafficking of PE-GFP truncated mutants was affected by treatments such as neuraminidase and addition of CTB that could alter the availability of SA moieties, proteins were applied to NP Caco-2 in the presence of 3.5 μM CTB with or without a 1 U/ml neuraminidase treatment. Fluorescence signals inside treated cells were greatly decreased for all PE-GFP mutants following CTB addition in the presence (Figure 5-11) or absence of neuraminidase treatment (Figure 5-12). The results suggest that the PE-GFP truncations behaved similarly to ntPE-GFP with regards to the actions of treatment that could affect SA levels in cells. Importantly, the carrier protein length did not seem to affect the internalisation process in NP cells; none of the truncated mutants described here appeared to be internalised in the absence of neuraminidase treatment while addition of this enzyme dramatically increased the uptake of all six proteins.

Interestingly, the A568-tagged counterparts of PE364-GFP and PE303-GFP seemed to be internalised, even in untreated cells (Section 5.3.3). Therefore, the observation that the full-length form, but not truncated forms of PE-GFP, was readily internalised, was surprising. It is possible that addition of a medium-sized cargo protein (MW_{GFP} = 27 kDa) to the C-terminal end of truncated forms of PE could have affected the intracellular fate of these materials relative to those tagged with a fluorescent molecule, altering their engagement with the lipid-associated pathway described in Section 4.4. Due to the inability to quantitatively compare the A568- and GFP-tagged proteins these observations are restricted to qualitative assessments. Alternatively, the GFP cargo protein might have been cleaved from the carrier domain before cell entry, which could account for the lack of intracellular fluorescence. This latter possibility seems unlikely, as there is no obvious reason for GFP to be cleaved off the truncated mutants but not the full-length protein.

The discrepancies observed between the estimated intracellular locations of A568-tagged and GFP-labelled versions of PE364 and PE303 following application to untreated cells could also be explained by differences in fluorophore stability. In fact, GFP is used here as a cargo protein as well as a fluorescent reporter. However, its nature makes it more sensitive to enzymatic degradation than the fluorescent tag A568, and perturbations of its tertiary structure are likely to cause a loss of fluorescence. As a consequence, it is possible

that even if a small amount of protein entered NP Caco-2 cells and was re-routed to the lysosome, variations in fluorophore stability would have led to A568-tagged molecules being visualised in the lysosomes, while the GFP-labelled mutants would have been undetected due to a more rapid inhibition of the fluorescence of GFP.

It is also possible that attachment of a cargo protein, such as GFP, could affect the intracellular destination of truncated forms of PE, possibly accelerating or enhancing routing to the lysosome (Section 5.3.3). While results from Chapter 4 suggested that neuraminidase treatment did not impact the intracellular protein location of A568-labelled ntPE, this same treatment seemed to have striking effects on the fate of ntPE-GFP. One possible interpretation of these data is that the protein could be caught in a trafficking loop possibly located between early and recycling endosomes.

Finally, in the hypothesis that GM1 is indeed involved in PE protein uptake, these findings complement earlier studies and suggest that the ganglioside binding site might be located between amino acids 1 and 303, as even the shortest fusion protein (PE303-GFP) entered the cells upon addition of neuraminidase. These results would be in agreement with conclusions drawn in Chapter 4 concerning the location of the GM1 binding site on PE domain II. However, this hypothesis relies on mere observation and would need confirmation by rigorous fluorescence quantification in each sample and additional truncation mutants.

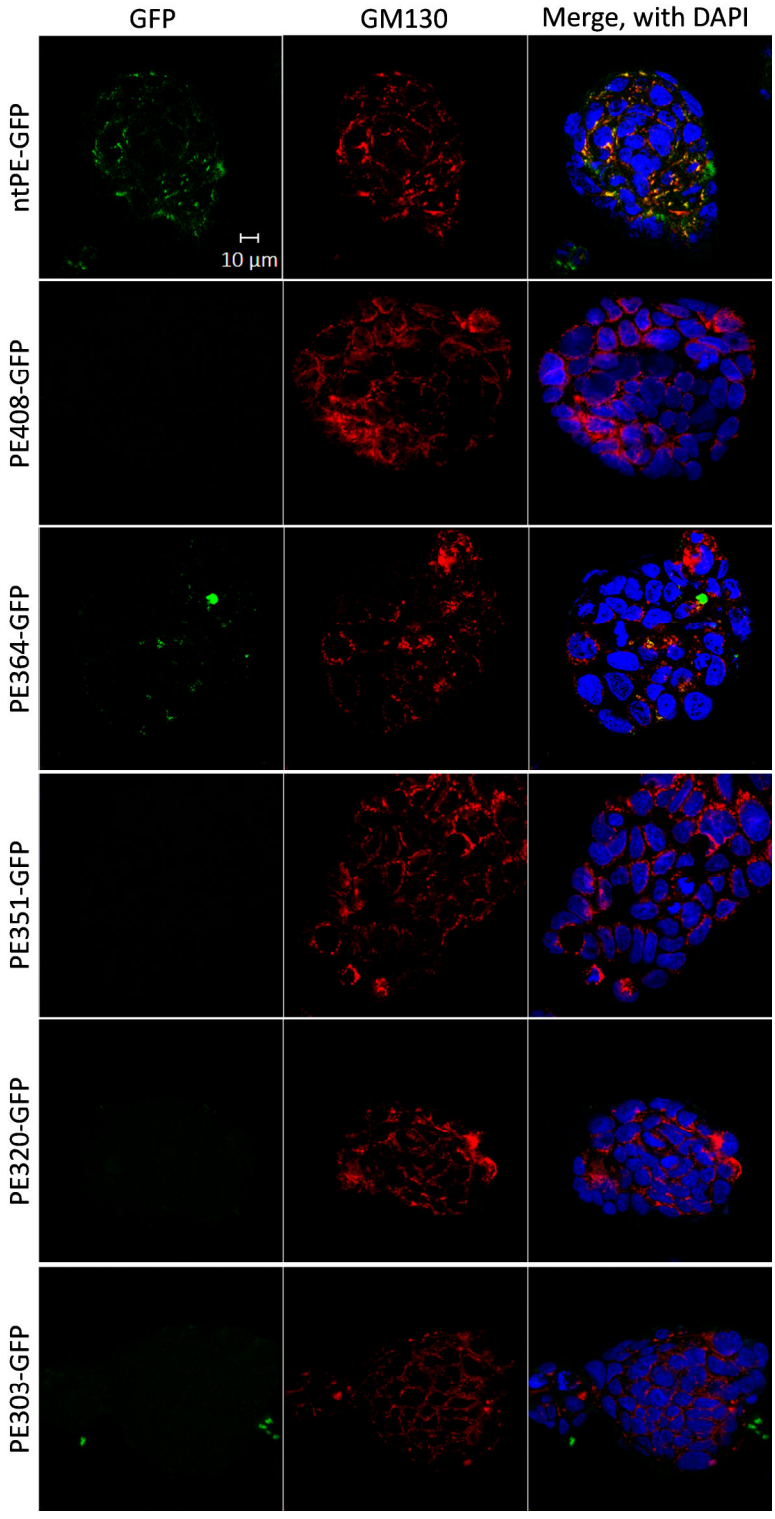

Figure 5-9 – PE-GFP mutant proteins are not internalised by NP epithelial cells. Fluorescent images of NP Caco-2 cells incubated for 2 h with 20 µg protein diluted in 100 µl complete growth medium. Molar concentrations are detailed in Table 5-2. Cell nuclei were stained with DAPI (blue) and expression of GM130 (red) was used to visualise the Golgi network. Images are representative of three independent experiments.

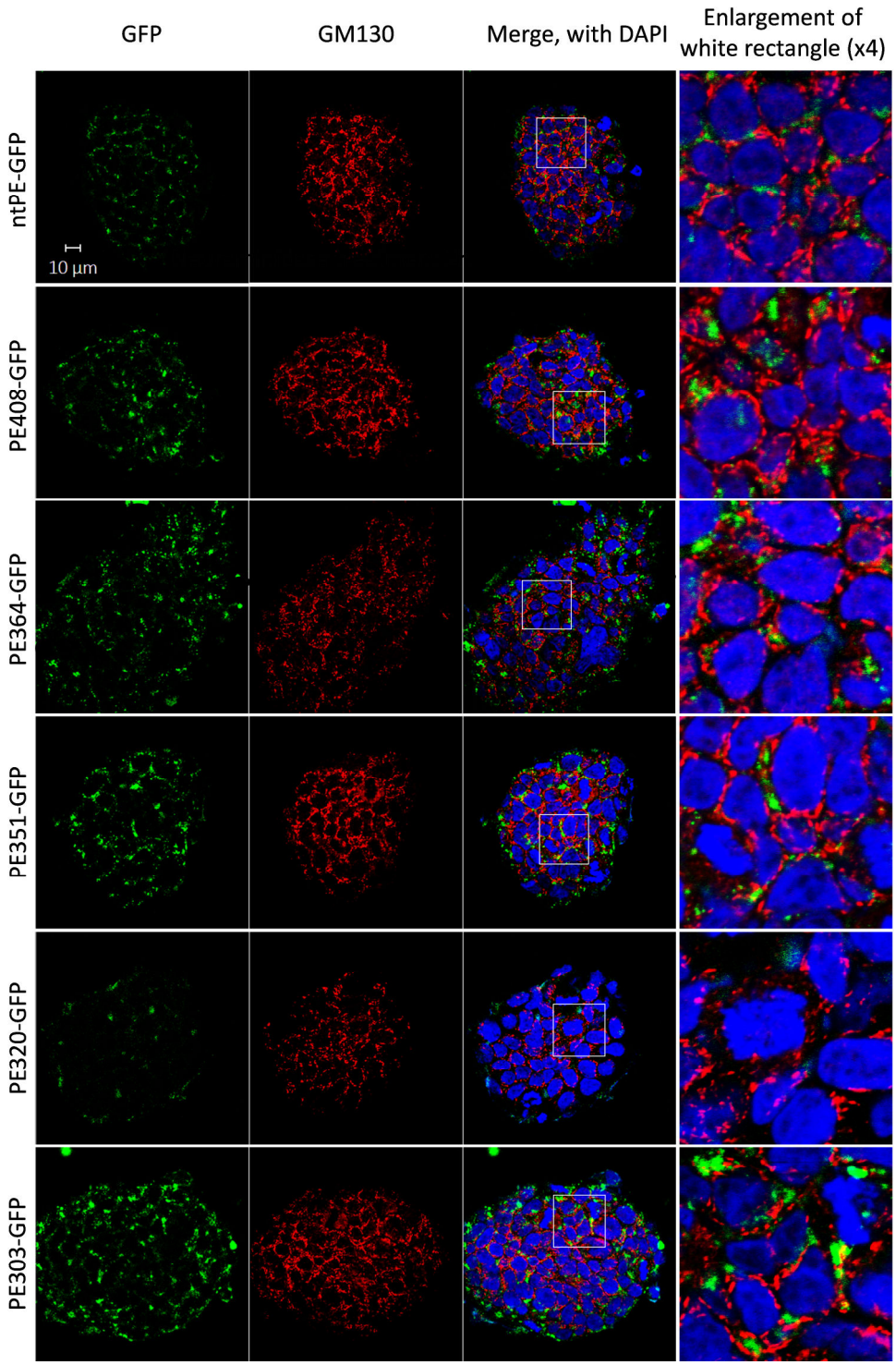

Figure 5-10 – Treating the cells with neuraminidase increases the uptake of PE-GFP mutants by NP epithelial cells. Fluorescent images of NP Caco-2 cells pre-incubated for 2 h with 1 U/ml neuraminidase followed by a further 2 h-incubation with 20 µg of protein diluted in 100 µl complete growth medium in the presence of 1 U/ml neuraminidase. Molar concentrations are detailed in Table 5-2. Cell nuclei were stained with DAPI (blue) and expression of GM130 (red) was used to visualise the Golgi network. Images are representative of three independent experiments.

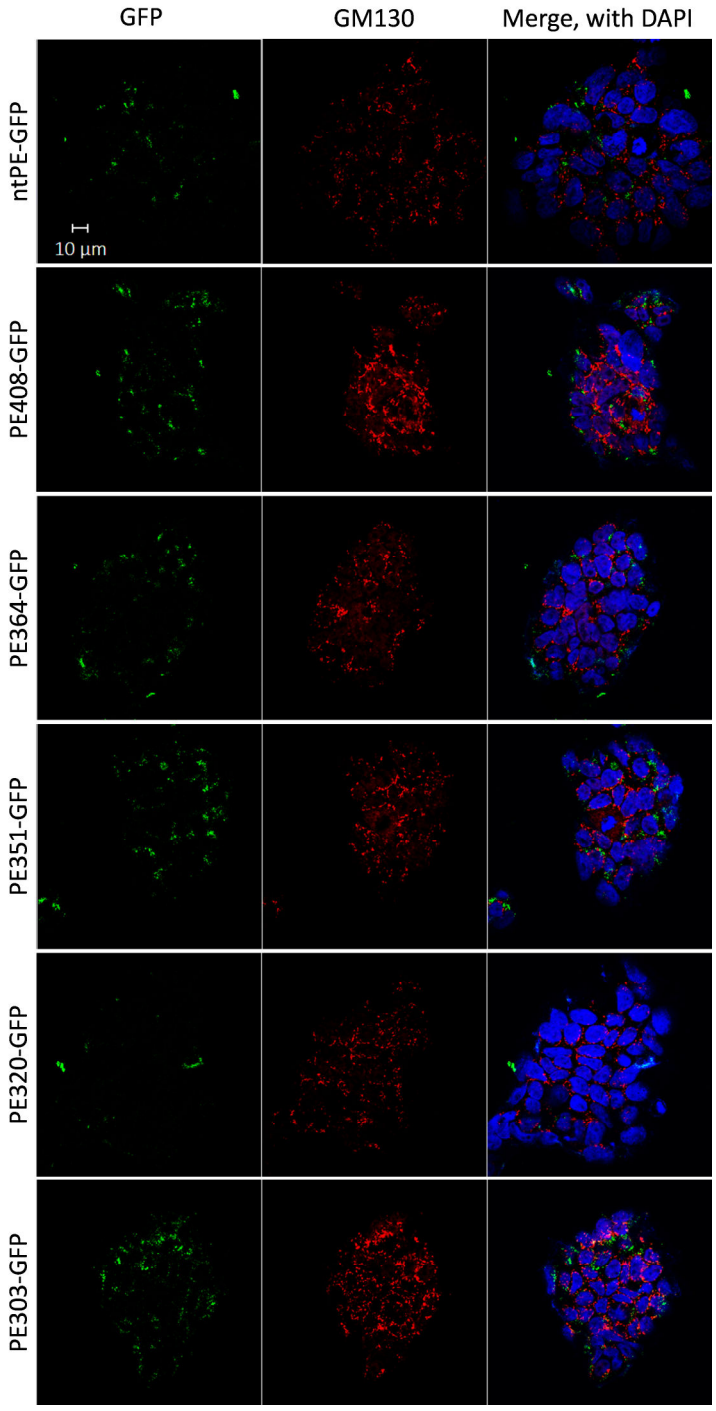

Figure 5-11 – CTB inhibits the internalisation of PE-GFP proteins by NP epithelial cells treated with neuraminidase. Fluorescent images of NP Caco-2 cells pre-incubated for 2 h with 1 U/ml neuraminidase before applying 20 µg of each protein diluted in 100 µl complete growth medium and 3.5 µM CTB in the presence of 1 U/ml neuraminidase for 2 h. Molar concentrations are detailed in Table 5-2. Cell nuclei were stained with DAPI (blue) and expression of GM130 (red) was used to visualise the Golgi network. Images are representative of three independent experiments.

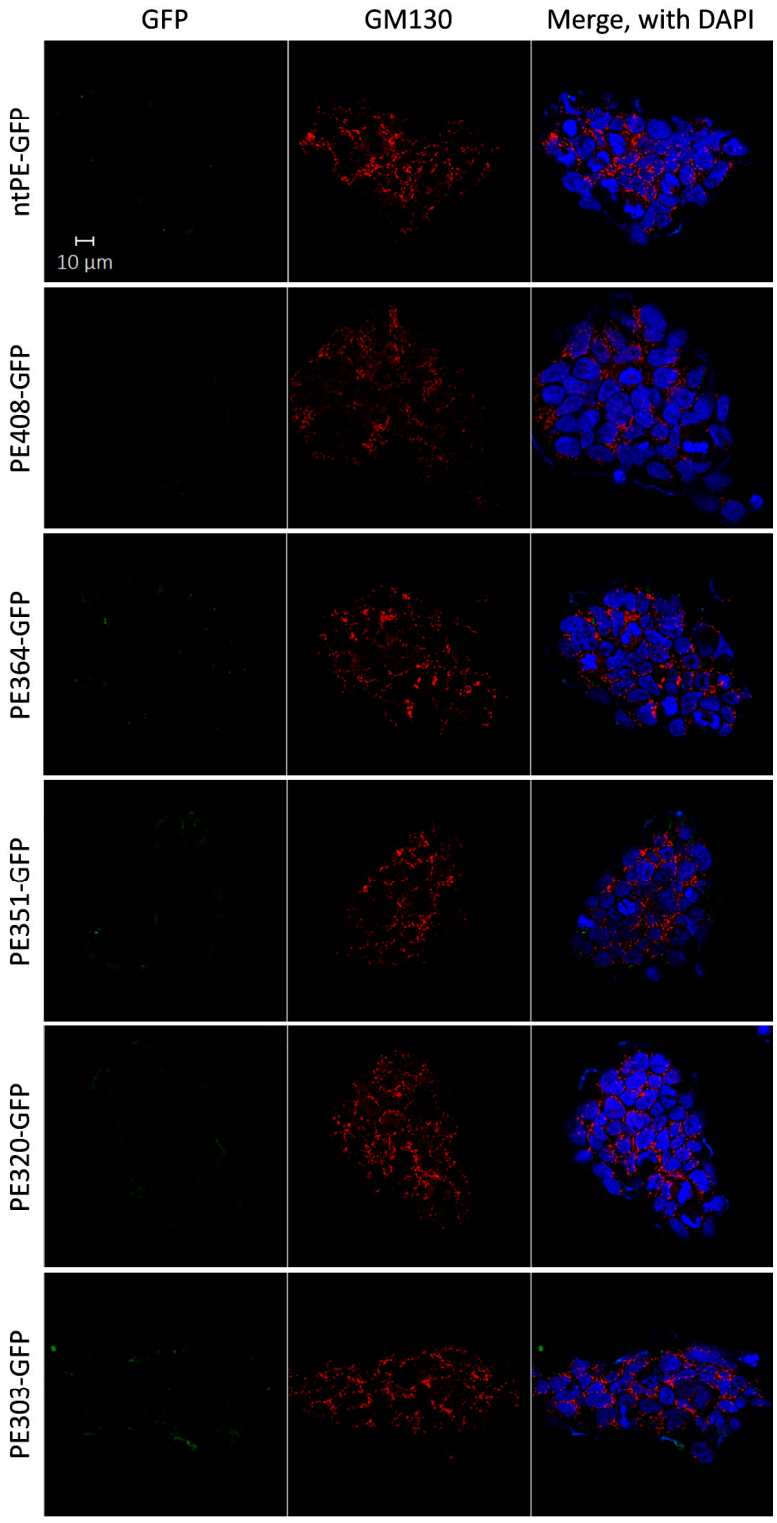

Figure 5-12 – CTB specifically inhibits the internalisation of PE-GFP mutants in NP cells. Fluorescent images of NP Caco-2 cells incubated for 2 h with 20 µg of each protein diluted in 100 µl complete growth medium and 3.5 µM CTB. Molar concentrations are detailed in Table 5-2. Cell nuclei were stained with DAPI (blue) and expression of GM130 (red) was used to visualise the Golgi network. Images are representative of three independent experiments.

5.3.5 In vitro transport of ntPE in polarised cells

Data obtained in the previous section showed that all six PE-GFP mutants were internalised by NP epithelial cells following neuraminidase treatment. However, the characteristics of polarised cells constituting the intestinal epithelium are different from those of their NP counterparts. This is highlighted by the fact that native, enzymatically active PE intoxicates and kills NP cells while it can transport across epithelial barriers without causing any perceptible cell damage. In order to determine the entry and transport characteristics of ntPE in polarised systems, Caco-2 cells were cultured on semi-permeable filters (Transwell®) to a confluent and polarised state. The Transwell® filters used in these studies were coated with a rat-tail Type I collagen matrix, which has been proposed to decrease the time needed for the cells to polarise by promoting cell attachment and cell growth [316]. The cells used here are the Caco-2 C2BBe1 clone (ATCC), which were reported to display a more homogeneous brush border expression and are therefore comparable to human enterocytes found in the small intestine [177, 317, 318]. When the cells became polarised following monolayer formation, a fluorescent protein was applied onto their apical surface, and transport across the monolayer was assessed by quantifying fluorescence in samples collected from the basolateral compartment (Figure 5-13). Functional monolayer integrity was evaluated by measuring both transepithelial electrical resistance (TEER) and dextran permeability through the paracellular pathway. Only wells presenting TEER > 350 $\Omega \cdot cm^2$ were used for the assay.

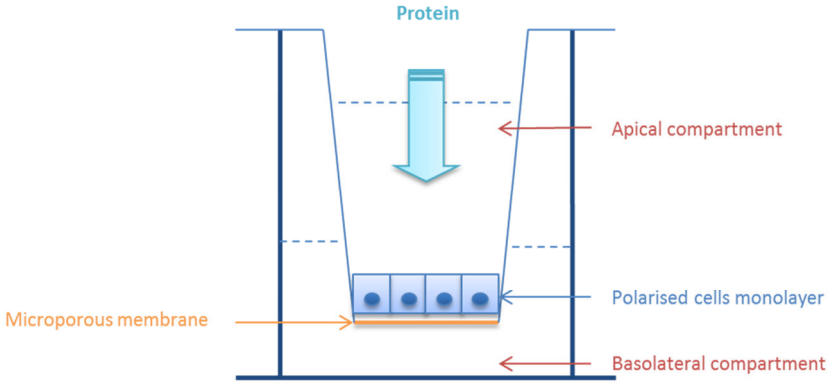

Figure 5-13 – Diagram for the Transwell® filter system for assessing protein transport across polarised cells. Cells are seeded on a semi-permeable membrane in the inner well and, once they polarise, protein is applied to their apical surface. Medium from the basolateral compartment is sampled at regular time intervals to assess the amount of protein that has crossed the cell monolayer. A non-permeable macromolecular marker, such as 4 kDa fluorescent dextran, added to the apical compartment can be used to monitor non-selective apical to basal flux.

First, 0.1 µM, 0.5 µM and 1.0 µM of full-length ntPE-A568 were applied to the apical surface of polarised cells (= 2, 10 and 20 µg diluted in 300 µl HBSS, respectively). Samples removed from the basolateral compartment at t = 15, 30, 60, 120 and 240 min were assayed for fluorescent content. Figure 5-14 represents the accumulation of total fluorescence collected from the basolateral compartment with time. It shows that transport of as little as 0.1 µM toxin could be detected and quantified by fluorescence. Furthermore, the total amount of protein transported increased linearly with incubation time for all three concentrations. Linearity of the fluorescence intensity with increasing amounts of protein was verified in the 0.001-0.1 mg/ml range (Figure 5-15). This implies that the saturation point of the system, and therefore the maximum transport rate, had not been reached. Measurements of dextran permeability indicated that between 8.2 and 16.2% of FITC-labelled 4 kDa dextran crossed the monolayer compared to the blank well. TEER values measured at the start and end of the assay (TEER > 350 $\Omega \cdot cm^2$) demonstrate that monolayer integrity was maintained throughout the experiment.

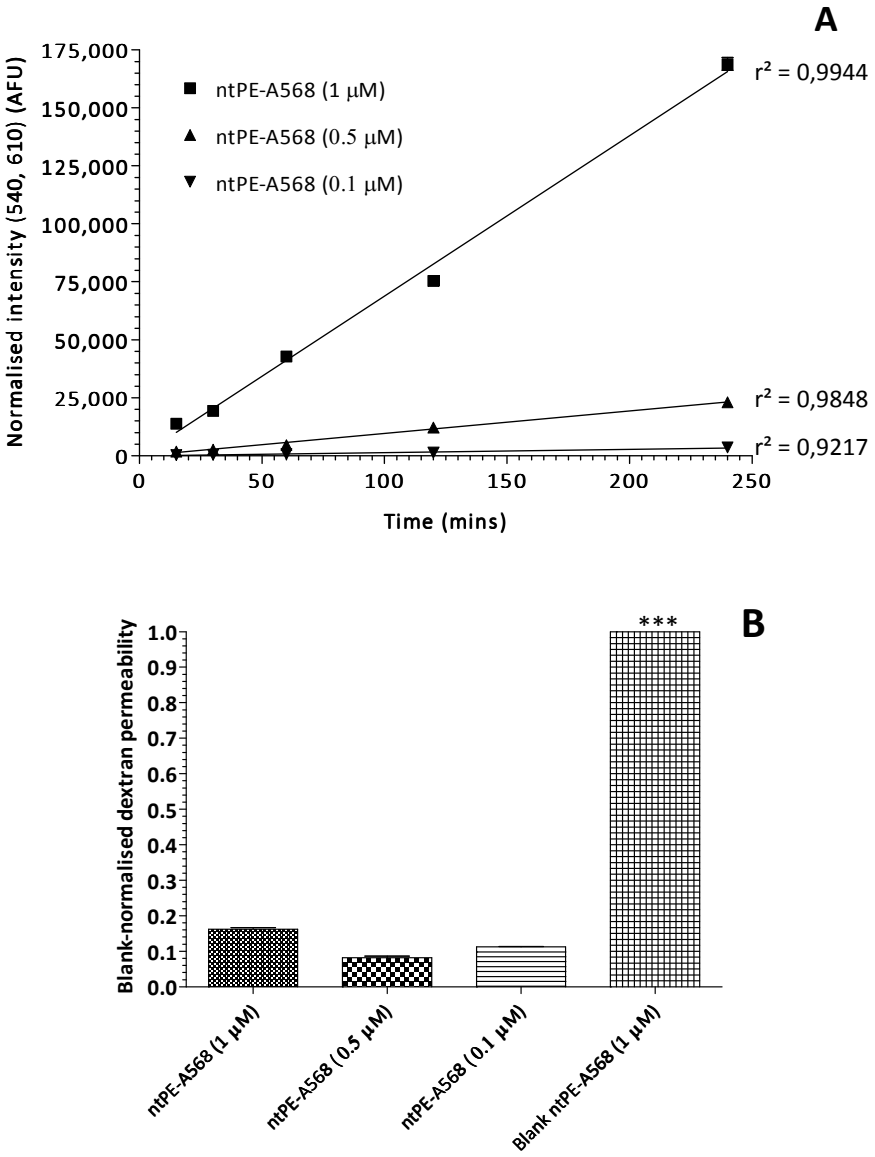

Figure 5-14 – Transport of full-length ntPE-A568 across polarised epithelial cells. (A) Normalised total fluorescence of 1.0 μM, 0.5 μM and 0.1 μM of ntPE-A68 present in the basolateral compartment over 240 min following initial application to the apical surface of Caco-2 monolayers. Data are presented as mean ± SD for each time point, for n = 3 independent samples. (B) Amount of FITC-labelled 4 kDa dextran present in the basolateral compartment 30 min after application to Transwell® filters (Blank) compared to Transwell® filters supporting a monolayer of polarised Caco-2 cells which were incubated with various amounts of ntPE-A568 for 240 min. Data are presented as mean ± SD for each sample, for n = 3 independent samples (* P < 0.001).**

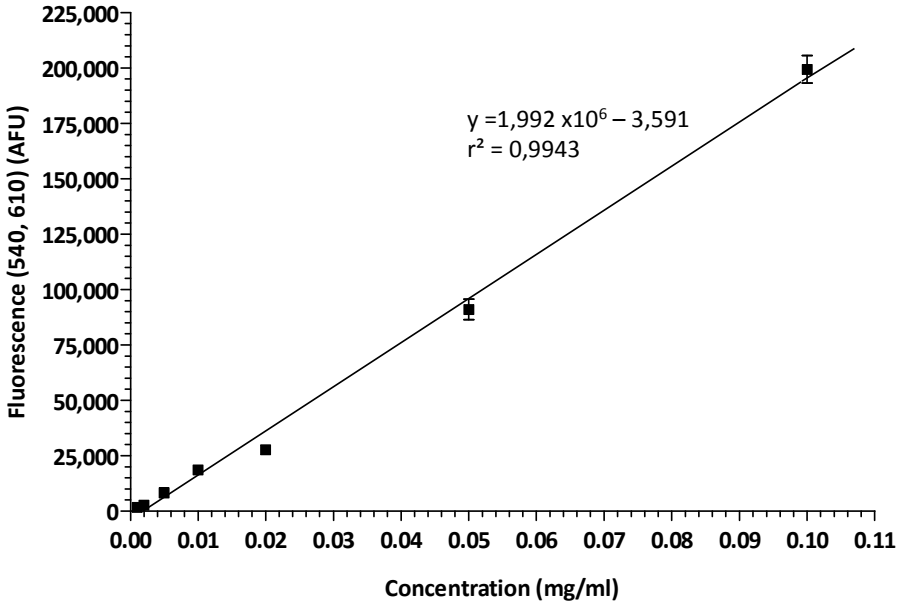

Figure 5-15 – Fluorescence intensity is linear in the 0.001-0.1 mg/ml range. Solutions of full-length ntPE-A568 at 0.1, 0.05, 0.02, 0.01, 0.005, 0.002 and 0.001 mg/ml were obtained by serial dilutions in HBSS from a 4.3 mg/ml stock solution in PBS. Data are presented as mean ± SD for each concentration, for n = 3 microplate wells.

Data here establishes that ntPE has the ability to transport a fluorescent tag across polarised cells without damaging the epithelium, as illustrated by conservation of the monolayer integrity throughout the assay. Furthermore, the tight intercellular contacts which prevent paracellular diffusion of 4 kDa dextran suggest that, due to its rather large molecular weight (66 kDa), the protein couldn't have permeated the monolayer via this pathway. As passive transcellular diffusion is also very unlikely, it would be safe to assume that ntPE transported across the cells by transcytosis, thereby confirming the presence of functional receptor(s) on the cell surface. This assay validates the potential of ntPE to transport across polarised monolayers in the experimental conditions described here.

In an attempt to test and compare the transport characteristics of several PE truncated mutants to those of the full-length protein, the assay was repeated with the PE-GFP protein series. However, the fluorescence detected in the basolateral compartment after 240 min was minimal, suggesting that no protein had transcytosed across the cells (Figure 5-16 and Table 5-3). ntPE-A568 was applied as a control, but did not seem to transport either. After several attempts to reproduce the results previously obtained for full-length ntPE-A568, no protein could be detected in the basolateral side. A series of tests were

performed in order to determine if this lack of transport was caused by the protein itself or instead a dysfunction of the cells.

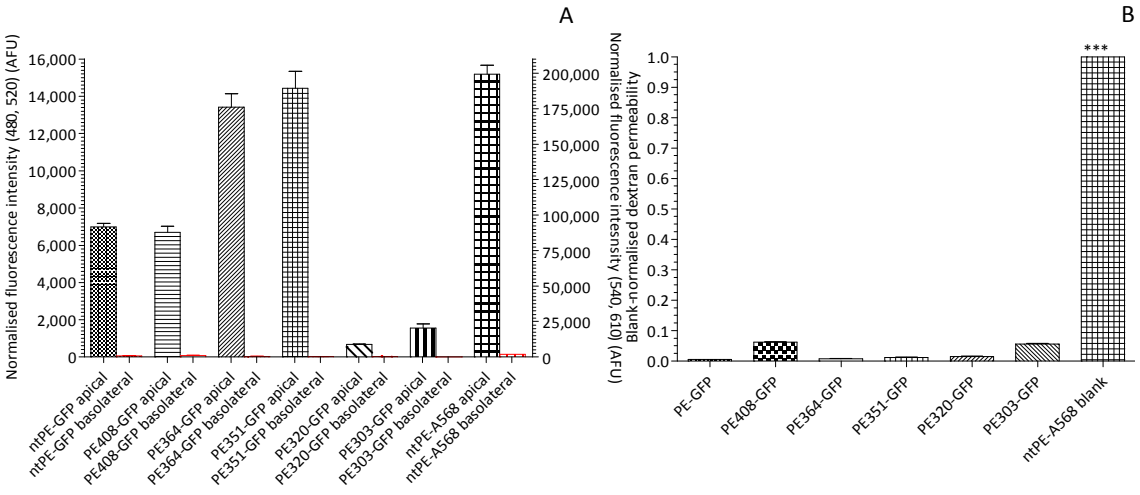

Figure 5-16 – (A) Amounts of PE-GFP mutants present in the apical (black) and basolateral (red) compartments after 240 min, following the application of 20 µg of protein in 300 µl HBSS to the apical surface of Caco-2 monolayers. Final molar concentrations for all proteins applied are given in Table 5-3. (B) Amounts of FITC-labelled 4 kDa dextran present in the basolateral compartment 30 min after apical application to Transwell® filters (blank) compared to Transwell® filters supporting a monolayer of polarised Caco-2 cells which were incubated with 20 µg protein for 240 min. Data presented as mean ± SD, for n = 3 wells, where *** P < 0.001.

Table 5-3 – Molar equivalent of 20 µg protein for the PE-GFP mutant series concentrations used in transport assays in polarised Caco-2 cells.

Protein designation	Molar equivalent of 20 µg protein (nmol)	Protein concentration in 300 µl medium (µM)
ntPE-GFP	0.21	0.70
PE408-GFP	0.28	0.93
PE364-GFP	0.29	0.97
PE351-GFP	0.29	0.97
PE320-GFP	0.31	1.03
PE303-GFP	0.32	1.07

Investigation of full-length ntPE functionality was carried out using different formats of this protein (ntPE GS TEV and ntPE-GFP) carrying various fluorescent reporters (A568,

A488, GFP). This strategy should have reduced the possibility that there might be a flaw in the protein being tested. For instance, it is possible that the protein could have been folded improperly or that the chemical coupling could have altered the protein; both events could have reduced its capacity to bind to receptors essential for transcytosis. Similarly, the use of two different fluorescent tags provided some assurance that detection was not the issue. Despite these efforts, neither ntPE-A568 nor ntPE-GFP was observed to transport across polarised monolayers of Caco-2 cells *in vitro* (Figure 5-17). The observation that two different full-length ntPE proteins carrying distinct fluorescent tags demonstrated undetectable transcytosis rates in the studied system suggests that they could be fully functional, and that the factor(s) preventing their transport across epithelial monolayers might be cell-related instead. This concept is supported by the fact that previous studies had shown efficient ntPE transcytosis (Figure 5-14). As a consequence, other tests were then performed on the cells themselves in an attempt to understand the nature of how their properties or status might affect ntPE transcytosis.

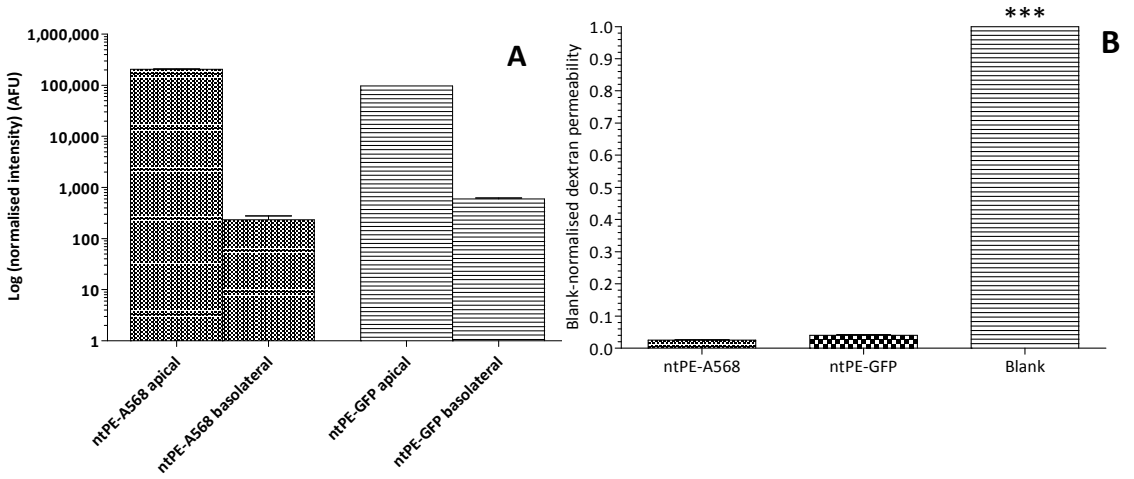

Figure 5-17 – (A) Amounts of ntPE-A568 and ntPE-GFP present in the apical and basolateral compartments after 240 min, following the application of 1.0 µM ntPE-A568 and 0.7 µM ntPE-GFP to the apical surface of Caco-2 monolayers. (B) Amounts of FITC-labelled 4 kDa dextran present in the basolateral compartment 30 min after apical application to Transwell® filters (blank) compared to Transwell® filters supporting a monolayer of polarised Caco-2 cells which were incubated with 1.0 µM ntPE-A568 or 0.7 µM ntPE-GFP for 240 min. Data presented as mean ± SD, for n = 3 wells, where *** P < 0.001.

Rat-tail collagen has been used in various laboratories to pre-coat Transwell® filters prior to the seeding of Caco-2 cells to facilitate their maturation into confluent, polarised cell monolayers [319]. A preparation of rat-tail collagen was isolated as previously described

[320] and used to coat Transwell® filters. This was compared to Transwell® filters coated with a commercial preparation of rat-tail collagen and Transwell® filters with no collagen coating. In all three cases, we failed to observe transport of full-length ntPE across Caco-2 monolayers.

We next tested if the medium used in the transport assay had an effect. Usually, cells were transferred from complete growth medium to HBSS 30 minutes before a transport study was initiated. Cells were either left in growth medium for the duration of the experiment or transferred to HBSS prior to addition of the full-length ntPE protein, in order to try to decrease or alternatively increase stress levels caused by medium change on the cells, respectively. Still no transport could be detected.

Conditions were then modified so that the cells were incubated in the presence of full-length ntPE protein at mildly acidic pH given that pH at the cell surface in diseased tissue during *Pseudomonas aeruginosa* infection is lower than in healthy systems [321]. In parallel, a mixture of various protease and phosphatase inhibitors (PI) was added to the cells in addition to the full-length ntPE protein to prevent potential degradation, which could hinder internalisation. While no transport could be detected at pH 5.88, a small increase in fluorescence intensity in the basolateral compartment was observed in presence of the PI. However, evaluation of dextran permeability indicated that the integrity of the monolayer had been partly compromised and therefore the observed increase in transport was probably due to protein leaking via the paracellular route rather than by transcytosis.

The proteins used here (ntPE-A568 and ntPE-GFP) appeared to be taken up by NP Caco-2 cells (Chapter 4 and Section 5.3.4), thereby implying that they were able to interact with their cell-surface receptor(s) in this system. Next, other cell lines were used for the transport assay: Calu-3 and MDCK that cells are lung adenocarcinoma and canine kidney epithelial cells, respectively. As LRP1 is located on the basolateral surface of MDCK cells, protein was added to the basolateral compartment of these cells and samples were taken out of the apical well [322]. However, neither protein seemed able to cross these cells better than they transported across Caco-2 monolayers. These results suggested that the problem was not caused by the polarised cell system used. Therefore the detection method was tested.

Samples were usually removed from the basolateral compartment and fluorescence intensity assessed using a microplate reader as detailed in Section 2.16.1 and Table 2-5. Here, Calu-3 cells were seeded in the inner well to polarise, and NP Caco-2 cells seeded on

coverslips as described in Section 2.14 were placed in the basolateral compartment. Any protein transporting across the Calu-3 monolayer should reach and enter the underlying NP cells, and therefore could be observed under confocal microscopy even if fluorescence measurements by the plate reader were faulty. However, no toxin could be detected in the NP Caco-2 cells. Then, protein was added to either the apical or basolateral side of cells in case cell polarity had shifted due to the presence or absence of cellular components [323]. Finally, new Caco-2 cells were acquired in case the line previously used had been passaged too far and their phenotypic characteristics had mutated [317]. In parallel, cells were grown on filters by another group (Prof. M. Gumbleton, Cardiff University). None of these conditions resulted in the transport of full-length ntPE protein. Some of the results described above are presented in Figure 5-18.

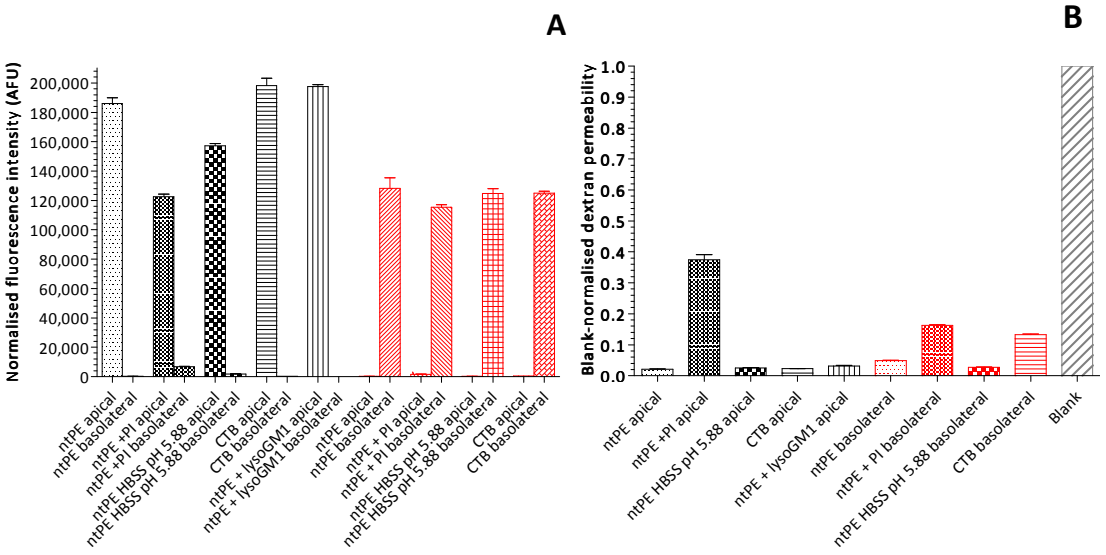

Figure 5-18 – (A) Amounts of ntPE-A568 or CTB-A488 collected from the apical and basolateral compartments after 240 min, following the application of 0.30 nmol ntPE-A568 or 0.35 nmol CTB-A488 to the apical (black) or basolateral (red) surface of Caco-2 monolayers. (B) Amount of FITC-labelled 4 kDa dextran present in the basolateral compartment 30 min after apical application to Transwell® filters (blank) compared to Transwell® filters supporting a monolayer of polarised Caco-2 cells incubated with either protein for 240 min. Data presented as mean ± SD for n = 3 wells.

Altogether, these results indicate that while the protein could be internalised by NP Caco-2 cells, its entry and transport in polarised monolayers was inconsistent for the *in vitro* systems of polarised epithelial cells that were studied, despite initial success using the

Caco-2 model. The fact that full-length ntPE protein and several truncated forms appeared to be taken up by NP cells suggests that it could still interact with its surface receptor(s). Tests aiming to eliminate experimental factors causing zero interaction did not prove conclusive either, since modifying the incubation conditions or even switching the system to new cells or different cell lines did not result in protein transport. CTB, which binds to the monosialoganglioside GM1 and can be used as a positive control for receptor-mediated endocytosis and transcytosis, was not able to cross or even traffic effectively in polarised Caco-2 cell monolayers (Figure 5-18 and Figure 5-19). If GM1 plays as important a role in the internalisation and potentially the transport of PE as was suggested by previous data (Chapter 4), its inability to traffic from the apical membrane would explain why transcytosis of ntPE across Caco-2 monolayers was not observed. How and why GM1 would be retained at the apical surface is unclear.

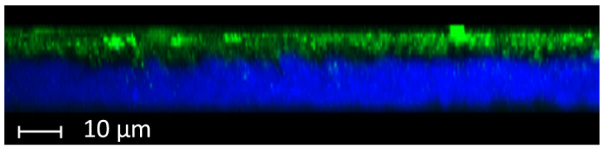

Figure 5-19 – CTB does not transport across polarised epithelial cells. Z-stack image of a Caco-2 monolayer 240 min after application of 0.35 nmol CTB-A488 (green) to the apical surface. Cell nuclei were stained with DAPI (blue).

5.3.6 In vivo transport of PE364-hGH

Results described in this chapter have shown that several truncated versions of PE linked to a C-terminal GFP molecule were internalised by NP cells *in vitro*. Moreover, it was demonstrated that full-length ntPE could carry a fluorescent tag across a polarised monolayer of intestinal epithelial cells. However, no data were obtained regarding the transport of a cargo protein across polarised cells, which is essential with regards to oral protein delivery, possibly due to problems that may be related to the *in vitro* system. To determine if this could be achieved, the uptake and trafficking of a truncated version of PE (PE364) carrying a molecule of human growth hormone (hGH) were studied *in vivo* (Figure 5-20 (A)). hGH was selected as a model protein drug because its molecular weight is comparable to that of PE domain III, and because the mature protein is a non-glycosylated monomer and could therefore be expressed in *E. coli* (Figure 5-20 (B)).

PE364-hGH diluted in PBS was first injected directly into the lumen of a rat's small intestine. A sample segment was collected 15 min after administration and tissues were

processed and immunostained as described in Section 2.17.2. PE364 and hGH were individually detected with antibodies targeting each protein, used in conjunction with corresponding fluorescent secondary antibodies. The white light channel was used to visualise individual villi as well as the borders of epithelial cells composing them. Controls (naïve tissue) are presented in Appendix 5.

The fluorescence pattern observed in Figure 5-21 showed that both PE364 (red) and hGH (green) were present inside the enterocytes lining the villi. Moreover, the detection of yellow fluorescence patches revealed that the two proteins co-localised within these polarised cells in both apical and basal regions. Further, some cells in the submucosa showed internal labelling for both PE364 and hGH, suggesting that these materials completed the transcytosis process and were internalised by some of these cells. On the contrary, other cells present in the submucosal space displayed only red or green labelling, suggesting that in some instances, the carrier and cargo proteins could have separated following transepithelial transport.

It has been shown in various cell types that following interaction with plasma membrane receptors, hGH is internalised by endocytosis [324]. The protein-receptor complex does not dissociate at low pH and is directed towards either the lysosome for degradation (degradative pathway, ~75%) or recycled to the cell surface, where intact hGH is released (non-degradative pathway, ~25%) [325]. As a consequence, the presence of intracellular hGH suggests that, in all likelihood, this protein was still attached to PE364. This idea is supported by the detection of both proteins at the basal pole of enterocytes, which implies that transcytosis occurred and that PE364 acted as a carrier and transported hGH within the cells, away from degradation or recycling pathways.

Detection of yellow fluorescence in the submucosal space suggests that the fusion protein transported across the enterocytes and reached cells present in the underlying mucosa. In fact, it has been shown that these cells share some of their cell-surface receptors with polarised enterocytes and are able to internalise PE [27]. The observed fluorescence pattern would therefore be consistent with the administered material undergoing transepithelial transport before being internalised by some cell populations in the submucosal space. Targeted co-localisation studies would need to be performed in order to identify which cell types may have internalised the transported material (e.g. macrophages, dendritic cells).

These findings demonstrate that neither truncation of PE down to residue 364, nor replacement of domain III by a different cargo protein, eliminated the protein's ability to transcytose across polarised enterocytes *in vivo*.

Although the protein was injected at high dose directly at the site of absorption, the *in vivo* model used here incorporates dynamic components such as blood circulation and gastrointestinal transit which can affect protein absorption and are not considered in the Caco-2 polarised system [318, 326]. Moreover, studies by Lennernäs *et al* (1995) reported lower expression of membrane-associated carrier proteins in Caco-2 monolayers than *in vivo*, possibly resulting in saturation of the carrier and leading to significantly lower effective permeability *in vitro* [327]. If this were applicable to membrane receptors, reduced LRP1 and/or GM1 expression in Caco-2 cells might explain why no transcytosis was observed *in vitro* (Section 5.3.5), whereas PE364 appears to effectively transport across polarised epithelial cells *in vivo*.

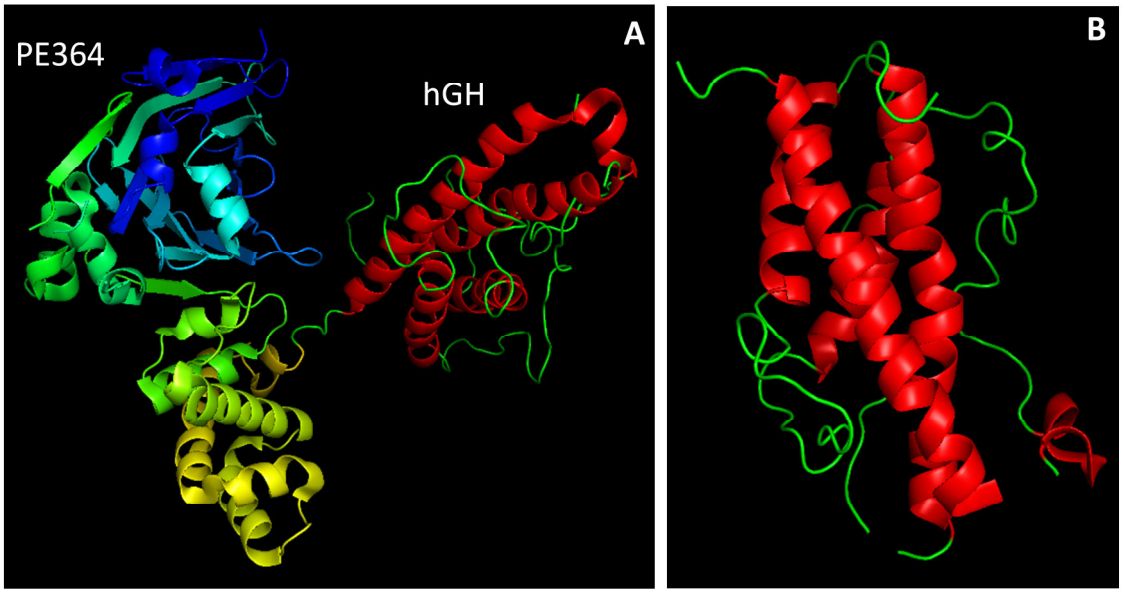

Figure 5-20 – Ribbon representations of (A) PE364-hGH and (B) human growth hormone (hGH) (PDB_ID: 1HGU). The mature hGH is a monomer composed of four α-helices and is non-glycosylated. α-helices and loops are displayed in red and green, respectively. Structures were generated using PyMOL [128].

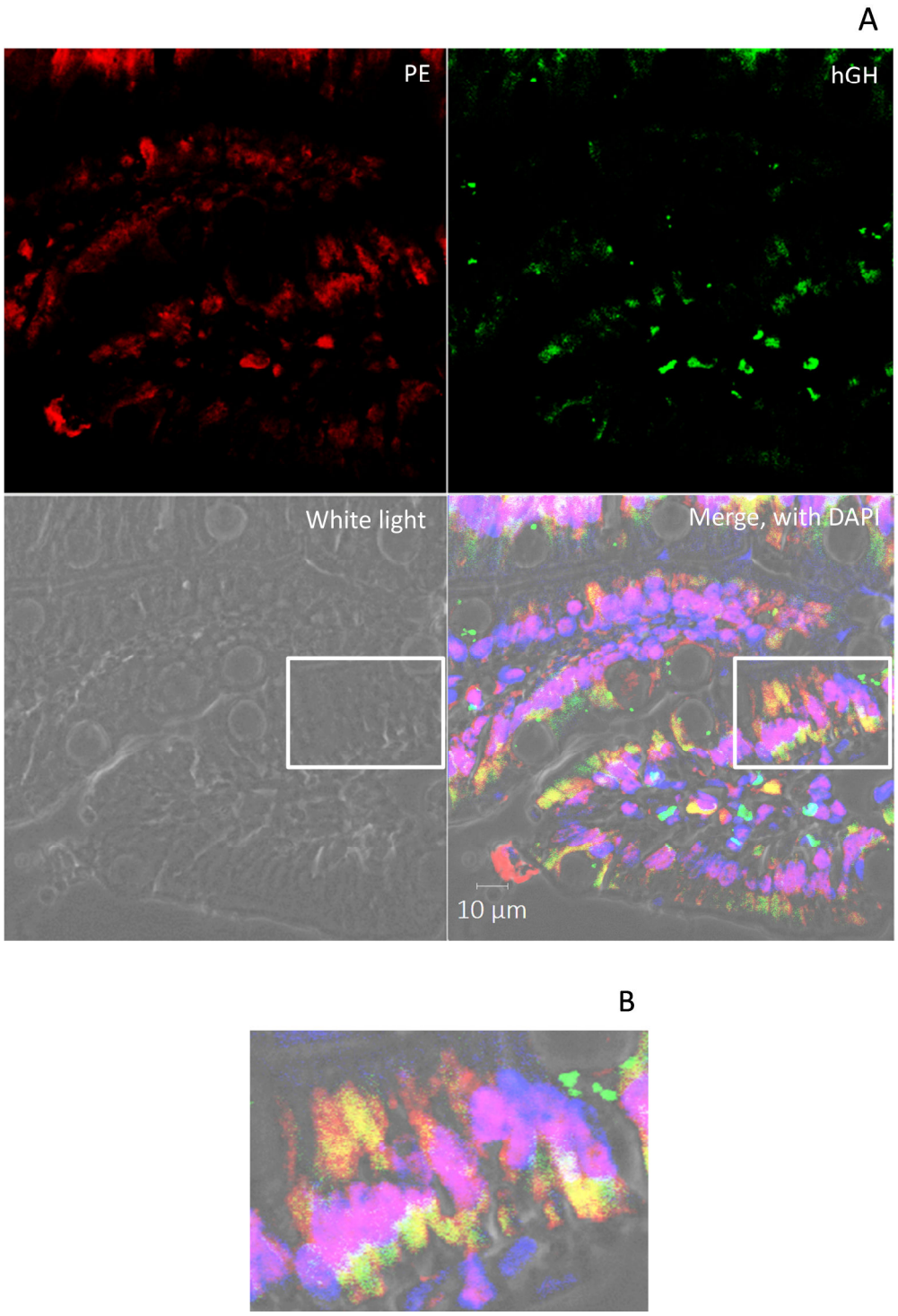

Figure 5-21 – Transport of PE364-hGH across rat small intestinal cells. (A) A section of rat intestinal tissue (5 µm) was indirectly immunostained with antibodies to PE (red) and hGH (green). Cell nuclei were stained with DAPI (blue). (B) Higher magnification of white rectangle from merge of image (A).

5.4 General discussion

This chapter describes efforts to characterise the properties of PE as a device for oral delivery of macromolecular drugs. Previous reports suggested that the three structural domains of PE may have independent functions [159] and that PE domain III was not required for cellular uptake or transcytosis of the protein in polarised epithelial cells [328]. To further investigate these concepts, six fusion proteins were used in the studies reported here, in addition to the PE GS TEV constructs. Each of them was composed of a carrier domain of variable length (one of the PE GS TEV proteins) linked to a C-terminal cargo molecule (GFP). The internalisation and transport properties of these proteins were studied in polarised and non-polarised cells. In addition to this, the transepithelial transport of a fusion protein composed of PE364 genetically linked to hGH was investigated *in vivo*.

Caco-2 cells have been widely described as a model for human intestinal absorption as they differentiate into monolayers of polarised enterocyte-like cells, characterised by the presence of a brush border, metabolic enzymes and tight junctions that establish cell-cell contacts [329, 330]. Caco-2 cells were used here to investigate protein uptake and transcytosis across intestinal epithelial cells. *In vitro* uptake assays in NP cells showed that two of PE's shorter mutants, truncated either at the end or middle of domain II and carrying a fluorescent Alexa Fluor® tag (PE364-A568 and PE303-A568, respectively), seemed to be internalised by NP Caco-2 cells. This is consistent with earlier reports indicating that the catalytic domain is dispensable for cell entry [328] and suggests that half of domain II might also be removed without affecting the protein's ability to be taken up by cells. Fluorescence patterns observed for each of the three versions of PE tested appeared to differ, suggesting that truncation of the carrier domain could interfere with PE's trafficking properties in NP cells. This could be due to truncated proteins being perceived as misfolded by quality control sensors, and therefore being redirected to the lysosome for degradation. Alternatively, a fraction of the protein could remain trapped within endosomal compartments. However no co-localisation studies were carried out, and therefore no conclusions can be drawn regarding the destination of these proteins or the extent of this truncation effect.

As a conclusion, truncation of PE did not seem to affect its ability to enter NP cells in this study. This is consistent with the attribution of binding activity to PE domain I, which remained intact in the truncated proteins that were prepared and tested. However, the

data described could also point to the possibility that excessive shortening of the protein might result in its premature clearance and degradation by intracellular quality control systems.

Similar uptake assays were performed on NP Caco-2 cells using the PE-GFP mutants in order to investigate the impact of a cargo protein on internalisation. Following the application of each protein to untreated cells, intracellular fluorescence could only be visualised for the full-length ntPE, suggesting that none of the five shorter mutants were able to be internalised by the cells. This could be due to the presence of the cargo protein at the C-terminal end of PE. As previous results highlighted the importance of specific PE-GM1 interactions for uptake, the role of GM1 in the entry process of the PE-GFP protein series was examined here using the same set of experiments that were used for the full-length ntPE in Chapter 4. Results denoted the same dependency upon GM1 for efficient entry of PE-GFP proteins in NP cells as was observed for full-length ntPE-A568. Therefore, it could be assumed that the mechanism used by the PE-GFP mutants to enter the cells was similar to the one used by full-length ntPE. In this case, the fact that all truncated proteins seemed to enter the cells implies that the presence of a cargo domain which is different from domain III, but of similar size, did not affect receptor-mediated endocytosis. Furthermore, as all proteins showed a marked improvement in internalisation following neuraminidase treatment, these studies appear to confirm results from Chapter 4 and support the hypothesis that the GM1 binding site could be located between amino acids 1 and 303 of PE.

These results establish that PE would constitute a suitable carrier for protein delivery in NP cells. However, this system does not completely reflect the mechanisms observed in polarised cells. For instance, polarised cells can display different endocytic mechanisms depending on whether the uptake occurs from their apical or basolateral membranes [311, 331], and the population of surface lipids, proteins and receptors also reflects the asymmetric cell organisation [332, 333]. As the intestinal epithelial barrier is composed of polarised cells, understanding transport mechanisms in these cells is necessary to evaluate the potential of PE as a carrier for oral protein delivery. Therefore, uptake and transcytosis of PE were assessed using polarised Caco-2 cell monolayers. Using this model, the ability of a fluorescently-tagged full-length ntPE to cross intact epithelial barriers was established. However, no information could be obtained about the transport characteristics of the PE-GFP protein series due to the collapse of the model for transport outcomes. Therefore, both the individual and combined impacts of truncation and presence of a cargo on transcytosis *in vitro* remain unknown. To further assess the

effect(s) of these factors, the transepithelial transport of PE364-hGH was then investigated *in vivo*. Results showed that following direct injection in the intestinal lumen, the fusion protein appeared to be internalised by enterocytes, translocated across these cells, and possibly taken up by some cells of the submucosal space. These findings therefore establish that replacement of PE domain III by a protein drug such as hGH does not block transcytosis of a truncated form of PE *in vivo* and that the cargo protein can be delivered to the underlying mucosa.

In conclusion, these results confirm that truncated forms of PE may provide a promising system for intracellular as well as oral delivery of biologics. Although shorter versions of PE carrying a C-terminal cargo protein did not seem able to be internalised by untreated NP cells, uptake of all mutants could be restored by activation of the DRM-mediated transport pathway (Section 4.4). Moreover, removal of domain III did not seem to alter protein trafficking and cargo delivery *in vivo*. Shortening the length of the carrier domain could therefore represent a significant advantage as it could dramatically decrease immune response upon administration. It must be underlined that the use of PE as a carrier for protein therapeutics would overcome the poor permeability of the intestinal epithelium, but would not protect the drug against the other obstacles encountered during oral delivery. Therefore, PE and its cargo protein would need to be associated with other protection devices, e.g. enzyme inhibitor or pH-dependent coating, to avoid degradation in the GIT, and potentially supplemented by adherent systems to bring it closer to the intestinal mucosa and ensure maximum effect.

6 RESULTS 4 – CHOLIX

6.1 Introduction

Jørgensen *et al* (2008) characterised the ADP-ribosylating protein that can be secreted by *Vibrio cholerae*, a protein that has been named cholix toxin (Cho) [105]. Cholix (70.4 kDa) structurally resembles PE, as it is a single polypeptide chain of 634 amino acids divided into three distinct domains, which appear to have the same respective functions as that of PE (Figure 6-1). Cho contains the same furin cleavage site required for activation (Arg292), has a C-terminal KDEL sequence, and has disulphide bridges that are positioned in an alignment similar to PE (C11-C15, C208-C225, C278-C300, C394-C401) [113]. Importantly, the cell intoxication produced by PE and Cho is a result of targeting the same residue on eEF2 [105]. Residue Glu581 has been identified as the equivalent of Glu553 for PE since mutant proteins carrying an Alanine residue at position 581 showed little or no activity in mouse fibroblasts [105]. Although cholix also recognises the LRP receptor [105], it uses a different receptor to enter CHO cells [27] and no evidence has yet been found that it uses the same intracellular pathway as PE [145]. Overall, sequence alignment between PE and cholix shows that the two proteins share only 33% sequence identity [105], yet alignment of their X-ray crystal structures are nearly superimposable (see Appendix 6 and Figure 6-1).

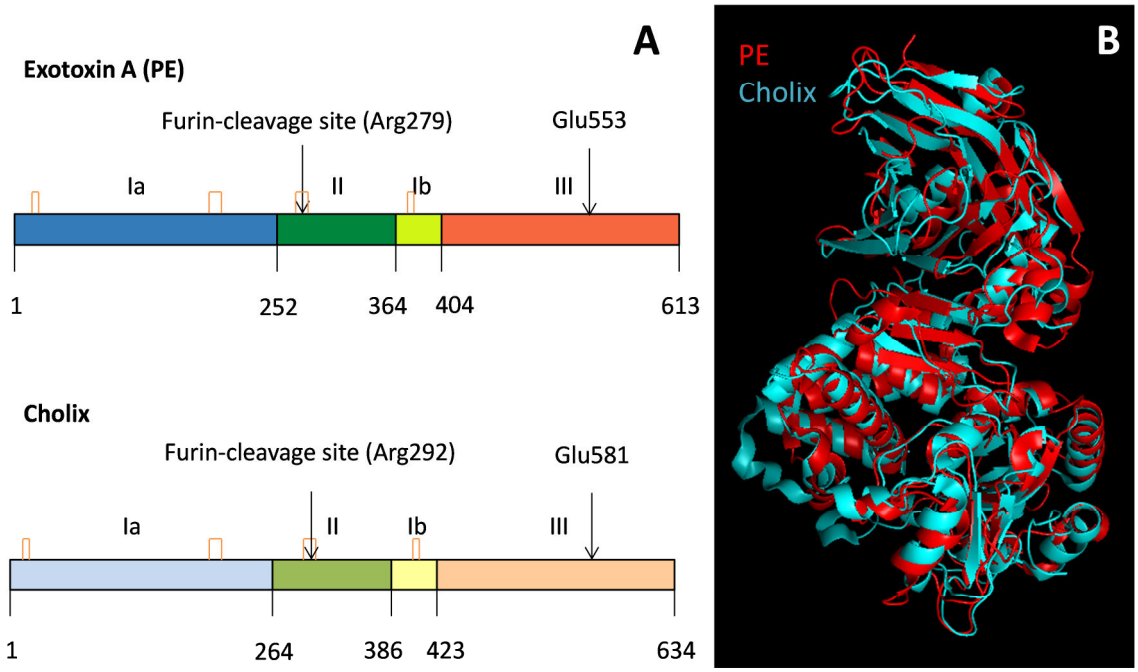

Figure 6-1 – The structure of cholix presents striking similarities with that of PE. (A) Schematic representation of PE and cholix structures. Both proteins are divided into distinct domains: Ia is responsible for cell recognition and receptor binding, domain II controls protein translocation and contains the furin-cleavage site, and domain III is the enzymatic domain of the toxin. The function of domain Ib, which is positioned between domains II and III, has yet to be elucidated. Disulphide bonds are represented orange and amino acids at the limit of each domain are indicated below. The furin cleavage site is indicated by an arrow. Note the deletions of PE-E553 and Cho-E581 in domain III that render PE and cholix non-toxic (ntPE and ntCho). (B) Ribbon representation of PE and cholix structures highlighting their similarity. The figure was generated using PyMOL [128].

The great structural and functional similarities between PE and cholix suggest that these two toxins could possibly use comparable mechanisms to both intoxicate non-polarised cells and transport across polarised monolayers. Therefore, the following chapter describes an effort to characterise the intracellular behaviour of cholix using some of the techniques that have previously been employed to investigate the properties of PE. In particular, the behaviour of cholix at acidic pH, its interaction with GM1, and its potential as a drug delivery system were examined.

6.2 Methods

Determination of trypsin cleavage sites from digestion fragments

Following digestion of Cho GS TEV mutants by trypsin, the size of the resulting fragments was used to estimate potential cleavage sites. The protein sequence used (PDB_ID: 2Q5T) contains an N-terminal 6X His tag which was removed for calculations. The remaining sequence was run into PeptideCutter and only digestion sites with a 100% cleavage probability were displayed [183]. The molecular weight of the resulting fragments was then calculated with ProtParam [181].

6.3 Results and discussion

6.3.1 Protein expression and coupling

6.3.1.1 Summary of proteins expressed

In this chapter, the behaviour of truncated versions of Cho GS TEV and Cho-GFP were studied. The expression and purification outcomes of these proteins, as well as their physiochemical properties, are presented in Tables 6-1 and 6-2 below.

Table 6-1 – Summary of expression and purification outcomes for both Cho GS TEV and Cho-GFP truncated mutants and for Cho386-hGH.

Protein designation	Solubility	Expression protocol used	Purification	Yield
ntCho GS TEV	Soluble	Soluble	IX, GF	Good
Cho428 GS TEV	Insoluble	Inclusion bodies	IX, GF	None
Cho386 GS TEV	Insoluble	Inclusion bodies	IX, GF	Good
Cho368 GS TEV	Insoluble	Inclusion bodies	IX, GF	Good
Cho332 GS TEV	Insoluble	Inclusion bodies	IX, GF	Good
Cho313 GS TEV	Insoluble	Inclusion bodies	IX, GF	Good
ntCho-GFP	Soluble	Soluble	IMAC, GF	Good
Cho428-GFP	Soluble	Soluble	IMAC, GF	Good
Cho386-GFP	Insoluble	Inclusion bodies	IMAC, GF	Low
Cho368-GFP	Insoluble	Inclusion bodies	IMAC, GF	Low
Cho332-GFP	Insoluble	Inclusion bodies	IMAC, GF	Low
Cho313-GFP	Insoluble	Inclusion bodies	IMAC, GF	Low
Cho386-hGH	Insoluble	Inclusion bodies	IX, GF	Medium

Table 6-2 – Physicochemical properties of Cho GS TEV and Cho-GFP mutants and of Cho386-hGH. Both pI and molecular weight were calculated using ExPASy ProtParam [181].

Protein designation	Calculated pI	Calculated molecular weight (kDa)
ntCho GS TEV	5.31	71.8
Cho428 GS TEV	5.31	48.0
Cho386 GS TEV	5.42	43.7
Cho368 GS TEV	5.37	41.6
Cho332 GS TEV	5.65	37.5
Cho313 GS TEV	5.59	35.4
ntCho-GFP	5.21	97.9
Cho428-GFP	5.18	74.9
Cho386-GFP	5.12	71.6
Cho368-GFP	5.08	69.7
Cho332-GFP	5.16	65.3
Cho313-GFP	5.19	63.1
Cho386-hGH	5.27	66.3

6.3.1.2 Expression and purification of Cho GS TEV mutants

Truncated versions of ntCho GS TEV were expressed following the same procedure as for PE GS TEV mutants. Only ntCho GS TEV was soluble. The other five proteins were insoluble and expressed as inclusion bodies. Below are presented, as an example, the chromatograms and Coomassie-stained SDS-PAGE obtained after purification of Cho386 GS TEV.

Following expression in inclusion bodies, Cho386 GS TEV was loaded on an AE column and eluted with a NaCl gradient. A single peak could be observed at 20-60% NaCl (= 0.2-0.6 M NaCl) (Figure 6-2 (A)).

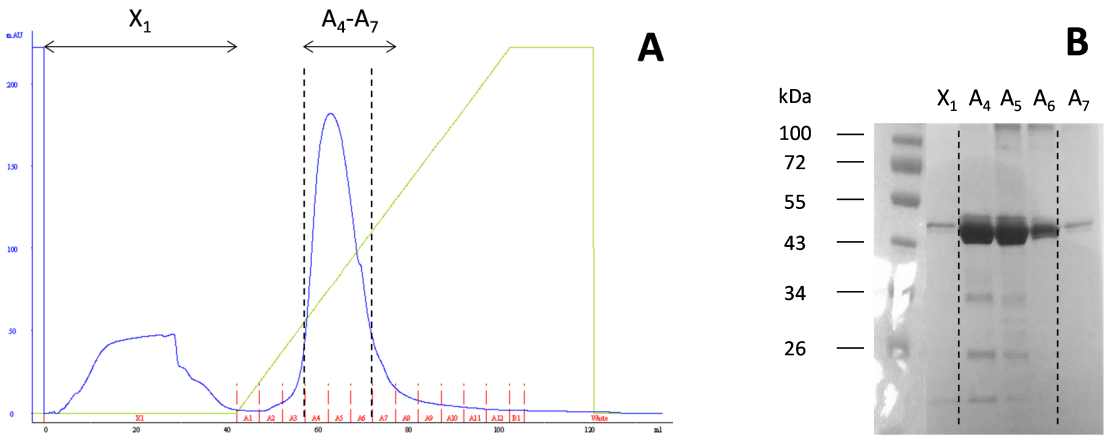

Figure 6-2 – Initial enrichment of Cho386 GS TEV by AE chromatography. (A) Chromatogram obtained for AE separation. (B) Coomassie-stained SDS-PAGE of AE fractions shown in (A) containing the flow-through and protein peaks. X- and A-labelled lanes in (B) correspond to arbitrary tray row and column reference on the fraction collector and are illustrated by the red dashes on (A). Fractions covered by the arrow in (A) indicate the complete range of fractions displayed in (B). The black dotted lines marked on both (A) and (B) indicate the fractions containing Cho386 GS TEV that were collected.

Fractions corresponding to the peak and flow-through were separated by SDS-PAGE (Figure 6-2 (B)). Although a very faint band the same size as the protein (~45 kDa) could be seen, the amount of Cho386 GS TEV present in the flow-through was negligible. On the contrary, fractions A_4-A_6 contained a large amount of protein which was collected, concentrated to a 1 ml volume, and further purified by size exclusion chromatography (Figure 6-3 (A)).

Fractions corresponding to the UV-absorbing material were separated by SDS-PAGE (Figure 6-3 (B)). Cho386 GS TEV was present in the combined fractions D_5-D_{14} and its purity was assessed to be acceptable for the following studies.

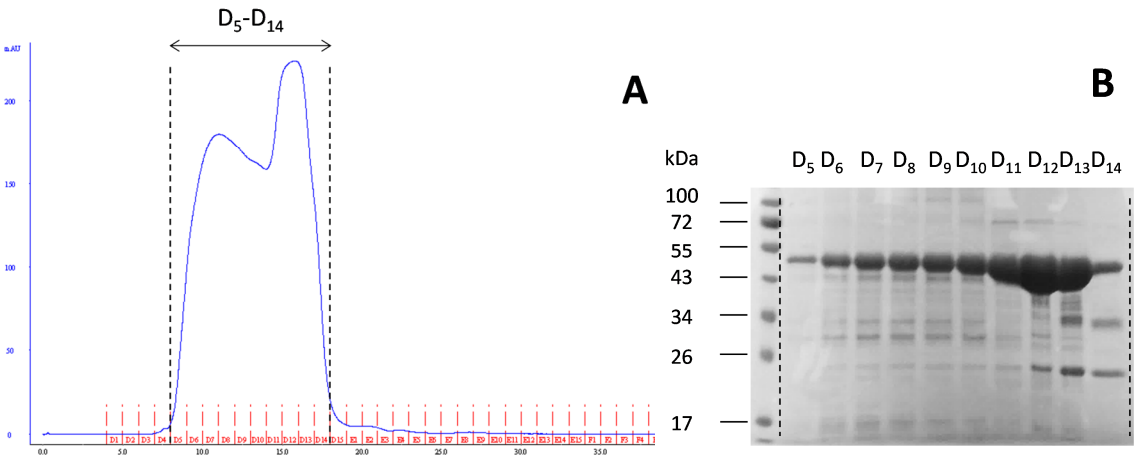

Figure 6-3 – Further enrichment of Cho386 GS TEV by GF chromatography. (A) Chromatogram obtained for GF column separation. (B) Coomassie-stained SDS-PAGE of fractions corresponding to the UV peak. D-labelled lanes in (B) correspond to arbitrary tray row and column reference on the fraction collector and are illustrated by the red dashes on (A). Fractions covered by the arrow in (A) indicate the complete range of fractions displayed in (B). The black dotted lines marked on both (A) and (B) indicate the fractions containing Cho386 GS TEV that were collected.

6.3.1.3 Expression and purification of Cho-GFP mutants

The proteins described in this section were cloned in collaboration with Dr Julia Mackay, who also assisted with their expression.

ntCho-GFP is a fusion protein where full-length Cho lacking residue E581 is connected by the previously described poly glycine-serine flexible linker to a C-terminal GFP molecule (Figure 6-4). The resulting protein carries an N-terminal 6X His tag which allows ntCho-GFP to be purified by IMAC.

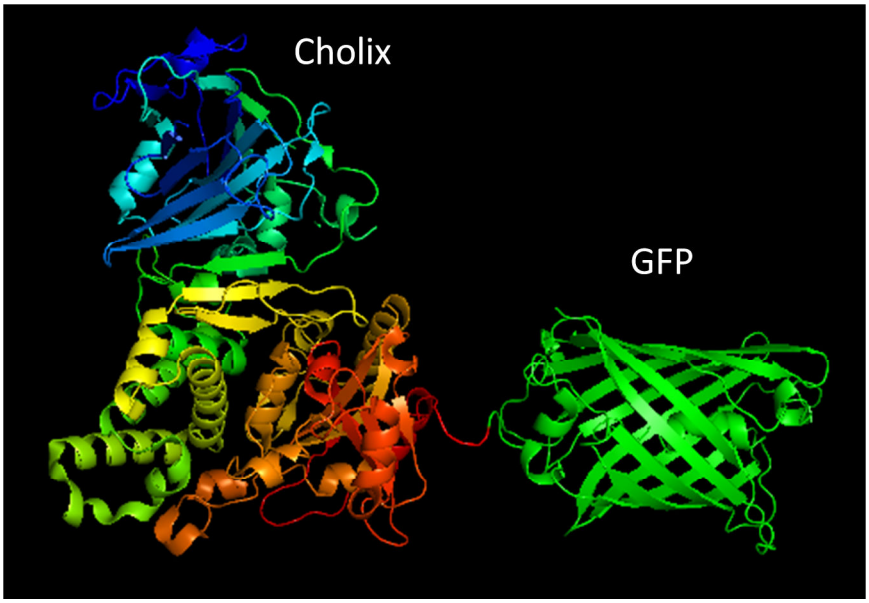

Figure 6-4 – Ribbon representation of ntCho-GFP structure. Cholix was fused with a C-terminal molecule of GFP. The figure was generated using PyMOL [128].

Five truncated versions of Cho-GFP were also produced, corresponding to the Cho GS TEV protein series: Cho428-GFP, Cho386-GFP, Cho368-GFP, Cho332-GFP and Cho313-GFP. Numbers indicate the last amino acid of the truncated Cho protein. Some physiochemical properties of these proteins are presented in Table 6-2.

While ntCho-GFP and Cho428-GFP were soluble and directly secreted by *E. coli*, the four shorter proteins were insoluble and therefore expressed as inclusion bodies. The presence of a GFP molecule and the resulting green colour facilitated the evaluation of soluble protein content following expression. A summary of the expression and purification outcomes is presented in Table 6-1. As the expression yield for the shortest mutants was fairly low, only ntCho-GFP purification details are provided below as an example.

Enrichment of His-tagged Cho protein was achieved using a nickel column that was eluted using an imidazole gradient. Two peaks of UV-absorbing material could be detected: the first peak (~400 mAU) corresponded to the flow-through (fraction X_4). The second peak (~175 mAU, fractions A_2-A_5) was a smaller peak eluting from 63 to 215 mM imidazole (9-41%) (Figure 6-5). This elution peak was well defined and, due to the specificity of IMAC, fractions A_2-A_5 were collected and enriched further using GF chromatography. The protein was eluted with PBS and only the content of fluorescent fractions (A_{12}-A_{14}) was separated by SDS-PAGE (Figure 6-6). The resulting Coomassie-stained gel revealed that these fractions did contain the protein of interest, and were therefore collected for future use.

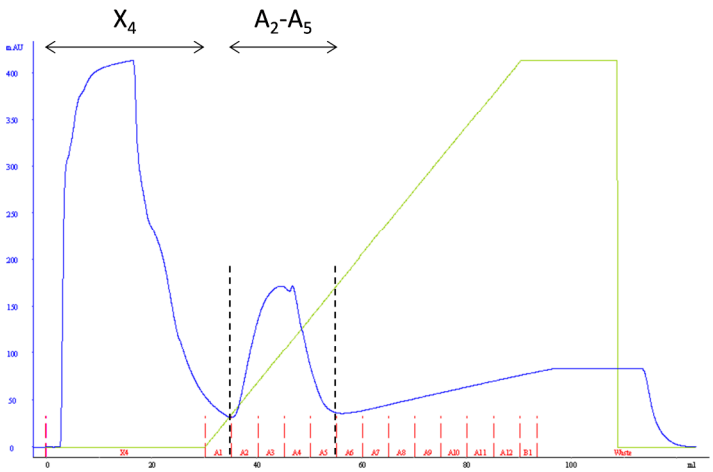

Figure 6-5 – Initial enrichment of ntCho-GFP by IMAC. X- and A-labelled lanes correspond to arbitrary tray row and column reference on the fraction collector and are illustrated by the red dashes. Fractions covered by the arrow indicate the complete range of fractions mentioned. The black dotted lines indicate the fractions containing ntCho-GFP that were collected.

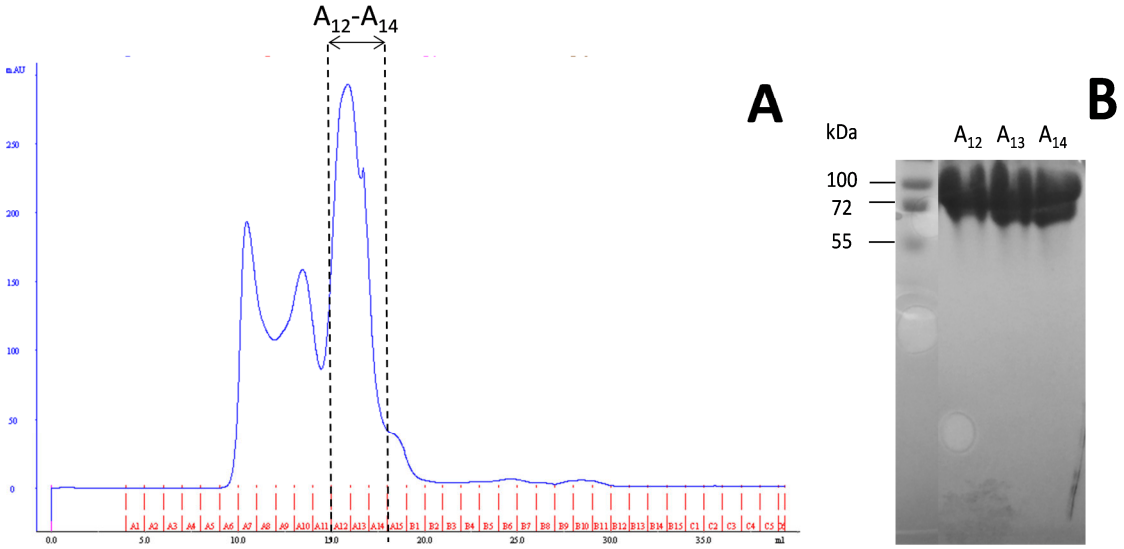

Figure 6-6 – Further enrichment of ntCho-GFP by GF chromatography. (A) Chromatogram obtained for GF column separation. (B) Coomassie-stained SDS-PAGE of UV peak fractions. A-labelled lanes in (B) correspond to arbitrary tray row and column reference on the fraction collector and are illustrated by the red dashes on (A). Fractions covered by the arrow in (A) indicate the complete range of fractions displayed in (B). The black dotted lines marked on both (A) and (B) indicate the fractions containing ntCho-GFP that were collected.

6.3.1.4 Cloning, expression and purification of Cho386-hGH

Cloning of Cho386-hGH

Cho386 was amplified from pETCHO, a vector containing the full length non-toxic cholix (Figure 9-1), using the three same buffers which were used for amplification of hGH (GC, GC + DMSO and HF) (Figure 6-7 (A) and (B)). The primers included the NdeI and SpeI restriction sites. PCR using GC + DMSO produced only a very faint band at ~1.2 kbp, which would correspond to Cho386. However, amplification using either GC buffer or HF buffer produced a stronger band of correct size. For all three conditions, two other bands could be observed at ~3 and ~9 kbp, which could result from the aggregation of several inserts. As HF is the recommended buffer for high-fidelity amplification, the PCR was scaled up using this buffer with the resulting Cho386 being digested by NdeI and SpeI-HF®. In parallel, pPE364-hGH (DH5α) was digested at these same restriction sites in order to release PE364 (~1.2 kbp) (Figure 6-7 (C)). The ~4 kbp band corresponding to the remaining plasmid was purified on agarose gel.

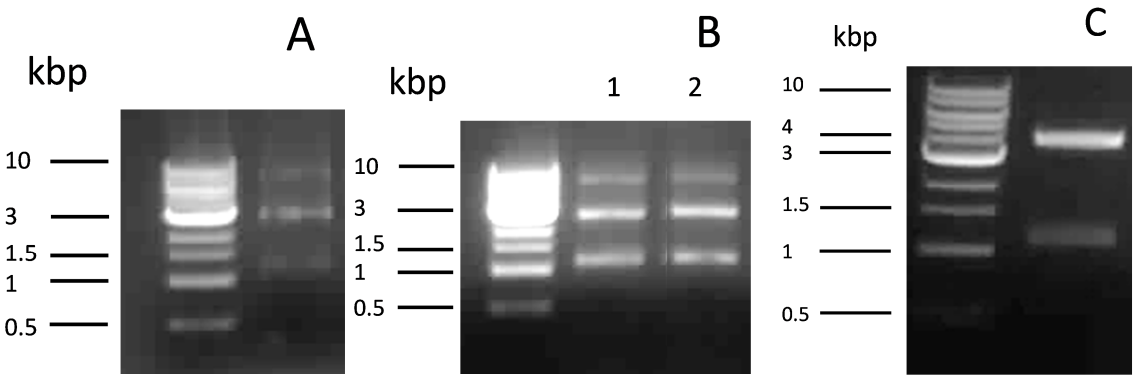

Figure 6-7 – Amplification of Cho386 by PCR in (A) GC buffer + DMSO or (B) GC or HF buffer only (Lanes 1 and 2, respectively). (C) Fragments obtained following digestion of pPE364-hGH by NdeI and SpeI-HF®.

pCho386-hGH (DH5α) was obtained after ligation of Cho386 and digested pPE364-hGH (DH5α) and further transformation of the resulting plasmid in competent DH5α cells. The presence of both Cho386 and hGH were confirmed by sequencing. pCho386-hGH (DH5α) was finally transferred into competent Shuffle cells to obtain pCho386-hGH (Shuffle), the plasmid used for expression of Cho386-hGH.

Expression and purification of Cho386-hGH

Cho386-hGH was insoluble when expressed in *E. coli*, as shown in Figure 6-8: after expression and centrifugation of bacterial cells, little protein was present in the supernatant, while pellets were loaded with protein.

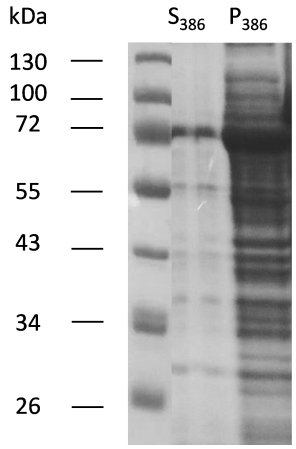

Figure 6-8 – Cho386-hGH is insoluble when expressed in *E. coli*. S_{386}, sample containing the soluble protein fractions (supernatant) and P_{386}, sample containing the insoluble protein fractions (pellet).

As a consequence, Cho386-hGH was expressed as inclusion bodies. Despite the presence of an N-terminal His tag, the expressed protein was not retained on a His column (Figure 6-9). It was therefore purified using AE and GF chromatography. First, Cho386-hGH was eluted from an AE column with a NaCl gradient. A single peak could be observed at 15-55% NaCl (0.15-0.55 M NaCl) (Figure 6-10 (A)). Fractions corresponding to this peak as well as the flow-through were separated by SDS-PAGE (Figure 6-10 (B)). A single band at ~72 kDa was detected in fractions H_4-H_8. As the band observed in the flow-through fraction (X_1) was very faint compared to bands detected in fractions H_4-H_8, these fractions were combined and were concentrated to 1 ml for further purification by size exclusion chromatography (Figure 6-11 (A)).

Following this second purification step, fractions corresponding to the UV-absorbing material were separated by SDS-PAGE. As the UV peak obtained was less well defined, an SDS-PAGE of individual column fractions was used to assess the amount and purity of the protein of interest in order to select fractions that were pooled; Cho386-hGH was collected from fractions D_5-D_{12} (Figure 6-11 (B)). Analysis of the Coomassie dye staining on the gel showed one dominant band visible at ~40 kDa in fractions D_{13}-D_{14}. This band could have corresponded to incompletely expressed Cho386-hGH.

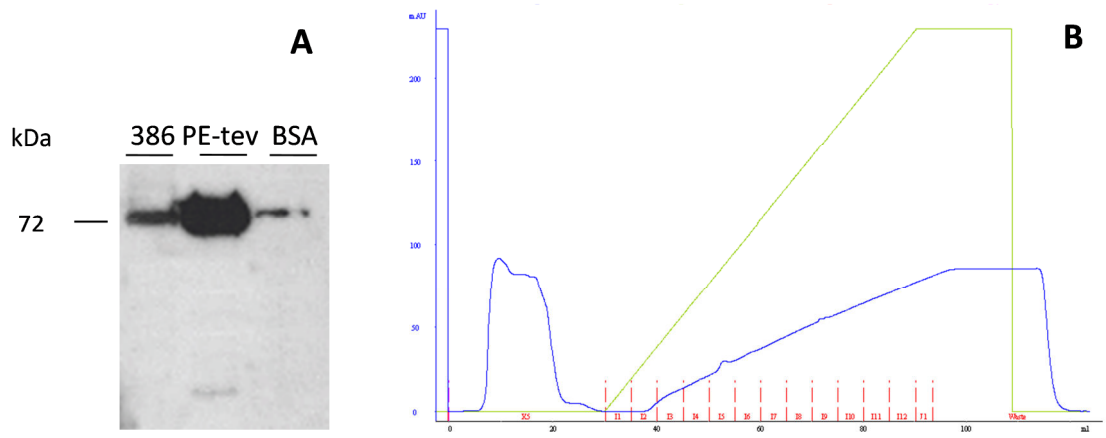

Figure 6-9 – Despite carrying an N-terminal His tag, Cho386-hGH was not retained on a His column. (A) WB of the purified Cho386-hGH. 10 µg protein was separated by SDS-PAGE and transferred to a PVDF membrane that was probed with an anti-His antibody diluted at 1 in 3,500 in TBS-T. PE-tev is a version of PE carrying a C-terminal His tag that was used as a positive control. BSA was used as a negative control. (B) Chromatogram obtained following elution of Cho386-hGH on a Ni^{2+}-functionalised column.

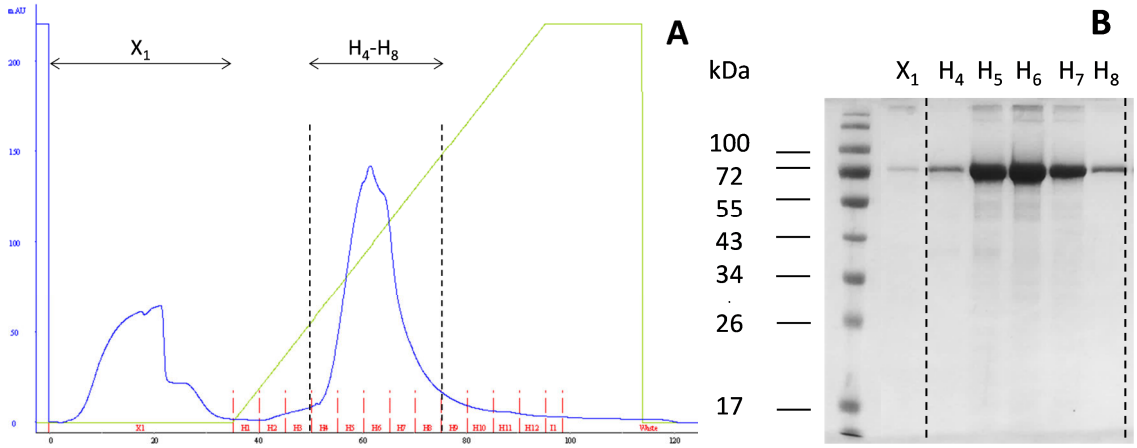

Figure 6-10 – Initial enrichment of Cho386-hGH by AE chromatography. (A) Chromatogram obtained for AE separation. (B) Coomassie-stained SDS-PAGE of fractions corresponding to the UV peaks. X- and H-labelled lanes in (B) correspond to arbitrary tray row and column reference on the fraction collector and are illustrated by the red dashes on (A). Fractions covered by the arrow in (A) indicate the complete range of fractions displayed in (B). The black dotted lines marked on both (A) and (B) indicate the fractions containing Cho386-hGH that were collected.

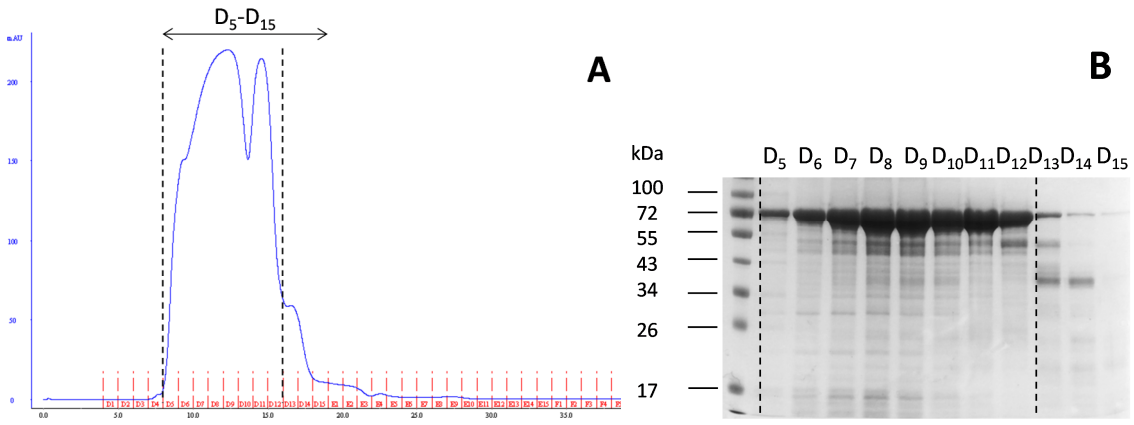

Figure 6-11 – Further enrichment of Cho386-hGH by GF chromatography. (A) Chromatogram obtained for GF column separation. (B) Coomassie-stained SDS-PAGE of fractions corresponding to the UV peaks. D-labelled lanes in (B) correspond to arbitrary tray row and column reference on the fraction collector and are illustrated by the red dashes on (A). Fractions covered by the arrow in (A) indicate the complete range of fractions displayed in (B). The black dotted lines marked on both (A) and (B) indicate the fractions containing Cho386-hGH that were collected.

6.3.1.5 Coupling of cholix to a fluorescent tag

All couplings were performed and purified using the same protocol. As an example, coupling of full-length cholix to Alexa Fluor® 568 is described below.

After cleavage of the C-terminal TEV sequence with a commercial AcTEV protease, ntCho GS TEV was incubated with a maleimide-functionalised Alexa Fluor® 568 tag (ntCho-A568). In order to separate the tagged protein from unreacted materials (uncoupled tag), the sample was loaded on a size exclusion column and purified by FPLC (Figure 6-12 (A)). The different components were eluted with PBS and the fractions corresponding to the UV-absorbing peaks were separated by SDS-PAGE (Figure 6-12 (B)).

Purification by GF chromatography resulted in the elution of one main UV-absorbing compound (fractions M_{10}-M_{14}) corresponding to a ~72 kDa band on Coomassie-stained gel. The very small peak eluting in fractions N_4-N_7 is likely to have contained the unbound dye. Only one very faint secondary band could be detected at ~55 kDa, indicating that the level of purity of the coupled material was satisfactory, and fractions M_{10}-M_{14} were thus concentrated together for further use.

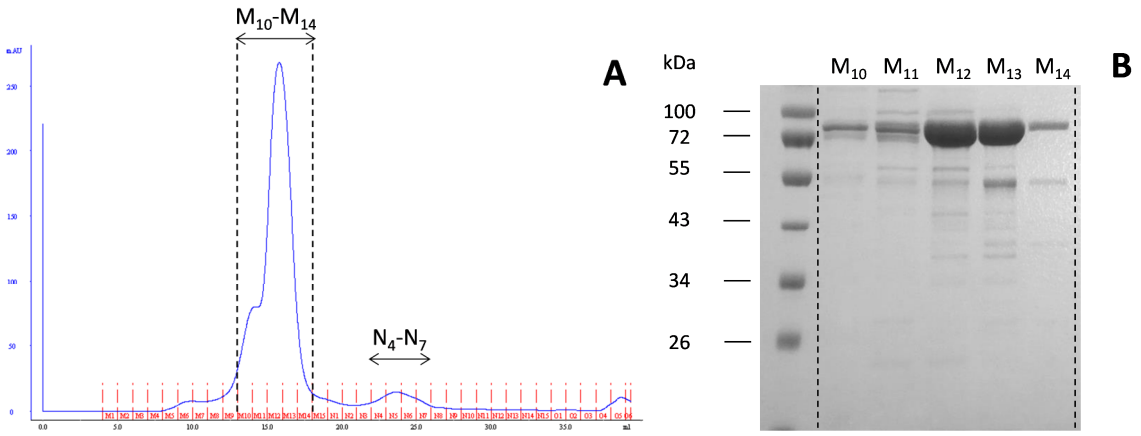

Figure 6-12 – Enrichment of ntCho-A568 by GF chromatography. (A) Chromatogram obtained for GF column separation. (B) Coomassie-stained SDS-PAGE of the fractions corresponding to the UV peak. M-labelled lanes in (B) correspond to arbitrary tray row and column reference on the fraction collector and are illustrated by the red dashes on (A). Fractions covered by the arrow in (A) indicate the complete range of fractions mentioned. The black dotted lines marked on both (A) and (B) indicate the fractions containing ntCho-A568 that were collected.

6.3.1.6 Preparation of biotin-labelled cholix

In order to obtain a biotinylated version of the protein, the C-terminal TEV sequence of ntCho GS TEV was digested with a commercial AcTEV protease; 1.09 mg (15 nmol) of cleaved ntCho GS TEV was collected in 3.5 ml PBS and incubated in the presence of 50-molar excess sulfhydryl-reactive EZ-Link® Maleimide-PEG_2-Biotin reagent (950 nmol ≡ 0.5 mg) for 3 h at RT. Following desalting, buffer exchange and concentration, 150 µl of ntCho-biotin at 2.8 mg/ml was collected in PBS.

6.3.2 Cholix undergoes a pH-induced conformational change which presents similar characteristics to that experienced by PE

In order to investigate the behaviour of cholix at mildly acidic pH, a set of experiments including trypsin digestion on the full-length protein and truncated mutants, size measurement using DLS and HPLC, and assessment of relative surface hydrophobicity by spectrofluorometry were performed.

6.3.2.1 Cholix undergoes a reversible pH-induced conformational change

In order to determine whether cholix presented the same pH-dependency as PE, the protein was digested with trypsin as previously described (Section 3.3.1). Analysis by SDS-PAGE revealed that the digestion pattern differed significantly depending on the pH (Figure 6-13). In fact, at physiological pH ntCho was hardly cleaved, as indicated by the presence of a strong band at ~72 kDa corresponding to the undigested protein (Figure 6-19). Two secondary bands could be detected at ~55 kDa and 50 kDa. This suggests that the major enzyme cleavage site was not fully exposed at pH 7.4. On the contrary, the pattern obtained at pH 5.8 revealed that virtually no undigested protein remained, and four main bands were seen at ~57, 53, 47 and 25 kDa. Moreover, the change proved completely reversible (REV sample) when the sample was adjusted from pH 5.8 to pH 7.4 (Figure 6-13).

These results suggest that cholix presents a pH-dependent behaviour similar to that observed for PE; the protein being increasingly digested as the pH is lowered due to a reversible conformational change. As in the case of PE, this complete reversibility suggests that the protein does not undergo major structural changes during this pH-dependent conformational switch, and implies a more local variation in structure.

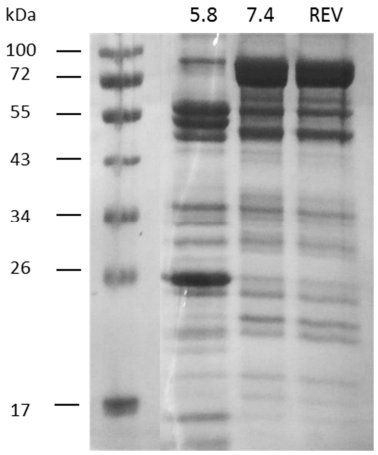

Figure 6-13 – pH-dependency of cholix digestion by trypsin is reversible. Coomassie-stained SDS-PAGE of ntCho GS TEV in citrate-phosphate buffer at pH 5.8 or 7.4 and of a sample incubated at pH 5.8 for 5 min and returned to pH 7.4 by dialysis (REV). All samples were digested using 0.4 µg trypsin at 4 °C for 30 min. SDS-PAGE of the undigested protein sample appears in Figure 6-19 (B).

6.3.2.2 Characterisation of the transition pH by DLS and trypsin digestion

In an effort to refine the pH range where the pH-dependent conformational changes might occur, the size of ntCho over the 5.8-7.4 range was determined by DLS. Variations in the protein's hydrodynamic diameter at various pH values and the statistical analysis used to assess that information are presented in Figure 6-14 (A) and (B), respectively. Statistical analysis revealed that only values at pH 6.2 and 7.4 were significantly different from other size measurements. Three distinct zones could be observed: when pH ≥ 6.4, a progressive decrease in protein size from12.1 ± 0.5 nm to 10.1 ± 0.3 nm (~16.5%) could be observed as the pH was lowered. When 6.0 < pH < 6.4, protein size seemed to re-increase to a maximum at 12.1 ± 1.0 nm. Finally, when the pH was ≤ 6.0, the hydrodynamic diameter of Cho seemed to stabilise around 10.7 ± 0.5 nm.

Samples used for DLS measurements were digested with trypsin and separated by SDS-PAGE. The gel was successively Coomassie- and silver-stained (Figure 6-15) and revealed that the conformational change occurred as a continuous transition between pH 7.4 and 5.8. In fact, band 1 (~72 kDa, ntCho) constituted the main band at pH 7.4 and 6.8, but gradually decreased in intensity until it completely disappeared at pH 5.8. The opposite progression could be observed for both bands 2 and 4 (~47 and 26 kDa, respectively). Finally, band 3 (~34 kDa) seemed to follow a similar transition but its intensity at pH 5.8 was significantly decreased. These results suggest that lowering the pH results in the progressive exposure of the trypsin cleavage sites, which only become completely accessible below pH 6.0. Using these four bands' relative intensities, three areas could be observed on these gels: when the pH was ≥ 6.8, the amount of digested protein remained minimal. However, when the pH was between 6.0 and 6.4 the protein became increasingly digested and maximum cleavage occurred at pH < 6.0. The significant increase in digestion observed at pH 5.8 could be due to protein denaturation, but this seems unlikely as it was previously shown that the conformational change at this pH was completely reversible.

These results indicate that as the pH decreases, cholix undergoes a progressive conformational change from a state in which the protein is resistant to trypsin cleavage to a state where its degradation by this protease is much more pronounced. This suggests that Cho presents at least one cleavage site in acidic conditions that is not present at neutral pH, with more cleavage sites becoming accessible following the initial trypsin cut. The three pH zones observed varied slightly depending on the technique used (DLS or trypsin digestion), but they confirmed that the transition between the two conformations adopted by cholix occurred in the pH region of 5.8-6.2. The marked increase in size

observed at pH 6.2 could imply that during its rearrangement from one conformation to the other, the protein might acquire different shapes of similar sizes. However, this conformational change did not tremendously affect the size of cholix, suggesting again that it might not be a global rearrangement of the protein's tertiary structure. In order to investigate further the extent of the unfolding and its impact on the protein's overall size, cholix was run on HPLC GF.

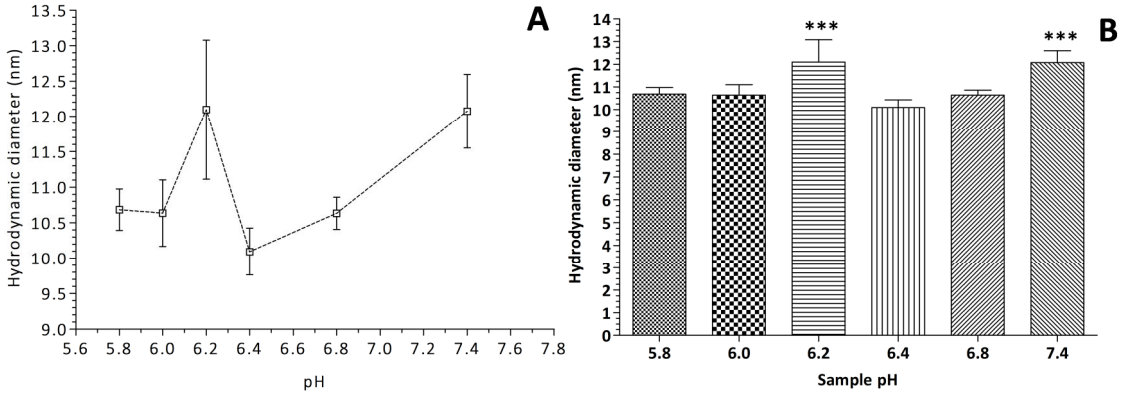

Figure 6-14 – (A) Measurement of the size of ntCho GS TEV at different pH values in citrate-phosphate buffer using DLS. (B) Statistical analysis of the results obtained in (A). Bars show mean ± SD for n = 6 independent samples where *** P < 0.001.

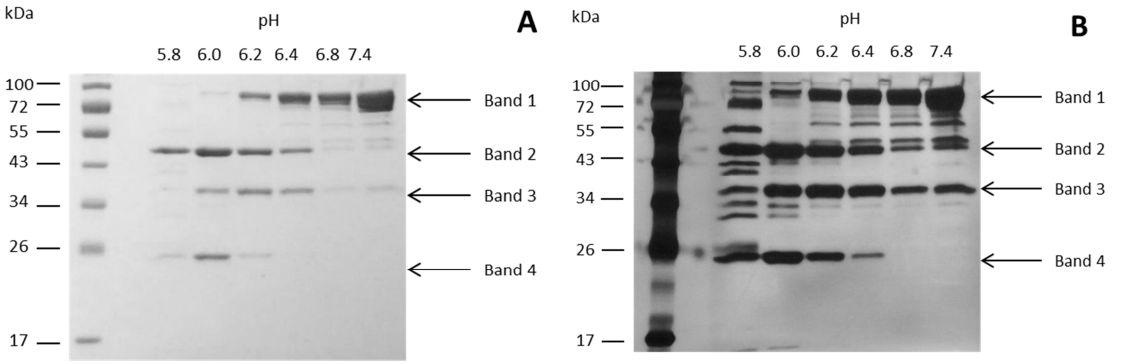

Figure 6-15 – Determination of the transition point between the two protein conformations by trypsin digestion. (A) Coomassie-stained and (B) silver-stained SDS-PAGE of DLS samples following digestion of 10 µg sample with 0.4 µg of trypsin at 4 °C for 30 min.

6.3.2.3 The conformational change experienced by cholix is not a global change in tertiary structure

A preparation of cholix was separated using an HPLC GF column in potassium-phosphate buffer (kPB) containing 0.1 M NaCl at pH 5.8 and 7.4. The main peak eluted from the

column at ~8.9 min, which is in agreement with the retention times determined for PE (~9.3-9.4 min). PE is smaller than cholix and therefore elutes slightly later from the column. Chromatograms collected for cholix at different pH values (Figure 6-16) showed that the two conformations of the protein eluted at very close retention times (8.936 and 8.870 min at pH 7.4 and 5.8, respectively). This suggested that their overall sizes and shapes were very similar, and therefore that no major structure alterations occurred upon lowering the pH. This supported the idea that, just as in the case of PE, the pH-dependent conformational change that occurred in Cho was consistent with a local change in structure.

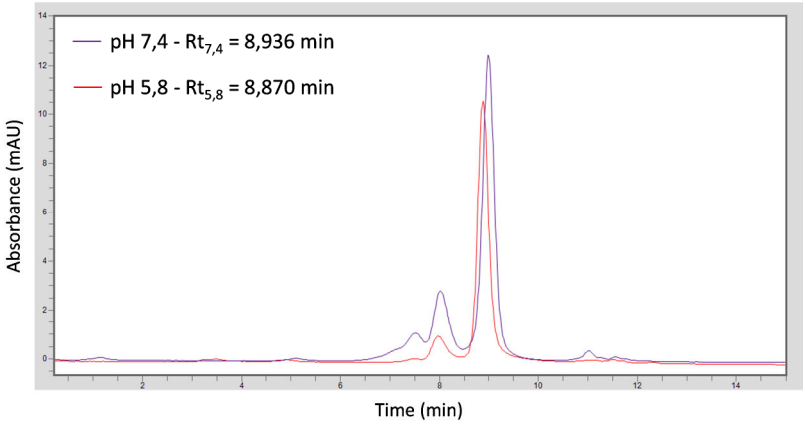

Figure 6-16 – HPLC chromatograms of cholix after elution on a GF column in 0.1 M kPB containing 0.1 M NaCl at pH 7.4 and 5.8 at 37 °C. UV measurements were performed at 254 nm. The chromatograms presented here were taken as representatives of 6 and 3 runs for pH 5.8 and 7.4, respectively.

6.3.2.4 Cholix conformational change results in the exposure of hydrophobic residues

In an attempt to further characterise the conformational change made by cholix in mildly acidic conditions, the surface hydrophobicity of the protein at different pH values was probed by measuring the variations in ANS fluorescence. The hypothesis to be tested was as follows: pH-dependent conformation changes in ntCho would result in alterations in surface accessible hydrophobic regions of the protein. This hypothesis was tested using a fluorescent dye and a protocol described previously for ntPE.

Fluorescence measurements were performed in citrate-phosphate buffer containing 0.1 M NaCl. The fluorescence emission spectrum was scanned between 400 and 700 nm, AUC values were calculated and values of $\lambda_{em,max}$ were determined (Figure 6-17 and Table 6-3). The same ANS blank and BSA controls as for PE were used in this study. Addition of 1.52 µM ntCho to 100 µM ANS at pH 7.4 resulted in a 1.25-fold increase in total fluorescence

compared to ANS alone and a blue shift in $\lambda_{em,max}$ from 518 to 507 nm. Upon lowering the pH, this shift became more pronounced with $\lambda_{em,max}$ further displaced at 498 nm and the fluorescence between ANS + ntCho 7.4 and ANS + ntCho 5.8 multiplied by ΔF = 2.143.

These observations suggested that, as in the case of ntPE, ANS was able to bind to solvent-exposed hydrophobic areas on the ntCho protein used in these studies. This was consistent with a molecular representation of cholix surface hydrophobicity, on which it was clear that hydrophobic residues were present on the protein surface at physiological pH (Figure 6-18). However, fluorescence intensity was much lower for cholix, suggesting that this toxin bears less surface exposed hydrophobic sites in its native state than PE. The dramatic increase in ΔF upon lowering the pH could indicate that following the conformational change(s) associated with the altered trypsin sensitivity, additional hydrophobic residues became exposed to the surface and available to bind the ANS dye.

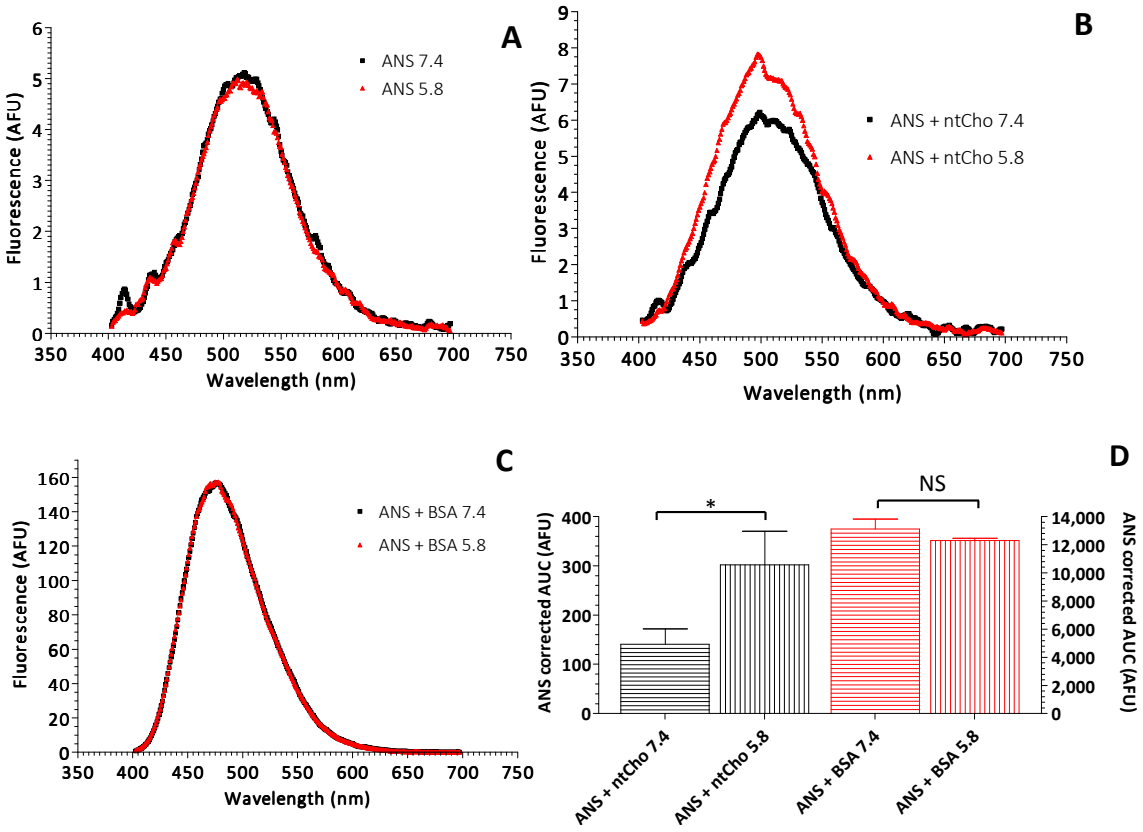

Figure 6-17 – Hydrophobic residues are exposed on the surface of cholix when the protein is exposed to acidic pH. Fluorescence spectra of (A) ANS, (B) ANS + ntCho and (C) ANS + BSA at pH 5.8 (red) and 7.4 (black) for [ANS] = 100 µM and [ntCho] = [BSA] = 1.52 µM. (D) Areas under the fluorescence curves of ntCho and BSA at both pH values. Black bars legend on left y axis, red bars legend on right y axis. Bars show mean ± SD from n = 3 independent samples where * P < 0.05 and NS is non-significant.

Table 6-3 – Values of *ΔF* and $\lambda_{em,max}$ collected by spectrofluorometry for samples composed of ANS, ANS + ntCho or ANS + BSA.

Sample	*ΔF*	$\lambda_{em,max}$ (nm)
ANS 7.4	0.976	518
ANS 5.8		517
ANS + ntCho 7.4	2.143	507
ANS + ntCho 5.8		498
ANS + BSA 7.4	0.938	476
ANS + BSA 5.8		475

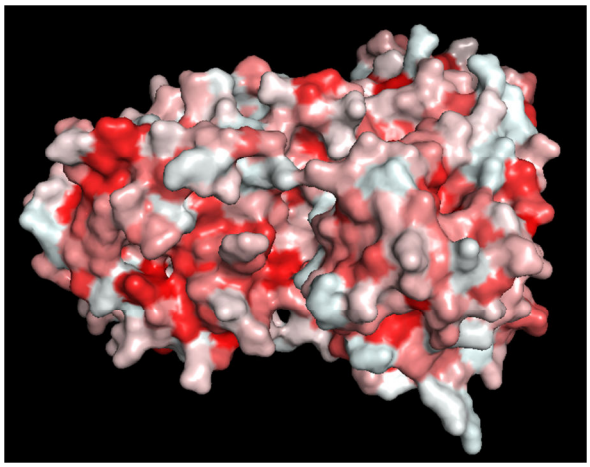

Figure 6-18 – Surface hydrophobicity of cholix at pH 7.4 (based upon crystal structure information). Red and white refer to hydrophobic and hydrophilic residues, respectively. Even at neutral pH, cholix presents a significant number of surface-exposed hydrophobic sites which could bind ANS. The figure was generated using PyMOL [128].

6.3.2.5 Truncation of cholix results in the increased exposure of trypsin cleavage sites

All six Cho GS TEV protein mutants were individually digested with trypsin at 4 °C for 30 min at pH 5.8 and 7.4. Samples were separated by SDS-PAGE and stained with Coomassie blue (Figure 6-19).

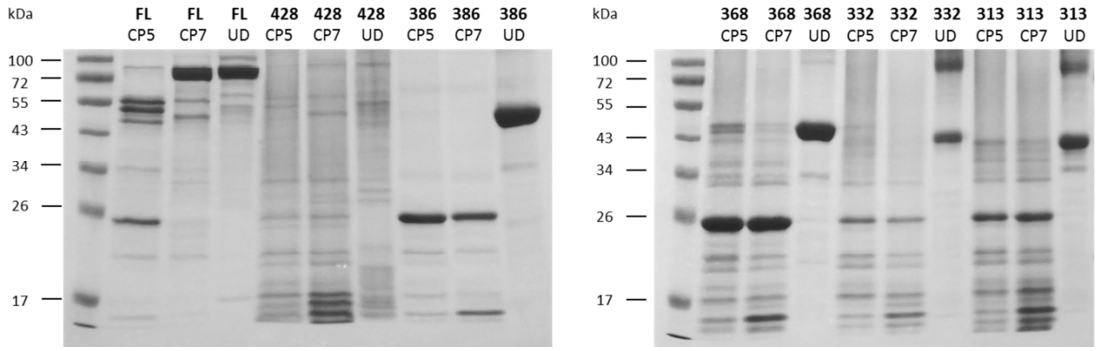

Figure 6-19 – Trypsin digestion of Cho GS TEV mutants. 10 µg of protein was incubated with 0.4 µg trypsin for 30 min at 4 °C and separated by SDS-PAGE. Undigested samples were incubated in PBS without trypsin. Top line indicates the mutant used: full-length ntCho GS TEV (FL), Cho428 GS TEV (428), Cho386 GS TEV (386), Cho368 GS TEV (368), Cho332 GS TEV (332) or Cho313 GS TEV (313). Bottom line indicates the conditions of the digestion: in citrate-phosphate at pH 5.8 or 7.4 (CP5 and CP7, respectively) or undigested protein (UD).

As previously described, the digestion pattern observed for the full-length (FL) non-toxic cholix was significantly different depending on the pH. Cleavage at neutral pH produced only very faint bands at ~57 and 47 kDa, and most of the protein remained undigested. These bands are similar to those obtained following trypsin digestion of native PE at Arg490 [225]. Sequence alignment between the two proteins suggests that Arg519 would be the equivalent amino acid in cholix. Cleavage at this position would create two fragments of 57.9 and 12.8 kDa, respectively [181, 183], which would be consistent with the observations reported above, and with the absence of the lowest band on the gel. Cleavage at pH 5.8 was much more pronounced, producing four bands of ~57, 53, 47 and 25 kDa. Virtually no undigested protein remained after incubation with the enzyme for 30 min at 4 °C. N-terminal sequencing of the different bands did not prove successful, but assuming that digestion of PE and cholix occurred in similar ways, it could be conjectured that cholix was cut at several distinct positions, and that the 25 kDa fragment observed here corresponded to the N-terminal end of the protein following one of these cleavages. Trypsin digestion of PE was proposed to occur after Arg186 or Arg213 (Cleavage 1, C1) and Arg279 (Cleavage 2, C2, main cutting site) (Section 3.3.4). Sequence alignment with cholix revealed that corresponding sites could be identified at positions Arg197 and Arg292. The latter would match cholix's furin-cleavage site but would generate two fragments of 32.9 and 37.9 kDa respectively, which would not coincide with the detected gel bands. Therefore, unlike PE, it would seem improbable that the main trypsin cleavage occurred at this position. Based on the approximate molecular weight of the fragments

detected, four cleavage sites are proposed here; Lys128, Arg138 or Lys145 and Arg197 (see Table 6-4 and Figure 6-20). While the latter would give the two 47 and 25 kDa observed on the gel, the three other cleavage sites would only produce one ~55 kDa visible band each, the other being too small and running off the gel.

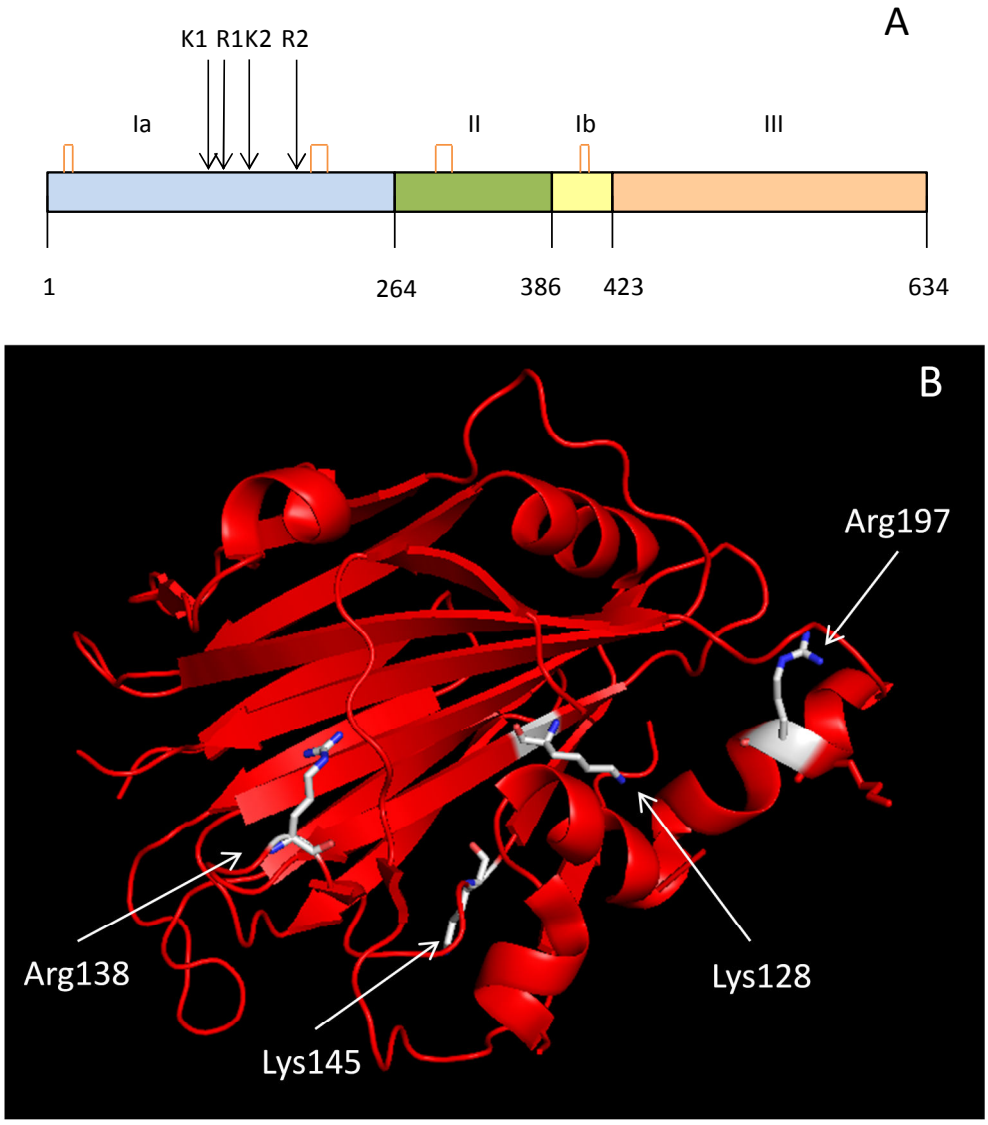

Figure 6-20 – Positions of the potential trypsin cleavage sites corresponding to the 25 and 47 kDa fragments that were detected in Figure 6-19. (A) Schematic representation of full-length cholix and (B) Ribbon representation of Cho domain I. Arg138 (R1) and Lys145 (K2) are both located on loops, while Lys128 (K1) is in the middle of a β-strand and Arg197 (R2) is located within a α-helix. Disulphide bonds are indicated orange in (A). Figure (B) was generated using PyMOL [128].

Table 6-4 – Potential trypsin cleavage sites corresponding to the 25 and 47 kDa fragments detected in Figure 6-19. ExPASy Peptide Cutter and ExPASy ProtParam were used to generate the fragments and calculate their molecular weight, respectively [181, 183]. Only 100% probability cleavage sites are displayed.

Position of cleavage site	MW (fragment 1) (kDa)	MW (fragment 2) (kDa)
Arg77	8.6	62.2
Lys128	14.3	56.4
Arg138	15.5	55.2
Lys145	16.3	54.5
Lys160	18.1	52.6
Lys186	21.0	49.7
Arg197	22.3	48.5
Lys244	27.6	43.2

Trypsin digestion of the five truncated mutants revealed that four of them (Cho386 GS TEV, Cho368 GS TEV, Cho332 GS TEV and Cho313 GS TEV) presented very similar patterns at both pHs, with cleavage being slightly more pronounced at pH 7.4. No undigested material remained in any case. The ~25 kDa band previously described for ntCho GS TEV appeared for all mutants at both pHs and represented the main fragment. This supports the idea that it corresponds to an N-terminal digestion fragment, as any C-terminal fragment would see its size vary due to protein truncation. For some reason which remains unexplained, digested fragments of Cho428 GS TEV were difficult to detect and even the undigested protein was not readily observed.

These results appear very similar to those obtained following digestion of the PE GS TEV protein series by trypsin. Again, the patterns observed suggest that additional trypsin cleavage sites were revealed in full-length ntCho upon lowering of the pH. On the contrary, the truncated proteins did not seem to need acidification of their environment to be cleaved by the protease, and the similarity between the patterns obtained at both pHs suggests that exposure of the cleavage sites were comparable in either conditions. This could imply that, as was previously proposed for PE, domain III (residues 423-634) could either conceal trypsin cleavage sites at neutral pH, or impose constraints on the protein structure that would prevent the enzyme from accessing these sites. The second possibility would seem more likely as, according to earlier observations, the conformational change experienced by cholix at mildly acidic pH remains local and therefore would be unlikely to trigger a change in position of the whole third domain to

reveal the hidden cleavage sites. Although the difference here is much more subtle than what was observed for ntPE, digestion was not completely identical at pH 7.4 and 5.8. This implies that the truncated mutants might still undergo a change in conformation when the pH is lowered, although not as extensive as that which occurs on the FL protein. It is therefore possible that the trigger for this conformational switch is located between amino acids 1 and 313.

Reversibility of the conformational change in the truncated mutants was tested as previously described for the full-length protein. As Cho428 GS TEV did not seem to provide any useful results after several attempts, it was not used here. Samples were incubated at pH 5.8 and returned to physiological pH by dialysis before being digested with trypsin and separated by SDS-PAGE (Figure 6-21). The pattern observed suggested that any conformational change(s) experienced by the truncated mutants was/were reversible, similar to that observed for the FL protein. This suggests that removal of residues 314-634 may not impede conformational change(s), nor prevent the remainder of the protein from returning to its original conformation. Therefore, it seems likely that the origin of this reversible pH-dependent conformational change is located prior to amino acid 313.

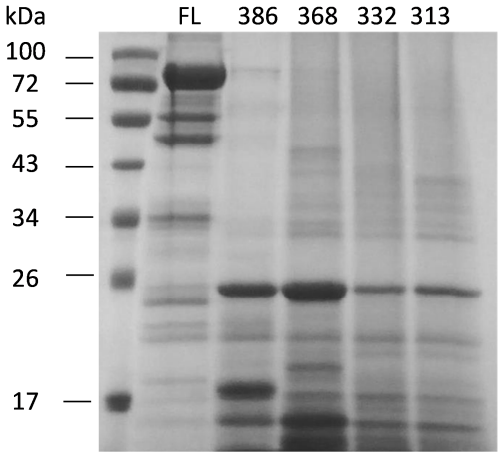

Figure 6-21 – Assessment of the reversibility of the pH-induced conformational change in Cho GS TEV mutants. Coomassie-stained SDS-PAGE of Cho GS TEV mutants incubated in citrate-phosphate buffer at pH 5.8 for 5 min and returned to pH 7.4 by dialysis. All samples were digested using 0.4 µg trypsin for 30 min at 4 °C.

6.3.3 Interaction of cholix with GM1

Studies reported above seem to suggest that cholix undergoes a conformational change whose characteristics are very similar to those described earlier for ntPE (Chapter 3).

Carter (2014) reported however that cholix does not interact with LRP1 at the surface of CHO cells, as the absence of this receptor does not prevent toxin internalisation by non-polarised cells [27]. Therefore, it is likely that in most cell lines PE and cholix use different receptors to gain entry into cells. Moreover, addition of CTB affected the transcytosis characteristics of cholix across Caco-2 cells, suggesting that GM1 influences protein transport across polarised monolayers of epithelial cells. For these reasons, a series of experiments were performed on cholix in order to investigate the nature and possible physiological implications of its interaction with GM1.

6.3.3.1 Quantitative characterisation of the interaction between cholix and GM1 using BLI

BLI was used here to investigate the characteristics of the interaction between cholix and GM1 at acidic pH. Biotin-labelled ntCho and the streptavidin-functionalised biosensor tips previously described in Section 2.13 were again used in this case. Biotinylated ntPE was run in parallel for comparative purposes. Measurements were performed in collaboration with Dr Thomas Hunter who had access to a BLI instrument; results are presented below.

Experiments were conducted at 37 °C in 0.1 M potassium-phosphate buffer at pH 5.5. GM1 concentration used here was 41.3 nM. The plate layout is presented in Figure 6-22 and details of the various step times are summarised in Table 6-5. Sensorgrams obtained for both cholix and PE (Figure 6-23) showed that the association and dissociation curves were biphasic for both proteins. The data obtained were fitted to a 2:1 heterogeneous ligand-binding model. A summary of the parameters obtained following fitting is presented in Table 6-6.

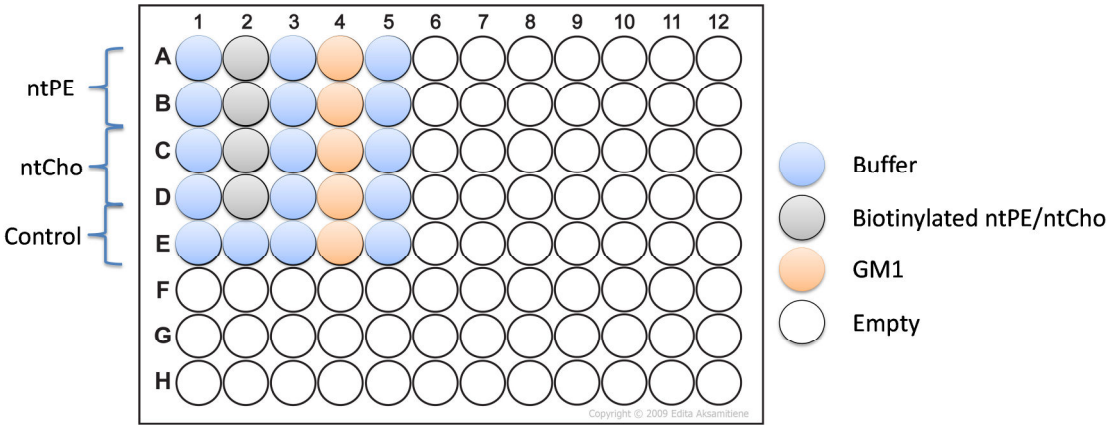

Figure 6-22 – Plate layout diagram for the kinetics assay.

Table 6-5 – Summary of kinetics assay procedure.

Step #	Step name	Time (sec)	Sample plate column
1	Equilibration	60	1
2	Loading	120	2
3	Baseline	15	3
4	Association	70	4
5	Dissociation	120	5

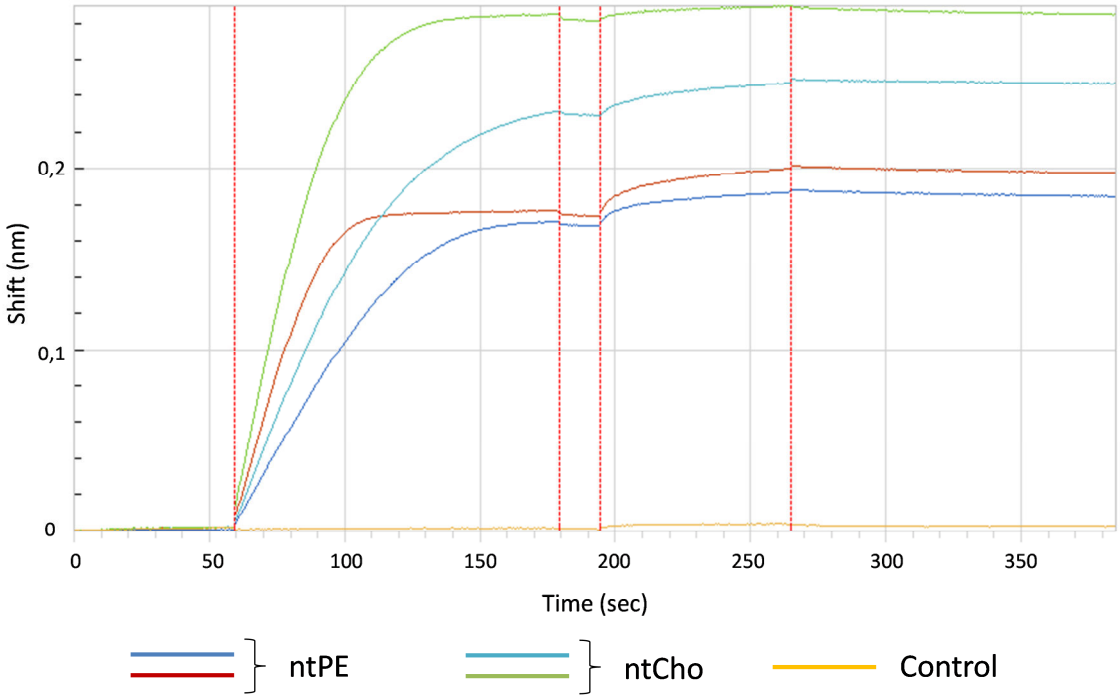

Figure 6-23 – Kinetic characterisation of the interaction between ntPE or ntCho and GM1 at pH 5.5. Sensorgrams obtained following interaction of GM1 and immobilised biotin-labelled ntPE or ntCho at pH 5.5.

Table 6-6 – Summary of the parameters obtained by fitting experimental data to a heterogeneous ligand binding model. Parameters represent the average of two individual lanes.

Sample	K_{D1} (M)	K_{D2} (M)	k_{a1} (1/M.s)	k_{a2} (1/M.s)	k_{d1} (s^{-1})	k_{d2} (s^{-1})	r^2
ntPE	$< 1 \times 10^{-12}$	1.96×10^{-10}	1.34×10^{6}	1.24×10^{7}	$< 1 \times 10^{-7}$	2.35×10^{-3}	0.987
ntCho	1.63×10^{-9}	7.17×10^{-10}	2.08×10^{6}	8.90×10^{6}	4.18×10^{-3}	4.18×10^{-3}	0.993

The r^2 values obtained confirmed that the 2:1 heterogeneous ligand model applied was the most fitting representation of the interactions involved between GM1 and each protein (r^2 = 0.987 and 0.993 for ntPE and ntCho, respectively). Results acquired for ntPE are of the same order of magnitude than those presented in Section 4.3.1.2. The differing step times for the association and dissociation phases might account for the minor variations in the calculated parameters.

Sensorgrams obtained for ntCho presented differences in the loading steps i.e. when the biotinylated protein was loaded on the surface of the streptavidin-functionalised tip. This might suggest that under the conditions of the assay the protein was in a conformation that slightly altered its interaction with the sensor tip, or that ntCho might not have been as efficiently labelled with the biotin compared to ntPE.

As previously described for ntPE, two distinct K_D values were calculated for ntCho at pH 5.5. This discrepancy again likely reflects a possible dynamic behaviour of the protein in acidic conditions and its presence under different conformations on the tip surface. However, K_{D1} and K_{D2} values remained close and the two k_d were of the same order of magnitude, suggesting that even if the protein was constantly shifting from one conformation to another, the respective affinities of all these conformations for GM1 was comparable.

K_D values calculated for ntCho at pH 5.5 were < 10^{-8} M, indicating that the interaction between the protein and the ganglioside was strong in acidic conditions. For a comprehensive understanding of the interactions taking place here, these studies would need to be repeated in optimised conditions.

6.3.3.2 Investigation of the GM1 binding site by spectrofluorometry

Spectrofluorometry was used here to investigate the location of the binding site between cholix and GM1. As the conformational change(s) undergone by ntCho resulted in the exposure of additional hydrophobic residues, GM1 interaction with a particular region uncovered as a result of decreased pH would trigger a change in ANS fluorescence. As mentioned earlier, GM1 was replaced by lysoGM1 in order to reduce ANS binding to the hydrophobic tail of the ganglioside. To test for specificity and ensure that the remaining hydrophobic tail of the ganglioside did not interfere with ANS fluorescence measurements, N-acetylneuraminic acid (NANA, sialic acid) was used as a control. Measurements were also performed after replacing lysoGM1 with sucrose to investigate whether potential

interactions were sugar-specific. Fluorescence spectra obtained for each sample are presented in Figure 6-24 and collected values of $\lambda_{em,\,max}$ and ΔF are gathered in Table 6-7.

It was previously shown that individual addition of lysoGM1, NANA or sucrose to ANS did not modify the fluorescence characteristics of the dye, with ΔF = 0.978 ± 0.03 and $\lambda_{em,\,max}$ = 517 ± 2 nm (Figure 6-25 (A)). When ntCho was added in solution to lysoGM1, NANA or sucrose, only variations between $AUC_{5.8}$(ANS + ntCho) and $AUC_{5.8}$(ANS + ntCho + lysoGM1) were calculated as statistically significant (Figure 6-25 (B)). However, the ΔF values for these two samples were not significantly different (Figure 6-25 (C)). The $\lambda_{em,max}$ values at both pHs also remained similar, whether or not lysoGM1 was present. These observations suggest that lysoGM1 did not induce any substantial changes in ANS fluorescence, implying that the molecules of lysoGM1 introduced in solution did not modify the dye binding enough for detection by a change in fluorescence intensity. However, as was already mentioned in the case of ntPE, these results do not prove that lysoGM1 did not bind to the protein, only that its presence did not affect the hydrophobic interactions between ANS and ntCho. This could be due to the receptor binding to the protein via non-hydrophobic interactions.

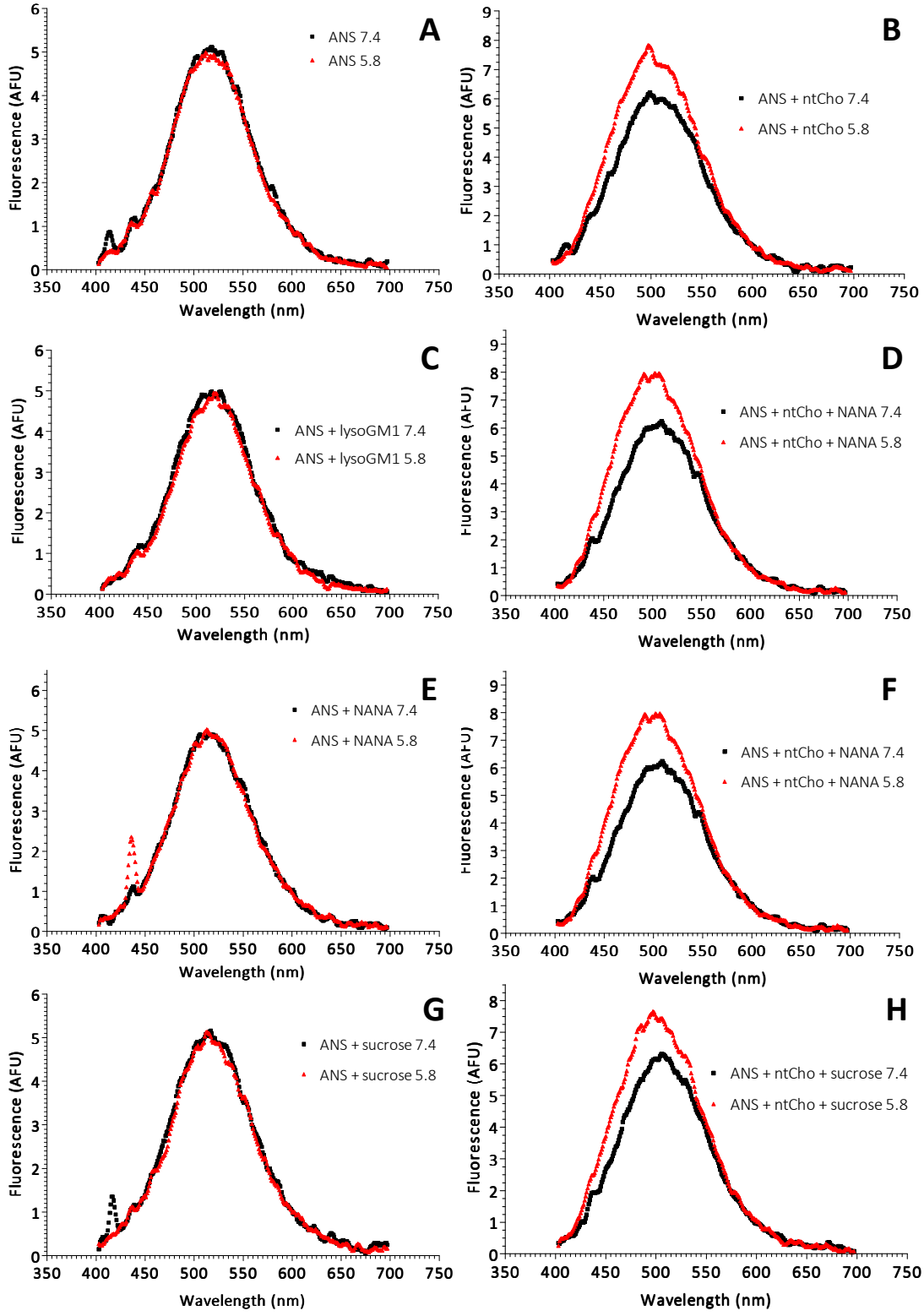

Figure 6-24 – Fluorescence spectra of (A) ANS, (B) ANS + ntCho, (C) ANS + lysoGM1, (D) ANS + ntCho + lysoGM1, (E) ANS + NANA, (F) ANS + ntCho + NANA, (G) ANS + sucrose and (H) ANS + ntCho + sucrose in CP 5.8 (red) and 7.4 (black). For all measurements, [ANS] = 100 µM, [ntCho] = 1.52 µM and [lysoGM1] = [NANA] = [sucrose] = 2 µM.

Table 6-7 – Values of ΔF and $\lambda_{em,max}$ collected by spectrofluorometry for different mixtures of ANS, ntCho and lysoGM1 or one of its substitutes.

Sample	ΔF	$\lambda_{em,max}$ (nm)
ANS 7.4	0,976	518
ANS 5.8		517
ANS + lysoGM1 7.4	0,952	520
ANS + lysoGM1 5.8		518
ANS + NANA 7.4	1,020	515
ANS + NANA 5.8		516
ANS + sucrose 7.4	0,964	516
ANS + sucrose 5.8		518
ANS + ntCho 7.4	2,143	507
ANS + ntCho 5.8		498
ANS + ntCho + lysoGM1 7.4	2,252	508
ANS + ntCho + lysoGM1 5.8		496
ANS + ntCho + NANA 7.4	1,985	504
ANS + ntCho + NANA 5.8		507
ANS + ntCho + sucrose 7.4	2,316	500
ANS + ntCho + sucrose 5.8		497

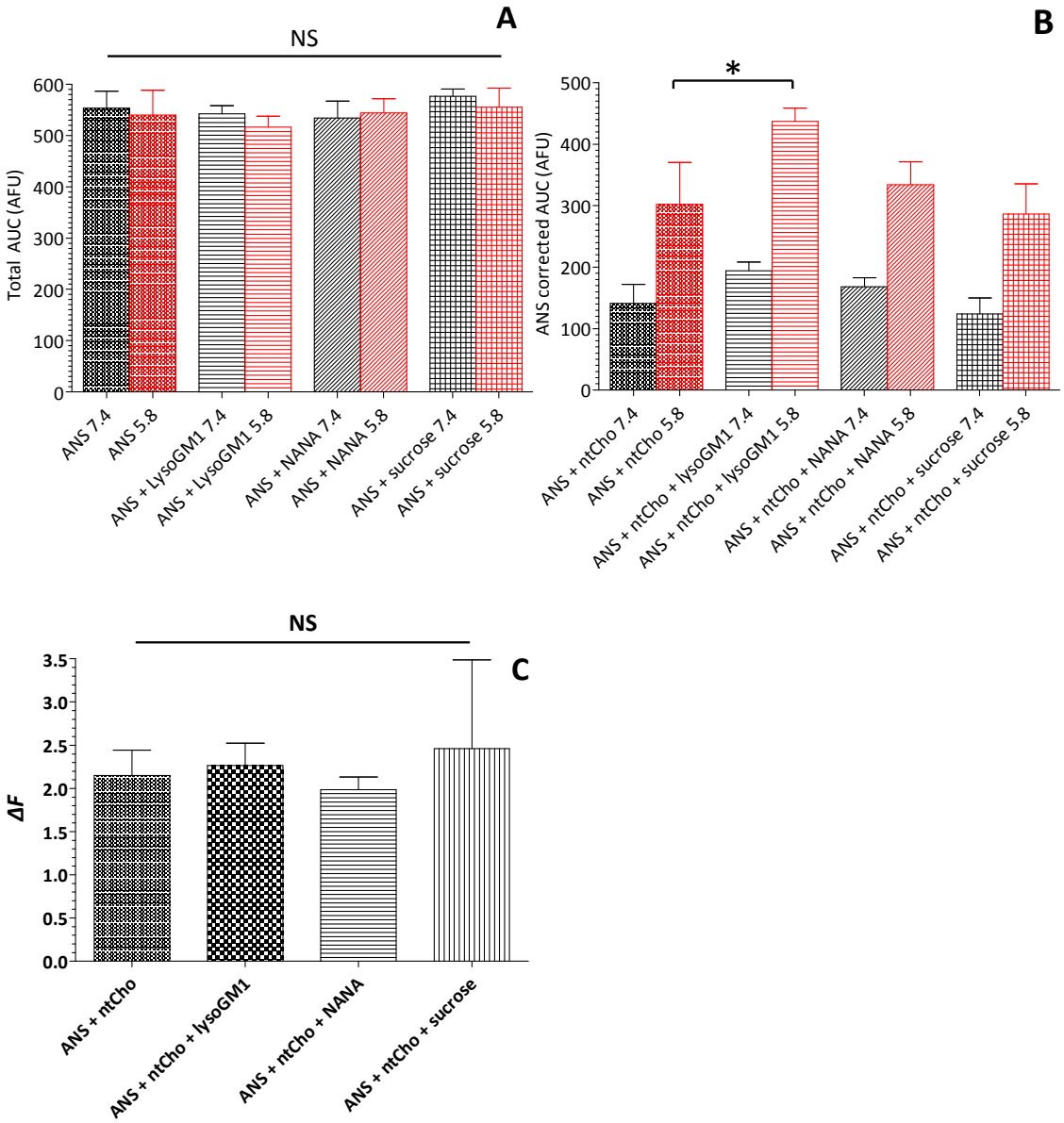

Figure 6-25 – Influence of lysoGM1, NANA and sucrose on ANS binding to cholix. Statistical analysis of the areas under the curves of (A) ANS and (B) ANS + ntCho in presence of lysoGM1, NANA and sucrose. (C) *ΔF* of cholix in presence of lysoGM1, NANA or sucrose. In (A) and (B), data at pH 7.4 and 5.8 are represented in black and red, respectively. Bars show mean ± SD for n = 3 independent samples where * P < 0.05, NS non-significant.

6.3.3.3 GM1 is involved in the uptake of cholix by non-polarised cells

BLI studies confirmed that GM1 could bind to ntCho at pH 5.5 with high affinity, which suggests that interaction(s) between the protein and the ganglioside could be important in a low pH intracellular compartment such as the endosome. Due to significant structural

similarities with PE, cholix might also bind to GM1 in more physiological conditions. This could imply a role for this ganglioside as a cell-surface receptor.

The role of GM1 in the uptake of cholix (Cho) by non-polarised (NP) cells was assessed by examining the effects of neuraminidase pre-treatment and/or the addition of CTB. This approach should also provide information about the role of the ganglioside's SA group in the interaction with the protein. NP Caco-2 cells were seeded on glass coverslips and incubated with 2.7 μM full-length, non-toxic Cho GS TEV protein modified to have a C-terminal Alexa Fluor® fluorescent tag (ntCho-A568). After 2 h, a limited amount of ntCho-A568 could be observed in NP cells, which appeared to localise at individual spots at the periphery of nuclei (Figure 6-26). When cells were pre-treated with 1 U/ml neuraminidase for 15 min before being incubated for 2 h with ntCho-A568 in presence of 1 U/ml neuraminidase, no major changes were detected. This is consistent with previous observations using ntPE, in which cellular uptake was not enhanced following a 15-minute neuraminidase pre-treatment (Chapter 4). Next, cells were pre-treated with neuraminidase for 2 h before applying the ntCho-A568/neuraminidase mixture for another 2 h. This seemed to trigger a significant increase in cell entry of the fluorescent tag, and the internalised material appeared to be more clearly localised, and in well-defined, individual areas close to the nuclei. Cells were also subjected to the same treatment plus 3.5 μM CTB; the level of cell-associated fluorescence did not seem to be affected by the addition of CTB. Finally, ntCho-A568 added to cells exposed to CTB but not neuraminidase appeared to enter at higher levels compared to those in untreated cells but slightly lower than those observed following 2 h neuraminidase treatment with or without CTB application. Co-localisation studies were not conducted for these experiments and would be required to determine accurately which intracellular compartment(s) were reached by the internalised ntCho-A568. However, observation of the fluorescence pattern could, as for PE, indicate that fluorescently-labelled ntCho might have trafficked as far as the Golgi network or possibly the ER. This would need to be confirmed by co-localising ntCho with a Golgi marker such as GM130 or TGN46.

These observations could indicate that ntCho can interact with GM1 at the cell surface in absence of neuraminidase treatment, as addition of CTB to untreated cells significantly enhanced protein entry. Moreover, possible cleavage of SA groups from cell surface components using neuraminidase seemed to have the same effect, suggesting that ntCho could interact with SA moieties; binding between ntCho and GM1 could therefore be mediated by this group on GM1. Overall, neuraminidase treatment should decrease the extent of GM1 present at the plasma membrane, even if the remaining ganglioside

molecules would be more exposed. Therefore, these results suggest that decreasing the toxin's potential to interact with GM1 (either with neuraminidase or by addition of CTB) resulted in a significant increase in ntCho uptake by NP cells. However, unlike ntPE, this interaction appears to lower the aptitude of ntCho to penetrate and traffic inside cells. It is therefore possible that interaction with GM1 could divert ntCho from a more efficient trafficking pathway. This interpretation would be consistent with data previously reported by Carter (2014) which suggested that addition of CTB enhanced ntCho transcytosis by potentially redirecting the toxin away from a secondary pathway involving GM1 in polarised cells [27].

Why cholix could interact with GM1 at the surface of untreated cells while PE did not seem able to do so remains unexplained. It could be related to a complex set of interactions involving cholix receptor, as GM1 is suggested here to only act as a secondary receptor for this protein. Finally, these observations underline that treating the cells with neuraminidase is not an absolute requirement for cholix to be internalised, as a low amount of protein was taken up even in the absence of the enzyme. As cholix is a potent toxin, penetration of even a low quantity of protein would be enough to intoxicate a cell [105]. However neuraminidase could play a role in enhancing the uptake of the virulence factor as previously discussed in Section 4.3.3.2 and by others [277-279].

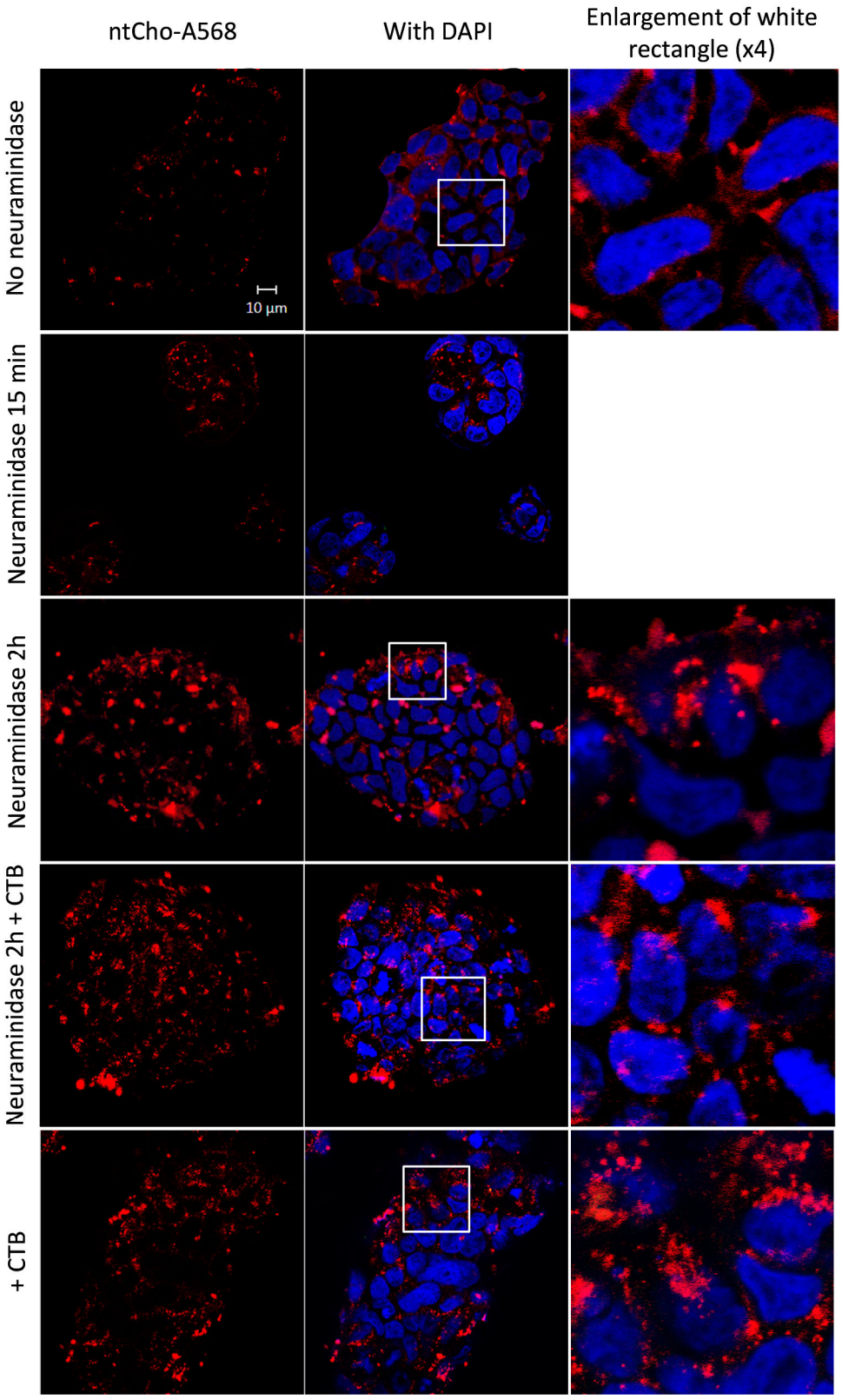

Figure 6-26 – Treatment with neuraminidase and CTB affects the entry of non-toxic cholix into NP epithelial cells. Fluorescent images of NP Caco-2 cells incubated for 2 h with 2.7 µM ntCho-A568 on its own or with 3.5 µM CTB, with or without cell treatment with 1 U/ml neuraminidase. Cell nuclei were stained with DAPI (blue). Images are representative of three independent experiments.

6.3.4 Study of cholix as a protein carrier for oral drug delivery

Due to its great structural similarities with PE, including the division of the full-length protein into three independent functional domains, cholix could potentially also be used as a delivery system to carry therapeutic proteins across the intestinal epithelium as was observed for PE. Moreover, cholix is a virulence factor secreted by an intestinal pathogen, while PE is secreted by a respiratory pathogen. Thus, cholix might prove more efficient than PE with respect to oral delivery as the system would be placed in an environment resembling more accurately that of the native toxin. In fact, Carter (2014) showed that cholix seemed to traffic more efficiently across polarised intestinal epithelial cells than PE.

Therefore, the internalisation of these proteins coupled to a fluorescent tag or fused with a GFP protein in NP epithelial cells was examined to determine the individual and combined effects on protein entry and intracellular transport of truncation and addition of a cargo protein. Transepithelial transport of full-length and truncated versions of cholix coupled to a fluorescent tag or cargo protein was also assessed *in vitro* and *in vivo*.

6.3.4.1 In vitro uptake of two truncated versions of cholix

In an attempt to get a better understanding of the behaviour of truncated versions of cholix, the ability of Cho386 GS TEV (medium-length mutant) and Cho313 GS TEV (short-length mutant) to be internalised by NP epithelial cells was assessed *in vitro*. NP Caco-2 cells cultured on glass coverslips were incubated with 20 µg fluorescently-tagged proteins diluted in 100 µl complete growth medium (concentration of ntCho-A568 = 2.8 µM, Cho386-A568 = 4.6 µM, and Cho313-A568 = 5.6 µM, respectively) for 2 h at 37 °C before being fixed and stained with DAPI. Fluorescent images obtained by confocal microscopy showed that, as observed in Section 6.3.3.3, a low amount of full-length ntCho appeared to be internalised by NP cells after 2 h. The two shorter proteins, Cho386-A568 and Cho313-A568, did not seem able to enter the cells (Figure 6-27).

These results could suggest that while FL ntCho might be able to carry a fluorescent tag inside NP cells, shortened versions of the protein were unable to be internalised. A possible explanation is that removal of amino acids 387-634 or 314-634 (Cho386-A568 and Cho313-A568, respectively) led to improper folding, resulting in the protein's inability to penetrate the cells. Alternatively, it was suggested that the GM1 binding site on PE would be located before residue 303 (between α-helices A and B). Sequence alignment revealed that this amino acid corresponds to Iso316 in cholix (Appendix 6). The two toxins

were shown to display similar pH-dependent behaviours and, assuming that the GM1 epitopes could also have comparable locations on both proteins and be revealed upon exposure to low pH, the GM1 binding site could be located between residues 1-316 on cholix. Therefore, this sequence might be more accessible on the truncated mutants than the full-length protein, even at neutral pH. As GM1 was suggested to reduce the efficiency of ntCho entry into cells (Section 6.3.3.3), an increase in binding to the ganglioside could diminish the ability of the truncated mutants (Cho386-A568 and Cho313-A568) to penetrate the cells, which could account for the lack of intracellular fluorescence.

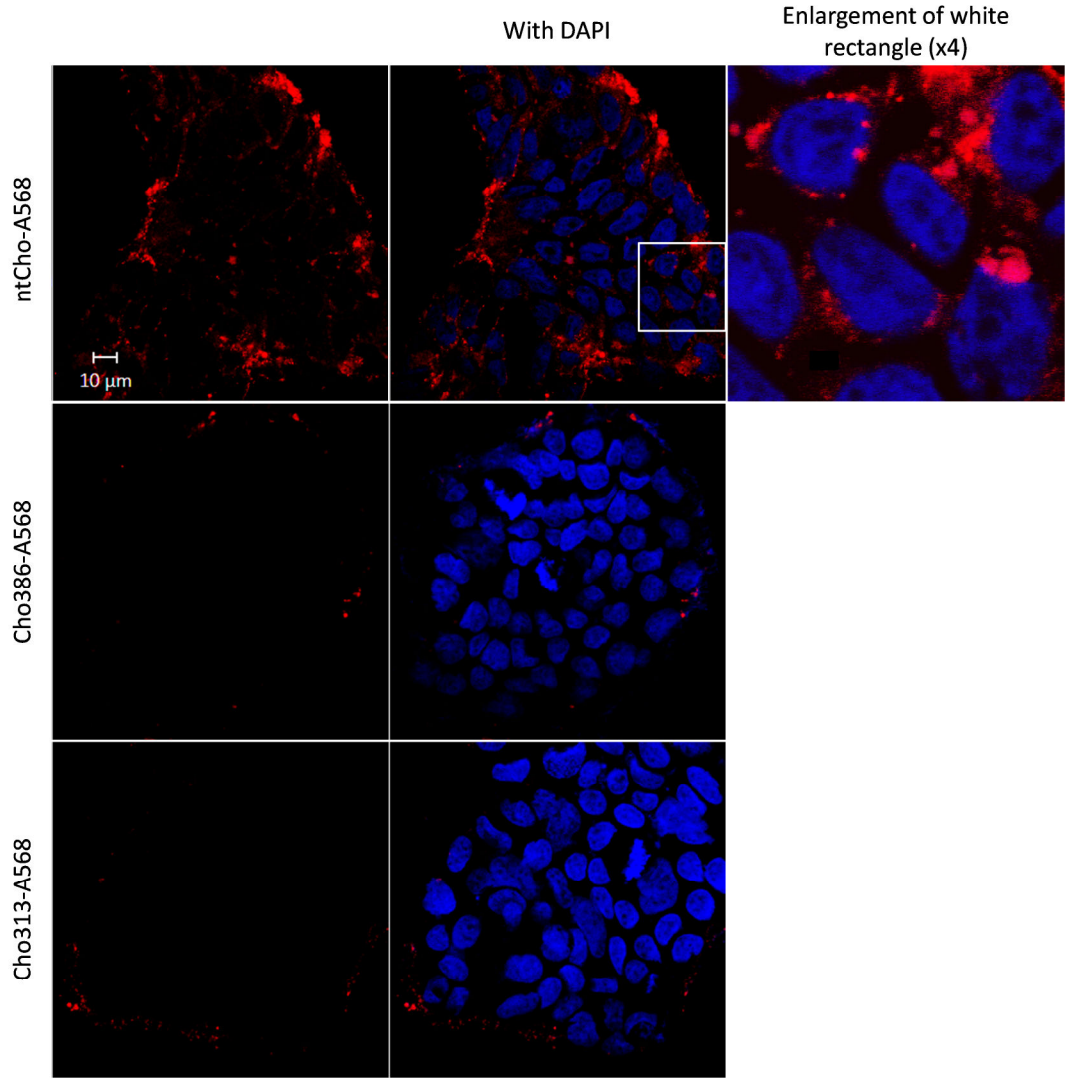

Figure 6-27 – Truncated forms of Cho have reduced rates of cell association by NP epithelial cells compared to the FL ntCho. Fluorescent images of NP Caco-2 cells incubated for 2 h with 20 µg of protein tagged with Alexa Fluor® 568 and diluted in 100 µl complete growth medium (red). Final protein concentrations were 2.8 µM ntCho-A568, 4.6 µM Cho386-A568 and 5.6 µM Cho313-A568. Cell nuclei were stained with DAPI (blue). Images are representative of three independent experiments.

6.3.4.2 In vitro uptake of Cho-GFP mutants –effects of neuraminidase

In order to determine the trafficking properties of full-length, non-toxic cholix as well as several truncated versions of this protein to transport a cargo (e.g. therapeutic protein) into NP cells, six Cho truncation mutants were expressed as fusion proteins carrying a C-terminal GFP molecule. 20 µg of each protein diluted in 100 µl complete growth medium was applied to NP Caco-2 cells and incubated at 37 °C for 2 h. Final molar concentrations for all proteins applied are given in Table 6-8. Cells were then fixed with PFA, labelled with an anti-GM130 antibody, and prepared for confocal microscopy. GM130 expression was used here to visualise the Golgi network [314].

Confocal images suggested that very little ntCho-GFP was internalised by these NP Caco-2 cells (Figure 6-28). Very little GFP fluorescence could be detected in cells incubated in the presence of any of the five shorter mutants. This is consistent with results described previously for ntCho-A568, Cho386-A568 and Cho313-A568. As neuraminidase treatment was previously shown to enhance the uptake of ntCho-A568, cells were pre-treated with 1 U/ml neuraminidase for 2 h before proteins were individually applied in presence of the same concentration of enzyme for another 2 h (Figure 6-29). Neuraminidase treatment significantly increased the uptake of ntCho-GFP (Figure 6-29, top) and also appeared to slightly enhance the penetration of Cho428-GFP.

Conversely, no major increase in intracellular fluorescence could be observed for any of the other mutants. In order to confirm that the absence of intracellular fluorescence was due to the lack of protein entry, the fluorescence intensity of 20 µg of each protein diluted in 100 µl HBSS was measured (Figure 6-30 and Table 6-8). ntCho-GFP and Cho428-GFP both presented detectable fluorescence levels. On the other hand, all Cho386-GFP, Cho368-GFP, Cho332-GFP and Cho313-GFP displayed intensities of less than 1,000 AFU. Therefore, even if any of these proteins had entered into the cells, it is highly unlikely that it would have been detected. The lack of fluorescence from five truncated versions of ntCho-GFP could be explained by improper protein folding, as the properties of GFP rely upon its tertiary structure [334]. This assumption would be in agreement with the expression outcomes for these proteins. Cholix is usually more soluble than PE when expressed in *E. coli*, and addition of GFP should have further improved the solubility of the fusion proteins. As all PE-GFP mutants were expressed as soluble proteins, it was surprising that most of the Cho-GFP proteins had to be expressed as inclusion bodies. Thus, misfolding could have accounted for both reduced protein solubility and a lack of fluorescence.

As a result, further tests were performed using only ntCho-GFP. In an attempt to determine if the relationship between the GFP-labelled ntCho and GM1 was comparable to that of ntCho-A568, cells were pre-treated with neuraminidase, and ntCho-GFP was subsequently added at the same time as CTB (Figure 6-31). This resulted in increased intracellular fluorescence levels in NP Caco-2 cells. When both ntCho-GFP and CTB were applied to NP cells, the fluorescence levels observed after 2 h were higher than in cells not treated with CTB, but appeared to be lower than in neuraminidase-treated cells either in the presence or absence of CTB. Expression of GM130 was used in all samples to visualise the Golgi network and investigate the destination of internalised ntCho-GFP. However, observation of confocal images revealed that co-localisation between GFP (green) and GM130 (red) was rather low, suggesting that very little protein localised in the Golgi network after 2 h.

These observations indicate that cell incubation with neuraminidase as well as application of CTB resulted in enhanced uptake of ntCho-GFP. They also suggest that either cleavage of SA groups from surface proteins and lipids, or targeted GM1 blocking, led to increased protein internalisation, consistent with the hypothesis that these elements hinder the entry process of ntCho-GFP. This would be in agreement with results previously described for ntCho-A568, which seemed to show that GM1 could interact with cholix via its SA moiety and that binding to the ganglioside would interfere with efficient protein internalisation and trafficking. These data would therefore indicate that addition of the C-terminal cargo protein GFP does not block the mechanism of ntCho entry. Co-localisation studies between ntCho-GFP and GM130, a protein situated exclusively in the Golgi matrix, revealed that ntCho-GFP did not traffic to this compartment following internalisation. The fluorescence patterns observed here are very similar to those detected for the various PE-GFP mutants, which were suggested to be retained within endocytic vesicles following cell penetration. It is therefore conceivable that ntCho-GFP experiences a similar fate upon cell uptake.

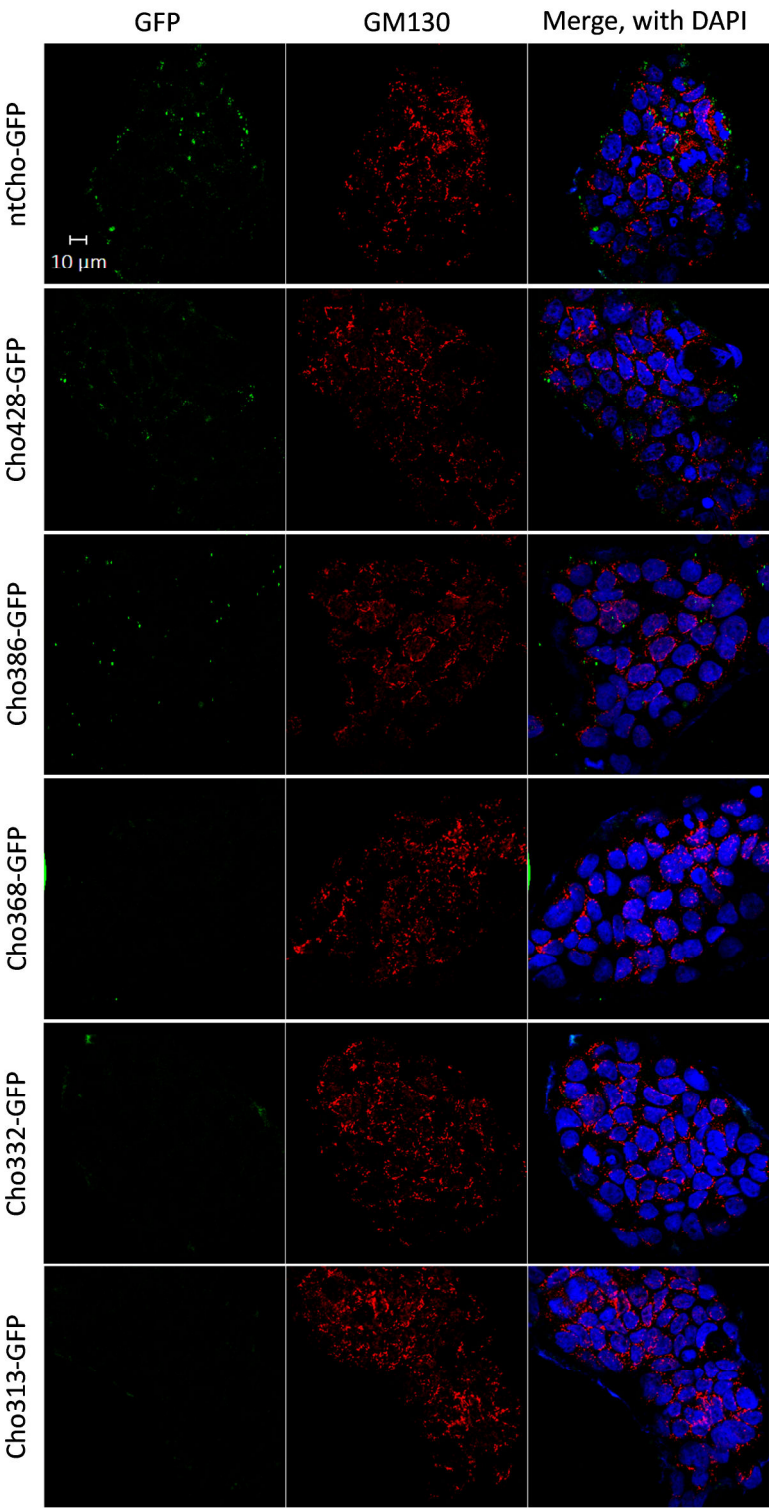

Figure 6-28 – Cho-GFP mutant proteins are not internalised by NP epithelial cells. Fluorescent images of NP Caco-2 cells incubated for 2 h with 20 µg of protein diluted in 100 µl complete growth medium. Molar concentrations are detailed in Table 6-8. Cell nuclei were stained with DAPI (blue) and expression of GM130 (red) was used to visualise the Golgi network. Images are representative of three independent experiments.

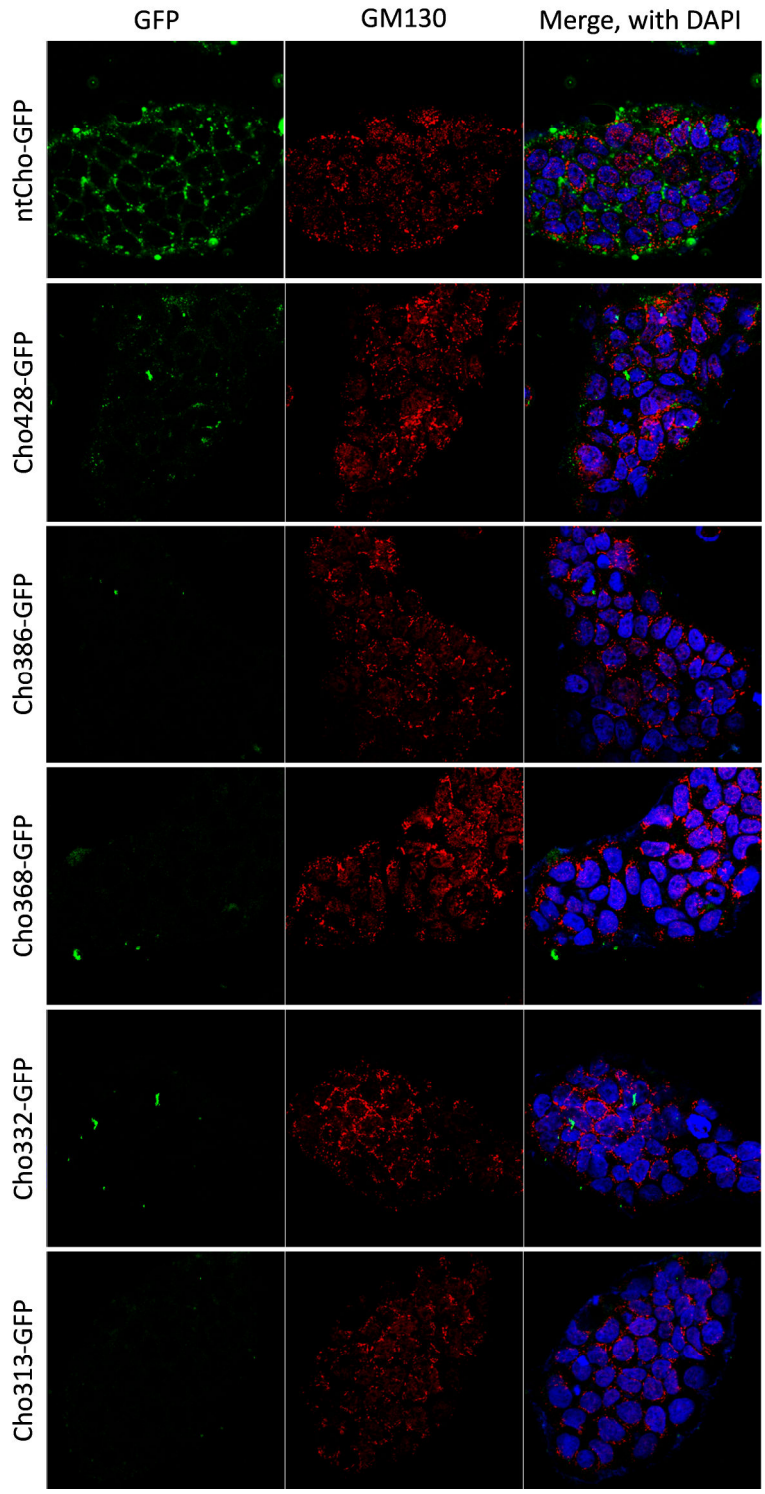

Figure 6-29 – Treating cells with neuraminidase does not increase the uptake of all Cho-GFP mutants by NP epithelial cells. Fluorescent images of NP Caco-2 cells pre-incubated for 2 h with 1 U/ml neuraminidase followed by another 2 h-incubation with 20 µg of protein diluted in 100 µl complete growth medium in presence of 1 U/ml neuraminidase. Molar concentrations are detailed in Table 6-8. Cell nuclei were stained with DAPI (blue) and expression of GM130 (red) was used to visualise the Golgi network. Images are representative of three independent experiments.

Table 6-8 – Molar equivalent of 20 µg protein for the Cho-GFP mutant series and concentrations used in uptake assays in NP Caco-2 cells.

Protein designation	Molar equivalent of 20 µg protein (nmol)	Protein concentration in 100 µl medium (µM)
ntCho-GFP	0.20	2.0
Cho428-GFP	0.27	2.7
Cho386-GFP	0.28	2.8
Cho368-GFP	0.29	2.9
Cho332-GFP	0.31	3.1
Cho313-GFP	0.32	3.2

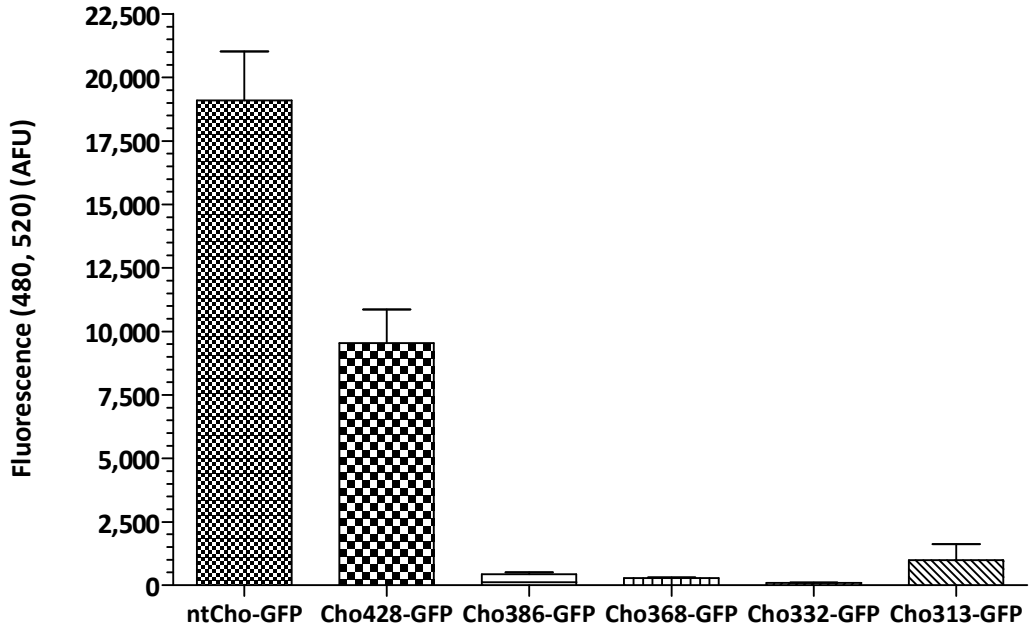

Figure 6-30 – Fluorescence of Cho-GFP mutant proteins. Fluorescence intensity of 20 µg of fusion protein in HBSS (λ_{ex} = 480 nm, λ_{em} = 520 nm). Corresponding molar concentrations are presented in Table 6-8. Data are presented as mean ± SD for each sample, for n = 3 microplate wells.

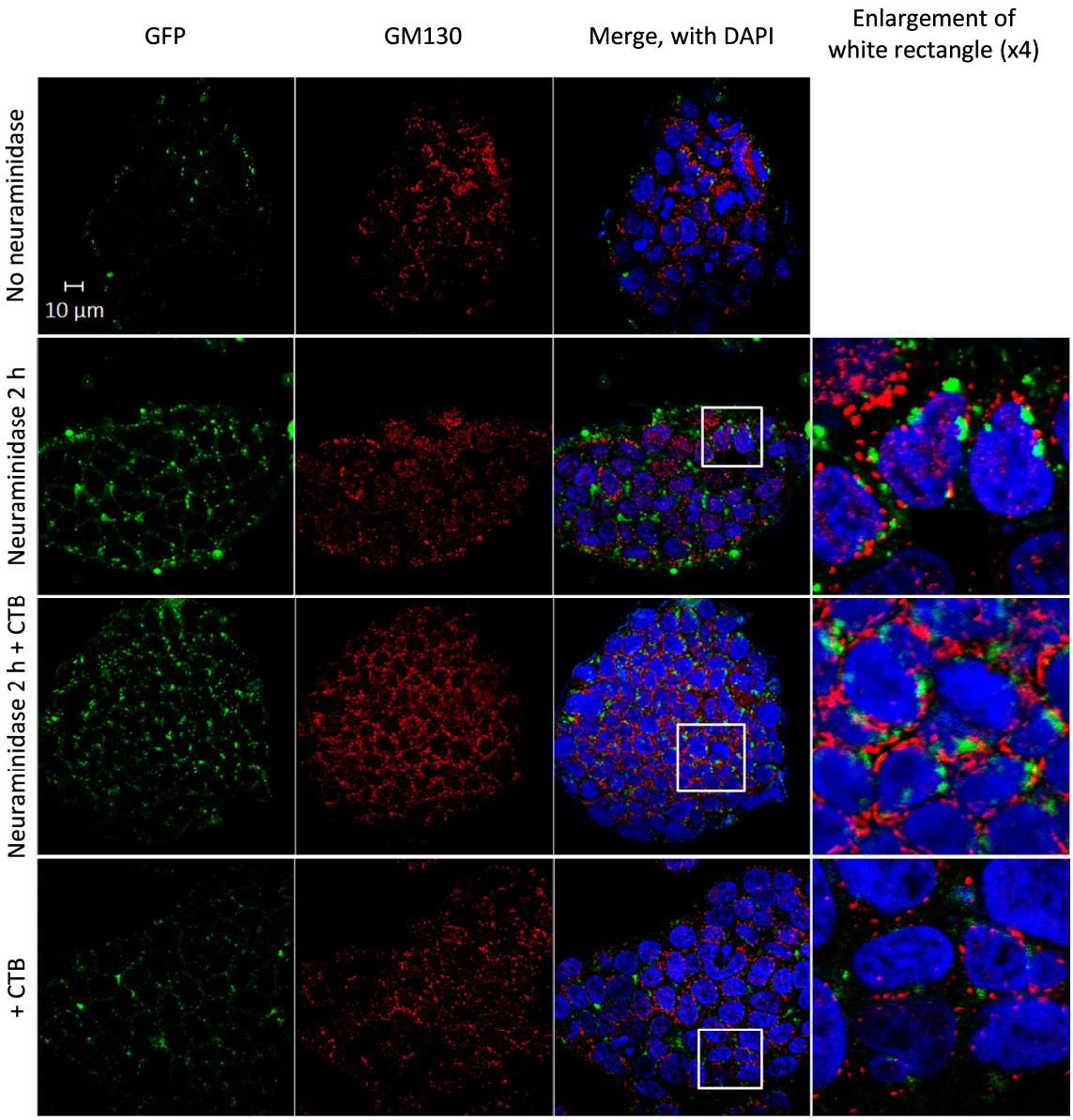

Figure 6-31 – Treatment with neuraminidase and CTB affects the entry of ntCho-GFP in NP epithelial cells. Fluorescent images of NP Caco-2 cells incubated for 2 h with 2.0 µM ntCho-GFP alone or with 3.5 µM CTB, with or without cell treatment with 1 U/ml neuraminidase. Cell nuclei were stained with DAPI (blue) and expression of GM130 (red) was used to visualise the Golgi network. Images are representative of three independent experiments.

6.3.4.3 In vitro transport of cholix in polarised cells and comparison with PE

To investigate the ability of ntCho to transport across epithelial cells, the FL protein was labelled with a fluorescent Alexa Fluor® tag (A568) and 0.09 µM, 0.47 µM and 0.93 µM of ntCho-A568 (= 2, 10 and 20 µg diluted in 300 µl HBSS, respectively) were applied to the apical surface of polarised cells as described in Sections 2.16 and 5.3.5. Samples were

taken from the basolateral well at t = 15, 30, 60, 120 and 240 min and assayed for fluorescence content.

Linearity of the fluorescence intensity with increasing amounts of protein was verified for the concentration range of 0.001-0.1 mg/ml (Section 5.3.5, Figure 5-15). Results showed that the total fluorescence intensity in samples collected from the basolateral side increased linearly over time for the three curves, indicating that surface receptors were not saturated and that the maximum transport rate had not been reached (Figure 6-32 (A)). Measurements of 4 kDa dextran permeability after incubation indicated that between 7.6 and 13.3% dextran crossed the monolayer compared to the blank well (Figure 6-32 (B)). When associated to the TEER values taken at the start of the assay (TEER > 350 $\Omega \cdot cm^2$), these results demonstrate that the integrity of the monolayer was maintained throughout the experiment.

These data establish that ntCho is able to carry a fluorescent tag across polarised cells without damaging the epithelium, as illustrated by conservation of the monolayer integrity throughout the assay. Moreover, ntCho has a molecular weight (72 kDa) comparable to that of PE (66 kDa) and therefore paracellular transport is also unlikely to account for the transport of either protein across Caco-2 cells. Although the receptor for cholix remains unknown, data obtained here suggest that it seems to be present on the cell surface of polarised Caco-2 cells. As a conclusion, this assay validates the potential of ntCho to transport and carry a fluorescent tag across polarised monolayers of Caco-2 cells in these experimental conditions.

Transport of ntPE and ntCho across polarised monolayers were then compared by application of 20 µg of either ntPE-A568 or ntCho-A568 (= 0.30 and 0.28 nmol, respectively) to the apical compartment. Samples were taken from the basolateral well at the same time points as previously mentioned and assessed for fluorescence content. The material remaining in the apical compartment after 240 min was also collected. This time, transport was not linear and both curves reached a plateau (Figure 6-33 (A)). This indicates that the maximum transcytosis rate had been attained and that surface receptors were saturated. Although the molar concentrations of the two proteins differed slightly, these results also showed that ntPE appeared to transport more efficiently than ntCho across polarised Caco-2 cells. In fact, the total fluorescence detected in the basolateral compartment after 240 min was approximately twice as high for ntPE than for ntCho while total fluorescence (apical + basolateral after 240 min) was approximately equal for both proteins (Figure 6-33 (B)). These results were surprising as cholix is naturally an intestinal pathogen and was expected to transport more efficiently than PE, a respiratory

toxin. Moreover, Carter (2014) previously showed that in identical conditions the total amount of ntCho in the basolateral compartment after 240 min was higher than for ntPE [27].

The nature of the system used here could account for discrepancies observed in the proteins' transport profiles (linear vs. non-linear transport curves). In fact, it is a cell-based model, and although results seem to be reproducible within the same experiment, variations in cell characteristics, for example passage number, appear to have an impact on data. Indeed, one experiment resulted in linear transport of 0.93 µM cholix and a total fluorescence of ~175,000 AFU after 240 min, while another experiment conducted with the same amount of protein led to saturation of the system and detection of total fluorescence ~30,000 AFU.

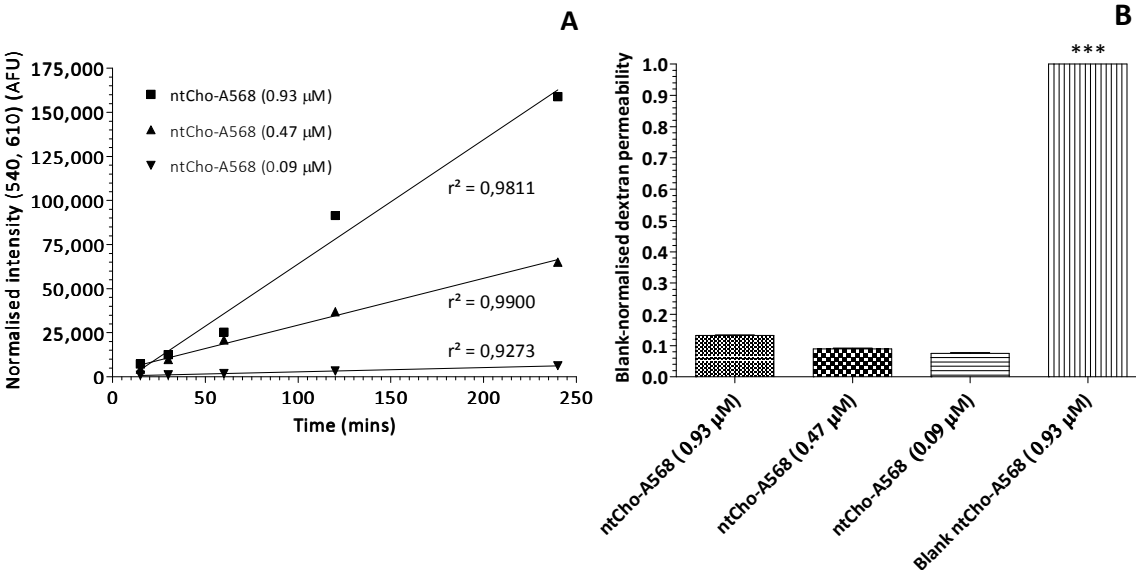

Figure 6-32 – Transport of ntCho-A568 across polarised epithelial cells. (A) Normalised total fluorescence of 0.93 µM, 0.47 µM and 0.09 µM of ntCho-A68 present in the basolateral compartment over 240 min following initial application to the apical surface of polarised Caco-2 monolayers. Data are presented as mean ± SD for each time point, totalling three individual samples. (B) Amount of FITC-labelled 4 kDa dextran present in the basolateral compartment 30 min after application to a blank Transwell® filter compared to Transwell® filters supporting a monolayer of polarised Caco-2 cells which had been incubated with various amounts of ntCho-A568 for 240 min. Data are presented as mean ± SD for each sample, for n = 3 samples where *** P < 0.001.

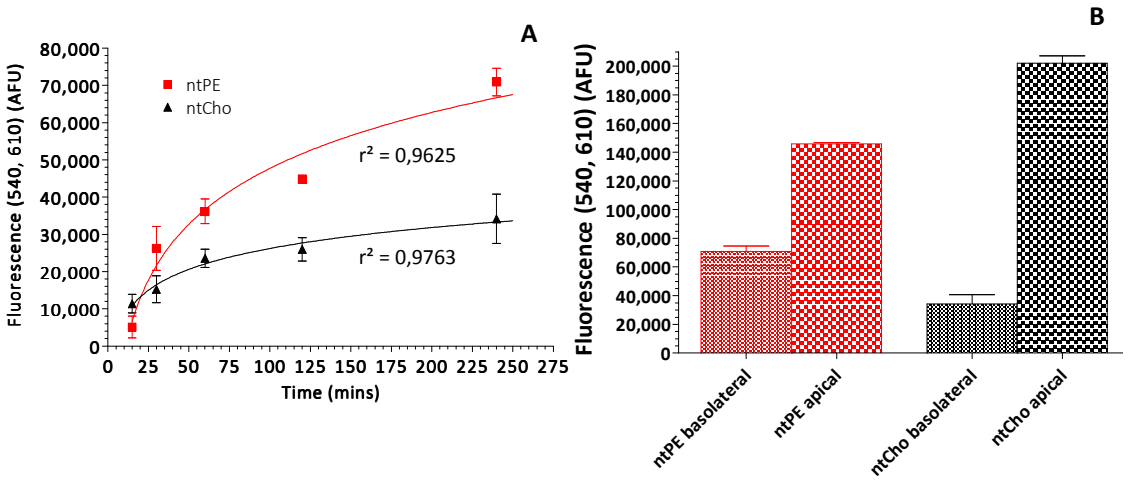

Figure 6-33 – Transport of ntPE-A568 and ntCho-A568 across polarised cells. (A) Normalised total fluorescence of 20 µg ntPE-A568 (= 0.30 nmol) (red) and ntCho-A568 (= 0.28 nmol) (black) present in the basolateral compartment over 240 min following initial application to the apical surface of Caco-2 monolayers. (B) Amounts of ntPE-A568 (red) and ntCho-A568 (black) collected from the apical and basolateral compartments after 240 min, following the application of 20 µg protein to the apical or basolateral surface of Caco-2 monolayers. Data are presented as mean ± SD for each time point (n = 3 wells).

6.3.4.4 In vivo transport of ntCho-A546 and Cho386-A546

Results described in this chapter showed that full-length non-toxic cholix (ntCho) labelled with a fluorescent tag can transport a fluorescent tag across a monolayer of polarised Caco-2 cells *in vitro*. To determine if this could be achieved *in vivo*, the uptake and trafficking of full-length and truncated versions of cholix attached to a fluorescent tag (ntCho-A546 and Cho386-A546) were studied in rat small intestine.

ntCho-A546 and Cho386-A546 were diluted in PBS and injected directly in the lumen of a rat small intestine *in vivo*. Sample segments were collected 20 min after administration and tissues were processed as described in Section 2.17.2. Controls (naïve tissue) are presented in Appendix 7.

Microscopic examination of isolated intestinal tissue revealed that most of the administered ntCho-A546 did not penetrate the cells soon after intraluminal injection, with the protein apparently being trapped at the mucosal surface (Figure 6-34, top). The fluorescence pattern observed for Cho386-A546 was significantly different when it was evaluated similarly to ntCho-A546. In this case, the white light channel was used to visualise the border of the villus and epithelial cells (Figure 6-34). At the tip of the villus,

fluorescence could be detected at the apical and basolateral poles of the enterocytes whereas further down the sides, a clear fluorescent line could be visualised mostly at the basolateral cell surface and in the submucosa. This demonstrates that Cho386-A546 was rapidly internalised by enterocytes, transported across these cells and reached the cells of the underlying mucosa.

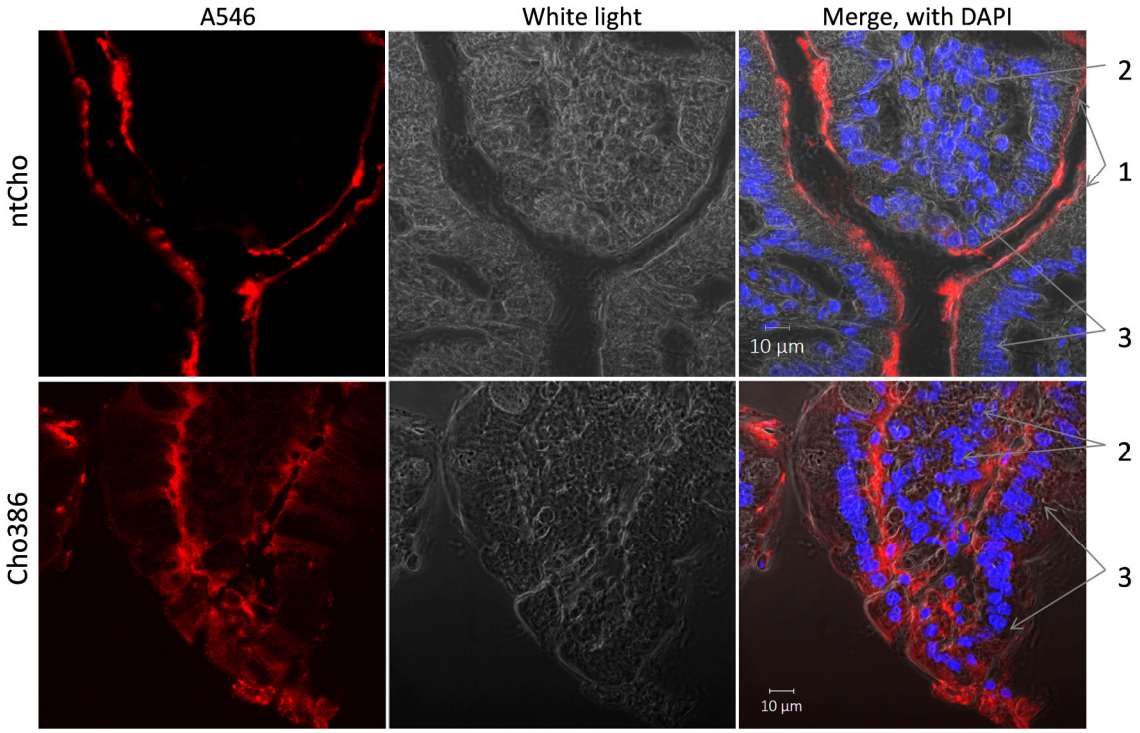

Figure 6-34 – *In vivo* transport of ntCho-A546 and Cho386-A546 across rat small intestinal cells. While ntCho-A546 appeared to be retained at the surface of the villi, Cho386-A546 was internalised and underwent transepithelial transport across enterocytes. Cell nuclei were stained with DAPI (blue). 1 = intestinal villi, 2 = cells of the space underlying the villi and 3 = absorptive enterocytes.

These results confirm that Cho386 is able to carry a fluorescent tag across a monolayer of polarised epithelial cells *in vivo*. On the contrary, full-length non-toxic cholix (ntCho) was not taken up as efficiently by enterocytes. In the small intestine, these cells are covered with a mucus coat, separated from the epithelial cells by a thin layer of glycocalyx [83, 86]. The observed fluorescence pattern would be consistent with the idea that the entry of ntCho-A546 was hindered by the presence of this glycocalyx and thereby kept away from the epithelial cell surface. Variations in cell penetration observed between full-length and truncated cholix versions could therefore be due to differences in mucus content between animals. Alternatively, these discrepancies could be explained by degradation of the carrier protein by digestive enzymes in the small intestine. In fact, these enzymes are not

uniformly distributed and it is therefore possible that ntCho-A546 was injected at an area containing large concentrations of enzymes, and subsequently degraded. Only the remaining undigested fluorescent tag would then be observed at the mucosal surface.

These findings confirmed that a truncated version of cholix lacking the cytotoxic domain and linked to a fluorescent label was able to undergo transepithelial transport. To investigate whether Cho386 could carry a cargo protein in a similar fashion, it was genetically fused with a molecule of hGH and transport of the resulting Cho386-hGH was assessed *in vivo*.

6.3.4.5 In vivo transport of Cho386-hGH

Cho386 was shown to be able to transport a fluorescent tag across polarised enterocytes to the submucosa *in vivo*. To further characterise the potential of cholix to be used as a carrier for oral delivery of protein therapeutics, Cho386 was genetically fused at its C-terminus to the N-terminal of hGH molecule (Figure 6-35). The expressed and purified chimera protein was administered to the apical surface of enterocytes by direct injection into the small intestine of a rat. The dosed intestinal segment was collected 15 min after administration and tissues were processed and immunostained as described in Section 2.17.2. Cho386 and hGH were individually detected with antibodies targeting each protein, used in conjunction with corresponding fluorescent secondary antibodies. The white light channel was used to visualise individual villi as well as the borders of epithelial cells composing them. Controls (naïve tissue) are presented in Appendix 8.

Red and green fluorescence could be detected inside enterocytes lining the villus, showing that Cho386 and hGH were both present inside these cells (Figure 6-36). Moreover, observation of yellow fluorescence areas revealed that the two antibodies co-localised within the cells. Due to the trafficking characteristics of internalised hGH (see Section 1.2.7), the detection of intracellular hGH implied that this protein remained connected to Cho386 and that the fusion protein was intact.

Although this yellow signal was mainly visualised apically, it could also be detected at the basal pole of some of the enterocytes and in some cells of the submucosal space. This suggests that the fusion protein underwent transepithelial transport from the apical to the basolateral surface before being released from epithelial cells and taken up by some of the cells present in the underlying mucosa. Only red fluorescence signals could be visualised in other cells, implying that only the carrier domain was detected in these cases.

These findings confirm the ability of Cho386 to transport a C-terminal cargo across a monolayer of polarised cells *in vivo*. The detection of co-localised Cho386 and hGH inside epithelial cells and in the submucosa suggests that a fraction of the fusion protein reached the submucosal space intact. These data establish the potential of Cho386 to act as a drug carrier for oral delivery of therapeutic proteins.

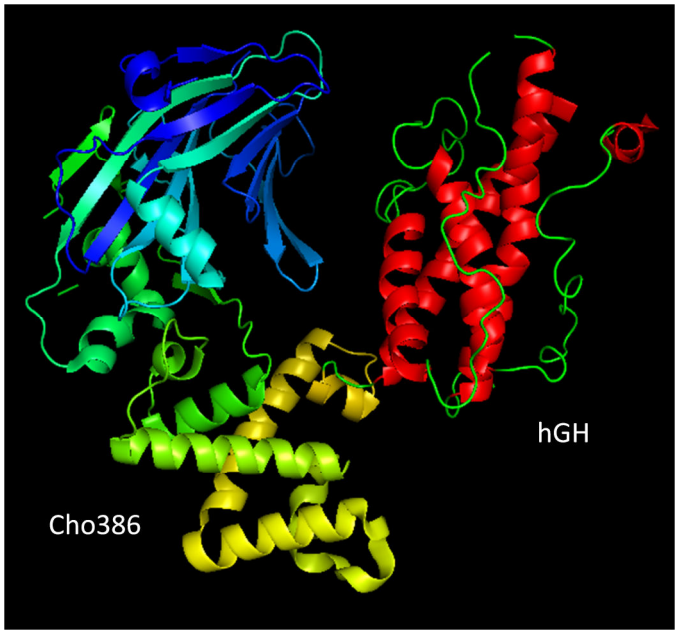

Figure 6-35 – Ribbon representations of Cho386-hGH. α-helices (red) and loops (green) of hGH are displayed in red and green, respectively. Structures were generated using PyMOL [128].

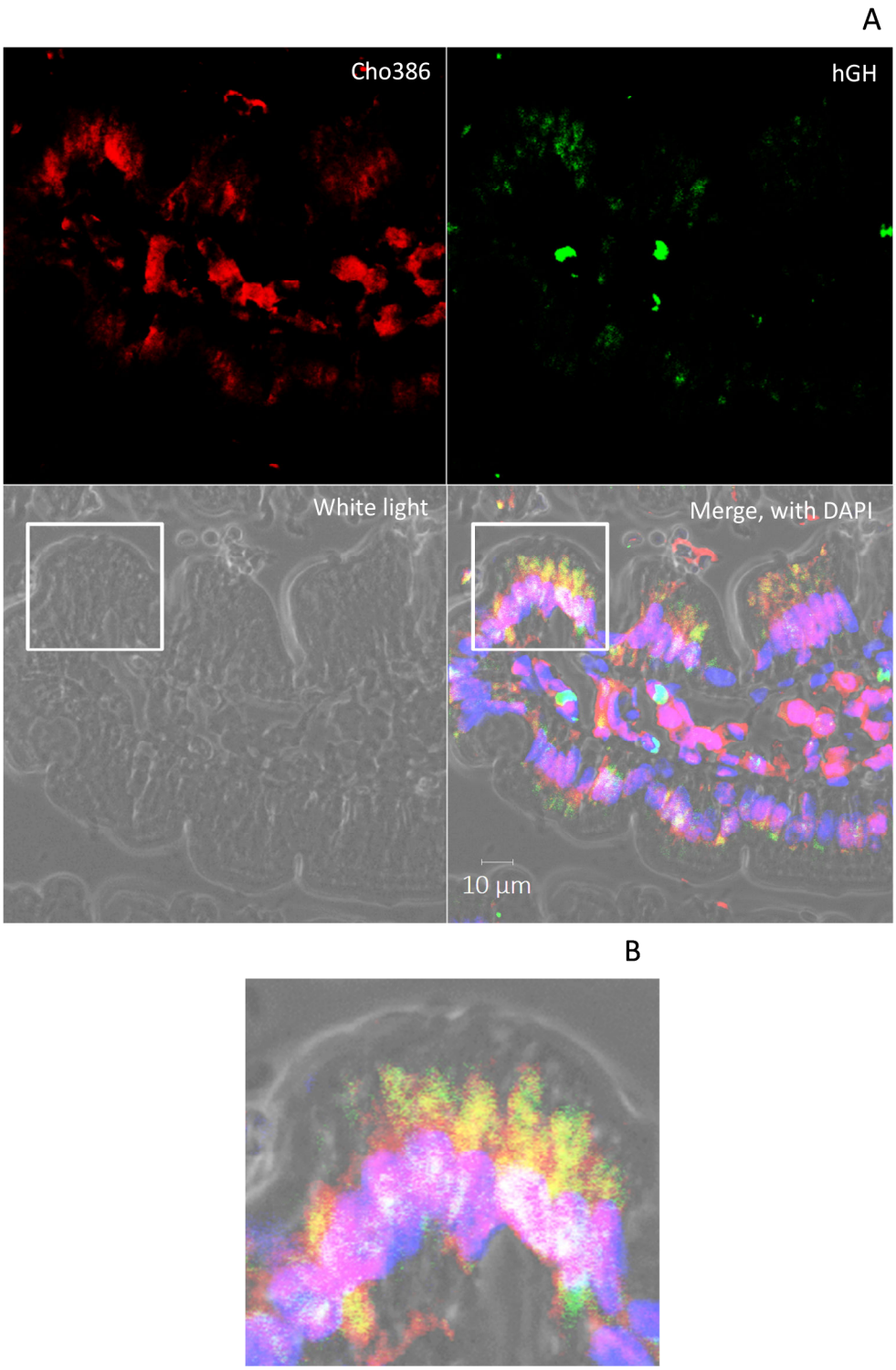

Figure 6-36 –Transport of Cho386-hGH across rat small intestinal cells. (A) A section of rat intestinal tissue (5 µm) was indirectly immunostained with antibodies to Cho386 GS TEV (red) and hGH (green). Cell nuclei were stained with DAPI (blue). (B) Higher magnification of white rectangle from merge of image (A).

6.4 General discussion

This chapter describes studies to characterise some of the aspects of the intracellular fate of ntCho in order to assess its potential to be used for the delivery of therapeutic proteins. The behaviour of the cholix toxin (tested here as full-length non-toxic and truncated forms) at acidic pH and its interaction with GM1 were discussed; potential applications as a drug delivery system were also examined. All these features were compared to the properties of a full-length non-toxic form and truncated versions of PE described in previous chapters.

Conformational change

Trypsin digestion showed that lowering the pH from 7.4 down to 5.8 triggers a conformational change in ntCho that appears to be completely reversible, but which results in the exposure of additional trypsin cleavage sites and hydrophobic residues. DLS and HPLC analysis revealed that a conformational transition could happen between pH 5.8 and 6.2, but that it does not seem to result in any dramatic changes in protein size or tertiary structure.

To date, little is known about the structure and trafficking pathway of cholix. Results obtained in this chapter suggest that the conformational change undergone by this toxin may present similarities to the one experienced by PE in mildly acidic conditions. In Chapter 3, three sets of residues were proposed to be involved in salt bridges, two of which (His249-Asp366 and His275-Glu80) were put forward as potentially crucial for the conformational change experienced by PE (Section 3.4). Alignment of PE and cholix sequences revealed that PE-His249 and PE-His262 directly align with two histidine residues in cholix (Cho-His262 and Cho-His275, respectively). However, PE-His275 does not align with a His but a Ser residue, whose side chain is much shorter and cannot become protonated upon lowering the pH. Therefore, this amino acid is highly unlikely to be involved in any conformational switch. Overlay of the crystal structures obtained at slightly alkaline conditions (pH 8) for PE and near neutrality (pH 7.5) for cholix showed that although they are very similar, they also present noticeable variations. Amongst these differences, the loop carrying the furin-cleavage site seems to be more exposed in cholix than in PE (Figure 6-37 and Figure 6-38), and the loop aligning directly with the loop carrying PE-Glu80 faces outward, making the amino acids of this segment improbable candidates for intramolecular interactions. However, the loop formed by cholix residues Thr95-Glu96-Asn97-Thr98 overlays with the loop bearing PE-Glu80, and Cho-Glu96 directly faces Cho-His262 (Figure 6-37). Moreover, the distance between these two

residues was estimated ~4 Å using PyMOL [128], suggesting that they could form a salt bridge upon protonation of the histidine at low pH [335]. Calculation of amino acid flexibilities using FlexPred [196] (Table 6-9) and ProtScale [181] (Figure 6-38) revealed that aligned residues present flexibility scores comparable to their corresponding residues in PE and that this region of cholix is on average more flexible and less buried than the rest of the protein. Therefore the residues constituting this segment could be involved in similar interactions, i.e. hydrogen bonds at neutral pH and salt bridges in acidic conditions. The two amino acids suggested here that might be involved in the formation of salt bridges at low pH (Cho-His262 and Cho-Glu96) are not located close to the furin loop. However, comparison of crystal structure information regarding this cleavage site suggests it to be more exposed in cholix than its equivalent on PE (crystal structure). Therefore, cholix may be induced to undergo a structural rearrangement that exposes its furin-cleavage site following a subtler pH-dependent prompt than that required for PE. This would be consistent with results obtained by trypsin digestion of truncated cholix mutants as, following removal of domain III, the digestion pattern varied only slightly between pH 5.8 and 7.4. This could indicate that the conformational change undergone by these truncated proteins is not as important as the one experienced by the full-length toxin, possibly due to a decrease in structural constraints caused by removal of domain III.

Altogether, these observations could indicate that due to an increased initial exposure of the furin-cleavage site at neutral pH, only a very subtle and localised conformational change is required for furin to cleave cholix. Therefore the formation of a single salt bridge rather than a combination of interactions might be enough to trigger this change in cholix.

This conformational change seems to occur at pH ~6.0, suggesting that the transition experienced by the protein could also occur soon after internalisation, in the early endocytic pathway and might be important in directing the protein toward an efficient trafficking route.

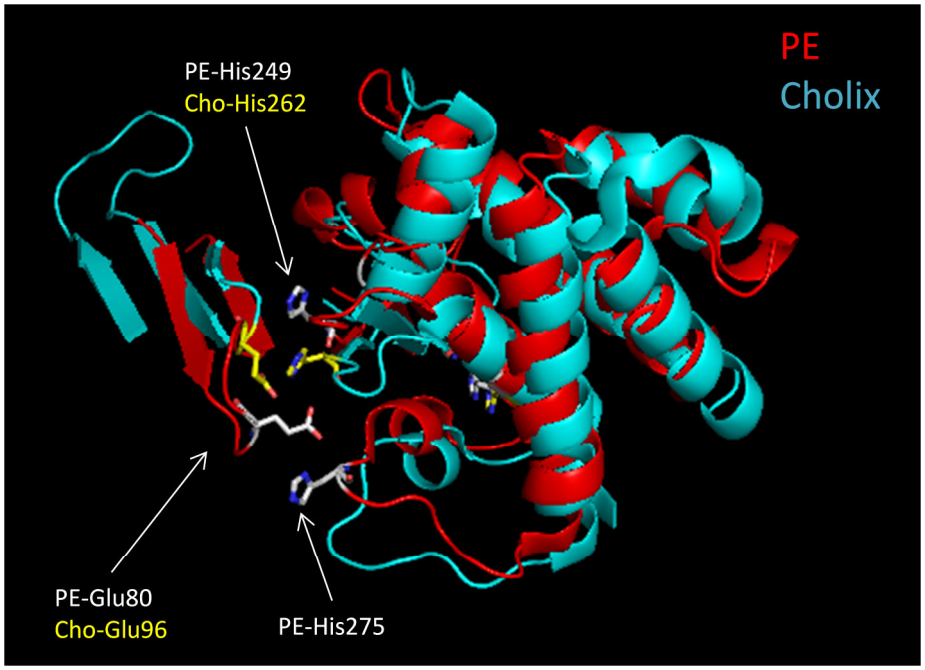

Figure 6-37 – Ribbon representation and overlay of domain II and a loop of domain I of PE (red) and cholix (blue). The residues potentially involved in salt bridges are indicated in white (PE) and yellow (cholix).The figure was generated using PyMOL [128].

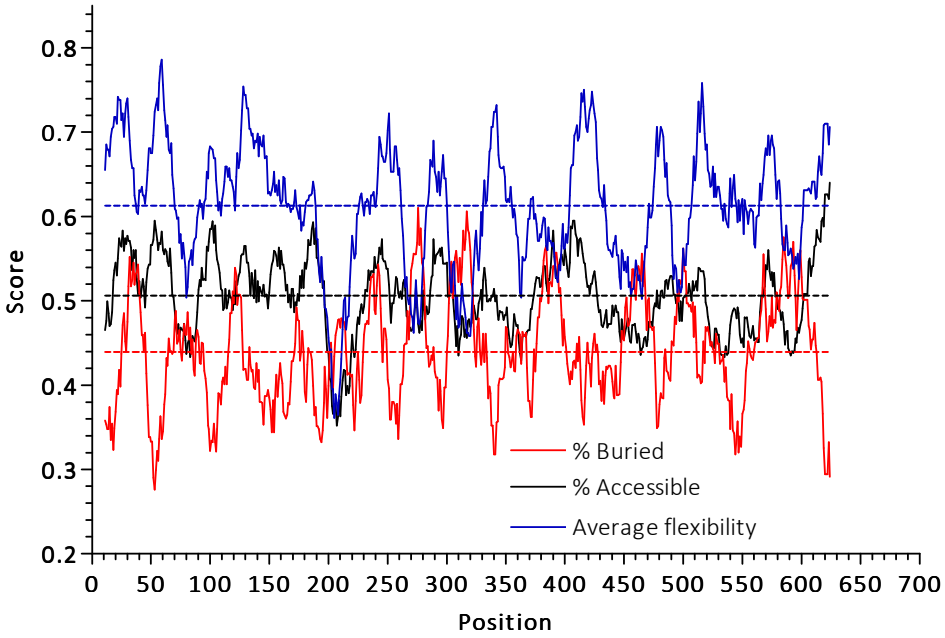

Figure 6-38 – Graphic representation of the relative degree of amino acid flexibility, accessibility and concealment from the surface. Dotted lines represent the respective average values for each curve. (Data were generated using ExPASy ProtScale [181]).

Table 6-9 – Relative individual flexibility of the residues involved in the formation of salt bridges with His. (Flexibility scores were calculated using FlexPred [196] and distances were measured using PyMOL [128]).

Protein	Acceptor residue	Flexibility score	Donor residue	Flexibility score	Distance (Å)
PE	Glu80	0.8680	His275	0.7302	3.2
	Asp366	0.4120	His249	0.4210	2.8
Cho	Glu96	0.8105	His262	0.4074	4.0

Interaction with GM1

In this chapter it was shown that cholix binds to GM1 with high affinity in mildly acidic conditions. This could indicate that interaction with the ganglioside occurs within the same compartment as, or possibly even following the conformational change. Uptake assays also suggested that exposure of the ganglioside at the plasma membrane had a direct effect on protein uptake and therefore it could also interact with cholix at a pH closer to physiological values. These studies also indicated that binding to GM1, potentially via its SA group, could interfere with the efficient trafficking of cholix. This could occur at the cell surface, where GM1 binding could possibly prevent internalisation by preventing access of cholix to its receptor. Alternatively, cholix binding to GM1 could occur following endocytosis, possibly in the early endosome where the environment becomes acidic, and result in alterations in the protein's intracellular trafficking pathway. Assuming that cholix can bind GM1 with high affinity both at neutral and low pH, these events could even combine to reroute the protein to a secondary trafficking pathway. Finally, it cannot be excluded that neuraminidase itself might modify the trafficking route exploited by the toxin by disturbing its ability to traffic with GM1. Further studies would be required in order to determine accurately which stage(s) of the trafficking process are affected by GM1 binding. For instance, GM1 could be knocked out and protein entry could be compared to control cells.

No conclusion could be drawn from the current studies regarding the location of GM1 binding site on cholix. However, if the functions of the toxin's respective domains correspond to those of PE, then it could be assumed that cholix might interact with its main receptor on the cell-surface via its domain I and with GM1 possibly via domain II. In order to verify this hypothesis, the host receptor(s) used by cholix to penetrate epithelial cells would need to be identified.

Cholix as a carrier for protein delivery

The potential of cholix as a carrier system for protein delivery into non-polarised systems and across the polarised intestinal epithelium was investigated. Unlike PE, shortening cholix appeared to significantly affect its uptake by NP epithelial cells. In fact, while full-length ntCho-A568 seemed to be internalised, neither Cho386-A568 nor Cho313-A568 were observed inside the cells. Two explanations were suggested to account for these observations. First, truncation of the protein could have led to improper folding during expression that limited receptor interactions required for uptake. This option is supported by the fact that all truncated versions of cholix were directed to inclusion bodies as an insoluble form rather than to the periplasm as a soluble protein. The refolding process from inclusion bodies may have resulted in mis- or poorly-folded forms of the truncated Cho proteins that affected their receptor-binding domain, possibly explaining why these proteins were unable to be taken up by cells. Alternatively, an increased interaction with GM1 could be responsible for the observed lack of intracellular fluorescence. In fact, it was proposed that the GM1 binding domain could be located at the beginning of cholix domain II (residues 264-313). In this case, removal of domain III and of half of domain II could have resulted in an increased exposure of the binding site and therefore enhanced the interaction between the protein and the ganglioside. Since GM1 binding was shown to decrease the amount of fluorescence detected inside NP cells (Section 6.3.3.3), this would lead to a decreased quantity of Cho truncated proteins that could be internalised compared to FL ntCho. Addition of a cargo protein at the C-terminus of full-length ntCho did not seem to affect its ability to be internalised by NP cells. In fact, blocking of GM1 had similar effects on both ntCho-A568 and ntCho-GFP. These findings are consistent with previous results observed for the PE-GFP protein series and confirm that FL cholix can be used to deliver a cargo protein in NP cells.

In order to establish the potential of ntCho as a carrier system for oral protein delivery, its ability to transport a fluorescent tag across a monolayer of polarised intestinal epithelial cells was investigated *in vitro* and *in vivo*. Although cholix was shown to transport efficiently across polarised monolayers of Caco-2 cells and data was consistent in each assay, the characteristics of transport varied greatly between *in vitro* experiments. In fact, while in one case up to 0.93 μM protein could be applied to the apical compartment without saturating surface receptors, in another the same initial concentration of material resulted in receptor saturation as demonstrated by a plateau phase in the transport data. The total quantity of protein trafficking from the apical to the basolateral compartment also varied. This demonstrates that the system used here remains an *in vitro* model and

that the biology of polarised monolayers of Caco-2 cells related to ntCho is not completely understood yet. Surprisingly, results obtained here also showed that the transport of ntPE across polarised cells appeared to be more efficient than that of cholix. This was unexpected as PE is a virulence factor originating from an airway pathogen, unlike cholix, which is secreted by an intestinal bacterium, and was therefore anticipated to transport more efficiently across the cells used here. However, these results would need to be confirmed either *in vitro* or *in vivo* using established and reliable models.

In vivo studies revealed that ntCho-A546 appeared to be retained at a distance from the mucosal surface, whereas Cho386-A546 penetrated the enterocytes and transported to the basolateral pole of the cells, and further to the submucosa. It was suggested that these discrepancies could be caused by variations in the thickness of the mucus layer or in the concentration of digestive enzymes at the site of injection. Next, the fluorescent label was replaced by hGH, a therapeutic protein currently administered by injection. The fusion protein was detected both at the apical and basolateral poles of intestinal enterocytes, as well as in some of the cells of the submucosal space. These findings therefore establish that replacement of cholix domain III by a protein drug does not affect its ability to transcytose *in vivo* and that the cargo protein can be delivered to the underlying mucosa.

As a conclusion, cholix was demonstrated to be able to carry a cargo protein inside non-polarised cells *in vitro*, and its potential to deliver a protein drug across the intestinal epithelium was confirmed *in vivo*. These results establish the potential of this toxin to be used as a carrier system for both intracellular and oral delivery of protein therapeutics.

7 GENERAL CONCLUSIONS AND FUTURE WORK

The principal aims of this research were two-fold. Firstly, the project involved the characterisation of the intracellular pathway exploited by PE in order to assess the potential of this toxin to act as a carrier for oral protein delivery. This implied the examination of possible conformational changes experienced by PE that might affect its ability to interact with potential cell receptors such as the scavenger receptor LRP1 and the ganglioside GM1; interactions that could affect its internalisation and intracellular trafficking. It also involved the evaluation of PE's ability to transport a cargo protein inside NP cells *in* vitro and across polarised enterocytes *in* vivo. Secondly, a comparison between the trafficking mechanisms of PE and another ADP-ribosylating protein, cholix toxin, was carried out. In fact, cholix structurally resembles PE and could therefore also be reprogrammed for therapeutic purposes, as was shown in this thesis.

PE conformational change

The aim of this chapter was to gain a better understanding of the intracellular trafficking pathway exploited by PE by studying the conformational change experienced by the toxin at low pH. Results described here suggest that this conformational switch involved fairly subtle structural changes (the overall shape and size of the toxin remaining unchanged) occurring in the acidic environment of the endosome. More specifically, two pairs of residues (His275-Glu80 and His249-Asp366) were proposed to be crucial in this process: exposure to low pH would result in the protonation of these His residues and would trigger the transition from one conformation to the other by formation of salt bridges.

To test this hypothesis, point mutations could be carried out on the amino acids suggested to be involved in the switch. His249 and His275 could be either individually or simultaneously mutated to residues which would i) form an H bond at physiological pH, but would not become protonated at lower pH (no formation of salt bridges) (example residues would be serine, asparagine or glutamine) or ii) form an H bond and electrostatic interaction (salt bridge) at both physiological and acidic pH (e.g. arginine or lysine). Glutamine and lysine would appear to best conserve the side-chain length compared to His. While the introduction of glutamine should not affect trypsin cleavage sites on the protein, introduction of an additional lysine might lead to an additional cleavage site and this would have to be considered in studies involving trypsin digestion at pH 5.8 and 7.4. Alternatively, new disulphide bridges could be strategically created in order to impose higher structural constraints on the protein and thereby prevent movements between domains.

Data presented in this chapter are consistent with the idea that the conformational change undergone by PE plays a major role in the protein's escape from lysosomal degradation following endocytosis. In fact, it would allow the toxin to dissociate from its cell-surface receptor LRP1, thereby permitting complete binding to a secondary receptor, which could lead it away from the degradation compartment.

PE interaction with GM1

This chapter aimed to investigate the possible interaction between PE and the host receptor for CT, monosialoganglioside GM1, in order to determine whether this ganglioside could act as a secondary receptor for PE. High-affinity binding was confirmed at acidic pH and a possible role for GM1 on the cell surface was suggested, as protein entry appeared to be significantly increased after the ganglioside was made more accessible. These studies concluded that exposure of GM1 was required for efficient protein internalisation by NP cells.

Although interaction between the protein and GM1 was confirmed, the binding site of GM1 on PE could not be identified. It was suggested that it might be located between residues 1 and 303 of PE. In order to verify this proposal, BLI studies could be conducted on truncated versions of the toxin (PE GS TEV mutants). Comparison of the binding affinity between GM1 and the various mutants would help refine the location of the binding site. Next, the potential of specific point mutations to trigger a significant decrease in binding affinity could be examined.

PE as a carrier for intracellular and oral delivery of therapeutic macromolecules

In this chapter, several versions of PE were shown to transport a cargo protein inside non-polarised cells *in vitro* and across a monolayer of polarised intestinal enterocytes *in vivo*. To confirm the potential of PE as a delivery vehicle for macromolecular drugs, the cargo protein would have to be detected in the bloodstream, quantified, and its biological activity would need to be confirmed following transport. Eventually, the poly glycine-serine linker connecting the carrier and cargo protein domains would be replaced by a cleavable linker that would allow for separation of PE from its payload following transcytosis, and would lead to the subsequent release of the therapeutic molecule in the bloodstream.

The results presented established that a protein of molecular weight comparable to that of PE domain III could be transported across polarised cells *in vivo*. The repertoire of cargo molecules that could be delivered using this system remains to be elucidated, and the impact of factors such as size and glycosylation, for instance, would need to be investigated.

Cholix

Cholix demonstrates great structural similarity with PE and its potential as a vehicle for oral drug delivery was therefore studied and compared to that of PE. Results showed that the two proteins experience a similar conformational switch and that cholix also binds to GM1 with high affinity at low pH. However, the ganglioside seems to play a different role in the entry of cholix, as increasing its exposure appeared to reduce protein entry in non-polarised cells. This indicates that despite their many similarities, the two proteins do not exploit identical intracellular trafficking routes. Cholix was also shown to carry a cargo protein inside NP cells *in vitro* and across a monolayer of polarised enterocytes *in vivo*. These results highlighted the importance of considering truncated versions of the toxin as delivery vehicles, as these should present a lower risk of inducing a host immune response upon repeated administration. The relative transport efficiencies of PE and cholix would next have to be compared *in vivo* to determine which protein would constitute the better candidate for delivery of biologics across the intestinal epithelial barrier.

Final remarks

The therapeutic benefits of bacterial toxins were first discovered with the creation of immunotoxins, which are now widely used in the treatment of various types of cancers. The studies described in this thesis reveal that the potential of these proteins to be reprogrammed for therapeutic purposes is even greater. It was demonstrated that both

cholix and PE could be used to deliver a therapeutic payload into and across cells. Numerous systems are being continually developed and enhanced in order to increase bioavailability following oral administration of a therapeutic protein by preventing degradation, increasing residence time in the intestine or facilitating contact with the mucosa. Bacterial toxins represent powerful tools that, in association with these other technologies, could lead to new, improved and more convenient ways to orally administer biologics.

8 References

1. Pavlou, A.K. and J.M. Reichert, *Recombinant protein therapeutics—success rates, market trends and values to 2010.* Nature Biotechnology, 2004. **22**(12): p. 1513-1519.
2. IMS Health. 04/05/2015]; Available from: http://www.imshealth.com/portal/site/imshealth.
3. BCC research. 04/05/2015]; Available from: http://www.bccresearch.com/pressroom/bio/global-market-protein-therapeutics-grow-$179.1-billion-2018.
4. Killewe, J. *The world's 10 best-selling prescription drugs*. 27/04/2014 04/05/2015]; Available from: http://www.theguardian.com/business/table/2014/mar/27/world-best-selling-prescription-drugs-pharmaceuticals-industry.
5. AbbVie Inc. 2013 04/05/2015]; Available from: https://www.humira.com/global/how-to-inject-humira.
6. Amgen Inc. 2015 04/05/2015]; Available from: http://www.enbrel.com/inject-ENBREL.jspx.
7. Jansen Biotech Inc. 2015 04/05/2015]; Available from: http://www.remicade.com/shared/product/remicade/prescribing-information.pdf.
8. GlaxoSmithKline Inc. 2014 04/05/2015]; Available from: http://www.gsk.ca/english/docs-pdf/product-monographs/Advair.pdf.
9. GlaxoSmithKline Inc. 2009 04/05/2015]; Available from: https://gsk.com.au/resources.ashx/prescriptionmedicinesproductschilddataproinfo/946/FileName/1D61E9ACB522688E1C1111CF331E2177/Seretide_Accuhaler_MDI_2.pdf.
10. Sanofi-Aventis. 2015 04/05/2015]; Available from: http://www.lantus.com/hcp/about-lantus/how-lantus-works.
11. Genentech Inc. 2014 04/05/2015]; Available from: http://www.rituxan.com/hem/hcp/dosing.
12. Datapharm communication Ltd. 04/05/2015]; Available from: https://www.medicines.org.uk/emc/.
13. Genentech USA Inc. 2015 04/05/2015]; Available from: http://www.herceptin.com/hcp/treatment/adjuvant/dosing.
14. AstraZeneca. 2015 04/05/2015]; Available from: https://www.crestortouchpoints.com/about-crestor/dosing-administration/.

References

15. Chung, S.W., T.A. Hil-lal, and Y. Byun, *Strategies for non-invasive delivery of biologics.* Journal of Drug Targeting, 2012(00): p. 1-21.
16. Leader, B., Q.J. Baca, and D.E. Golan, *Protein therapeutics: a summary and pharmacological classification.* Nature Reviews Drug Discovery, 2008. **7**(1): p. 21-39.
17. Grewal, I.S., *Emerging protein biotherapeutics*. 2009: CRC Press.
18. Mahato, R.I., et al., *Emerging trends in oral delivery of peptide and protein drugs.* Critical reviews in therapeutic drug carrier systems, 2003. **20**(2-3): p. 153-214.
19. Lee, V., *Peptide and protein drug delivery*. Vol. 4. 1990: CRC Press.
20. Hanas, R. and J. Ludvigsson, *Experience of pain from insulin injections and needle-phobia in young patients with IDDM.* Practical Diabetes, 1997. **14**(4): p. 95-99.
21. Irshad, S. and N. Maisey, *Considerations when choosing oral chemotherapy: identifying and responding to patient need.* European Journal of Cancer Care, 2010. **19**(s1): p. 5-11.
22. Shaji, J. and V. Patole, *Protein and peptide drug delivery: Oral approaches.* Indian journal of pharmaceutical sciences, 2008. **70**(3): p. 269.
23. Park, K., I.C. Kwon, and K. Park, *Oral protein delivery: Current status and future prospect.* Reactive and Functional Polymers, 2011. **71**(3): p. 280-287.
24. Karsdal, M., et al., *Lessons Learned From the Development of Oral Calcitonin: The First Tablet Formulation of a Protein in Phase III Clinical Trials.* The Journal of Clinical Pharmacology, 2011. **51**(4): p. 460-471.
25. Pastan, I., et al., *Immunotoxin therapy of cancer.* Nature Reviews Cancer, 2006. **6**(7): p. 559-565.
26. Mrsny, R.J., et al., *Bacterial toxins as tools for mucosal vaccination.* Drug Discov Today, 2002. **7**(4): p. 247-58.
27. Carter, E., *The Involvement of Phosphoinositide 3-kinase in Murine Lung Branching Morphogenesis and Insights into Protein Mediated Drug Delivery*. 2014, University of Bath.
28. Davenport, H.W., *Physiology of the digestive tract*. 1982: Year book medical publishers.
29. Paulsson, M., *Basement membrane proteins: structure, assembly, and cellular interactions.* Crit Rev Biochem Mol Biol, 1992. **27**(1-2): p. 93-127.
30. Kalluri, R., *Basement membranes: structure, assembly and role in tumour angiogenesis.* Nature Reviews Cancer, 2003. **3**(6): p. 422-433.
31. Timpl, R., *Macromolecular organization of basement membranes.* Current opinion in cell biology, 1996. **8**(5): p. 618-624.
32. Borradori, L. and A. Sonnenberg, *Structure and function of hemidesmosomes: more than simple adhesion complexes.* Journal of Investigative Dermatology, 1999. **112**(4): p. 411-418.
33. Bloom, W. and D.W. Fawcett, *A textbook of histology 8th ed.* WB Saunders Co., Philadelphia, 1962.
34. Wheater, P.R., H.G. Burkitt, and V.G. Daniels, *Functional histology. A text and colour atlas*. 1979: Churchill Livingstone, 23 Ravelston Terrace, Edinburgh, EH4 3TL.
35. Caplan, M.J., *Membrane polarity in epithelial cells: protein sorting and establishment of polarized domains.* American Journal of Physiology-Renal Physiology, 1997. **272**(4): p. F425-F429.
36. Delva, E., D.K. Tucker, and A.P. Kowalczyk, *The desmosome.* Cold Spring Harbor perspectives in biology, 2009. **1**(2): p. a002543.
37. Garrod, D. and M. Chidgey, *Desmosome structure, composition and function.* Biochimica et Biophysica Acta (BBA)-Biomembranes, 2008. **1778**(3): p. 572-587.
38. Shen, L., *Tight junctions on the move: molecular mechanisms for epithelial barrier regulation.* Annals of the New York Academy of Sciences, 2012. **1258**(1): p. 9-18.

39. Hartsock, A. and W.J. Nelson, *Adherens and tight junctions: structure, function and connections to the actin cytoskeleton.* Biochimica et Biophysica Acta (BBA)-Biomembranes, 2008. **1778**(3): p. 660-669.
40. Giepmans, B.N. and S.C. van IJzendoorn, *Epithelial cell–cell junctions and plasma membrane domains.* Biochimica et Biophysica Acta (BBA)-Biomembranes, 2009. **1788**(4): p. 820-831.
41. van Meer, G. and K. Simons, *The function of tight junctions in maintaining differences in lipid composition between the apical and the basolateral cell surface domains of MDCK cells.* The EMBO journal, 1986. **5**(7): p. 1455.
42. Schneeberger, E.E. and R.D. Lynch, *The tight junction: a multifunctional complex.* American Journal of Physiology-Cell Physiology, 2004. **286**(6): p. C1213-C1228.
43. Tsukita, S., M. Furuse, and M. Itoh, *Multifunctional strands in tight junctions.* Nat Rev Mol Cell Biol, 2001. **2**(4): p. 285-93.
44. Krug, S.M., et al., *Charge-selective claudin channels.* Ann N Y Acad Sci, 2012. **1257**: p. 20-8.
45. Van Itallie, C.M. and J.M. Anderson, *Claudins and epithelial paracellular transport.* Annu. Rev. Physiol., 2006. **68**: p. 403-429.
46. Peterson, L.W. and D. Artis, *Intestinal epithelial cells: regulators of barrier function and immune homeostasis.* Nature Reviews Immunology, 2014. **14**(3): p. 141-153.
47. Daugherty, A.L. and R.J. Mrsny, *Transcellular uptake mechanisms of the intestinal epithelial barrier Part one.* Pharmaceutical science & technology today, 1999. **2**(4): p. 144-151.
48. Simons, K. and E. Ikonen, *Functional rafts in cell membranes.* Nature, 1997. **387**(6633): p. 569-572.
49. Danielsen, E.M. and G.H. Hansen, *Lipid rafts in epithelial brush borders: atypical membrane microdomains with specialized functions.* Biochimica et Biophysica Acta (BBA)-Biomembranes, 2003. **1617**(1): p. 1-9.
50. Calder, P.C. and P. Yaqoob, *Lipid rafts—composition, characterization, and controversies.* The Journal of nutrition, 2007. **137**(3): p. 545-547.
51. Simons, K. and D. Toomre, *Lipid rafts and signal transduction.* Nature Reviews Molecular Cell Biology, 2000. **1**(1): p. 31-39.
52. Verdugo, P., *Goblet cells secretion and mucogenesis.* Annual review of physiology, 1990. **52**(1): p. 157-176.
53. Specian, R.D. and M.G. Oliver, *Functional biology of intestinal goblet cells.* American Journal of Physiology-Cell Physiology, 1991. **260**(2): p. C183-C193.
54. Neutra, M.R. and J.-P. Kraehenbuhl, *Transepithelial transport and mucosal defence I: the role of M cells.* Trends in cell biology, 1992. **2**(5): p. 134-138.
55. Neutra, M.R., N.J. Mantis, and J.-P. Kraehenbuhl, *Collaboration of epithelial cells with organized mucosal lymphoid tissues.* Nature immunology, 2001. **2**(11): p. 1004-1009.
56. Bevins, C.L. and N.H. Salzman, *Paneth cells, antimicrobial peptides and maintenance of intestinal homeostasis.* Nature Reviews Microbiology, 2011. **9**(5): p. 356-368.
57. Anderson, J.M. and C.M. Van Itallie, *Physiology and function of the tight junction.* Cold Spring Harb Perspect Biol, 2009. **1**(2): p. a002584.
58. Tomita, M., et al., *Enhancement of colonic drug absorption by the paracellular permeation route.* Pharmaceutical research, 1988. **5**(6): p. 341-346.
59. Rubas, W., et al., *Flux measurements across Caco-2 monolayers may predict transport in human large intestinal tissue.* Journal of pharmaceutical sciences, 1996. **85**(2): p. 165-169.
60. Van Itallie, C.M., et al., *The density of small tight junction pores varies among cell types and is increased by expression of claudin-2.* Journal of cell science, 2008. **121**(3): p. 298-305.
61. Chiba, H., et al., *Transmembrane proteins of tight junctions.* Biochim Biophys Acta, 2008. **1778**(3): p. 588-600.

62. Sugano, K., et al., *Coexistence of passive and carrier-mediated processes in drug transport.* Nature Reviews Drug Discovery, 2010. **9**(8): p. 597-614.
63. Hediger, M.A., et al., *The ABCs of solute carriers: physiological, pathological and therapeutic implications of human membrane transport proteins.* Pflügers Archiv, 2004. **447**(5): p. 465-468.
64. Doherty, G.J. and H.T. McMahon, *Mechanisms of endocytosis.* Annual review of biochemistry, 2009. **78**: p. 857-902.
65. Mayor, S. and R.E. Pagano, *Pathways of clathrin-independent endocytosis.* Nature Reviews Molecular Cell Biology, 2007. **8**(8): p. 603-612.
66. Mabbott, N.A., et al., *Microfold (M) cells: important immunosurveillance posts in the intestinal epithelium.* Mucosal immunology, 2013. **6**(4): p. 666-677.
67. Swanson, J.A. and C. Watts, *Macropinocytosis.* Trends in cell biology, 1995. **5**(11): p. 424-428.
68. McMahon, H.T. and E. Boucrot, *Molecular mechanism and physiological functions of clathrin-mediated endocytosis.* Nature reviews Molecular cell biology, 2011. **12**(8): p. 517-533.
69. Rojas, R. and G. Apodaca, *Immunoglobulin transport across polarized epithelial cells.* Nature Reviews Molecular Cell Biology, 2002. **3**(12): p. 944-956.
70. Tuma, P.L. and A.L. Hubbard, *Transcytosis: crossing cellular barriers.* Physiological reviews, 2003. **83**(3): p. 871-932.
71. Marks, B., et al., *GTPase activity of dynamin and resulting conformation change are essential for endocytosis.* Nature, 2001. **410**(6825): p. 231-235.
72. Donovan, M.D., G.L. Flynn, and G.L. Amidon, *Absorption of polyethylene glycols 600 through 2000: the molecular weight dependence of gastrointestinal and nasal absorption.* Pharmaceutical research, 1990. **7**(8): p. 863-868.
73. Camenisch, G., et al., *Estimation of permeability by passive diffusion through Caco-2 cell monolayers using the drugs' lipophilicity and molecular weight.* European journal of pharmaceutical sciences, 1998. **6**(4): p. 313-319.
74. Nishikawa, M., et al., *Electrical charge on protein regulates its absorption from the rat small intestine.* American Journal of Physiology-Gastrointestinal and Liver Physiology, 2002. **282**(4): p. G711-G719.
75. Castell, J., et al., *Intestinal absorption of undegraded proteins in men: presence of bromelain in plasma after oral intake.* American Journal of Physiology-Gastrointestinal and Liver Physiology, 1997. **273**(1): p. G139-G146.
76. Pauletti, G.M., F.W. Okumu, and R.T. Borchardt, *Effect of size and charge on the passive diffusion of peptides across Caco-2 cell monolayers via the paracellular pathway.* Pharmaceutical research, 1997. **14**(2): p. 164-168.
77. He, Y.-L., et al., *Oral absorption of D-oligopeptides in rats via the paracellular route.* Pharmaceutical research, 1996. **13**(11): p. 1673-1678.
78. Singh, R., S. Singh, and J.W. Lillard, *Past, present, and future technologies for oral delivery of therapeutic proteins.* Journal of pharmaceutical sciences, 2008. **97**(7): p. 2497-2523.
79. Charman, W.N., et al., *Physicochemical and physiological mechanisms for the effects of food on drug absorption: the role of lipids and pH.* 1997.
80. Bernkop-Schnurch, A. and T. Schmitz, *Presystemic metabolism of orally administered peptide drugs and strategies to overcome it.* Current drug metabolism, 2007. **8**(5): p. 509-517.
81. Lee, V.H., *Changing needs in drug delivery in the era of peptide and protein drugs.* Peptide and Protein Drug Delivery, 1991: p. 1-56.
82. Ganong, W.F. and K.E. Barrett, *Review of medical physiology*. Vol. 21. 2005: McGraw-Hill Medical ^ eNew York New York.
83. Johansson, M.E., et al., *Composition and functional role of the mucus layers in the intestine.* Cellular and Molecular Life Sciences, 2011. **68**(22): p. 3635-3641.

84. Ensign, L.M., R. Cone, and J. Hanes, *Oral drug delivery with polymeric nanoparticles: The gastrointestinal mucus barriers.* Advanced Drug Delivery Reviews, 2011.
85. Didierlaurent, A., et al., *How the gut senses its content.* Cellular microbiology, 2002. **4**(2): p. 61-72.
86. Kim, Y.S. and S.B. Ho, *Intestinal goblet cells and mucins in health and disease: recent insights and progress.* Curr Gastroenterol Rep, 2010. **12**(5): p. 319-30.
87. Verdugo, P., *Goblet cells secretion and mucogenesis.* Annu Rev Physiol, 1990. **52**(1): p. 157-176.
88. Cone, R.A., *Barrier properties of mucus.* Advanced Drug Delivery Reviews, 2009. **61**(2): p. 75-85.
89. Müller, C., I. Autenrieth, and A. Peschel, *Innate defenses of the intestinal epithelial barrier.* Cellular and molecular life sciences: CMLS, 2005. **62**(12): p. 1297-1307.
90. Maury, J., et al., *The Filamentous Brush Border Glycocalyx, a Mucin-like Marker of Enterocyte Hyper-Polarization.* European Journal of Biochemistry, 1995. **228**(2): p. 323-331.
91. Holmes, R. and R. Lobley, *Intestinal brush border revisited.* Gut, 1989. **30**(12): p. 1667-1678.
92. Frey, A., et al., *Role of the glycocalyx in regulating access of microparticles to apical plasma membranes of intestinal epithelial cells: implications for microbial attachment and oral vaccine targeting.* The Journal of experimental medicine, 1996. **184**(3): p. 1045-1059.
93. Sigurdsson, H.H., J. Kirch, and C.M. Lehr, *Mucus as a barrier to lipophilic drugs.* Int J Pharm, 2013. **453**(1): p. 56-64.
94. Ensign, L.M., R. Cone, and J. Hanes, *Oral drug delivery with polymeric nanoparticles: the gastrointestinal mucus barriers.* Adv Drug Deliv Rev, 2012. **64**(6): p. 557-70.
95. Schellekens, H., *Bioequivalence and the immunogenicity of biopharmaceuticals.* Nature reviews Drug discovery, 2002. **1**(6): p. 457-462.
96. Oberg, K., et al., *Treatment of malignant carcinoid tumors with recombinant interferon alfa-2b: development of neutralizing interferon antibodies and possible loss of antitumor activity.* Journal of the National Cancer Institute, 1989. **81**(7): p. 531-535.
97. De Groot, A.S. and D.W. Scott, *Immunogenicity of protein therapeutics.* Trends in immunology, 2007. **28**(11): p. 482-490.
98. Casadevall, N., et al., *Pure red-cell aplasia and antierythropoietin antibodies in patients treated with recombinant erythropoietin.* New England Journal of Medicine, 2002. **346**(7): p. 469-475.
99. Wang, X., et al., *Mechanism of oral tolerance induction to therapeutic proteins.* Advanced drug delivery reviews, 2013. **65**(6): p. 759-773.
100. Holmgren, J. and C. Czerkinsky, *Mucosal immunity and vaccines.* Nature medicine, 2005. **11**: p. S45-S53.
101. Falnes, P.Ø. and K. Sandvig, *Penetration of protein toxins into cells.* Current opinion in cell biology, 2000. **12**(4): p. 407-413.
102. Eidels, L., R. Proia, and D. Hart, *Membrane receptors for bacterial toxins.* Microbiological reviews, 1983. **47**(4): p. 596.
103. Lord, J.M., D.C. Smith, and L.M. Roberts, *Toxin entry: how bacterial proteins get into mammalian cells.* Cellular microbiology, 1999. **1**(2): p. 85-91.
104. Sandvig, K. and B. van Deurs, *Membrane traffic exploited by protein toxins.* Annual review of cell and developmental biology, 2002. **18**(1): p. 1-24.
105. Jørgensen, R., et al., *Cholix toxin, a novel ADP-ribosylating factor from Vibrio cholerae.* Journal of Biological Chemistry, 2008. **283**(16): p. 10671-10678.
106. Naglich, J.G., et al., *Expression cloning of a diphtheria toxin receptor: identity with a heparin-binding EGF-like growth factor precursor.* Cell, 1992. **69**(6): p. 1051-1061.
107. Collier, R., *Understanding the mode of action of diphtheria toxin: a perspective on progress during the 20th century.* Toxicon, 2001. **39**(11): p. 1793-1803.

108. Kounnas, M., et al., *The alpha 2-macroglobulin receptor/low density lipoprotein receptor-related protein binds and internalizes Pseudomonas exotoxin A.* Journal of Biological Chemistry, 1992. **267**(18): p. 12420-12423.
109. Holmgren, J., et al., *Interaction of cholera toxin and membrane GM1 ganglioside of small intestine.* Proceedings of the National Academy of Sciences, 1975. **72**(7): p. 2520-2524.
110. Merritt, E.A., et al., *Crystal structure of cholera toxin B-pentamer bound to receptor GM1 pentasaccharide.* Protein Science, 1994. **3**(2): p. 166-175.
111. Lencer, W.I. and D. Saslowsky, *Raft trafficking of AB 5 subunit bacterial toxins.* Biochimica et Biophysica Acta (BBA)-Molecular Cell Research, 2005. **1746**(3): p. 314-321.
112. Pastan, I., et al., *Immunotoxin treatment of cancer*.* Annu. Rev. Med., 2007. **58**: p. 221-237.
113. Sarnovsky, R., et al., *Initial characterization of an immunotoxin constructed from domains II and III of cholera exotoxin.* Cancer Immunology, Immunotherapy, 2010. **59**(5): p. 737-746.
114. Simon, N.C., K. Aktories, and J.T. Barbieri, *Novel bacterial ADP-ribosylating toxins: structure and function.* Nature Reviews Microbiology, 2014. **12**(9): p. 599-611.
115. Salvatore, G., et al., *Improved cytotoxic activity toward cell lines and fresh leukemia cells of a mutant anti-CD22 immunotoxin obtained by antibody phage display.* Clinical Cancer Research, 2002. **8**(4): p. 995-1002.
116. Arons, E., et al., *Pharmacokinetic Analysis Of Response In Hairy Cell Leukemia Treated By Anti-CD22 Recombinant Immunotoxin Moxetumomab Pasudotox.* Blood, 2013. **122**(21): p. 2871-2871.
117. Hassan, R., et al., *Phase I study of SS1P, a recombinant anti-mesothelin immunotoxin given as a bolus IV infusion to patients with mesothelin-expressing mesothelioma, ovarian, and pancreatic cancers.* Clinical Cancer Research, 2007. **13**(17): p. 5144-5149.
118. Kreitman, R.J., et al., *Phase I trial of continuous infusion anti-mesothelin recombinant immunotoxin SS1P.* Clinical Cancer Research, 2009. **15**(16): p. 5274-5279.
119. Weldon, J.E., et al., *A recombinant immunotoxin against the tumor-associated antigen mesothelin reengineered for high activity, low off-target toxicity, and reduced antigenicity.* Molecular cancer therapeutics, 2013. **12**(1): p. 48-57.
120. Alewine, C., R. Hassan, and I. Pastan, *Advances in Anticancer Immunotoxin Therapy.* The Oncologist, 2015: p. theoncologist. 2014-0358.
121. Olsen, E., et al., *Pivotal phase III trial of two dose levels of denileukin diftitox for the treatment of cutaneous T-cell lymphoma.* Journal of clinical oncology, 2001. **19**(2): p. 376-388.
122. Prince, H.M., et al., *Phase III placebo-controlled trial of denileukin diftitox for patients with cutaneous T-cell lymphoma.* Journal of clinical oncology, 2010. **28**(11): p. 1870-1877.
123. Onda, M., et al., *An immunotoxin with greatly reduced immunogenicity by identification and removal of B cell epitopes.* Proceedings of the National Academy of Sciences, 2008. **105**(32): p. 11311-11316.
124. Onda, M., et al., *Characterization of the B cell epitopes associated with a truncated form of Pseudomonas exotoxin (PE38) used to make immunotoxins for the treatment of cancer patients.* The Journal of Immunology, 2006. **177**(12): p. 8822-8834.
125. Yeung, V.P., et al., *Elimination of an immunodominant CD4+ T cell epitope in human IFN-β does not result in an in vivo response directed at the subdominant epitope.* The Journal of Immunology, 2004. **172**(11): p. 6658-6665.
126. Gelber, E.E. and E.S. Vitetta, *Effect of immunosuppressive agents on the immunogenicity and efficacy of an immunotoxin in mice.* Clinical cancer research, 1998. **4**(5): p. 1297-1304.

127. Hassan, R., et al., *Major cancer regressions in mesothelioma after treatment with an anti-mesothelin immunotoxin and immune suppression.* Science translational medicine, 2013. **5**(208): p. 208ra147-208ra147.
128. Schrodinger, LLC, *The PyMOL Molecular Graphics System, Version 1.3r1*. 2010.
129. Hessler, J.L. and R.J. Kreitman, *An early step in Pseudomonas exotoxin action is removal of the terminal lysine residue, which allows binding to the KDEL receptor.* Biochemistry, 1997. **36**(47): p. 14577-14582.
130. Pastrana, D.V., et al., *LRP1B functions as a receptor for Pseudomonas exotoxin.* Biochimica et Biophysica Acta (BBA)-Molecular Basis of Disease, 2005. **1741**(3): p. 234-239.
131. Fitzgerald, D., R.E. Morris, and C.B. Saelinger, *Receptor-mediated internalization of Pseudomonas toxin by mouse fibroblasts.* Cell, 1980. **21**(3): p. 867-873.
132. Willnow, T., et al., *The low-density-lipoprotein receptor-related protein (LRP) is processed by furin in vivo and in vitro.* Biochem. J, 1996. **313**: p. 71-76.
133. Li, Y., et al., *The YXXL motif, but not the two NPXY motifs, serves as the dominant endocytosis signal for low density lipoprotein receptor-related protein.* Journal of Biological Chemistry, 2000. **275**(22): p. 17187-17194.
134. Li, Y., et al., *Identification of a major cyclic AMP-dependent protein kinase A phosphorylation site within the cytoplasmic tail of the low-density lipoprotein receptor-related protein: implication for receptor-mediated endocytosis.* Molecular and cellular biology, 2001. **21**(4): p. 1185-1195.
135. Pivot, X., et al., *Preference for subcutaneous or intravenous administration of trastuzumab in patients with HER2-positive early breast cancer (PrefHer): an open-label randomised study.* Lancet Oncol, 2013. **14**(10): p. 962-70.
136. Gorovoy, M., et al., *Inflammatory mediators promote production of shed LRP1/CD91, which regulates cell signaling and cytokine expression by macrophages.* Journal of leukocyte biology, 2010. **88**(4): p. 769-778.
137. McKee, M.L. and D.J. FitzGerald, *Reduction of furin-nicked Pseudomonas exotoxin A: an unfolding story.* Biochemistry, 1999. **38**(50): p. 16507-16513.
138. Ogata, M., et al., *Cell-mediated cleavage of Pseudomonas exotoxin between Arg279 and Gly280 generates the enzymatically active fragment which translocates to the cytosol.* Journal of Biological Chemistry, 1992. **267**(35): p. 25396-25401.
139. Inocencio, N.M., J.M. Moehring, and T.J. Moehring, *Furin activates Pseudomonas exotoxin A by specific cleavage in vivo and in vitro.* Journal of Biological Chemistry, 1994. **269**(50): p. 31831-31835.
140. Ogata, M., et al., *Processing of Pseudomonas exotoxin by a cellular protease results in the generation of a 37,000-Da toxin fragment that is translocated to the cytosol.* Journal of Biological Chemistry, 1990. **265**(33): p. 20678-20685.
141. Jackson, M.E., et al., *The KDEL retrieval system is exploited by Pseudomonas exotoxin A, but not by Shiga-like toxin-1, during retrograde transport from the Golgi complex to the endoplasmic reticulum.* Journal of cell science, 1999. **112**(4): p. 467-475.
142. Smith, D.C., et al., *Internalized Pseudomonas Exotoxin A can Exploit Multiple Pathways to Reach the Endoplasmic Reticulum.* Traffic, 2006. **7**(4): p. 379-393.
143. Chaudhary, V.K., et al., *Pseudomonas exotoxin contains a specific sequence at the carboxyl terminus that is required for cytotoxicity.* Proceedings of the National Academy of Sciences, 1990. **87**(1): p. 308-312.
144. Koopmann, J.-O., et al., *Export of antigenic peptides from the endoplasmic reticulum intersects with retrograde protein translocation through the Sec61p channel.* Immunity, 2000. **13**(1): p. 117-127.
145. Weldon, J.E. and I. Pastan, *A guide to taming a toxin–recombinant immunotoxins constructed from Pseudomonas exotoxin A for the treatment of cancer.* FEBS Journal, 2011. **278**(23): p. 4683-4700.

146. Iglewski, B.H. and D. Kabat, *NAD-dependent inhibition of protein synthesis by Pseudomonas aeruginosa toxin.* Proceedings of the National Academy of Sciences, 1975. **72**(6): p. 2284-2288.
147. Iglewski, B.H., P.V. Liu, and D. Kabat, *Mechanism of action of Pseudomonas aeruginosa exotoxin Aiadenosine diphosphate-ribosylation of mammalian elongation factor 2 in vitro and in vivo.* Infection and immunity, 1977. **15**(1): p. 138-144.
148. Maxfield, F.R. and T.E. McGraw, *Endocytic recycling.* Nature Reviews Molecular Cell Biology, 2004. **5**(2): p. 121-132.
149. Mellman, I., *Endocytosis and molecular sorting.* Annual review of cell and developmental biology, 1996. **12**(1): p. 575-625.
150. Farahbakhsh, Z.T., R. Baldwin, and B. Wisnieski, *Effect of low pH on the conformation of Pseudomonas exotoxin A.* Journal of Biological Chemistry, 1987. **262**(5): p. 2256-2261.
151. Leka, O., et al., *Diphtheria toxin conformational switching at acidic pH.* FEBS Journal, 2014. **281**(9): p. 2115-2122.
152. McCann, J.A., et al., *Conformational changes in cholera toxin B subunit-ganglioside GM1 complexes are elicited by environmental pH and evoke changes in membrane structure.* Biochemistry, 1997. **36**(30): p. 9169-9178.
153. Ogata, M., I. Pastan, and D. FitzGerald, *Analysis of Pseudomonas exotoxin activation and conformational changes by using monoclonal antibodies as probes.* Infection and immunity, 1991. **59**(1): p. 407-414.
154. Idziorek, T., D. FitzGerald, and I. Pastan, *Low pH-induced changes in Pseudomonas exotoxin and its domains: increased binding of Triton X-114.* Infection and immunity, 1990. **58**(5): p. 1415-1420.
155. King, C.A. and W.E. van Heyningen, *Deactivation of cholera toxin by a sialidase-resistant monosialosylganglioside.* Journal of Infectious Diseases, 1973. **127**(6): p. 639-647.
156. Holmgren, J., I. Lönnroth, and L. Svennerholm, *Tissue receptor for cholera exotoxin: postulated structure from studies with GM1 ganglioside and related glycolipids.* Infection and immunity, 1973. **8**(2): p. 208-214.
157. Chinnapen, D.J.-F., et al., *Lipid sorting by ceramide structure from plasma membrane to ER for the cholera toxin receptor ganglioside GM1.* Developmental cell, 2012. **23**(3): p. 573-586.
158. Allured, V.S., et al., *Structure of exotoxin A of Pseudomonas aeruginosa at 3.0-Angstrom resolution.* Proceedings of the National Academy of Sciences, 1986. **83**(5): p. 1320-1324.
159. Hwang, J., et al., *Functional domains of Pseudomonas exotoxin identified by deletion analysis of the gene expressed in E. coli.* Cell, 1987. **48**(1): p. 129-136.
160. Siegall, C.B., et al., *Functional analysis of domains II, Ib, and III of Pseudomonas exotoxin.* Journal of Biological Chemistry, 1989. **264**(24): p. 14256-14261.
161. Douglas, C.M. and R. Collier, *Exotoxin A of Pseudomonas aeruginosa: substitution of glutamic acid 553 with aspartic acid drastically reduces toxicity and enzymatic activity.* Journal of bacteriology, 1987. **169**(11): p. 4967-4971.
162. Chiron, M.F., C.M. Fryling, and D.J. FitzGerald, *Cleavage of pseudomonas exotoxin and diphtheria toxin by a furin-like enzyme prepared from beef liver.* Journal of Biological Chemistry, 1994. **269**(27): p. 18167-18176.
163. Daugherty, A.L., et al., *Epithelial application of Pseudomonas aeruginosa exotoxin A results in a selective targeting to cells in the liver, spleen and lymph node.* Journal of Controlled Release, 2000. **65**(1): p. 297-302.
164. Mrsny, R.J., et al., *Bacterial toxins as tools for mucosal vaccination.* Drug discovery today, 2002. **7**(4): p. 247-258.
165. Mohammed, A.F., et al., *The< i> Pseudomonas aeruginosa</i> Exotoxin A translocation domain facilitates the routing of CPP-protein cargos to the cytosol of eukaryotic cells.* Journal of Controlled Release, 2012.

166. Strobl, J.S. and M. Thomas, *Human growth hormone.* Pharmacological Reviews, 1994. **46**(1): p. 1-34.
167. Carroll, P.V., et al., *Growth hormone deficiency in adulthood and the effects of growth hormone replacement: a review.* The Journal of Clinical Endocrinology & Metabolism, 1998. **83**(2): p. 382-395.
168. Schambelan, M., et al., *Recombinant human growth hormone in patients with HIV-associated wasting: a randomized, placebo-controlled trial.* Annals of internal medicine, 1996. **125**(11): p. 873-882.
169. Cázares-Delgadillo, J., A. Ganem-Rondero, and Y. Kalia, *Human growth hormone: new delivery systems, alternative routes of administration, and their pharmacological relevance.* European Journal of Pharmaceutics and Biopharmaceutics, 2011. **78**(2): p. 278-288.
170. Cai, Y., et al., *Developments in human growth hormone preparations: sustained-release, prolonged half-life, novel injection devices, and alternative delivery routes.* International journal of nanomedicine, 2014. **9**: p. 3527.
171. Godowski, P.J., et al., *Characterization of the human growth hormone receptor gene and demonstration of a partial gene deletion in two patients with Laron-type dwarfism.* Proceedings of the National Academy of Sciences, 1989. **86**(20): p. 8083-8087.
172. Asadullah, K., W. Sterry, and H. Volk, *Interleukin-10 therapy—review of a new approach.* Pharmacological reviews, 2003. **55**(2): p. 241-269.
173. Couper, K.N., D.G. Blount, and E.M. Riley, *IL-10: the master regulator of immunity to infection.* The Journal of Immunology, 2008. **180**(9): p. 5771-5777.
174. Marshall, J., *Ilodecakin. Schering-Plough Corp.* IDrugs: the investigational drugs journal, 1999. **2**(10): p. 1045-1058.
175. Dumont, F.J., *Therapeutic potential of IL-10 and its viral homologues: an update.* Expert Opinion on Therapeutic Patents, 2003. **13**(10): p. 1551-1577.
176. Moore, K.W., et al., *Interleukin-10 and the interleukin-10 receptor.* Annual review of immunology, 2001. **19**(1): p. 683-765.
177. Peterson, M. and M. Mooseker, *Characterization of the enterocyte-like brush border cytoskeleton of the C2BBe clones of the human intestinal cell line, Caco-2.* Journal of cell science, 1992. **102**(3): p. 581-600.
178. Goeddel, D.V., et al., *Direct expression in Escherichia coli of a DNA sequence coding for human growth hormone.* Nature, 1979. **281**(5732): p. 544.
179. Chaudhary, V.K., et al., *Role of domain II of Pseudomonas exotoxin in the secretion of proteins into the periplasm and medium by Escherichia coli.* Proceedings of the National Academy of Sciences, 1988. **85**(9): p. 2939-2943.
180. Hatefi, Y. and W. Hanstein, *Solubilization of particulate proteins and nonelectrolytes by chaotropic agents.* Proceedings of the National Academy of Sciences, 1969. **62**(4): p. 1129-1136.
181. Gasteiger, E., et al., *Protein identification and analysis tools on the ExPASy server*, in *The proteomics protocols handbook*. 2005, Springer. p. 571-607.
182. Thermo Fisher Scientific Inc. *Coomassie Plus (Bradford) Assay Reagent*. 2012 09/07/2015]; Available from: https://tools.lifetechnologies.com/content/sfs/manuals/MAN0011344_CoomassiePlus_Bradford_Asy_Reag_UG.pdf.
183. (SIB), S.I.o.B. *Peptide Cutter*. [cited 2014 12/06]; Available from: http://web.expasy.org/peptide_cutter/peptidecutter_enzymes.html#Tryps.
184. Malvern Instruments Ltd. *Dynamic Light Scattering: An Introduction in 30 Minutes*. 2012 [cited 2012 03/09]; Technical note MRK656-01]. Available from: http://www.malvern.com/common/downloads/campaign/MRK656-01.pdf.
185. Malvern Instruments Ltd. *Zetasizer Nano S/ZS Specifications - DLS Minimum Size Limit*. 2014 2014 [cited 2015 09/02]; Available from:

http://www.malvern.com/en/pdf/secure/TN101104ZetasizerNanoS_ZSMinimumSizeLimit.pdf.

186. Slavík, J., *Anilinonaphthalene sulfonate as a probe of membrane composition and function.* Biochimica et Biophysica Acta (BBA)-Reviews on Biomembranes, 1982. **694**(1): p. 1-25.
187. Brand, L. and J.R. Gohlke, *Fluorescence probes for structure.* Annual review of biochemistry, 1972. **41**(1): p. 843-868.
188. Fink, A.L., et al., *Classification of acid denaturation of proteins: intermediates and unfolded states.* Biochemistry, 1994. **33**(41): p. 12504-12511.
189. Goto, Y. and A.L. Fink, *Conformational states in. beta.-lactamase: molten-globule states at acidic and alkaline pH with high salt.* Biochemistry, 1989. **28**(3): p. 945-952.
190. Cardamone, M. and N. Puri, *Spectrofluorimetric assessment of the surface hydrophobicity of proteins.* Biochem. J, 1992. **282**: p. 589-593.
191. Kane, C.D. and D.A. Bernlohr, *A simple assay for intracellular lipid-binding proteins using displacement of 1-anilinonaphthalene 8-sulfonic acid.* Analytical biochemistry, 1996. **233**(2): p. 197-204.
192. Stryer, L., *The interaction of a naphthalene dye with apomyoglobin and apohemoglobin: a fluorescent probe of non-polar binding sites.* Journal of molecular biology, 1965. **13**(2): p. 482-495.
193. Cattoni, D.I., S.B. Kaufman, and F.L.G. Flecha, *Kinetics and thermodynamics of the interaction of 1-anilino-naphthalene-8-sulfonate with proteins.* Biochimica et Biophysica Acta (BBA)-Proteins and Proteomics, 2009. **1794**(11): p. 1700-1708.
194. Thompson, W. and K.L. Yielding, *8-Anilino naphthalene sulfonate binding as a probe for conformational changes induced in glutamate dehydrogenase by regulatory reagents.* Archives of biochemistry and biophysics, 1968. **126**(2): p. 399-406.
195. Tobias R. and Kumaraswamy S. *Biomolecular Binding Kinetics Assays on the Octet Platform*. 2013 [cited 2015 24/03]; Available from: http://csbi.mit.edu/instrumentation/ForteBio_App_Note_14.pdf.
196. Kuznetsov, I.B. and M. McDuffie, *FlexPred: a web-server for predicting residue positions involved in conformational switches in proteins.* Bioinformation, 2008. **3**(3): p. 134.
197. Kuznetsov, I.B., *Ordered conformational change in the protein backbone: Prediction of conformationally variable positions from sequence and low-resolution structural data.* Proteins: Structure, Function, and Bioinformatics, 2008. **72**(1): p. 74-87.
198. Janin, J., *Surface and inside volumes in globular proteins.* 1979.
199. Bhaskaran, R. and P. Ponnuswamy, *Positional flexibilities of amino acid residues in globular proteins.* International Journal of Peptide and Protein Research, 1988. **32**(4): p. 241-255.
200. Prior, T.I., D.J. FitzGerald, and I. Pastan, *Translocation mediated by domain II of Pseudomonas exotoxin A: transport of barnase into the cytosol.* Biochemistry, 1992. **31**(14): p. 3555-3559.
201. Jinno, Y., et al., *Domain II mutants of Pseudomonas exotoxin deficient in translocation.* Journal of Biological Chemistry, 1989. **264**(27): p. 15953-15959.
202. Méré, J., et al., *Acid-triggered membrane insertion of Pseudomonas exotoxin A involves an original mechanism based on pH-regulated tryptophan exposure.* Journal of Biological Chemistry, 2005. **280**(22): p. 21194-21201.
203. Sandvig, K. and S. Olsnes, *Diphtheria toxin entry into cells is facilitated by low pH.* The Journal of cell biology, 1980. **87**(3): p. 828-832.
204. Draper, R.K. and M.I. Simon, *The entry of diphtheria toxin into the mammalian cell cytoplasm: evidence for lysosomal involvement.* The Journal of cell biology, 1980. **87**(3): p. 849-854.

205. Taupiac, M.P., et al., *A deletion within the translocation domain of Pseudomonas exotoxin A enhances translocation efficiency and cytotoxicity concomitantly.* Molecular microbiology, 1999. **31**(5): p. 1385-1393.
206. Zalman, L.S. and B. Wisnieski, *Characterization of the insertion of Pseudomonas exotoxin A into membranes.* Infection and immunity, 1985. **50**(3): p. 630-635.
207. Sandvig, K. and J. Moskaug, *Pseudomonas toxin binds triton X-114 at low pH.* Biochem. J, 1987. **245**: p. 899-901.
208. Mere, J., *Acid-triggered Membrane Insertion of Pseudomonas Exotoxin A Involves an Original Mechanism Based on pH-regulated Tryptophan Exposure.* Journal of Biological Chemistry, 2005. **280**(22): p. 21194-21201.
209. Wedekind, J.E., et al., *Refined crystallographic structure of Pseudomonas aeruginosa exotoxin A and its implications for the molecular mechanism of toxicity.* Journal of molecular biology, 2001. **314**(4): p. 823-837.
210. Fryling, C., M. Ogata, and D. FitzGerald, *Characterization of a cellular protease that cleaves Pseudomonas exotoxin.* Infection and immunity, 1992. **60**(2): p. 497-502.
211. Baneyx, F. and M. Mujacic, *Recombinant protein folding and misfolding in Escherichia coli.* Nature biotechnology, 2004. **22**(11): p. 1399-1408.
212. Missiakas, D. and S. Raina, *Protein folding in the bacterial periplasm.* Journal of bacteriology, 1997. **179**(8): p. 2465.
213. Rudolph, R. and H. Lilie, *In vitro folding of inclusion body proteins.* The FASEB Journal, 1996. **10**(1): p. 49-56.
214. Villaverde, A. and M.M. Carrió, *Protein aggregation in recombinant bacteria: biological role of inclusion bodies.* Biotechnology letters, 2003. **25**(17): p. 1385-1395.
215. De Bernardez Clark, E., E. Schwarz, and R. Rudolph, *Inhibition of aggregation side reactions during in vitro protein folding.* Methods in enzymology, 1999. **309**: p. 217-236.
216. Arakawa, T., et al., *Suppression of protein interactions by arginine: a proposed mechanism of the arginine effects.* Biophysical chemistry, 2007. **127**(1): p. 1-8.
217. Baynes, B.M., D.I. Wang, and B.L. Trout, *Role of arginine in the stabilization of proteins against aggregation.* Biochemistry, 2005. **44**(12): p. 4919-4925.
218. Baynes, B.M. and B.L. Trout, *Rational design of solution additives for the prevention of protein aggregation.* Biophysical journal, 2004. **87**(3): p. 1631-1639.
219. Dockal, M., D.C. Carter, and F. Rüker, *Conformational transitions of the three recombinant domains of human serum albumin depending on pH.* Journal of Biological Chemistry, 2000. **275**(5): p. 3042-3050.
220. Bhattacharya, M., et al., *pH-induced conformational isomerization of bovine serum albumin studied by extrinsic and intrinsic protein fluorescence.* Journal of fluorescence, 2011. **21**(3): p. 1083-1090.
221. Li, Y., et al., *Effects of pH on the interactions and conformation of bovine serum albumin: comparison between chemical force microscopy and small-angle neutron scattering.* The Journal of Physical Chemistry B, 2008. **112**(12): p. 3797-3806.
222. Kun, R., M. Szekeres, and I. Dékány, *Isothermal titration calorimetric studies of the pH induced conformational changes of bovine serum albumin.* Journal of thermal analysis and calorimetry, 2009. **96**(3): p. 1009-1017.
223. Murthy, S., J. Kostman, and V.P. Dinoso Jr, *Effect of pH, substrate, and temperature on tryptic activity of duodenal samples.* Digestive diseases and sciences, 1980. **25**(4): p. 289-294.
224. Varkouhi, A.K., et al., *Endosomal escape pathways for delivery of biologicals.* Journal of Controlled Release, 2011. **151**(3): p. 220-228.
225. Brinkmann, U., et al., *Alteration of a protease-sensitive region of Pseudomonas exotoxin prolongs its survival in the circulation of mice.* Proceedings of the National Academy of Sciences, 1992. **89**(7): p. 3065-3069.

226. ChemAxon. *chemicalize.org*. 21/01/2015 [cited 2015 23/01]; Available from: http://www.chemicalize.org/.
227. Spector, A.A., *Fatty acid binding to plasma albumin.* Journal of lipid research, 1975. **16**(3): p. 165-179.
228. Spector, A.A., K. John, and J.E. Fletcher, *Binding of long-chain fatty acids to bovine serum albumin.* Journal of Lipid Research, 1969. **10**(1): p. 56-67.
229. Curry, S., et al., *Crystal structure of human serum albumin complexed with fatty acid reveals an asymmetric distribution of binding sites.* Nature Structural & Molecular Biology, 1998. **5**(9): p. 827-835.
230. Curry, S., P. Brick, and N.P. Franks, *Fatty acid binding to human serum albumin: new insights from crystallographic studies.* Biochimica et Biophysica Acta (BBA)-Molecular and Cell Biology of Lipids, 1999. **1441**(2): p. 131-140.
231. Bhattacharya, A.A., T. Grüne, and S. Curry, *Crystallographic analysis reveals common modes of binding of medium and long-chain fatty acids to human serum albumin.* Journal of molecular biology, 2000. **303**(5): p. 721-732.
232. Tulip, W.R., et al., *Refined crystal structure of the influenza virus N9 neuraminidase-NC41 Fab complex.* Journal of molecular biology, 1992. **227**(1): p. 122-148.
233. Vedadi, M., et al., *Chemical screening methods to identify ligands that promote protein stability, protein crystallization, and structure determination.* Proceedings of the National Academy of Sciences, 2006. **103**(43): p. 15835-15840.
234. Penmatsa, A., K.H. Wang, and E. Gouaux, *X-ray structure of dopamine transporter elucidates antidepressant mechanism.* Nature, 2013. **503**(7474): p. 85-90.
235. Ostermeier, C., et al., *Fv fragment-mediated crystallization of the membrane protein bacterial cytochrome c oxidase.* Nature Structural & Molecular Biology, 1995. **2**(10): p. 842-846.
236. Leppla, S.H., O.C. Martin, and L.A. Muehl, *The exotoxin of P. aeruginosa: a proenzyme having an unusual mode of activation.* Biochemical and biophysical research communications, 1978. **81**(2): p. 532-538.
237. Griffin, L. and A. Lawson, *Antibody fragments as tools in crystallography.* Clinical & Experimental Immunology, 2011. **165**(3): p. 285-291.
238. Prongay, A.J., et al., *Preparation and crystallization of a human immunodeficiency virus p24-Fab complex.* Proceedings of the National Academy of Sciences, 1990. **87**(24): p. 9980-9984.
239. Hunte, C. and H. Michel, *Crystallisation of membrane proteins mediated by antibody fragments.* Current Opinion in Structural Biology, 2002. **12**(4): p. 503-508.
240. Farahbakhsh, Z.T. and B.J. Wisnieski, *The acid-triggered entry pathway of Pseudomonas exotoxin A.* Biochemistry, 1989. **28**(2): p. 580-585.
241. Jiang, J.X. and E. London, *Involvement of denaturation-like changes in Pseudomonas exotoxin a hydrophobicity and membrane penetration determined by characterization of pH and thermal transitions. Roles of two distinct conformationally altered states.* Journal of Biological Chemistry, 1990. **265**(15): p. 8636-8641.
242. Casey, J.R., S. Grinstein, and J. Orlowski, *Sensors and regulators of intracellular pH.* Nature reviews Molecular cell biology, 2009. **11**(1): p. 50-61.
243. Wedekind, J.E., et al., *Refined crystallographic structure of Pseudomonas aeruginosa exotoxin A and its implications for the molecular mechanism of toxicity1.* Journal of molecular biology, 2001. **314**(4): p. 823-837.
244. Holden, N. and D. Lide, *CRC handbook of chemistry and physics*. 1991, CRC Press, Boca Raton, FL.
245. Chaudhary, V.K., et al., *Mutagenesis of Pseudomonas exotoxin in identification of sequences responsible for the animal toxicity.* Journal of Biological Chemistry, 1990. **265**(27): p. 16306-16310.
246. Kasturi, S., et al., *Alanine scanning mutagenesis identifies surface amino acids on domain II of Pseudomonas exotoxin required for cytotoxicity, proper folding, and*

secretion into periplasm. Journal of Biological Chemistry, 1992. **267**(32): p. 23427-23433.
247. Gething, M.-J., et al., *Studies on the mechanism of membrane fusion: site-specific mutagenesis of the hemagglutinin of influenza virus.* The Journal of cell biology, 1986. **102**(1): p. 11-23.
248. Doms, R.W. and A. Helenius, *Quaternary structure of influenza virus hemagglutinin after acid treatment.* Journal of virology, 1986. **60**(3): p. 833-839.
249. Daniels, R., et al., *Fusion mutants of the influenza virus hemagglutinin glycoprotein.* Cell, 1985. **40**(2): p. 431-439.
250. Qa'Dan, M., L.M. Spyres, and J.D. Ballard, *pH-Induced Conformational Changes inClostridium difficile Toxin B.* Infection and immunity, 2000. **68**(5): p. 2470-2474.
251. Puhar, A., et al., *Comparison of the pH-induced conformational change of different clostridial neurotoxins.* Biochemical and biophysical research communications, 2004. **319**(1): p. 66-71.
252. Stampfer, S.D., et al., *Structural basis of local, pH-dependent conformational changes in glycoprotein B from herpes simplex virus type 1.* Journal of virology, 2010. **84**(24): p. 12924-12933.
253. Kurnikov, I.V., et al., *pH-Triggered conformational switching of the diphtheria toxin t-domain: The roles of N-terminal histidines.* Journal of molecular biology, 2013. **425**(15): p. 2752-2764.
254. Svennerholm, L., *The gangliosides.* Journal of lipid research, 1964. **5**(2): p. 145-155.
255. de Chaves, E.P. and S. Sipione, *Sphingolipids and gangliosides of the nervous system in membrane function and dysfunction.* FEBS letters, 2010. **584**(9): p. 1748-1759.
256. Ledeen, R.W., et al., *The Role of GM1 and Other Gangliosides in Neuronal Differentiation Overview and New Findingsa.* Annals of the New York Academy of Sciences, 1998. **845**(1): p. 161-175.
257. Torgersen, M.L., et al., *Internalization of cholera toxin by different endocytic mechanisms.* Journal of cell science, 2001. **114**(20): p. 3737-3747.
258. Spooner, R.A., et al., *Retrograde transport pathways utilised by viruses and protein toxins.* Virol. J, 2006. **3**: p. 26.
259. Cho, J.A., et al., *Insights on the trafficking and retro-translocation of glycosphingolipid-binding bacterial toxins.* Frontiers in Cellular and Infection Microbiology, 2012. **2**.
260. Sonnino, S., et al., *Preparation of lyso-GM1 (II3Neu5AcGgOse4-long chain bases) by a one-pot reaction.* Journal of lipid research, 1992. **33**(8): p. 1221-1226.
261. Patist, A., et al., *On the measurement of critical micelle concentrations of pure and technical-grade nonionic surfactants.* Journal of Surfactants and Detergents, 2000. **3**(1): p. 53-58.
262. Krista Witte from ForteBio Inc. *New 2:1 Heterogeneous Ligand Model Now Available for Kinetic Analysis*. 10/2009 [cited 2015 12/02]; Available from: http://www.fortebio.com/interactions/October_2009/page4.html.
263. Sonnino, S., et al., *Aggregative properties of gangliosides in solution.* Chemistry and physics of lipids, 1994. **71**(1): p. 21-45.
264. Lasic, D.D. and Y. Barenholz, *Handbook of Nonmedical Applications of Liposomes: Theory and basic sciences*. Vol. 1. 1996: CRC Press.
265. Ulrich-Bott, B. and H. Wiegandt, *Micellar properties of glycosphingolipids in aqueous media.* Journal of lipid research, 1984. **25**(11): p. 1233-1245.
266. RAUVALA, H., *Monomer-Micelle Transition of the Ganglioside GM1 and the Hydrolysis by Clostridium perfringens Neuraminidase.* European Journal of Biochemistry, 1979. **97**(2): p. 555-564.
267. Formisano, S., et al., *Critical micelle concentrations of gangliosides.* Biochemistry, 1979. **18**(6): p. 1119-1124.
268. Shinoda, K., T. Nakagawa, and B.-I. Tamamushi, *Colloidal surfactants: some physicochemical properties*. 2013: Elsevier.

269. Velkov, T., et al., *The interaction of lipophilic drugs with intestinal fatty acid-binding protein.* Journal of Biological Chemistry, 2005. **280**(18): p. 17769-17776.
270. Thermo Fisher Scientific Inc. 2015 [cited 2015 10/02]; Available from: https://www.lifetechnologies.com/order/catalog/product/A20341.
271. Sauer, A.-K., et al., *Characterization of the sialic acid binding activity of Influenza A viruses using soluble variants of the H7 and H9 hemagglutinins.* PloS one, 2014. **9**(2).
272. Cacalano, G., et al., *Production of the Pseudomonas aeruginosa neuraminidase is increased under hyperosmolar conditions and is regulated by genes involved in alginate expression.* Journal of Clinical Investigation, 1992. **89**(6): p. 1866.
273. Ada, G., E. French, and P. Lind, *Purification and properties of neuraminidase from Vibrio cholerae.* Journal of general microbiology, 1961. **24**(3): p. 409-421.
274. Linden, S., et al., *Mucins in the mucosal barrier to infection.* Mucosal immunology, 2008. **1**(3): p. 183-197.
275. Hutchinson, D. and J. Kabayo, *Current thoughts on neuraminidase.* Trends in biochemical sciences, 1977. **2**(1): p. 1-3.
276. Soong, G., et al., *Bacterial neuraminidase facilitates mucosal infection by participating in biofilm production.* The Journal of clinical investigation, 2006. **116**(8): p. 2297.
277. Galen, J.E., et al., *Role of Vibrio cholerae neuraminidase in the function of cholera toxin.* Infection and immunity, 1992. **60**(2): p. 406-415.
278. Kabir, S., N. Ahmad, and S. Ali, *Neuraminidase production by Vibrio cholerae O1 and other diarrheagenic bacteria.* Infection and immunity, 1984. **44**(3): p. 747-749.
279. Moustafa, I., et al., *Sialic acid recognition by Vibrio cholerae neuraminidase.* Journal of Biological Chemistry, 2004. **279**(39): p. 40819-40826.
280. Svennerholm, L., *Biological function of gangliosides: proceedings of Nobel Symposium 83*. Vol. 101. 1994: Elsevier.
281. Tettamanti, G., *Ganglioside/glycosphingolipid turnover: new concepts.* Glycoconjugate journal, 2003. **20**(5): p. 301-317.
282. Alberts, B., et al., *Molecular Biology of the Cell (3rd edn).* Trends in biochemical sciences, 1995. **20**(5): p. 210-210.
283. Reichner, J., S. Whiteheart, and G. Hart, *Intracellular trafficking of cell surface sialoglycoconjugates.* Journal of Biological Chemistry, 1988. **263**(31): p. 16316-16326.
284. Brändli, A. and K. Simons, *A restricted set of apical proteins recycle through the trans-Golgi network in MDCK cells.* The EMBO journal, 1989. **8**(11): p. 3207.
285. Mathews, R.A., T. Johnson, and J. Hudson, *Synthesis and turnover of plasma-membrane proteins and glycoproteins in a neuroblastoma cell line.* Biochem. J, 1976. **154**: p. 57-64.
286. Brown, D. and E. London, *Functions of lipid rafts in biological membranes.* Annual review of cell and developmental biology, 1998. **14**(1): p. 111-136.
287. Mallard, F., et al., *Direct pathway from early/recycling endosomes to the Golgi apparatus revealed through the study of shiga toxin B-fragment transport.* The Journal of cell biology, 1998. **143**(4): p. 973-990.
288. Falguieres, T., et al., *Targeting of Shiga toxin B-subunit to retrograde transport route in association with detergent-resistant membranes.* Molecular biology of the cell, 2001. **12**(8): p. 2453-2468.
289. Seetharam, S., et al., *Increased cytotoxic activity of Pseudomonas exotoxin and two chimeric toxins ending in KDEL.* Journal of Biological Chemistry, 1991. **266**(26): p. 17376-17381.
290. Gordon, V.M., et al., *Proteolytic activation of bacterial toxins by eukaryotic cells is performed by furin and by additional cellular proteases.* Infection and immunity, 1995. **63**(1): p. 82-87.
291. Kenworthy, A.K., N. Petranova, and M. Edidin, *High-resolution FRET microscopy of cholera toxin B-subunit and GPI-anchored proteins in cell plasma membranes.* Molecular biology of the cell, 2000. **11**(5): p. 1645-1655.

292. Montesano, R., et al., *Non-coated membrane invaginations are involved in binding and internalization of cholera and tetanus toxins.* 1982.
293. Parton, R.G., *Ultrastructural localization of gangliosides; GM1 is concentrated in caveolae.* Journal of Histochemistry & Cytochemistry, 1994. **42**(2): p. 155-166.
294. Möbius, W., et al., *Intracellular distribution of a biotin-labeled ganglioside, GM1, by immunoelectron microscopy after endocytosis in fibroblasts.* Journal of Histochemistry & Cytochemistry, 1999. **47**(8): p. 1005-1014.
295. Fujinaga, Y., et al., *Gangliosides that associate with lipid rafts mediate transport of cholera and related toxins from the plasma membrane to endoplasmic reticulm.* Molecular biology of the cell, 2003. **14**(12): p. 4783-4793.
296. Kuziemko, G.M., M. Stroh, and R.C. Stevens, *Cholera toxin binding affinity and specificity for gangliosides determined by surface plasmon resonance.* Biochemistry, 1996. **35**(20): p. 6375-6384.
297. Massol, R.H., et al., *Cholera toxin toxicity does not require functional Arf6-and dynamin-dependent endocytic pathways.* Molecular biology of the cell, 2004. **15**(8): p. 3631-3641.
298. Lencer, W., et al., *Targeting of cholera toxin and Escherichia coli heat labile toxin in polarized epithelia: role of COOH-terminal KDEL.* The Journal of cell biology, 1995. **131**(4): p. 951-962.
299. Lencer, W.I. and B. Tsai, *The intracellular voyage of cholera toxin: going retro.* Trends in biochemical sciences, 2003. **28**(12): p. 639-645.
300. Kreitman, R.J. and I. Pastan, *Importance of the glutamate residue of KDEL in increasing the cytotoxicity of Pseudomonas exotoxin derivatives and for increased binding to the KDEL receptor.* Biochem. J, 1995. **307**: p. 29-37.
301. Lillis, A.P., et al., *LDL receptor-related protein 1: unique tissue-specific functions revealed by selective gene knockout studies.* Physiological reviews, 2008. **88**(3): p. 887-918.
302. Obermoeller-McCormick, L.M., et al., *Dissection of receptor folding and ligand-binding property with functional minireceptors of LDL receptor-related protein.* Journal of cell science, 2001. **114**(5): p. 899-908.
303. Neels, J.G., et al., *The second and fourth cluster of class A cysteine-rich repeats of the low density lipoprotein receptor-related protein share ligand-binding properties.* Journal of Biological Chemistry, 1999. **274**(44): p. 31305.
304. Petrus, A.K., T.J. Fairchild, and R.P. Doyle, *Traveling the vitamin B12 pathway: oral delivery of protein and peptide drugs.* Angewandte Chemie International Edition, 2009. **48**(6): p. 1022-1028.
305. Petrus, A.K., et al., *Vitamin B12 as a carrier for the oral delivery of insulin.* ChemMedChem, 2007. **2**(12): p. 1717-1721.
306. Carrasco, G.C., *Quantification of paper mass distributions within local picking areas.* 2007.
307. Bourdoncle, P., *Colocalization plugin in Java.* Institut Jacques Monod, Service Imagerie, Paris, France, 2003.
308. Rasband, W.S. *Image J, U.S. National Institues of Health, Bethesda, Maryland, USA*. 1997-2014; Available from: http://imagej.nih.gov/ij/.
309. New England Biolabs. 18/05/2015]; Available from: https://www.neb.com/protocols/2012/06/01/guidelines-for-pcr-optimization-with-phusion-high-fidelity-dna-polymerase.
310. Watson, P., A.T. Jones, and D.J. Stephens, *Intracellular trafficking pathways and drug delivery: fluorescence imaging of living and fixed cells.* Advanced drug delivery reviews, 2005. **57**(1): p. 43-61.
311. Iversen, T.-G., T. Skotland, and K. Sandvig, *Endocytosis and intracellular transport of nanoparticles: present knowledge and need for future studies.* Nano Today, 2011. **6**(2): p. 176-185.

312. Gruenberg, J. and F.R. Maxfield, *Membrane transport in the endocytic pathway.* Current opinion in cell biology, 1995. **7**(4): p. 552-563.
313. Trombetta, E.S. and A.J. Parodi, *Quality control and protein folding in the secretory pathway.* Annual review of cell and developmental biology, 2003. **19**(1): p. 649-676.
314. Nakamura, N., et al., *Characterization of a cis-Golgi matrix protein, GM130.* The Journal of cell biology, 1995. **131**(6): p. 1715-1726.
315. Grant, B.D. and J.G. Donaldson, *Pathways and mechanisms of endocytic recycling.* Nature reviews Molecular cell biology, 2009. **10**(9): p. 597-608.
316. Hidalgo, I.J., T.J. Raub, and R.T. Borchardt, *Characterization of the human colon carcinoma cell line (Caco-2) as a model system for intestinal epithelial permeability.* Gastroenterology, 1989(96): p. 736-49.
317. Sambuy, Y., et al., *The Caco-2 cell line as a model of the intestinal barrier: influence of cell and culture-related factors on Caco-2 cell functional characteristics.* Cell biology and toxicology, 2005. **21**(1): p. 1-26.
318. Artursson, P., K. Palm, and K. Luthman, *Caco-2 monolayers in experimental and theoretical predictions of drug transport.* Advanced Drug Delivery Reviews, 2012. **64**: p. 280-289.
319. Hubatsch, I., E.G. Ragnarsson, and P. Artursson, *Determination of drug permeability and prediction of drug absorption in Caco-2 monolayers.* Nature protocols, 2007. **2**(9): p. 2111-2119.
320. Cereijido, M., et al., *Polarized monolayers formed by epithelial cells on a permeable and translucent support.* The Journal of cell biology, 1978. **77**(3): p. 853-880.
321. Pezzulo, A.A., et al., *Reduced airway surface pH impairs bacterial killing in the porcine cystic fibrosis lung.* Nature, 2012. **487**(7405): p. 109-113.
322. Marzolo, M.P., et al., *Differential distribution of low-density lipoprotein-receptor-related protein (LRP) and megalin in polarized epithelial cells is determined by their cytoplasmic domains.* Traffic, 2003. **4**(4): p. 273-288.
323. Gassama-Diagne, A., et al., *Phosphatidylinositol-3, 4, 5-trisphosphate regulates the formation of the basolateral plasma membrane in epithelial cells.* Nature cell biology, 2006. **8**(9): p. 963-970.
324. Hizuka, N., et al., *Polypeptide hormone degradation and receptor regulation are coupled to ligand internalization. A direct biochemical and morphologic demonstration.* Journal of Biological Chemistry, 1981. **256**(9): p. 4591-4597.
325. Henriksen, J.H., *Degradation of Bioactive Substances: Physiology and Pathophysiology*. 1991: CRC Press.
326. Antunes, F., et al., *Models to predict intestinal absorption of therapeutic peptides and proteins.* Current drug metabolism, 2013. **14**(1): p. 4-20.
327. Lennernäs, H., et al., *Correlation between paracellular and transcellular drug permeability in the human jejunum and Caco-2 monolayers.* Int. J. Pharm, 1996. **127**: p. 103-107.
328. Mrsny, R.J., *Unpublished data*. 2011.
329. Wilson, G., et al., *Transport and permeability properties of human Caco-2 cells: an in vitro model of the intestinal epithelial cell barrier.* Journal of controlled release, 1990. **11**(1): p. 25-40.
330. Meunier, V., et al., *The human intestinal epithelial cell line Caco-2; pharmacological and pharmacokinetic applications.* Cell biology and toxicology, 1995. **11**(3-4): p. 187-194.
331. Sandvig, K. and B. van Deurs, *Delivery into cells: lessons learned from plant and bacterial toxins.* Gene therapy, 2005. **12**(11): p. 865-872.
332. Cao, X., M.A. Surma, and K. Simons, *Polarized sorting and trafficking in epithelial cells.* Cell Research, 2012.
333. Matter, K. and I. Mellman, *Mechamisms of cell polarity: sorting and transport in epithelial cells.* Current opinion in cell biology, 1994. **6**(4): p. 545-554.

334. Yang, F., L.G. Moss, and G.N. Phillips Jr, *The molecular structure of green fluorescent protein.* Dept. of biochemistry and cell biology, Rice University, 1997.
335. Donald, J.E., D.W. Kulp, and W.F. DeGrado, *Salt bridges: Geometrically specific, designable interactions.* Proteins: Structure, Function, and Bioinformatics, 2011. **79**(3): p. 898-915.

References

9 Appendices

Appendix 1 – Expression plasmids and physiochemical properties of the versions of PE and cholix

During cloning of Cho386-hGH, pETCHO was used for amplification of Cho386 sequence from full-length, non-toxic cholix, whose sequence had previously been cloned into pET-26 b (+) plasmid from Novagen (Millipore Limited, Watford, UK) (Figure 9-1).

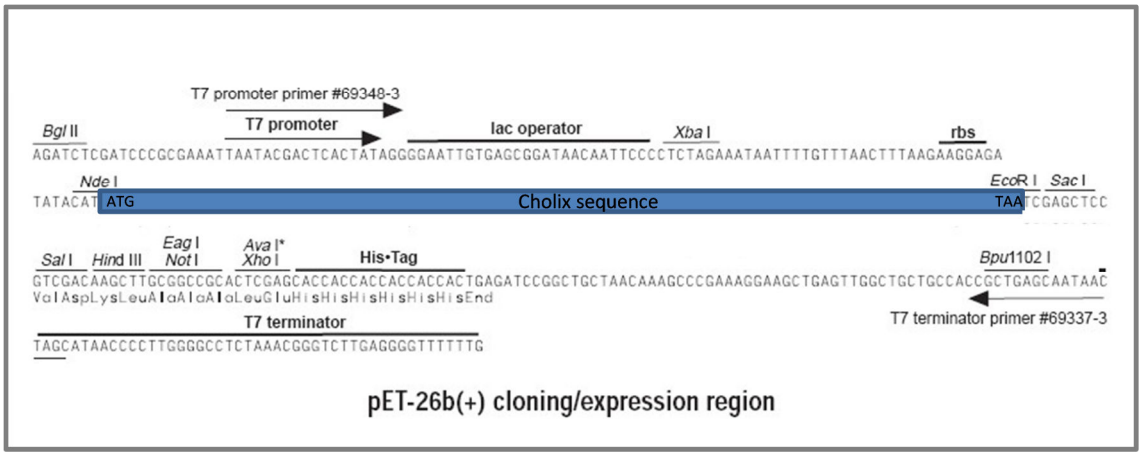

Figure 9-1 – Schematic representation of pETCHO expression construct. The sequence encoding for full-length, non-toxic, cholix was cloned into pET-26 b (+) between the NdeI and EcoRI restriction sites.

Table 9-1 presented below summarises the plasmids used in the expression process of the various versions of PE and cholix, as well as the calculated molecular weight and isoelectric point for these proteins. pET-26 b (+) was obtained from Novagen, while pET28 was obtained from the David Liu laboratory (Harvard University, Cambridge, MA, USA). pVC45D was a gift from Dr David FitzGerald (NCI/NIH, Bethesda, MD, USA).

Table 9-1 – Plasmids and physicochemical properties of PE and cholix versions. Both pI and molecular weight were calculated using ExPASy ProtParam [181].

Vector backbone	Expression plasmid	Protein	Calculated pI	Predicted molecular weight (kDa)
pUC13	pVC45D	ntPE	5.28	66.7
pET-26 b (+)	pntPE GS TEV	ntPE GS TEV	5.28	66.7
	pPE408 GS TEV	PE408 GS TEV	5.28	44.4
	pPE364 GS TEV	PE364 GS TEV	5.86	40.1
	pPE351 GS TEV	PE351 GS TEV	5.97	38.9
	pPE320 GS TEV	PE320 GS TEV	6.33	35.6
	pPE303 GS TEV	PE303 GS TEV	6.33	33.8
pET28	phisPE-GFP	ntPE-GFP	5.34	93.2
	phis408-GFP	PE408-GFP	5.36	71.4
	phis364-GFP	PE364-GFP	5.33	69.2
	phis351-GFP	PE351-GFP	5.41	67.6
	phis320-GFP	PE320-GFP	5.53	64.4
	phis303-GFP	PE303-GFP	5.53	62.5
pET28	phis364-hGH	PE364-hGH	5.84	66.4
pETCHO	pcholix	cholix	5.31	71.8
pET-26 b (+)	pntCho GS TEV	ntCho GS TEV	5.31	71.8
	pCho428 GS TEV	Cho428 GS TEV	5.31	48.0
	pCho386 GS TEV	Cho386 GS TEV	5.42	43.7
	pCho368 GS TEV	Cho368 GS TEV	5.37	41.6
	pCho332 GS TEV	Cho332 GS TEV	5.65	37.5
	pCho313 GS TEV	Cho313 GS TEV	5.59	35.4
pET28	phisCho-GFP	ntCho-GFP	5.21	97.9
	phis428-GFP	Cho428-GFP	5.18	74.9
	phis386-GFP	Cho386-GFP	5.12	71.6
	phis368-GFP	Cho368-GFP	5.08	69.7
	phis332-GFP	Cho332-GFP	5.16	65.3
	phis313-GFP	Cho313-GFP	5.19	63.1
pET28	phis386-hGH	Cho386-hGH	5.27	66.3

Appendix 2 – Summary of the antibodies used in the thesis

The tables below detail, for each primary and secondary antibody applied, the target, clonality, host species and supplier, as well as the blocking solution and dilution used.

Table 9-2 – Primary antibodies and dilutions used for Western blot (WB), immunofluorescence (IF) and/or immunohistochemistry (IHC).

Primary antibody	Clonality	Species	Blocking solution	Dilution	Supplier
Pseudomonas Exotoxin A	Whole antiserum	Rabbit	BSA	1/20,000 WB 1/1,000 IF/IHC	Sigma-Aldrich #P2318
M40-1	Monoclonal antibody	Mouse	Milk	1/10,000 WB	Expressed
Cho386 GS TEV	Whole antiserum	Rabbit	BSA	1/2,000 WB 1/500 IF/IHC	Innovagen AB, custom-made
6X His	Polyclonal antibody	Rabbit	BSA	1/3,500 WB	Abcam #ab125262
GM130	Polyclonal antibody	Rabbit	BSA	1/500 IF	Abcam #ab52649
Human growth hormone	Monoclonal antibody	Goat	BSA	1/100 IHC	R&D Systems #AF1067

Table 9-3 – Secondary antibodies and dilutions.

Secondary antibody	Dilution	Supplier
HRP-conjugated anti-rabbit IgG	1/4,000	GE Healthcare #NA934
HRP-conjugated anti-mouse IgG	1/4,000	GE Healthcare #NXA931
Fluorescein-conjugated anti-goat IgG	1/100	Vector Laboratories #FI-5000
Alexa Fluor® 546-conjugated anti-rabbit IgG	1/100	Invitrogen #A10004
Alexa Fluor® 568-conjugated anti-rabbit IgG	1/100	Invitrogen #A10042

Appendix 3 – Controls for uptake assays on PE-GFP and Cho-GFP mutants

CT, whose host cell-membrane receptor is GM1, is readily taken up by NP cells. Therefore CTB-A488 was used as a positive control in the assays investigating the role of this ganglioside in the uptake of ntPE, ntCho and various PE-GFP and Cho-GFP mutants (Sections 4.3.3.2, 5.3.4, 6.3.3.3 and 6.3.4.2). Unlike CT, GFP is not spontaneously internalised by NP cells and was therefore used as a negative control in the studies presented in the thesis. NP Caco-2 cells were incubated with 20 µg CTB-A488 or GFP in 100 µl complete growth medium (concentration CTB-A488 = 3.5 µM and GFP = 7.4 µM) at 37 °C for 2 h in the experimental conditions previously described. Cells were then fixed with PFA, labelled with an anti-GM130 antibody, and prepared for confocal microscopy. GM130 expression was also used here to visualise the Golgi network [314].

Following neuraminidase treatment, the amount of CTB-A488 internalised by NP cells was significantly reduced compared to untreated cells. Similarly, addition of CTB resulted in lower protein uptake (Figure 9-2). These observations are consistent with GM1 being the receptor for CT. Figure 9-3 shows that GFP was not readily taken up by untreated cells, and that neither treatment with neuraminidase or addition of CTB affected its entry as no intracellular fluorescence could be detected.

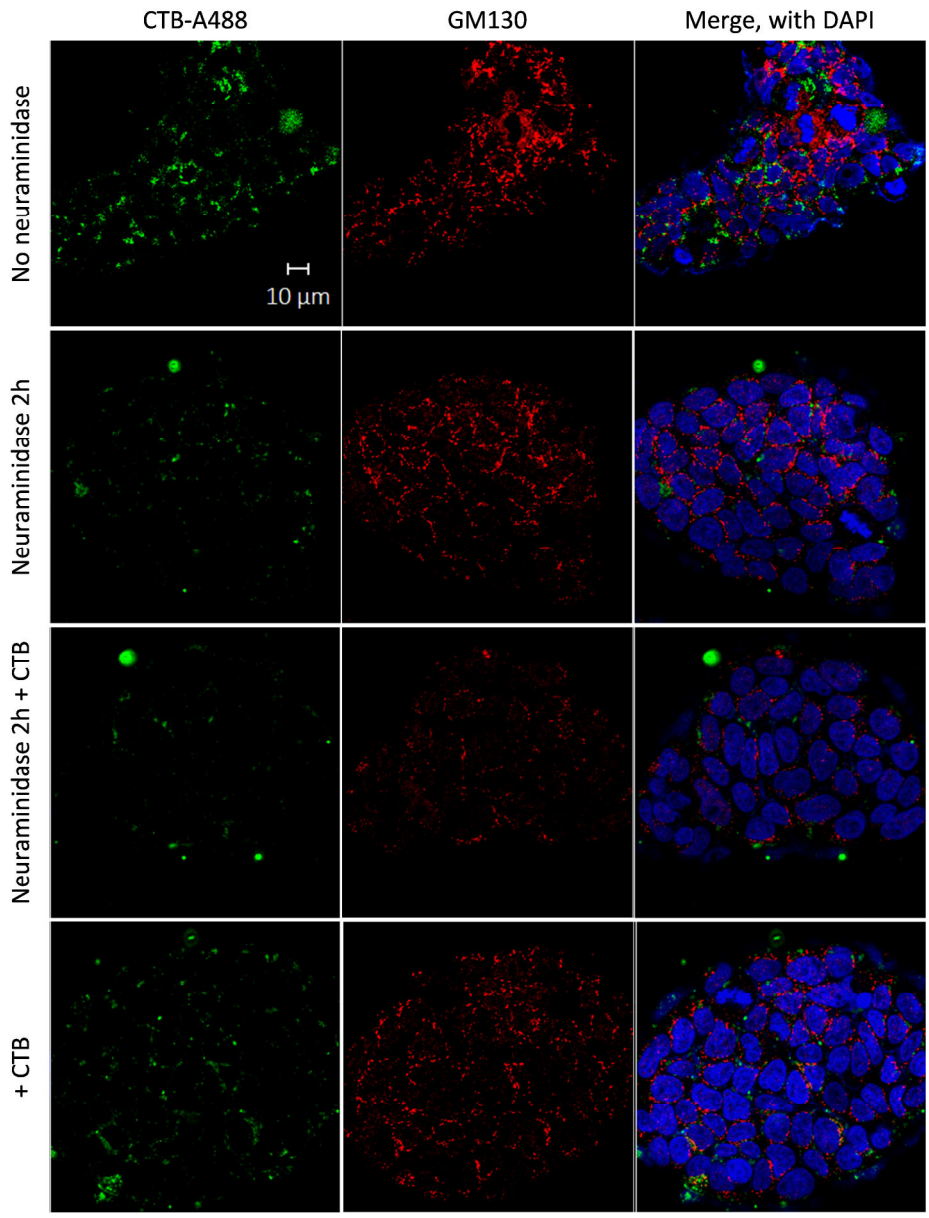

Figure 9-2 – Treatment with neuraminidase and CTB affects the entry of CTB-A488 in NP epithelial cells. Fluorescent images of NP Caco-2 cells incubated for 2 h with 3.5 µM CTB-A488 (green) alone or with 3.5 µM CTB, with or without cell treatment with 1 U/ml neuraminidase. Cell nuclei were stained with DAPI (blue) and expression of GM130 (red) was used to visualise the Golgi network. Images are representative of three independent experiments.

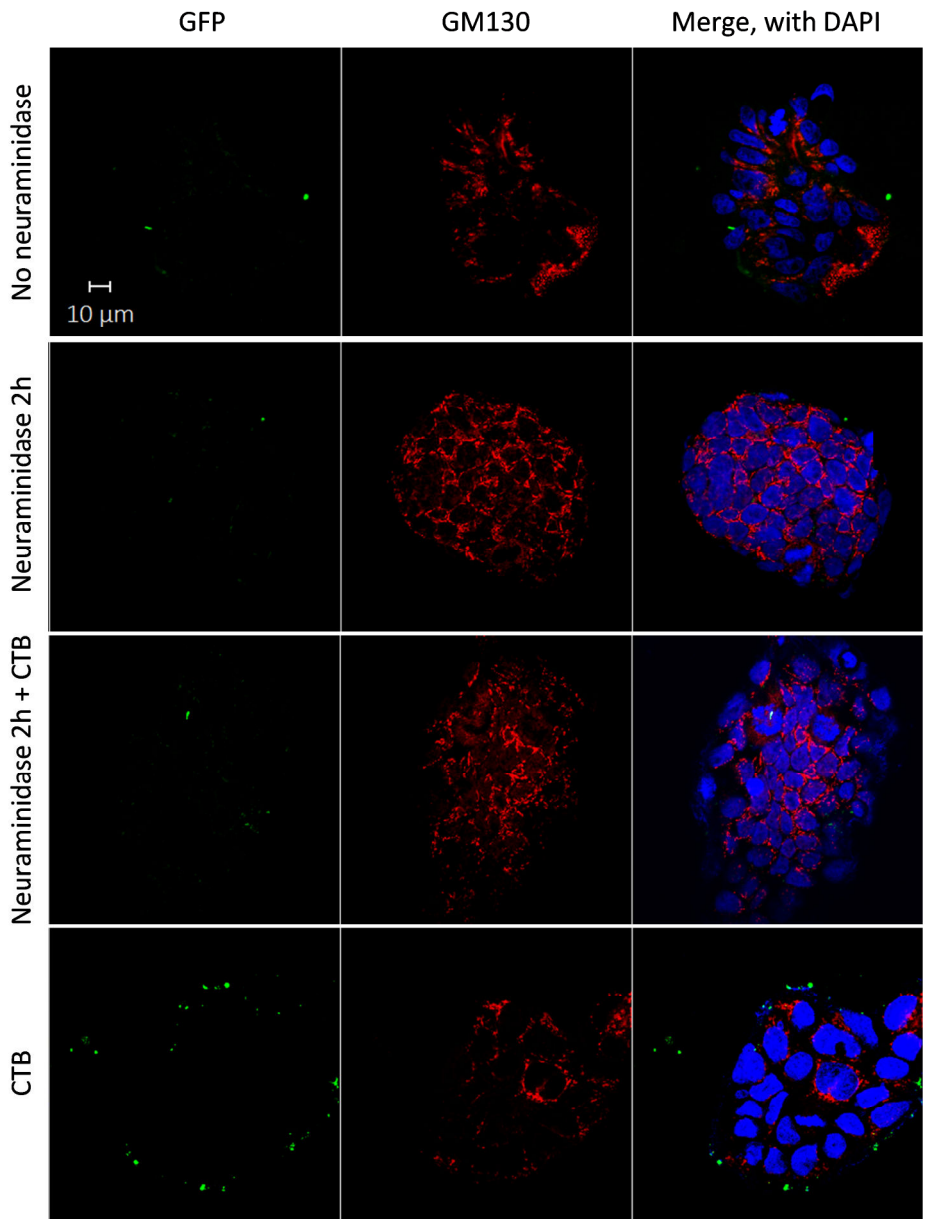

Figure 9-3 – GFP is not internalised by NP epithelial cells. Fluorescent images of NP Caco-2 cells incubated for 2 h with 7.4 µM GFP (green) alone or with 3.5 µM CTB, with or without cell treatment with 1 U/ml neuraminidase. Cell nuclei were stained with DAPI (blue) and expression of GM130 (red) was used to visualise the Golgi network. Images are representative of three independent experiments.

Appendix 4 – Correlation plots and masks for co-localisation of PE-GFP mutants and GM130 after 2 h neuraminidase treatment

NP cells were pre-treated with 1 U/ml neuraminidase for 2 h. Following this, 20 µg of protein diluted in 100 µl complete growth medium containing 1 U/ml neuraminidase was applied for another 2 h. Cells were then fixed with PFA, labelled with an anti-GM130 antibody, and prepared for confocal microscopy. GM130 expression was also used here to visualise the Golgi network [314]. A correlation plot and co-localisation mask were generated using Image Correlation J [306] and Colocalization [307] plugins on Image J [308], respectively (Figure 9-4 and Figure 9-5). Results showed that co-localisation of the PE-GFP mutants (green) with the Golgi network (red) was low in these conditions (Section 5.3.4 and Table 9-4).

Table 9-4 – Correlation coefficients for co-localisation of PE-GFP mutants and GM130 after 2 h neuraminidase treatment. r^2 values were obtained following generation of scatter plots using Image correlation J [306].

Protein	r^2
ntPE-GFP	0.04
PE408-GFP	0.15
PE364-GFP	0.02
PE351-GFP	0.19
PE320-GFP	0.04
PE303-GFP	0.10

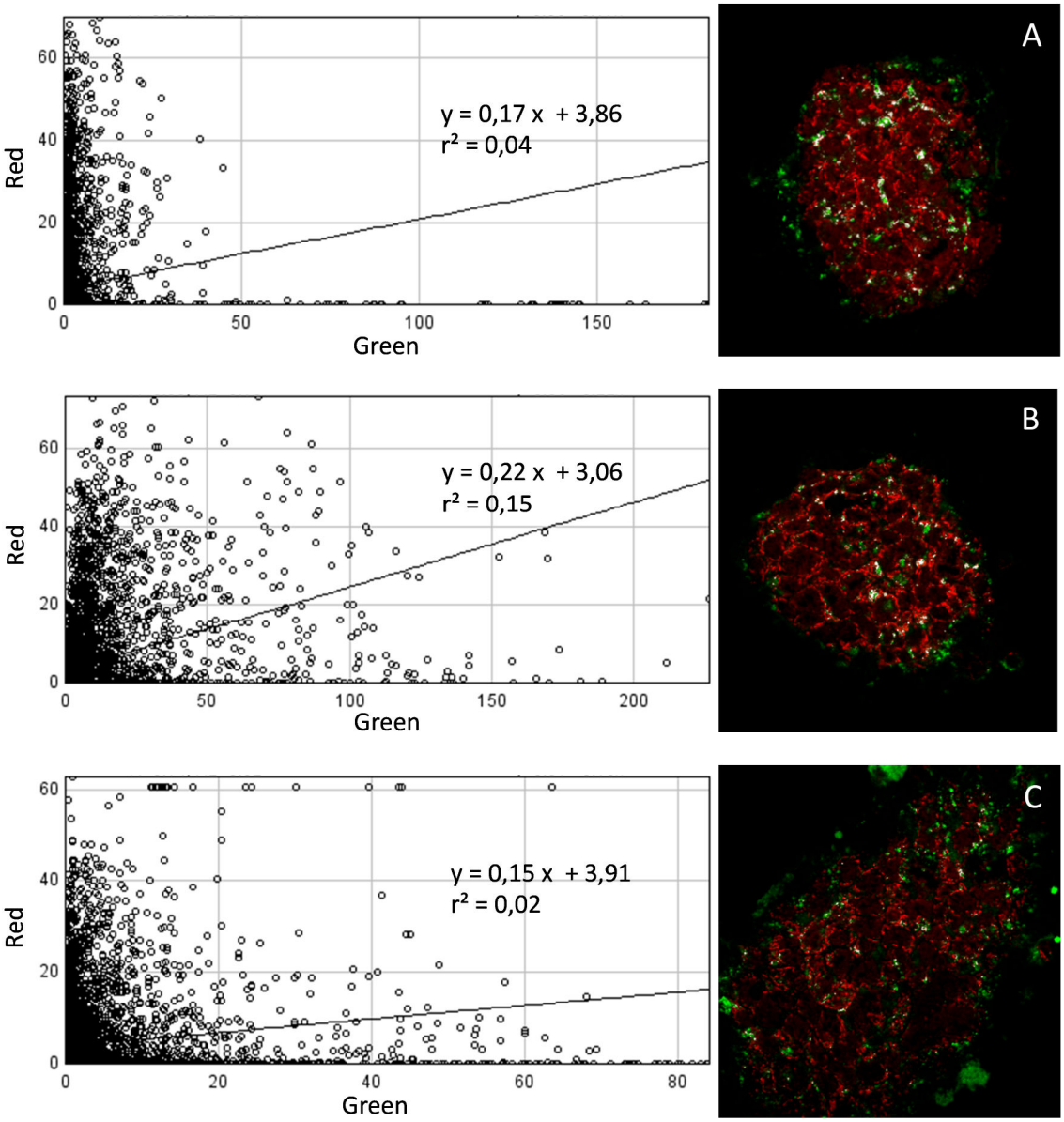

Figure 9-4 – Co-localisation of (A) ntPE-GFP, (B) PE408-GFP and (C) PE364-GFP with GM130 is low following internalisation by neuraminidase-treated cells. Scatter plots and co-localisation masks obtained following application of 20 µg protein (green) diluted in 100 µl complete growth medium containing 1 U/ml neuraminidase to NP Caco-2 cells pre-treated with 1 U/ml neuraminidase for 2 h at 37 °C. Cell nuclei were stained with DAPI (blue) and expression of GM130 (red) was used to visualise the Golgi network. Areas of co-localisation are white. Images are representative of three independent experiments.

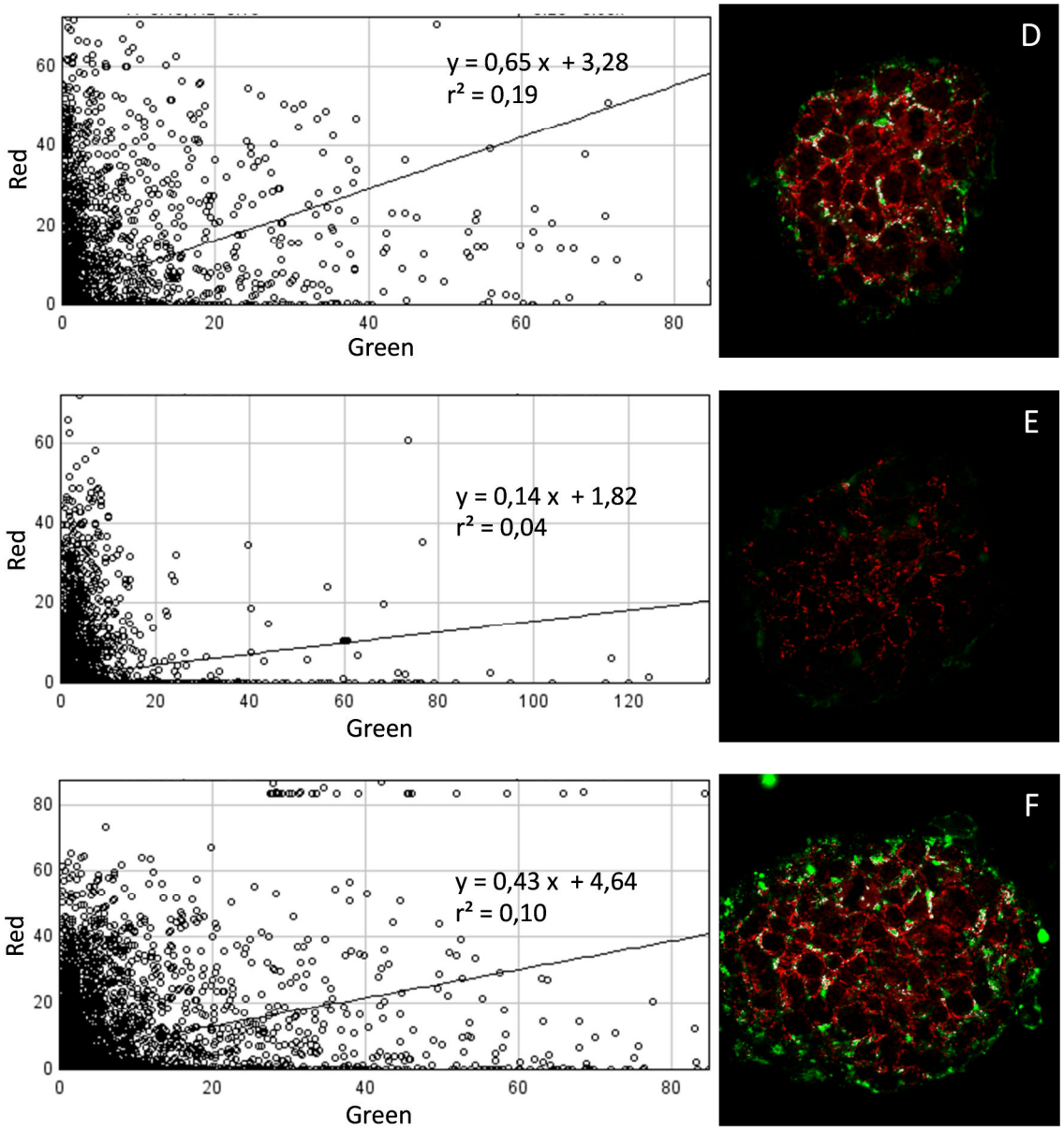

Figure 9-5 – Co-localisation of (D) PE351-GFP, (E) PE320-GFP and (F) PE303-GFP with GM130 is low following internalisation by neuraminidase-treated cells. Scatter plots and co-localisation masks obtained following application of 20 µg protein (green) diluted in 100 µl complete growth medium containing 1 U/ml neuraminidase to NP Caco-2 cells pre-treated with 1 U/ml neuraminidase for 2 h at 37 °C. Cell nuclei were stained with DAPI (blue) and expression of GM130 (red) was used to visualise the Golgi network. Areas of co-localisation are white. Images are representative of three independent experiments.

Appendix 5 – *In vivo* transport of PE364-hGH: Control tissue

To test the specificity of the method used to detect PE364-hGH *in vivo*, naïve tissue sections were sampled from the small intestine of a rat following administration of PBS by luminal injection. Tissues were processed as described in Chapter 2 and immunostained using primary antibodies against PE and hGH. These antibodies were themselves detected using anti-IgG secondary antibodies conjugated to A546 (PE, red) or fluorescein (hGH, green). No signal could be detected, confirming that the antibodies used specifically targeted PE and hGH, respectively (Figure 9-6).

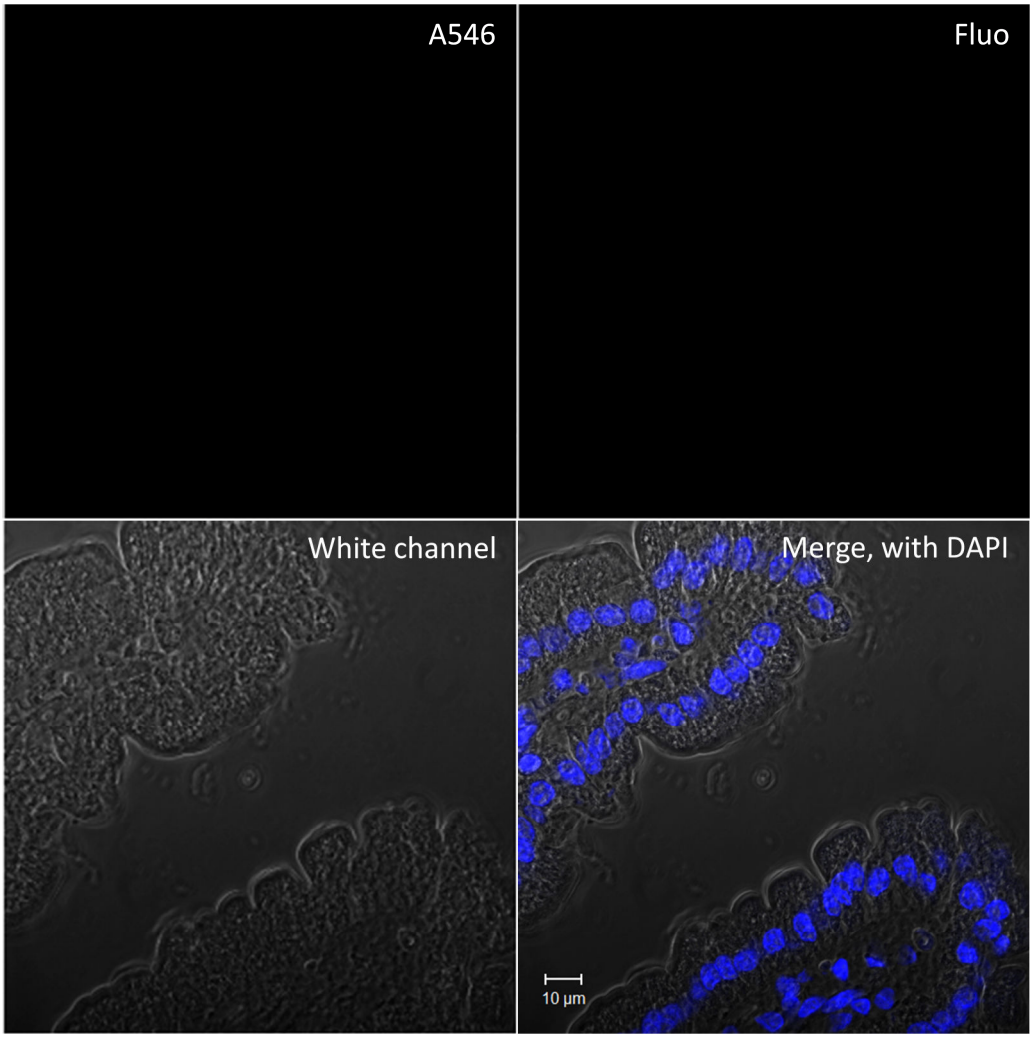

Figure 9-6 – Section of rat naïve intestinal tissue (5 µm) sampled 20 min following intraluminal injection of PBS. The section was indirectly immunostained with antibodies to PE (red) and hGH (green). Cell nuclei were stained with DAPI (blue).

Appendix 6 – Alignment of PE and cholix protein sequences

Protein sequences of full-length PE and cholix were aligned using the Align tool of NCBI's BLAST (BLASTP, http://blast.ncbi.nlm.nih.gov/). The Query and Subject sequences were those of PE (PDB_ID: 1IKQ) and cholix (PDB_ID: 2Q5T), respectively. Results showed that the two protein sequences showed 33% identity, with 49% positives and 10% gaps (Figure 9-7).

```
Query  1    AEEAFDLWNECAKACVLDLKDGV-RSSRMSVDPAIADTNGQGVLHYSMVLEGGNDALKLA  59
            E+  ++++EC   C L  + G    S++S+   +     +GVL+YSM +    + +K
Sbjct  1    VEDELNIFDECRSPCSLTPEPGKPIQSKLSIPSDVVL--DEGVLYYSMTINDEQNDIKDE  58

Query  60   IDNALSITSDG----------------------LTIRLEGGVEPNKPVRYSYTRQARGSW  97
            D   SI + G                        L I  E G +      YSY R+  G +
Sbjct  59   -DKGESIITIGEFATVRATRHYVNQDAPFGVIHLDITTENGTK-----TYSYNRK-EGEF  111

Query  98   SLNWLVPIGHEKPSNIKVFIHELNAGNQLSHMSPIYTIEMGDELLA--KLARDATFFVRA  155
            ++NWLVPIG + P++IK+ + EL+    +  +  +Y+I++ ++ L   K   + +F V
Sbjct  112  AINWLVPIGEDSPASIKISVDELDQQRNIIEVPKLYSIDLDNQTLEQWKTQGNVSFSVTR  171

Query  156  HESNEMQPTLAISHAGVSVVMAQAQPRREKRWSEWASGKVLCLLDPLDGVYNYLAQQRCN  215
            E N     +AIS   VS   AQ +  R KRW+ W +G  LC L P+D +YNY+ QQ C
Sbjct  172  PEHN-----IAISWPSVSYKAAQKEGSRHKRWAHWHTGLALCWLVPMDAIYNYITQQNCT  226

Query  216  LDDTWEGKIYRVLAGNP----AKHDLDIKPTVISHRLHFPEGGSLAALTAHQACHLPLET  271
            L D W G  Y  +AG P     K  ++ KP  +  R+HF +G +++AL AH+ C +PLET
Sbjct  227  LGDNWFGGSYETVAGTPKVITVKQGIEQKP--VEQRIHFSKGNAMSALAAHRVCGVPLET  284

Query  272  FTRHRQPRGWEQLEQCGYPVQRLVALYLAARLSWNQVDQVIRNAL--ASPGSG---GDLG  326
              R R+PR       C Y  Q +V+L++A R+ ++ +D V    L    P        DL
Sbjct  285  LARSRKPRDLTDDLSCAYQAQNIVSLFVATRILFSHLDSVFTLNLDEQEPEVAERLSDLR  344

Query  327  EAIREQPEQARLALTLAAAESERFVRQGTG----NDEAGAANADVVSLTCPVAAGECAGP  382
                 P      LT+A      +V    G       AGA  AD++SL CP A   C
Sbjct  345  RINENNPGMVTQVLTVARQIYNDYVTHHPGLTPEQTSAGAQAADILSLFCPDADKSCVA-  403

Query  383  ADSGDALLERNYPTGAEFLGDGGDVSFSTRGTQNWTVERLLQAHRQLEERGYVFVGYHGT  442
            +++  A +     +G  +L +   V  + +G  NWT + L   H+ L   GYVFVGYHGT
Sbjct  404  SNNDQANINIESRSGRSYLPENRAV-ITPQGVTNWTYQELEATHQALTREGYVFVGYHGT  462
```

```
Query  443  FLEAAQSIV--FGGV-RARSQDLDAIWRGFYIAGDPALAYGYAQDQE-------PDARGR  492
               AAQ+IV     V R  + + +  W G Y+A    +A+GYA+ +E       P    R
Sbjct  463  NHVAAQTIVNRIAPVPRGNNTENEEKWGGLYVATHAEVAHGYARIKEGTGEYGLPTRAER  522

Query  493  IRNGALLRVYVPRSSLPGFYRTSLTLAAPEAAGEVERLIGHPLPLRLDAITGPEEEGGRL  552
               G +LRVY+PR+SL  FYRT+  L   E    + ++IGH LPLR +A TGPE  GG
Sbjct  523  DARGVMLRVYIPRASLERFYRTNTPLENAEE--HITQVIGHSLPLRNEAFTGPESAGGED  580

Query  553  ETILGWPLAERTVVIPSAIPTDPRNVGGDLDPSSIPDKEQAISALPDY  600
             ET++GW +A   V IPS IP +       +D  ++  KEQ+IS  P Y
Sbjct  581  ETVIGWDMAIHAVAIPSTIPGNAYEELA-IDEEAVA-KEQSISTKPPY  626
```

Figure 9-7 – Protein sequence alignment between PE and cholix. The furin-cleavage site is red in the two amino acid sequences.

Appendix 7 – *In vivo* transport of ntCho-A546 and Cho386-A546: control tissue

Naïve tissue sections were sampled from the small intestine of a rat following administration of PBS by luminal injection. Tissues were processed as described in Chapter 2. No signal could be detected, confirming that the signal detected in presence of Cho386-A546 (red) was not an artefact due to intrinsic sample fluorescence (Figure 9-8).

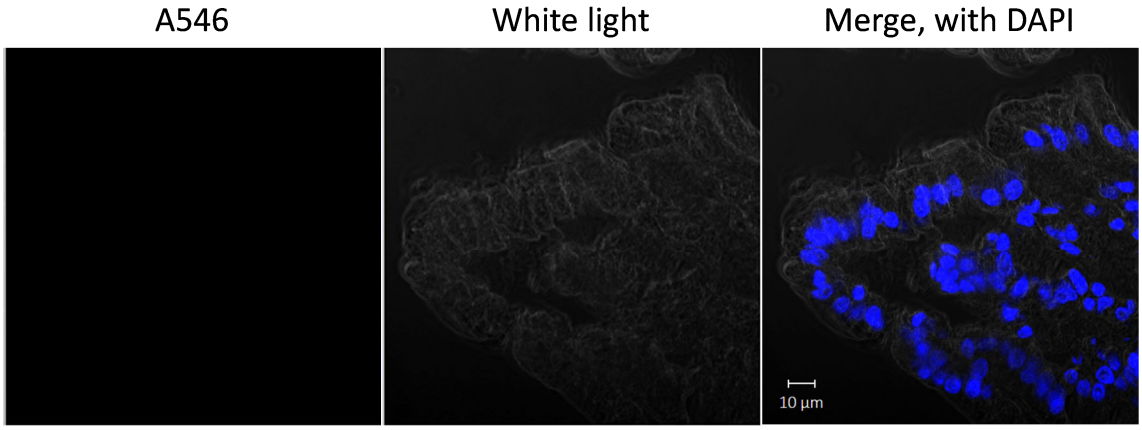

Figure 9-8 – Section of rat naïve intestinal tissue (5 µm) sampled 20 min following intraluminal injection of PBS. Cell nuclei were stained with DAPI (blue).

Appendix 8 – *In vivo* transport of Cho386-hGH: control tissue

To test the specificity of the method used to detect Cho386-hGH *in vivo*, naïve tissue sections were sampled from the small intestine of a rat following administration of PBS by luminal injection. Tissues were processed as described in Chapter 2 and immunostained using primary antibodies against Cho386 GS TEV and hGH. These antibodies were themselves detected using anti-IgG secondary antibodies conjugated to A546 (Cho386, red) or fluorescein (hGH, green). No signal could be detected, confirming that the antibodies used specifically targeted Cho386 and hGH, respectively (Figure 9-9).

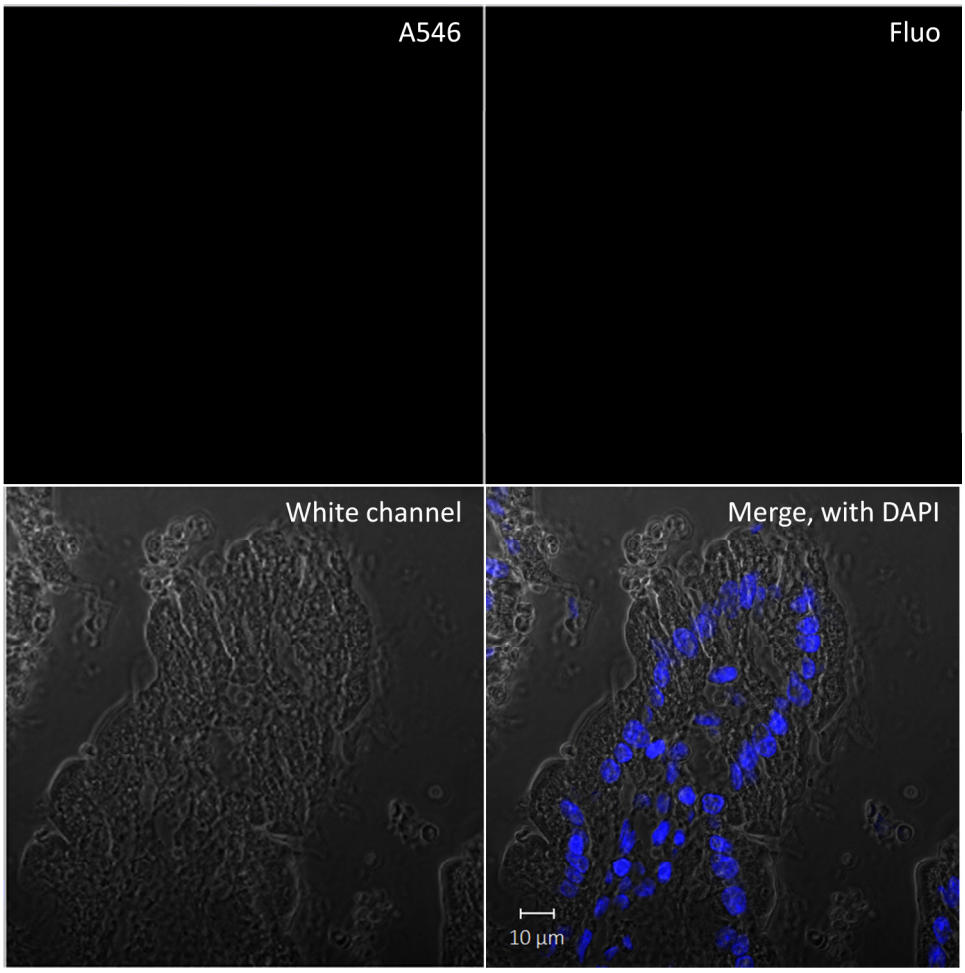

Figure 9-9 – Section of rat naïve intestinal tissue (5 µm) sampled 20 min following intraluminal injection of PBS. The section was indirectly immunostained with antibodies to Cho386 GS TEV (red) and hGH (green). Cell nuclei were stained with DAPI (blue).

Appendices

10 DISSEMINATION

Oral presentation at an international meeting

Research Highlight Talk: "*Pseudomonas* exotoxin A as a drug carrier for oral protein delivery", presented at the 42nd Annual Meeting and Exposition of the Controlled Released Society – July 26-29th, 2015 – Edinburgh, Scotland

Poster presentation at an international meeting

"*Pseudomonas* exotoxin A as a carrier for intracellular protein delivery", presented at the 42nd Annual Meeting and Exposition of the Controlled Released Society – July 26-29th, 2015 – Edinburgh, Scotland

Publications

Book chapter in preparation

Laurent, F., Hillery, A.M., Mrsny, R.J. (2015), Overview of Epithelial Cell Barriers. In Drug Delivery and Targeting: Fundamentals, Applications and Future Directions, A.M. Hillery, J. Swarbrick and K. Park, eds. (Taylor and Francis)